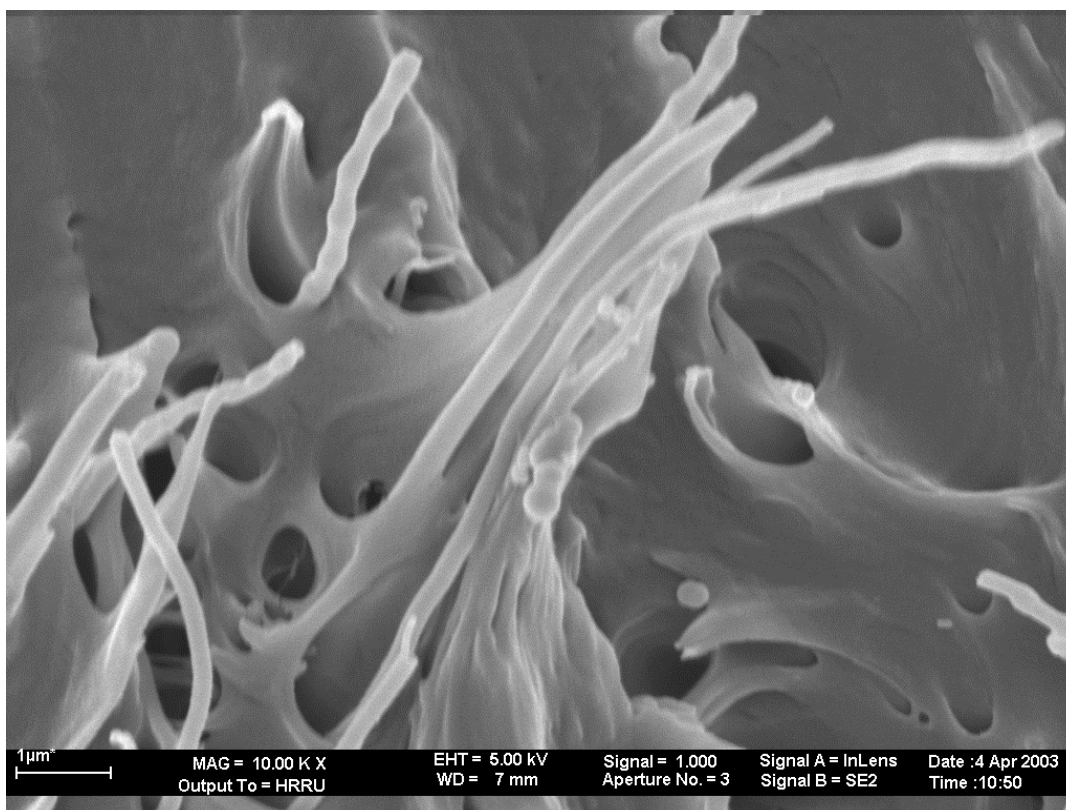






# Synthesis of Polypropylene Nanocomposites by *in situ* Polymerization of Propylene with Metallocene/MAO Catalysts



## Dissertation

Submitted to  
Fachbereich Chemie  
Universität Hamburg

In partial fulfillment of the requirements  
for the German academic degree  
Dr. rer. nat.

**Katharina Wiemann**

Hamburg, 2004





Gutachter/Reviewers:

Prof. Dr. W. Kaminsky

Prof. Dr. W.- M. Kulicke

Disputation: December 17<sup>th</sup>, 2004

This thesis was prepared between October 2001 and November 2004 at the Institute of Technical and Macromolecular Chemistry of the University of Hamburg.

Great thanks I owe to my honored teacher, Prof. Dr. W. Kaminsky, for the interesting subject and the freedom given during the preparation of this work.

This work would not have been possible without the help of the research group's, the institute's, and the department's members. Special thanks to:

- Andrea who was always open for discussions and who always had a helping hand
- Christian and Tanja for the GPC-measurements and for the fruitful discussions
- Andreas for the work during his practical training
- Björn, the “metallocene-whisperer”
- Phu, Fabian, Matthias and Mercia for the DSC-measurements
- Olivera, Isabel, Jens and Björn for the measurement of NMR-samples
- Ben for solving computer-related problems
- Stefan for the determination of the viscosimetric molecular weights.
- Mrs. Hagemeister for the incineration analyses
- Uta Sazama (research group Albert) for the TGA-measurements
- Matthias Wulff and Sven Gerber (research group Vill) for their help with the microscope
- Mrs. Ralya (PC) and Dr. Kathrin Hofmann (AC) for some SEM-measurements
- Holger for the works involving electronics
- Kathleen, Klaus, Jens P. and K. Fischer for the smooth ordering procedures
- Peter for the glass works
- The team of the workshop, especially Mr. Horbaschk, for the prompt and precise mechanical works.

I would also like to thank Dr. Joachim Loos (research group Lemstra, TU Eindhoven) for some of the SEM-photographs and Florian Gojny (research group Schulte, TUHH) for electron micrographs and some of the tensile tests. Thanks go also to Prof. Koning and Nadia Grossiord (TU Eindhoven) for making the conductivity measurements possible.

Bob and Patty, I would like to thank for being my “parents abroad”, and especially Patty for editing this thesis.

Very special thanks go to my parents and my sister for making my studies possible with all their support.

I also owe loads of thanks to Jan for always being there and cheering me up when things had somehow gone wrong again.

## CONTENTS

<b>1</b>	<b>ABBREVIATIONS .....</b>	<b>IV</b>
<b>2</b>	<b>SUMMARY.....</b>	<b>1</b>
<b>3</b>	<b>ZUSAMMENFASSUNG .....</b>	<b>3</b>
<b>4</b>	<b>INTRODUCTION.....</b>	<b>5</b>
4.1	SYNTHESIS OF POLYPROPYLENE WITH METALLOCENE/MAO CATALYSTS .....	6
4.1.1	<i>Discovery and Development.....</i>	6
4.1.2	<i>Mechanism of Olefin Polymerization.....</i>	7
4.1.3	<i>Stereochemistry of the Propylene Insertion .....</i>	9
4.2	NANOCOMPOSITES .....	11
4.2.1	<i>Synthesis of Nanocomposites .....</i>	13
4.2.2	<i>Fillers .....</i>	17
4.2.3	<i>Properties of Nanocomposites .....</i>	19
<b>5</b>	<b>AIM OF THIS WORK .....</b>	<b>25</b>
<b>6</b>	<b>RESULTS AND DISCUSSION.....</b>	<b>27</b>
6.1	GENERAL ASPECTS.....	27
6.1.1	<i>Dispersion of the Fillers and Adhesion of the Polymer to the Filler.....</i>	28
6.1.2	<i>Pre-Reaction of the Fillers with MAO .....</i>	29
6.1.3	<i>Crystallization Behavior of the Nanocomposites.....</i>	30
6.1.4	<i>Thermal Stability of the Nanocomposites.....</i>	34
6.1.5	<i>Electrical Conductivity of the Nanocomposites .....</i>	35
6.1.6	<i>Tensile Properties of the Nanocomposites .....</i>	36
6.2	POLYPROPYLENE/MONOSPHER NANOCOMPOSITES .....	38
6.2.1	<i>Adhesion and Stability.....</i>	38
6.2.2	<i>Variation of MAO Amount .....</i>	39
6.2.3	<i>Variation of Temperature, Propylene Concentration and Catalyst Amount ...</i>	42
6.2.4	<i>Gasphase Polymerizations .....</i>	47
6.3	POLYPROPYLENE/GLASS FIBER NANOCOMPOSITES.....	51
6.4	ISOTACTIC POLYPROPYLENE/CARBON NANOFIBER NANOCOMPOSITES.....	57
6.4.1	<i>Dispersion of the Carbon Nanofibers .....</i>	57

6.4.2	<i>Adhesion of the Polypropylene Matrix to the Carbon Nanofibers</i> .....	63
6.4.3	<i>Crystallization and Melting Behavior of the iPP/CNF Nanocomposites</i> .....	65
6.5	SYNDIOTACTIC POLYPROPYLENE/CARBON NANOFIBER NANOCOMPOSITES.....	69
6.5.1	<i>Dispersion of the Carbon Nanofibers</i> .....	69
6.5.2	<i>Adhesion of the Polypropylene Matrix to the Carbon Nanofibers</i> .....	74
6.5.3	<i>Crystallization and Melting Behavior of the sPP/CNF nanocomposites</i> .....	77
6.5.4	<i>Thermal Stability of the sPP/CNF Nanocomposites</i> .....	81
6.5.5	<i>Electrical Conductivity of the sPP/CNF Nanocomposites</i> .....	82
6.5.6	<i>Tensile Properties of the sPP/CNF Nanocomposites</i> .....	82
6.6	SYNDIOTACTIC POLYPROPYLENE/CARBON NANOTUBE NANOCOMPOSITES .....	86
6.6.1	<i>Dispersion of the Carbon Nanotubes</i> .....	86
6.6.2	<i>Adhesion of the Polypropylene to the Carbon Nanotubes</i> .....	92
6.6.3	<i>Crystallization and Melting Behavior of the sPP/MWNT Nanocomposites</i> ....	95
6.6.4	<i>Thermal Stability of the sPP/MWNT Nanocomposites</i> .....	103
6.6.5	<i>Electrical Conductivity of the sPP/MWNT Nanocomposites</i> .....	106
6.6.6	<i>Tensile Properties of the sPP/MWNT Nanocomposites</i> .....	106
6.7	SYNDIOTACTIC POLYPROPYLENE/CARBON BLACK NANOCOMPOSITES .....	110
6.7.1	<i>Dispersion of the Carbon Black</i> .....	110
6.7.2	<i>Crystallization and Melting Behavior of the sPP/CB Nanocomposites</i> .....	112
6.7.3	<i>Thermal Stability of the sPP/CB Nanocomposites</i> .....	114
6.7.4	<i>Electrical Conductivity of the sPP/CB Nanocomposites</i> .....	115
6.7.5	<i>Tensile Properties of the sPP/CB Nanocomposites</i> .....	115
6.8	COMPARISON OF sPP/CNF, sPP/MWNT AND sPP/CB NANOCOMPOSITES. 117	
6.8.1	<i>PP/GF and PP/M250 Nanocomposites</i> .....	117
6.8.2	<i>PP/CNF, PP/MWNT and PP/CB Nanocomposites</i> .....	117
<b>7</b>	<b>CONCLUSIONS AND PROSPECTS .....</b>	<b>126</b>
<b>8</b>	<b>EXPERIMENTAL PART .....</b>	<b>128</b>
8.1	MATERIALS .....	128
8.1.1	<i>Gases</i> .....	128
8.1.2	<i>Solvents</i> .....	128
8.1.3	<i>Fillers</i> .....	128
8.1.4	<i>Metallocenes</i> .....	129
8.1.5	<i>Cocatalyst and Scavenger</i> .....	129

8.1.6	<i>Quench-Solution</i> .....	129
8.2	PRETREATMENT OF THE FILLERS .....	130
8.2.1	<i>Silica Gel</i> .....	130
8.2.2	<i>Glass Fibers</i> .....	130
8.2.3	<i>Monosphers 250</i> .....	130
8.2.4	<i>Carbon Nanotubes and Nanofibers</i> .....	130
8.3	POLYMERIZATIONS.....	131
8.3.1	<i>Polymerizations in the Presence of Monosphers</i> .....	132
8.3.2	<i>Polymerizations in the Presence of Carbon Nanotubes and Carbon Nanofibers</i> .....	132
8.4	ANALYTICAL TECHNIQUES.....	133
8.4.1	<i>Filler Content</i> .....	133
8.4.2	<sup>13</sup> C-NMR-Spectroscopy.....	133
8.4.3	<i>Differential-Scanning-Calorimetry (DSC)</i> .....	133
8.4.4	<i>Electron Microscopy</i> .....	134
8.4.5	<i>Microscopy</i> .....	134
8.4.6	<i>Viscosimetry</i> .....	134
8.4.7	<i>Gel-Permeation-Chromatography</i> .....	134
8.4.8	<i>Tensile Testing</i> .....	135
8.4.9	<i>Incineration</i> .....	135
8.4.10	<i>Thermo-Gravimetric Analysis</i> .....	135
8.4.11	<i>Conductivity Measurements</i> .....	135
8.5	SAFETY .....	136
<b>9</b>	<b>LITERATURE .....</b>	<b>138</b>

## 1 ABBREVIATIONS

$\delta$	Chemical Shift (NMR)
$\eta$	Hapticity
$\rho$	Resistivity (electrical)
$\sigma$	Stress
$\varepsilon$	Strain
a	Mark-Houwink-Constant
BOPP	Biaxially Oriented Polypropylene
c	Concentration
CVD	Chemical Vapor Deposition
CNF	Carbon Nanofibers
CNT	Carbon Nanotubes
Cp	Cyclopentadienyl
DB	Doublebond(s)
DSC	Differential Scanning Calorimetry
E	Young's Modulus (Elastic Modulus)
Et	Ethylene-
g	Gramms
GF	Glass Fibers
GPC	Gel-Permeation-Chromatography
h	Hour(s)
<i>h</i>	Thickness
HDPE	High Density Polyethylene
i-Bu	iso-Butyl-Group
IndH <sub>4</sub>	Tetrahydroindenyl-
K	Mark-Houwink-Constant
l	Liter
<i>l</i>	length
LDPE	Low Density Polyethylene
M250	Monosphers
MAO	Methylaluminoxane
Me	Methyl-Group
IV	

mg	Milligramms
min	Minutes
ml	Milliliters
mm	Millimeters
MMA	Methylmethacrylate
MWNT	Multi-Walled Carbon Nanotubes
n	Avrami Exponent
NMR	Nuclear Magnetic Resonance
PE	Polyethene
PMMA	Polymethylmethacrylate
PP	Polypropylene
R	Organic Group
<i>R</i>	Resistance (electrical)
SEM	Scanning-Electron-Microscopy
sPP	Syndiotactic Polypropylene
SWNT	Single-Walled Carbon Nanotubes
t	Time
T	Temperature
$t_{0.5}$	Half-Time of Crystallization
<sup>t</sup> Bu	<i>tert</i> -Butyl-Group
$T_c$	Crystallization Temperature
$T_g$	Glass Temperature
$T_m$	Melting Temperature
$T_{max}$	Temperature of Maximum Weight Loss Rate
$T_{on}$	Etrapolated Onset Temperature of Degradation
$T_p$	Polymerization Temperature
TCE-d2	<i>bis</i> -Deutero-Tetrachloroethane
TGA	Thermo-Gravimetric Analysis
TIBA	Triisobutylaluminum
TMA	Trimethylaluminum
V	Volume
<i>w</i>	Width
$X_c$	Crystalline Fraction

---



## 2 SUMMARY

In the past years, a lot of research has focused on the field of nanocomposites because of their potential as materials with novel properties. Exceptionally strong materials could be synthesized by combination of a soft polymer matrix with nano-sized, rigid filler particles. Moreover, the intrinsic properties of the nanofillers, like electrical conductivity or barrier properties, can add to the value of the nanocomposite material.

The forecasted potential of these nanocomposites is frequently not accomplished in practice which can be attributed to an insufficient load transfer between the matrix and the filler. A homogeneous distribution and a good interfacial adhesion are crucial for the successful preparation of nanocomposites but often difficult to achieve by simple melt-compounding. Especially fillers with high aspect ratio like carbon nanofibers and carbon nanotubes tend to stay aggregated during this process. The *in situ* polymerization of monomers in the presence of nanofillers is a promising approach for a homogeneous distribution because of the close contact of polymer and filler during synthesis.

In this work, *in situ* polymerization of propylene with metallocene/MAO catalysts in the presence of monospheres (silica nanospheres), glass fibers, nano-sized carbon black, carbon nanofibers (CNFs) and multi-walled carbon nanotubes (MWNTs) was performed to prepare the respective (nano-)composites. Nanocomposites of syndiotactic polypropylene (sPP) and carbon nanotubes have not been synthesized before. An ultrasonic treatment before the polymerizations was necessary for all nanofillers to ensure a homogeneous distribution.

A good coverage of glass fibers with syndiotactic polypropylene was achieved when MAO was heterogenized on etched glass fibers. The monospheres could be homogeneously dispersed and covered well in gas-phase polymerizations of propylene after heterogenization of MAO on the monospher surface. A filler content of up to 60 weight-% could be realized by this process.

A rather homogeneous distribution of carbon nanofibers in isotactic (iPP) and syndiotactic polypropylene and of carbon black in syndiotactic polypropylene could be achieved by *in situ* polymerization of propylene after dispersion of the fillers with ultrasound. The best sonication conditions were dependant on the nanofiller used. In addition to sonication, a pre-reaction of

carbon nanotubes with MAO for 24 hours was necessary to obtain a homogeneous dispersion of this type of filler.

The properties of the PP/carbon nanofiber, PP/carbon black, and PP/carbon nanotube nanocomposites were investigated taking the filler type and the filler content into account. The electrical conductivity, the thermal stability, the tensile properties, and the crystallization behavior of the nanocomposites were studied.

Due to the low filler loadings (0.1 to 1 %), no electrical conductivity of nanocomposites containing carbon black or carbon nanotubes was detected. In contrast to this, the sPP/carbon nanofiber nanocomposites already exhibited a slight electrical conductivity at filler contents of 3 to 4 %.

The presence of carbon black, carbon nanofibers and carbon nanotubes improved the thermal stability of the polypropylene matrix. An improvement of the yield strength was found for all three nanocomposites, which was most evident in the case of carbon nanofibers. Further enhancements in the yield strength could be possible by amelioration of the distribution and adhesion.

The most apparent effect of the fillers was detected in the crystallization behavior of the nanocomposites. They all exhibited crystallization temperatures higher than those of the pure PP, which also increased with rising the filler content. The half-time of crystallization was significantly reduced upon addition of carbon black, carbon nanofibers or carbon nanotubes. Moreover, the rate constant of crystallization obtained from Avrami analysis of isothermal DSC (differential scanning calorimetry) measurements was notably increased. The above findings prove a nucleating effect of the nanofillers. This enhancement of the crystallization rate was by far most pronounced in the case of carbon nanotubes and was observed for the first time for these nanocomposites.

### 3 ZUSAMMENFASSUNG

In den letzten Jahren ist das Interesse der Forschung an Nanocomposites wegen ihres Potentials als Materialien mit ganz neuen Eigenschaften sprunghaft angestiegen. Sehr steife Materialien konnten durch Kombination einer weichen Polymermatrix mit harten Nanofüllstoffen hergestellt werden. Darüber hinaus können die speziellen Eigenschaften der Nanofüllstoffe, wie zum Beispiel die elektrische Leitfähigkeit oder die Barriereigenschaften, das Eigenschaftsspektrum der Nanocomposite-Materialien erweitern.

Die erwartete Verbesserung der Eigenschaften wird in der Praxis häufig nicht erreicht, was wahrscheinlich auf eine nicht ausreichende Übertragung der Lasten von dem Polymer auf den Füllstoff zurückzuführen ist. Eine homogene Verteilung und eine gute Haftung, die durch Schmelz-Compoundierung jedoch häufig nur schwer zu erreichen sind, sind ausschlaggebend für die erfolgreiche Herstellung von Nanocomposites. Besonders Füllstoffe mit hohem Aspektverhältnis wie Kohlenstoff-Nanofasern und Kohlenstoff-Nanoröhrchen bleiben leicht agglomeriert. Die *in situ* Polymerisation in Gegenwart von Nanofüllstoffen ist wegen der räumlichen Nähe zwischen Füllstoff und entstehendem Polymer ein vielversprechender Ansatz, um eine homogene Verteilung zu erreichen.

In dieser Arbeit wurden *in situ* Polymerisationen von Propen mit Metallocen/MAO Katalysatoren in Gegenwart von Monosphers (Silica Nanokugeln), Glasfasern, Ruß (Partikelgröße 30 nm), Kohlenstoff-Nanofasern (CNF) und Kohlenstoff-Nanoröhrchen (MWNT) zur Herstellung der jeweiligen (Nano-)Composites durchgeführt. Nanocomposites aus syndiotaktischem Polypropen (sPP) und Kohlenstoff-Nanoröhrchen wurden erstmals hergestellt. Um eine homogene Verteilung zu erreichen, war die Behandlung der Füllstoffe mit Ultraschall vor der Polymerisation notwendig.

Eine fast vollständige Umhüllung der Glasfasern mit syndiotaktischem Polypropen konnte durch Heterogenisierung von MAO auf den angeätzten Glasfasern erreicht werden. Auch die Monosphers konnten durch Gasphasenpolymerisationen von Propen nach Heterogenisierung des MAO auf der Monospher-Oberfläche homogen verteilt und gut umhüllt werden. Es konnte dabei ein Füllstoffgehalt von bis zu 60 Gewichts-% realisiert werden.

Eine überwiegend homogene Verteilung von Kohlenstoff-Nanofasern in isotaktischem (iPP) und syndiotaktischem Polypropen und von Ruß in sPP konnte durch *in situ* Polymerisation von Propen nach Behandlung der Füllstoffe mit Ultraschall erreicht werden. Zusätzlich zu der Ultraschallbehandlung war eine Vorreaktionszeit von 24 Stunden mit MAO nötig, um eine ebenfalls homogene Verteilung der Kohlenstoff-Nanoröhrchen zu erreichen.

Die Eigenschaften der PP/CNF-, der PP/Ruß- und der PP/MWNT-Nanocomposites wurden unter Berücksichtigung des Füllstofftyps und des jeweiligen Füllstoffgehaltes untersucht. Dazu wurden die elektrische Leitfähigkeit, die Zug-Dehnungseigenschaften und das Kristallisationsverhalten der Nanocomposites analysiert.

Wegen der niedrigen Füllstoffgehalte (0,1 bis 1 %) wurde bei Ruß oder Kohlenstoff-Nanoröhrchen enthaltenden Nanocomposites keine Leitfähigkeit gemessen. Im Gegensatz dazu konnte für sPP/Kohlenstoff-Nanofaser Nanocomposites mit einem Füllstoffgehalt von 3 bis 4 % bereits eine leicht erhöhte Leitfähigkeit beobachtet werden.

Die Anwesenheit von Ruß, Kohlenstoff-Nanofasern oder Kohlenstoff-Nanoröhrchen verbesserte die thermische Stabilität der Polypropenmatrix. Für alle drei Füllstoffe wurde eine Verbesserung der Fließspannung gemessen, die im Falle der Kohlenstoff-Nanofasern am stärksten ausfiel. Weitere Erhöhungen der Fließspannung könnten durch eine noch bessere Verteilung und Adhäsion der Füllstoffe im Polymer möglich sein.

Den deutlichsten Effekt zeigte die Anwesenheit der Füllstoffe auf das Kristallisationsverhalten der Nanocomposites. Alle Kristallisationstemperaturen lagen über denen des reinen Polypropens und stiegen mit steigendem Füllstoffgehalt. Die Kristallisationshalbzeit wurde durch Zusatz von Ruß, Kohlenstoff-Nanofasern oder Kohlenstoff-Nanoröhrchen signifikant verringert. Darüber hinaus wurde die Geschwindigkeitskonstante der Kristallisation, die aus Avrami Auswertungen der isothermen DSC-Messungen (differential scanning calorimetry) bestimmt wurde, deutlich gesteigert. Die obigen Ergebnisse belegen einen Nukleierungseffekt der Füllstoffe für Polypropen. Diese Beschleunigung der Kristallisation war für sPP/Kohlenstoff-Nanoröhrchen Nanocomposites am stärksten ausgeprägt und wurde für diese Nanocomposites erstmals nachgewiesen.

## 4 INTRODUCTION

Polyolefins are an interesting class of materials, because of their versatility with respect to physical and mechanical properties, their nontoxicity, the energy efficient and economic production, their low cost and easily available raw materials<sup>[1]</sup>. Among these commodity polymers, polypropylene (PP) has shown the highest growth rates. In 2002, the production capacity of PP was roughly 39 mio. tons, exhibiting an average annual growth rate of 14.9 %<sup>[1,2]</sup>. The world consumption of PP in 2003 and its estimated consumption in 2010 are shown in Fig. 1. The most common commercial form of PP is isotactic PP (iPP) which features good stiffness, high melting temperature and yield strength, good chemical resistance and excellent moisture barrier properties<sup>[3]</sup>. Isotactic and syndiotactic PP (sPP) exhibit a high crystallinity and melting temperature. In addition, sPP shows good elastic properties in a wide deformation range<sup>[4]</sup>. It is softer and has a higher clarity than iPP<sup>[5]</sup>. On the other hand, the low crystallization rate hinders the commercial application<sup>[6]</sup>.

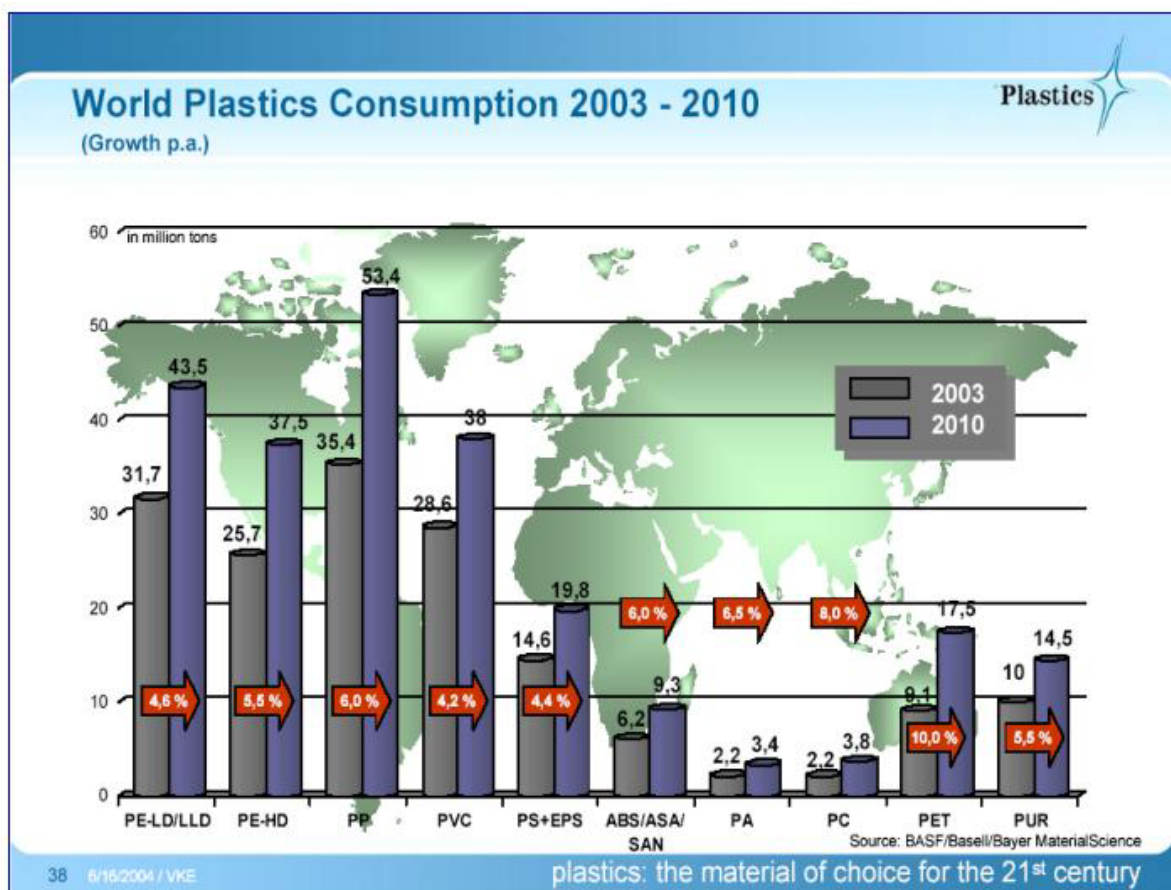


Fig. 1: World Plastics Consumption 2003 (taken from [www.vke.de/de/infomaterial/downloads](http://www.vke.de/de/infomaterial/downloads))

Polypropylene and its copolymers are, for example, used in packaging (films, BOPP-films, containers etc.), domestic appliances (e.g. kitchenware and tool handles), electrical, fiber and

automotive applications<sup>[7-9]</sup>. It is also applied for medical, sanitary, construction and agricultural materials<sup>[10]</sup>. Its properties depend largely on the microstructure, the molecular weight and the molecular weight distribution and can be tuned over a wide range to fit the desired application. In some cases, comonomers are incorporated for a further modification of the physical and mechanical properties.

Commercially available PP is usually synthesized with Ziegler-Natta type catalysts, but also metallocene-PP is now accessible<sup>[11,12]</sup>. In 2001, about 0.3 % of the produced PP was synthesized with metallocene catalysts<sup>[10]</sup>. Different grades of metallocene synthesized syndiotactic PP and syndiotactic PP copolymers are available from Atofina, for example<sup>[11,13]</sup>. The possibility to fine-tune the properties of metallocene-PP by variation of the metallocene structure to get materials with new properties makes these resins interesting for a broadening of the product portfolio.

Advances of polypropylene into new markets could also be possible by preparing PP-nanocomposites with new properties, thus permitting the substitution of environmentally less favorable or more expensive polymers. Additionally, the good processing characteristics, the low density, and the good cost-benefit-balance make PP an interesting material for the substitution of other materials<sup>[12]</sup>. Compounded PP is used in areas, where unmodified PP couldn't compete with other polymers, like bumpers for cars, outdoor garden furniture and temperature resistant car under hood applications<sup>[9]</sup>. To further expand the PP portfolio, and replace other polymers on the market, the incorporation of nano-sized fillers into this matrix polymer is interesting. The consulting group STA, USA, estimates that the next great step in polypropylene technology will be polypropylene nanocomposites<sup>[14]</sup>. Very small particles dispersed in a polymer matrix can have a tremendous impact on the physical properties of polymers, such as the stiffness, the impact strength, the gas barrier properties, the thermal stability, and the optical appearance. In 2010, a million tons of nanocomposites could be produced per year.

## **4.1 Synthesis of Polypropylene with Metallocene/MAO Catalysts**

### **4.1.1 Discovery and Development**

The foundation for today's extensive use of polyolefins was laid about 50 years ago, when Ziegler polymerized ethylene with the system  $\text{TiCl}_4/\text{Et}_3\text{Al}$ <sup>[15,16]</sup>. A year later, in 1954, Natta

used the same system for the polymerization of propylene to a mixture of atactic and isotactic polypropylene<sup>[17,18]</sup>. Already very soon afterwards, the above system was implemented for industrial application. The relatively poor properties of the produced polypropylene have led to numerous improvements of the catalysts and production processes with respect to their activity and stereospecificity since the 1960s. Today, heterogeneous titanium catalysts are the most commonly used catalysts for the polymerization of propylene. Modern industrial catalysts are constituted of  $MgCl_2/TiCl_4$  and a Lewis base, such as ethylbenzoate, alkylphthalate, alkoxysilane or a 1,3-diether, as electron donor. They are typically activated by triethyl-aluminum (TEA) and produce highly isotactic polypropylene with high activities<sup>[18,19]</sup>.

The first metallocenes produced only atactic polypropylene with low activities above 0°C and became interesting as olefin polymerization catalysts only after the discovery of Sinn and Kaminsky in 1976 that the addition of methylaluminoxane (MAO) extremely boosts the activity of these systems<sup>[20,21]</sup>. A further step towards their applicability was the discovery of chiral *ansa*-metallocenes by Brintzinger in 1982<sup>[22]</sup>, which were used for the isotactic polymerization of propylene by Kaminsky in 1985<sup>[23]</sup>. Since then, the structure of the metallocenes has been modified in many ways to provide now a vast array of different catalyst-structures which can be used to synthesize highly isotactic, syndiotactic, atactic or hemi-isotactic polypropylenes with different molecular weights and different degrees of tacticity <sup>[24-28]</sup>. Besides that, the incorporation of many different comonomers is possible.

Although providing higher activities and a tunable stereocontrol, metallocenes are still not widely used in industrial applications. One of the problems to be overcome is the homogeneous nature of the catalyst, which prevents these systems from being used in existing plants without further modifications. In spite of these problems, metallocene-PP is on the market and is, for example, used by airline caterers because of its good thermal and chemical resistance, the very good transparency and its low cost<sup>[29]</sup>. It has substituted Polymethylmethacrylate (PMMA) in this application.

#### **4.1.2 Mechanism of Olefin Polymerization**

Of the different mechanisms that have been proposed for the catalytic olefin polymerization, the one proposed by Cossée and Arlmann is now widely accepted<sup>[30]</sup>. This mechanism was originally proposed for the olefin insertion into a metal-alkyl group bond in the heterogeneous

polymerization of olefins, but it can also be used to describe the basic steps in olefin polymerization with metallocene/MAO catalysts. The reaction can proceed via two different paths, the first step of both paths being the double methylation of the metallocene-dichloride by the MAO and the abstraction of the chloro-ligands, followed by elimination of one of the methyl groups. This process yields a cationic species that is active in propylene (olefin) polymerization with MAO as non-coordinating counter-ion. The proposed mechanism for the olefin insertion is shown in Fig. 2.

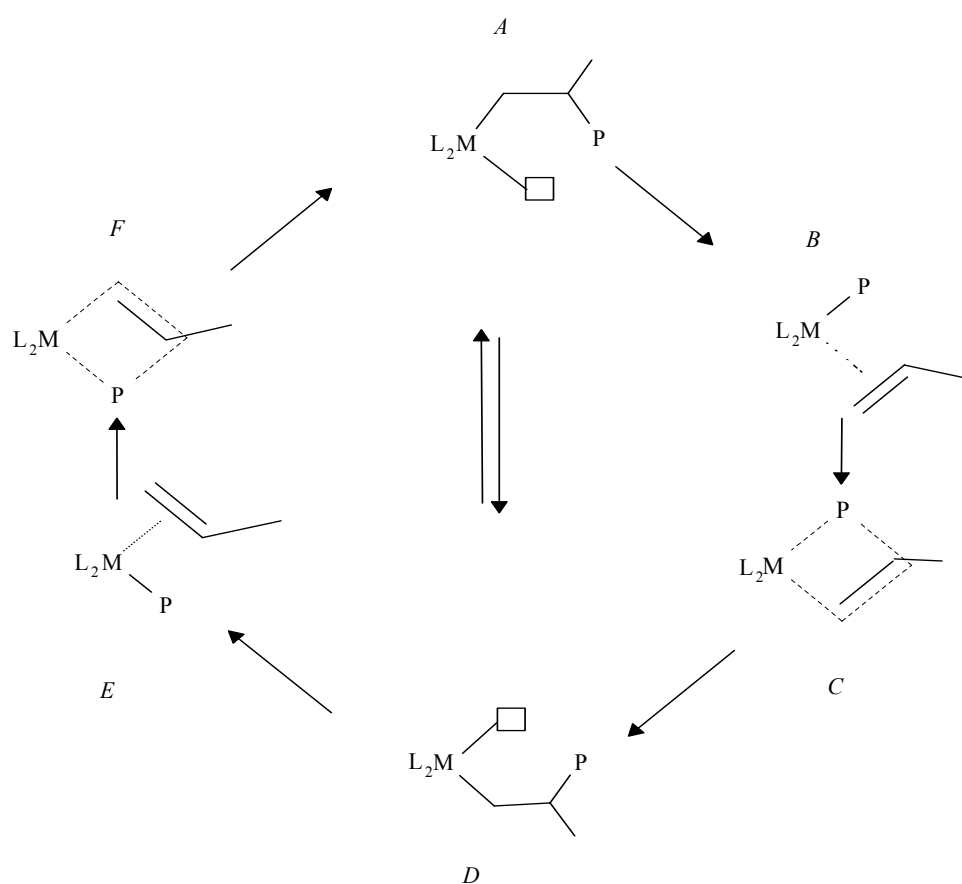


**Fig. 2: Possible paths for the insertion of olefins into the metal-polymer-bond.**

The olefin approaches the free coordination-site of the metallocene (A) to subsequently form a  $\pi$ -complex (B). Via a four-membered transition-state (C), the olefin-unit is inserted into the growing chain (D). The next insertion can either follow immediately by coordination and insertion of the next olefin molecule (E and F). This is called an alternating mechanism. For the retention mechanism (back skip), an inversion of the configuration at the stereocenter (D to A) is followed by coordination and insertion of the next olefin molecule (A to D).

Different mechanisms can lead to the termination of the growing chain. These are shown in Fig. 3 to Fig. 5<sup>[31]</sup>.



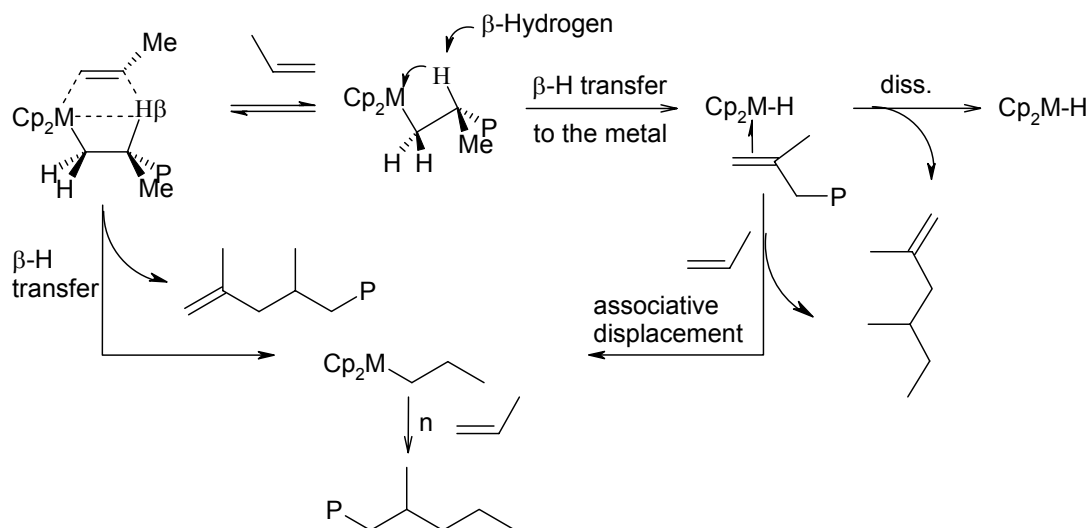


Fig. 3: Chain-termination by  $\beta$ -hydride transfer to the metal or to the monomer.

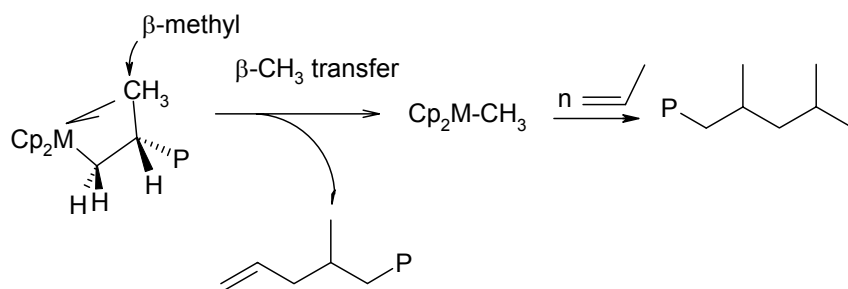


Fig. 4: Chain-termination by  $\beta$ -methyl transfer to the metal.

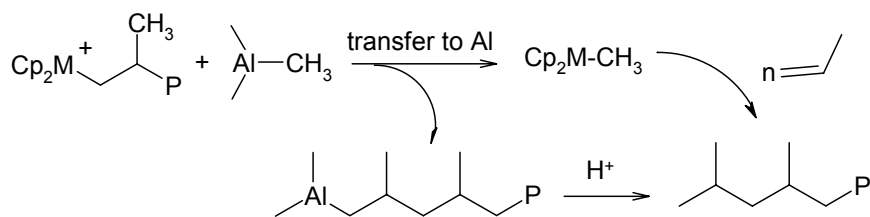


Fig. 5: Chain-termination by chain-transfer to aluminum.

### 4.1.3 Stereochemistry of the Propylene Insertion

Propylene can be polymerized in different ways by metallocene/MAO catalysts because it is a prochiral monomer. The last inserted monomer unit (chain-end control) or the stereochemistry of the metallocene (enantiomeric site control) determine the microstructure of the resulting polypropylene. If the metal center can distinguish between the prochiral sides of the propylene, the stereochemistry of the resulting polypropylene is determined by the structure of the metallocene. To provide for a stereoregular chain, the metallocene geometry has to stay

the same for thousands of insertions. This can be accomplished by a bridge between the upper and lower ring systems<sup>[32]</sup>.

Generally, the formation of two diastereomeric complexes is possible, the one with the growing polymer chain pointing into the sterically less crowded quadrant being energetically more favorable. In case of the  $C_s$ -symmetric metallocene shown in Fig. 6, the two lower quadrants are more crowded because of the fluorenyl ring, forcing the polymer chain to point into the upper quadrant. In the transition state forming upon approach of a propylene molecule, the monomer adopts a conformation with the methyl group pointing in the opposite direction of the polymer chain, which is energetically more favorable<sup>[33,34]</sup>. For steric reasons, the methyl group also points away from the metal center which causes a 1,2-insertion of the monomer.

Upon insertion, the polymer chain migrates to the other side of the metal center, thus liberating a coordination site for the next incoming monomer. The growing chain again moves to the quadrant with the lower steric crowding, pointing upward in the case of a  $C_s$ -symmetric metallocene. By numerous repetitions of these processes, a syndiotactic (see Fig. 7) polymer chain is formed.

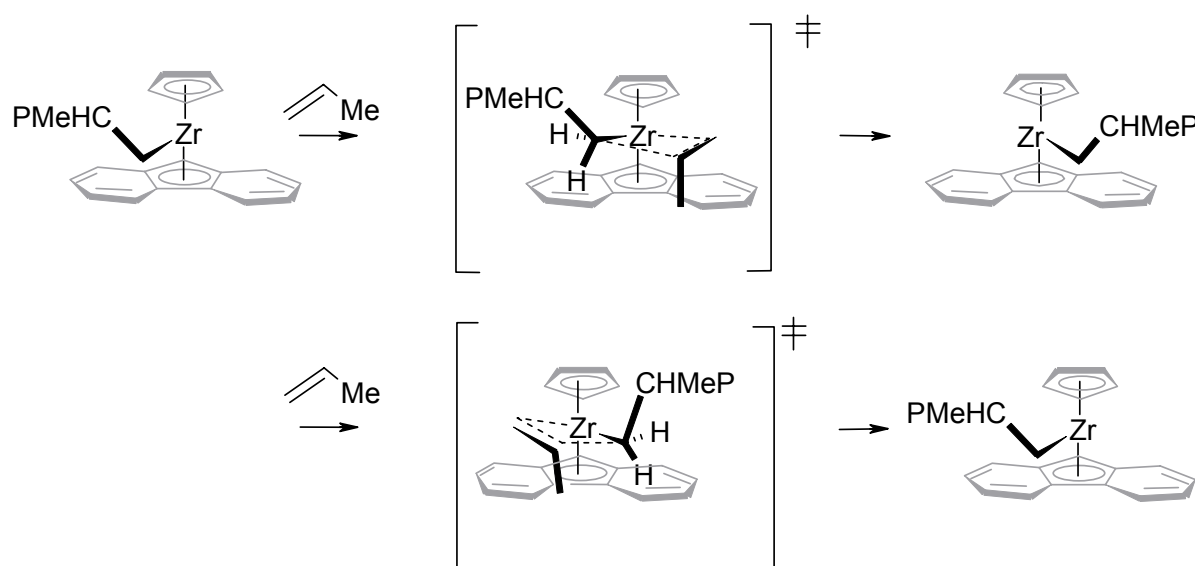


**Fig. 6:** Stereoselective insertion of propylene into the metal polymer bond of a  $C_s$ -symmetric metallocene (for simplification, the bridge between the upper and lower ring systems is not shown, nor are any additional ligands)<sup>[35]</sup>.

Different metallocene structures produce different microstructures which are shown in Fig. 7. They can be atactic, e. g. with  $Cp_2ZrCl_2$ , isotactic with  $C_2$ -symmetric metallocenes like *rac*-[Et-(IndH<sub>4</sub>)<sub>2</sub>]ZrCl<sub>2</sub> or syndiotactic with  $C_s$ -symmetric systems like [(p-MePh)<sub>2</sub>C(Cp)](2,7-bis-

<sup>t</sup>BuFlu)]ZrCl<sub>2</sub>. Apart from that, hemi-isotactic microstructures can, for example, be accomplished with the C<sub>1</sub>-symmetric system [Me<sub>2</sub>C(3-MeCp)(Flu)]ZrCl<sub>2</sub>. An example for a metallocene producing stereoblock PP is [(2-phenylindenyl)<sub>2</sub>]ZrCl<sub>2</sub> which can change between chiral and non-chiral conformations by rotation of the aromatic rings.

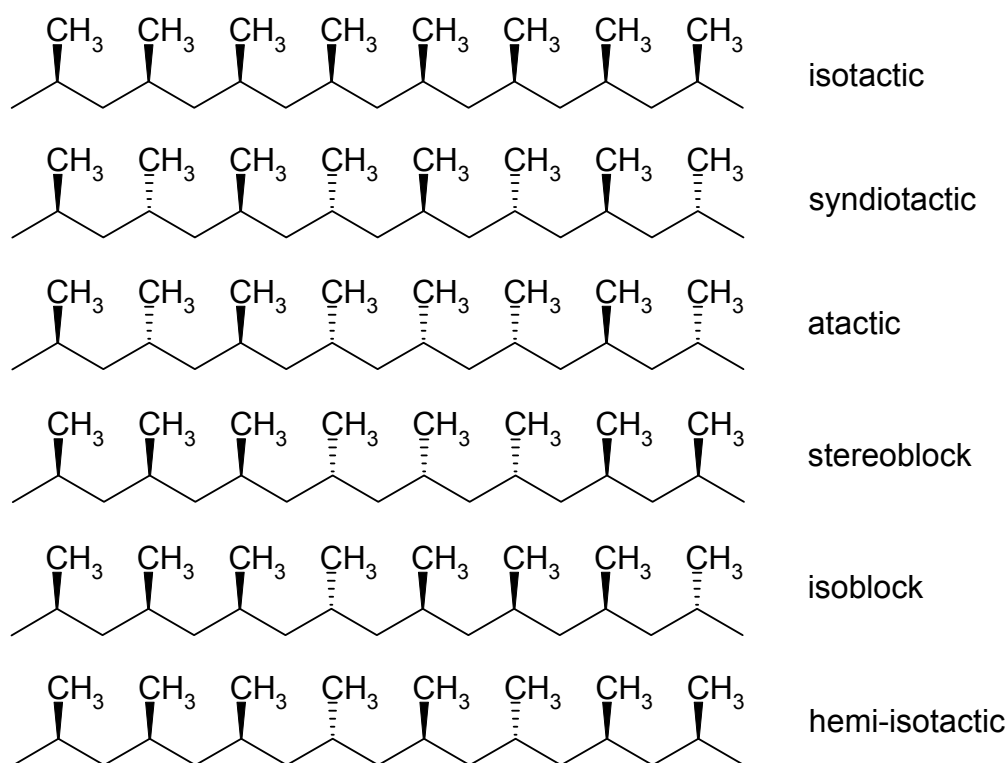


**Fig. 7: Possible PP-microstructures**

The fraction of isotactic or syndiotactic pentads can be determined by nmr-analysis, which also provides information regarding the regio-errors. The dependence of the polymer microstructure on the metallocene structure has been extensively investigated and reviewed<sup>[27,28,31,36-38]</sup> and will not be discussed further in this work.

## 4.2 Nanocomposites

Research in the area of nanocomposites is inspired by nature, which has created materials with exceptional properties by combination of a hard, skeleton-like structure combined with a continuous flexible phase<sup>[39]</sup>. Analogously, the addition of fillers to a polymer matrix opens up the route to materials with completely new properties.

Fillers can serve as weight- and cost-reducing agent, which often was the primary purpose in the past. Typically, the fillers employed were micron-sized. Polypropylene has, for example, been filled with inorganic materials such as talcum or calcium carbonate <sup>[40,41]</sup> to reduce the

cost and/or the weight. Examples of use are domestic appliances and automotive applications<sup>[7]</sup>. Apart from that, the thermal conductivity could be markedly improved by the incorporation of aluminum powder or aluminum platelets into a polypropylene matrix<sup>[42],[43]</sup>. Another interesting class of fillers for PP are natural products, such as starch <sup>[44]</sup>, rice husk ash <sup>[45,46]</sup>, and cellulose<sup>[47]</sup> because they can easily be grown again. On the other hand, the mechanical properties can be ruined in wet surroundings, because of water uptake.

Recently, a new interest in filled polymers has awakened, when it became apparent, that fillers with a size on the nano-scale in at least one dimension could equip the matrix polymer with intriguing new properties. One of the main reasons for the different behavior of these nano-fillers as compared to their micron-sized counterparts is the conversion of the bulk-polymer to an interface-polymer<sup>[39]</sup> (Fig. 8). The volume fraction of composite occupied by a filler with an average particle diameter of 1mm is shown in the left part of the graphic representation. The right part shows the same volume filled with the same weight percentage of a filler with an average particle diameter of 1nm. It is obvious that the volume fraction occupied by the filler particles is much larger in this case.

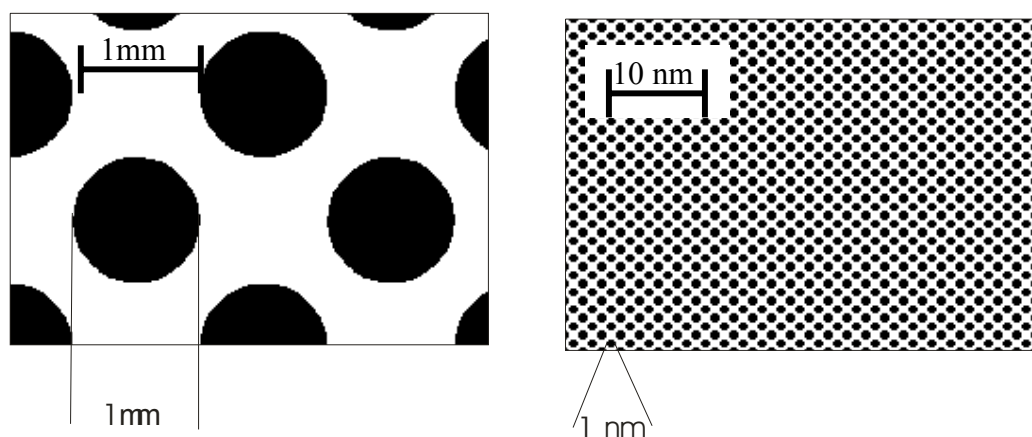


**Fig. 8: Conversion of bulk-polymer to interface-polymer upon change from micron- to nano-sized fillers (The total volume is the same in both cases and so is the weight percentage of the filler).**

Already at low filler contents, a major part of the polymer is located close to the surface of the nano-fillers. The properties are consequently largely influenced by the interface between the polymer and the filler.

When discussing the benefits of nanocomposites, it should be considered, that, so far, little is known about the health risks posed by nanoparticles. They could possibly cause problems in the respiratory tract or irritate the skin. Currently, studies are in progress concerning the

health hazards of particles that could potentially serve as reinforcing agents in nanocomposites<sup>[48]</sup>.

As the field of nanocomposites is developing rapidly, there will be more new materials with exciting properties in the future. Apart from improvements of the mechanical properties of the polymer matrix by addition of nanofillers, the intrinsic properties of the nanoparticles, like electrical conductivity, can also be of use. Some theoretical calculations regarding the potential of polymers filled with nanoparticles are already available<sup>[49,50]</sup>.

#### **4.2.1 Synthesis of Nanocomposites**

To prepare a good nanocomposite that exploits the full potential of the individual constituents, it is necessary to ensure a uniform distribution of the nanofillers in the polymer matrix. Especially for fillers with very small dimensions, this can be a major problem. The separation of agglomerates and bundles into individual particles or fibers is often not possible without the application of great forces. These can be shear forces during melt-compounding or forces exerted by ultrasound during solution blending or before *in situ* polymerization, which can damage not only the involved polymer matrix, but also the filler itself. It has been reported, that prolonged ultrasonic treatment leads to a damage and shortening of carbon nanotubes, for example<sup>[51]</sup>. This impedes profit of the full range of properties of these nanofillers. On the other hand, mechanical mixing often does not suffice to separate the individual particles from each other. Hence, it is necessary to find a suitable method that ensures a homogeneous dispersion without doing much damage to the filler or the polymer.

Another important factor for the quality of a nanocomposite is an excellent adhesion of the matrix polymer to the filler surface. That is important for the load transfer during mechanical stress. In practice, the interfacial adhesion is often poor. Especially if polar fillers like silicates are to be incorporated into an unpolar polymer, such as polypropylene, it can be a problem. This can be overcome by modification of the filler surface or the polymer. By chemically linking the matrix to the filler, the interfacial properties can be notably improved.

There are four principal routes to produce filled polymers<sup>[52-54]</sup> each of them exhibiting advantages and disadvantages with regard to the aforementioned difficulties. Their effectiveness depends strongly on the individual constituents of the system which should be considered before choosing a method.

#### 4.2.1.1 Solution Blending

If a nanocomposite is prepared via solution blending, the filler is mixed with a polymer in solution. In addition to mechanical mixing, ultrasound can be used to separate the filler particles. When the dispersion is satisfactory, the solvent is evaporated to yield the filled polymer. This method is suitable for systems that consist of a polymer which is soluble in a common solvent<sup>[55]</sup>, in which also the nanofiller can be dispersed well. Highly tactic polypropylene is poorly soluble in most organic solvents, which makes this method problematic for the preparation of polypropylene nanocomposites.

#### 4.2.1.2 Synthesis of the Nanofillers in the Presence of the Polymer

Silica nanocomposites are an example of composites that can be prepared by the synthesis of nanofillers in the presence of the matrix polymer. The silica nanoparticles are formed in situ from tetraethoxysilane (TEOS) or tetramethoxysilane in the polymer solution. It is important, that the synthesis of the desired nanofillers does not promote the degradation of the polymer and that the polymer does not inhibit the formation of the nanoparticles<sup>[54]</sup>. Like in solution blending, the polymer has to be well soluble.

#### 4.2.1.3 Melt-Compounding

Nanocomposites can also be prepared by a melt mixing process (melt intercalation). Molten polymer and the nanofiller are mixed intensively under the influence of shear forces. Different kinds of mixing devices, such as a twin-screw extruder, are available for this task. It is important, that the shear forces exerted by the mixer are sufficient to tear the individual particles apart. Especially in the case of carbon nanotubes (CNTs), this can be a serious problem because they have a high tendency to agglomerate due to a very high surface energy. Highly viscous melts of polymers are also inadequate for this method, because the mixing is hindered, and the high shear forces can lead to a partial degradation of the polymer. Not only the polymer, but also the nanotubes can be damaged during this process. The mean tube length was found to decrease with increasing energy input during melt-compounding<sup>[55]</sup>. A good dispersion of particles in polyolefin matrices is often hard to achieve by simple melt-compounding, especially at a high filler content<sup>[56]</sup>. That is why, in the case of polypropylene, surfactants and modifiers are frequently used to improve the dispersion and the interfacial adhesion, especially if the fillers are polar<sup>[57-59]</sup>.

Nevertheless, melt-compounding is a widely used method for the preparation of PP/clay nanocomposites. As pointed out above, a coupling agent is often necessary. This can, for example, be constituted of maleic anhydride modified polypropylene oligomers<sup>[57]</sup> or other compounds. The influence of the compatibilizer functionality has been investigated by Reichert et al.<sup>[60]</sup>. A different approach is the functionalization of the PP-matrix<sup>[61]</sup>.

#### 4.2.1.4 *In situ* Polymerization

Analogously to the synthesis of the nanoparticles in the presence of the polymer, it is possible to synthesize the polymer in the presence of the filler by *in situ* polymerization. A good adhesion of the matrix can be achieved by directly connecting the catalyst or cocatalyst and the filler, which also promotes the separation of the individual particles during the polymerization process.

If the *in situ* polymerization approach is to be used for the preparation of nanocomposites, it is indispensable that the filler can be pre-treated in a way to prevent it from deactivating the catalysts. It is also essential that the nanofiller bears chemical groups on its surface with which the catalyst or cocatalyst can react. In the case of olefin polymerization, the heterogenization of the cocatalyst (MAO) on the surface of the nanofiller (see section 6.1.2) is a convenient procedure for anchoring of the catalyst. The presence of the active species on the surface of the nanofiller after the addition of the metallocene and during the polymerization should facilitate a homogeneous dispersion of the filler. *In situ* polymerization of polyolefins is a versatile method for the production of nanocomposites, which has already been used for the generation of nanocomposites of PE (or a copolymer with an  $\alpha$ -olefin) and layered silicates, glass beads, nickel powder, graphite and others<sup>[62,63]</sup>. Moreover, it has been employed for the preparation of PP/clay nanocomposites<sup>[64]</sup> and for the preparation of syndiotactic PP/M250 (silica beads) nanocomposites<sup>[65,66]</sup>.

It could be shown for PE/graphite composites, that the dispersion of the particles within the polymeric matrix is more homogeneous, when the composites are prepared by *in situ* polymerization than by melt-mixing. The best results were obtained when the catalyst was anchored on the filler surface. Simple melt-compounding was insufficient to homogeneously disperse the carbon black as was proven by measurements of the electrical conductivity<sup>[67]</sup>. Similar results were obtained for silica nanospheres (Monospher, M250) that have been dispersed in PP by melt compounding. The highest filler amount that was reached by this

method was 5 %, above which aggregation of the particles became too strong to separate them<sup>[41]</sup>. The dispersion of the silica nanospheres could be considerably improved when the nanocomposites were prepared by *in situ* polymerization of propylene with metallocenes<sup>[65]</sup>. They have also served as fragmentable cocatalyst-carrier for ethylene polymerizations<sup>[68]</sup>.

Different methods for the preparation of polyolefin/layered silicate nanocomposites by *in situ* polymerization with metallocenes have been patented in 1999 by the Dow chemical company<sup>[69]</sup>, in 2000 by BASF AG<sup>[70]</sup> and by Tang, Wei and Huang<sup>[71]</sup> in 2003. Several more publications deal with the formation of PP/clay nanocomposites via *in situ* polymerization with metallocene catalysts in the presence of layered silicates<sup>[63,71,72]</sup>. In addition to that, Brookhart-type catalysts anchored to the surface of the silicate have been successfully employed to prepare PE/layered silicate nanocomposites via *in situ* polymerization<sup>[52]</sup>.

Some other silica fillers have been incorporated into a polyolefin matrix by this method as well. For instance, a PE/polyargoskite (silica nanowhiskers) nanocomposite has been prepared by *in situ* polymerization with a Ziegler-Natta catalyst<sup>[73,74]</sup>. PP/SiO<sub>2</sub> nanocomposites were also prepared by the *in situ* polymerization of propylene with a fourth generation Ziegler-Natta catalyst in the presence of silica nanoparticles that had been modified with octadecyltrimethoxysilane as coupling agent<sup>[75]</sup>.

Not only silica fillers but also carbon nanotubes have served as fillers in the *in situ* polymerization of all kinds of monomers. Nanocomposites from different types of carbon nanotubes with acrylic monomers have, for example, been synthesized by this method. In some cases, the nanotubes were pretreated, like in the *in situ* emulsion polymerization of acrylic monomer in the presence of oxidized nanotubes<sup>[76]</sup>. The same was true in the polymerization of MMA- and tert-butyl acrylate by ATRP with initiators anchored on the surface of the SWNTs. Especially the resulting poly(tert-butyl acrylate)/SWNT nanocomposites had an improved solubility in organic solvents compared to the raw SWNTs<sup>[77]</sup>. The initiator was also hooked to the surface of the nanotubes for the preparation of PMMA/MWNT or PS nanocomposites by *in situ* polymerization. This method provides for an anchoring of the polymer chains on the filler<sup>[78]</sup>. In a different approach, the initiation of the polymerization was accomplished by ultrasound during the preparation of poly(n-butyl acrylate)/MWNT and PMMA/MWNT nanocomposites<sup>[79]</sup>.



Polyaniline/MWNT composites<sup>[80]</sup> and electrically conductive polyimide/SWNT nanocomposites have been prepared by *in situ* polymerization. The conductivity, as well as mechanical properties and thermal stability were improved<sup>[81]</sup>.

The *in situ* polymerization approach has also been used in the synthesis of polyolefin/CNT composites. PE/SWNT nanocomposites have, for example, been prepared by *in situ* polymerization with Ziegler-Natta catalysts. These were then compounded with PE, which improved the interfacial properties of the resulting PE/SWNT nanocomposites<sup>[82]</sup>. *In situ* polymerization has so far not been used for the synthesis of PP/CNT nanocomposites.

PP/glass fiber (GF) composites have been prepared by *in situ* polymerization of propylene in the presence of pre-treated glass fibers. The PP close to the GF could not be extracted with hot heptane, indicating a good interfacial adhesion<sup>[83]</sup>.

## **4.2.2 Fillers**

### **4.2.2.1 Clays and Other Silica Fillers**

Layered silicates like montmorillonite consist of platelets usually arranged in stacks that form micron-sized particles, which can be handled with ease<sup>[39]</sup>. On the other hand, it is not so easy to homogeneously disperse them in unpolar polymer matrices. Polar silica fillers often have to be modified to achieve a homogeneous distribution and a good adhesion in unpolar polymers. Other silicas that have been used as fillers for polymers are polyargoskite (silica nanowhiskers) and spherical silica particles of different diameters.

### **4.2.2.2 Carbon Nanofibers (CNFs)**

Carbon nanofibers are interesting as fillers for polymers, because they represent an intermediate between traditional carbon fibers of a large diameter and carbon nanotubes with a diameter in the range of nanometers. They are available in large quantities at low costs<sup>[84-86]</sup>, which makes them even more attractive. Carbon Nanofibers can be synthesized catalytically. Gaseous hydrocarbons are decomposed in the gas phase in the presence of a transition metal catalyst to form the CNFs<sup>[87]</sup>.

### 4.2.2.3 Carbon Nanotubes (CNTs)

Carbon nanotubes are an especially attractive class of fillers for polymers because of their intriguing mechanical and thermal properties. They can consist of only one graphitic sheet rolled up to form a single-walled carbon nanotube (SWNT, Fig. 9) or concentric tubes forming multi-walled carbon nanotubes (MWNTs). Currently, the costs of carbon nanotubes are still extremely high, and the quantities that can be produced are relatively small, which hinders their commercial application<sup>[88]</sup>. This will probably change in the near future, as a lot of research focuses on finding cheaper production processes for nanotubes<sup>[89,90]</sup>. In the future, large quantities of pure, low-cost multi-walled carbon nanotubes produced by chemical vapor deposition (CVD) are expected to be available<sup>[55]</sup>.

Different methods are employed for the manufacturing of carbon nanotubes. Arc-discharge furnishes stiff, near-perfect, whisker-like MWNT, but the amount that can be produced is limited. In chemical vapor deposition (CVD), catalytic metal particles are exposed to a medium containing hydrocarbon gaseous species, and nanofibrils are formed catalytically in that atmosphere<sup>[90]</sup>. Besides that, laser ablation and gas-phase catalytic growth from carbon monoxide can be used to prepare carbon nanotubes<sup>[88]</sup>.

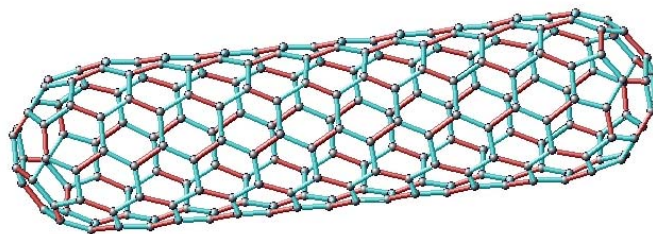


**Fig. 9: Schematic representation of a single-walled carbon nanotube (by courtesy of F. Gojny, TU Harburg).**

Carbon nanotubes represent one of the strongest and toughest materials known. The elastic modulus in the direction of the tube length is estimated to be at least 1 TPa and the strength 30 GPa<sup>[88,90]</sup>. Furthermore, they are highly flexible, which gives them an advantage over CNFs. This is important during processing, because they are less likely to break under the applied forces. Although the mechanical properties of carbon nanotubes are exceptional, their influence on the macroscopic mechanical properties is still controversial<sup>[91]</sup>.

Because of their good electrical conductivity, carbon nanotubes can also serve for antistatic applications<sup>[92]</sup>. Many polymers are used in packaging applications for electronic devices. For this purpose, their insulating properties can be overcome by the addition of conductive fillers, such as carbon black, carbon fibers, and others. To achieve the desired modification, it is often necessary to add large amounts of these fillers, thereby deteriorating their mechanical properties. This can be avoided by the use of CNTs, which only have to be added in small quantities<sup>[87,93]</sup>. Conventional conductive fillers could, therefore, be replaced by CNT in some applications<sup>[55]</sup>.

Some other interesting properties of CNTs are their inertness, their low density, and their large surface area<sup>[90]</sup> along with their high aspect ratio. Carbon nanotubes should be well suited for preparing composites that have a smooth surface and are also easy to process and recycle<sup>[86]</sup>.

Unfortunately, CNTs exhibit some less favorable properties as well. They are, for example, insoluble in organic solvents<sup>[90]</sup>, which makes their application tricky and obstructs the preparation of CNT nanocomposites. This difficulty can be overcome by functionalization of the nanotubes, which facilitates their dispersion in solvents<sup>[78]</sup>. Apart from a difficult handling with regard to the chemical properties of the nanotubes, a lot of research is still necessary to estimate the health risk of CNT, which is still largely unknown. In TEM investigations, a striking similarity of MWNTs originating from fuel gas combustion and asbestos fibers has been observed. Nevertheless, not only the morphology of the tubes, but also their mechanical properties have to be taken into account when evaluating their toxicity. In contrast to asbestos, carbon nanotubes are flexible, which means that the cell response to both materials could differ significantly<sup>[48]</sup>. Nevertheless, these risks should be taken into account when discussing carbon nanotube composites.

### **4.2.3 Properties of Nanocomposites**

Many interesting properties of nanocomposites have been observed but some of the results are controversial. In the following section, some areas in which an enhancement of the properties could be accomplished, are presented.

#### 4.2.3.1 Barrier Properties

The barrier properties could especially be improved by the addition of platelet fillers like clays. Dispersed into individual platelets, they enhance the gas-barrier properties and act as flame-retardants<sup>[94-97]</sup> for the matrix polymer. The former could, for example, be increased dramatically by the addition of a very small amount of clay platelets to a polyamide<sup>[92]</sup>, even more in combination with an oxygen scavenger. These compounds could be used in combination with PET for the production of bottles<sup>[98]</sup>.

#### 4.2.3.2 Mechanical Properties

The macroscopic properties of a polymer can be influenced by a wall (e. g. a filler surface) even at a distance of up to several 100nm<sup>[98]</sup>. This can lead to an extraordinary improvement of the mechanical properties. In comparison to traditional fillers, like glass fibers, the amount of nanofiller that is necessary for the same mechanical improvement is considerably reduced<sup>[92]</sup>.

Although the mechanism of polymer reinforcement still largely remains in the dark<sup>[98]</sup>, it is known that nano-fillers with a high aspect ratio are especially favorable for the mechanical properties of the nanocomposite. Their size is on the nano-scale in one or two dimension(s), whereas the other dimension(s) is (are) in the micron-range. Layered silicates like montmorillonite, which have a platelet structure are exemplary of this type of filler<sup>[39]</sup>. Fibrous materials, especially nanofibers and nanotubes, also belong to this group of fillers. To be able to profit from the excellent properties of the CNTs, a strong interface between the nanotubes and the polymeric matrix and a homogeneous distribution of the individual tubes are necessary<sup>[90,99]</sup>. The improvement in mechanical properties upon addition of carbon nanotubes is often not as high as expected, which is probably due to an insufficient load transfer from the matrix polymer to the filler<sup>[100]</sup> or a poor dispersion.

There has been extensive research concerning layered silicate nanocomposites since the discovery of Toyota researchers that the properties of nylon could be enhanced by the addition of these clays<sup>[101-103]</sup>. Clay nanocomposites have also been prepared with polyolefins as matrix polymers. Efforts are underway to improve polypropylene mechanical properties by incorporation of natural<sup>[104]</sup> or modified clays such as montmorillonite or bentonite<sup>[52,70,97,105-107]</sup>. As the polar clay and the unpolar PP are incompatible, a coupling

agent is usually necessary for the effective dispersion of the silicate layers in the polyolefin matrix. The silicates used as fillers were typically modified by alkyl-ammonium cations to improve the interfacial properties of the composite. A coupling agent was also necessary to separate the layers from each other in sPP/organophilic layered silicate nanocomposites prepared by melt-compounding. The improvement in mechanical properties and the increase in crystallization temperature was strongly dependant on the modifier amount<sup>[105]</sup>.

Moreover, spherical silica particles have been used as fillers to improve the mechanical properties of polyolefins. It is especially favorable to use silica modified by grafting with other polymers such as poly(ethylacrylate) if melt-compounding is the preparation technique used. Otherwise a poor interfacial adhesion can lead to a strength inferior to that of the unfilled polymer. A polypropylene/silica nanocomposite with improved Young's modulus and improved elongation to break could be obtained after modification of the silica particles<sup>[108]</sup>. By modification of the filler surface with a poly(butylacrylate), the interfacial adhesion between isotactic PP and silica nanoparticles (diameter: 10 nm) was improved and thus nanocomposites with superior properties to the unfilled system and that using unmodified silica were produced<sup>[109]</sup>. A good dispersion and interfacial adhesion are important because agglomerates of silica can act as stress concentrators that lead to failure of the nanocomposite under mechanical stress<sup>[109]</sup>.

PP has also served as matrix polymer for calcium carbonate nanocomposites. The modulus and impact strength could be significantly improved by the addition of calcium carbonate (diameter: 44 nm) to the polymer via melt-compounding<sup>[110]</sup>. Toughening of PP was achieved by the addition of calcium carbonate of different sizes to the neat polymer<sup>[111]</sup>.

The addition of CNFs has also been shown to improve the mechanical properties of polymers<sup>[86]</sup>. The modulus of PP fibers could, for example, be enhanced by the incorporation of CNFs, which was accomplished by melt spinning of the two components<sup>[112]</sup>. In another experiment, the yield strength of PP could be considerably improved by the addition of CNFs. The tensile properties were dependant on the surface properties of the nanofibers that had been subjected to different pretreatments. The best results were obtained for slightly etched fibers<sup>[113]</sup>. The interfacial adhesion could be improved by radically polymerizing isoprene on the surface of the nanofibers. The resulting nanocomposite fibers showed improved mechanical properties over the neat PP fibers, in addition to a slightly higher crystallinity<sup>[84]</sup>.

Especially since 2002, many publications have appeared describing the effect of carbon nanotubes on different polymeric matrices. These nanocomposites have been prepared by melt-compounding, solution blending, or *in situ* polymerization. Depending on the polymer matrix, the incorporation of multi-walled carbon nanotubes (MWNTs) has been quite successful. MWNT/Nylon-6 nanocomposites prepared by melt-compounding exhibit improved mechanical properties as compared to neat nylon-6<sup>[99]</sup>. When PS was used as matrix, the MWNTs were functionalized with a polystyrene copolymer by esterification with carboxyl groups on their surface to facilitate the distribution in the matrix<sup>[114]</sup>. PS/MWNT nanocomposites have also been prepared by solution blending, resulting in a material with superior tensile properties exhibited than those of the pristine polymer<sup>[115]</sup>.

When polyolefin/CNT nanocomposites were prepared, controversial effects of the filler on the mechanical properties were found. The mechanical properties remained largely unchanged in PP/SWNT nanocomposites prepared via melt-compounding. The authors attributed this fact to a poor dispersion of the SWNTs<sup>[116]</sup>. In contrast to this, films of UHMWPE/CNT composites showed better yield strength than the neat PE films<sup>[117]</sup>. An enhancement was also found, when CNTs were pan-milled before the melt-compounding with PP. The Young's modulus and the yield strength of polypropylene could be increased via this method<sup>[118]</sup>.

To improve the interfacial adhesion of PP to MWNTs, the later have been functionalized with n-butyl-lithium and then reacted with chlorinated PP. These composites have afterwards been solution blended with chlorinated PP to give nanocomposites with superior mechanical properties, such as an enhanced Young's Modulus<sup>[119]</sup>. The tensile properties of PP/SWNT nanocomposites prepared by solution blending and subsequent melt-spinning into fibers could also be significantly improved<sup>[120]</sup>. The same was found for films of melt-mixed PP/CNT nanocomposites that were post-drawn after the production<sup>[121]</sup>.

Theoretical quantum mechanical calculations predict that a high stress-transfer from PE to carbon nanotubes in the presence of radical generators should be possible by the formation of covalent bonds<sup>[122]</sup>. Also other properties of polyolefin/CNT nanocomposites have been explored by theoretical calculations. Accordingly, it could be shown, that it is necessary to take the differences of the tube diameters into account when modeling the composite's properties, because the distribution of the diameter has an impact on the overall properties of

the composite<sup>[100]</sup>. The temperature dependant structural behavior of PE/CNT nanocomposites has been investigated by quantum mechanical calculations<sup>[123]</sup>.

The flow-induced properties of polypropylene are influenced by the addition of MWNT. Upon extrusion, the strand of nanocomposite was found to contract, whereas the pure PP strand expands when it is extruded. This behavior is significant for the processing of these nanocomposites<sup>[124]</sup>.

#### 4.2.3.3 Electrical Conductivity

In addition to the mechanical properties, the electrical conductivity is influenced by the presence of CNFs or carbon nanotubes in the polymer matrix. A percolation threshold for electrical conductivity of 9-18 weight-% was found for carbon nanofibers dispersed in PP<sup>[85]</sup>.

Ultrahigh molecular weight polyethylene UHMWPE/MWNT nanocomposites have been successfully prepared by solution blending which exhibited a much lower percolation threshold than carbon black/PE composites<sup>[125]</sup>. Moreover, the electrical conductivity of PP could be increased significantly by the addition of MWNT<sup>[124]</sup>. This effect was especially pronounced for PP/MWNT films compared to films of neat PP and also compared to PP/CNF composites<sup>[55]</sup>.

Polymer masterbatches containing multi-walled carbon nanotubes and a polymer like PP or nylon are presently available from Hyperion Catalysis for automotive and electronic applications<sup>[93]</sup>. Nylon composites containing 1-5 % of nanotubes are, for example, used for fuel lines and electrostatically painted exterior body parts of cars<sup>[92]</sup>. The electrostatic painting of car parts is possible by using thermoplastic/nanotube composites because they are conductive but not brittle<sup>[126]</sup>.

#### 4.2.3.4 Crystallization Behavior

The crystallization behavior of polymers is an important factor during processing of these materials because cycle times also depend on the time needed for solidification of the manufactured parts. By addition of particulate fillers, the crystallization rate is often increased. The crystallization of PE was, for instance, accelerated by melt-copounding of nano silica particles covered with a silane coupling agent and PE<sup>[127]</sup>. Similarly, Calcium carbonate nanoparticles acted as nucleating agents for PP<sup>[110]</sup>.

The crystallization temperature and the rate of crystallization of PP could be enhanced by the addition of CNFs to the polymer matrix<sup>[128]</sup>. Moreover, carbon nanotubes have been shown to act as nucleating agents for some polymers. The crystallization temperature of UHMWPE could be raised when a coupling agent was used during the solution blending of the UHMWPE with CNTs<sup>[129]</sup>. A similar effect on PP has also been detected. In blends of PP and ethylene-propylene-diene rubber (EPDM), the addition of SWNTs has led to an increase in the crystallization rate of PP, which means, that the nanotubes acted as nucleating agents<sup>[130]</sup>. It was observed that the nanotubes also nucleated crystallization in PP/SWNT nanocomposites prepared via solution blending. The crystallization half-time was reduced, and the percent crystallinity was increased upon the addition of SWNTs<sup>[131]</sup>. Similar results were obtained when the PP/SWNT nanocomposites were prepared via melt-compounding. The crystallization rate and the crystallization temperature were increased by the addition of SWNTs to PP, and the spherulitic size was reduced<sup>[116]</sup>. When CNTs were pan-milled before the melt-compounding with PP, the crystallization temperature and crystallization rate could also be increased<sup>[118]</sup>.

#### 4.2.3.5 Thermal Stability

The thermal stability of the polymer matrix can be enhanced by the addition of carbon nanofibers or carbon nanotubes. The degradation properties of PP, for example, were improved by the presence of CNFs which could be shown for PP/CNF nanocomposites prepared by melt-compounding<sup>[128]</sup>.

Studies regarding the effect of MWNT on the thermal degradation of PP have also been conducted. They showed that the nanotubes raised the degradation temperature with respect to the pure polypropylene<sup>[132]</sup>. The incorporated CNTs were found to act as antioxidants<sup>[133]</sup>. In another study, the thermal conductance was enhanced as well, and the nanotubes behaved as flame retardants<sup>[134,135]</sup>.



## 5 AIM OF THIS WORK

Nature has created great materials of exceptional strength by combination of a soft matrix with a solid filler. Based on similar considerations, nanocomposites can be synthesized by combination of the ductile polymer matrix with nanofillers exhibiting good mechanical properties, and materials with new properties can be created.

The aim of this work was to synthesize new polypropylene nanocomposites by *in situ* polymerization of propylene with metallocene/MAO catalysts in the presence of different (nano-) fillers and explore the influence of the different fillers on the polymer properties. Syndiotactic polypropylene is an attractive matrix polymer due to its elastic properties. Special emphasis was to be laid on the achievement of a homogeneous distribution and a good interfacial adhesion with the help of this new preparation method. These two factors are especially important for an efficient load transfer from the matrix to the filler upon mechanical stress. The *in situ* polymerization should facilitate an intimate mixing of polymer and filler by formation of the polymer directly in the presence of the filler. The so prepared nanocomposites should be investigated with regard to the fillers' influence on the polymer properties.

High loads of hard, spherical silica particles (M250) should be homogeneously dispersed in the polymer matrix. Carbon nanofibers were chosen as fillers because of their similarity to carbon nanotubes. Their great advantage over carbon nanotubes is the low cost making them an ideal model system. An improvement of the mechanical properties of polymers upon addition of CNFs has been accomplished. Moreover, they were shown to act as nucleating agents and enhanced the thermal stability of polymer matrices. The CNFs were to be dispersed as homogeneously as possible in the polymer matrix while ensuring a good adhesion of the PP to the filler. The influence of the incorporated carbon nanotubes and their percentage on the mechanical and other polymer properties should be investigated.

Carbon nanotubes are expected to have a promising potential as fillers for polymers because of their unique property profile. In addition to extraordinary strength, they are highly flexible, conductive, inert, of low density and have a very high aspect ratio. Unfortunately, their cost is still very high but cheaper production of large quantities is forecasted for the future. In spite of their exceptional mechanical properties their full potential is still far from being explored,

and the effect of carbon nanotubes on the macroscopic polymer properties is still controversial. In this work, a distribution as homogeneous as possible and a good adhesion of the polypropylene matrix should be achieved. The influence of the filler and its percentage on the mechanical and other polymer properties was to be examined.

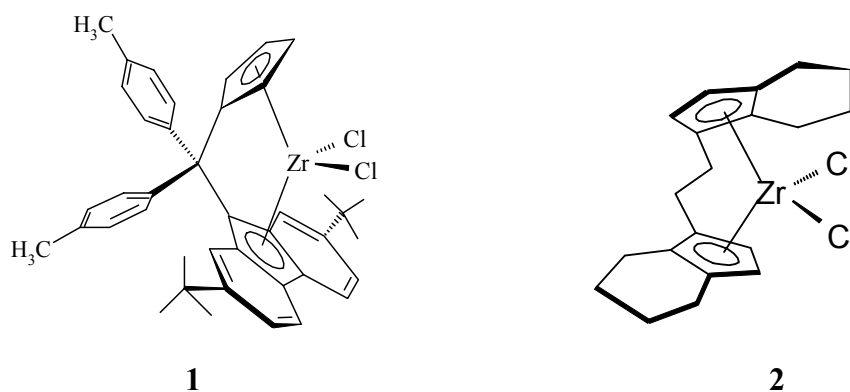
For comparison with CNFs and MWNTs, which are both fillers with a high aspect ratio, nano-sized carbon black was also utilized as filler. The influence of CB on the polymer properties should be investigated and compared to the effect of the two other carbon fillers.

## 6 RESULTS AND DISCUSSION

### 6.1 General Aspects

Polypropylene (nano-) composites with glass fibers (GF), silica nanospheres (monosphers, M250), carbon nanofibers (CNF) carbon black (CB) and multi-walled carbon nanotubes (MWNT) were prepared by *in situ* polymerization of propylene with metallocenes in the presence of the respective fillers. Depending on the filler, different pre-treatments and polymerization procedures were applied in order to achieve a homogeneous distribution of the fillers in the matrix. The nanocomposite properties for different filler contents were then investigated.

Polymerizations of propylene were performed with [(*p*-MePh)<sub>2</sub>C(Cp)(2,7-bis-<sup>t</sup>BuFlu)]ZrCl<sub>2</sub>/MAO (**1** in scheme 1) and with *rac*-[Et(IndH4)<sub>2</sub>]ZrCl<sub>2</sub> (**2** in scheme 1). The first metallocene produces highly syndiotactic polypropylene with a high molecular weight; whereas, polypropylene of a moderate isotacticity with a low molecular weight is obtained by use of the second one.



**Scheme 1: Metallocenes used in this study.**

A homogeneous distribution of the nanotubes or nanofibers in the polymer matrix is crucial for the enhancement of the mechanical properties. To achieve this, an ultrasonic treatment of the nanofillers before the polymerizations turned out to be necessary for all fillers except for the GF.

Nanocomposites containing CNFs, CB or MWNTs were synthesized by polymerization of propylene in toluenic suspension with metallocene 2. Additionally, iPP/CNF nanocomposites were synthesized with metallocene 1. Two different polymerization procedures (with and

without pre-reaction with the cocatalyst MAO) described in more detail in the next section were used to find out, if a pre-reaction with the cocatalyst would improve the distribution of the nanofillers in the polymer matrix and the adhesion of the polypropylene to the nanotubes and nanofibers.

The determined conditions that yielded the best distribution were applied for experiments in which the filler content was varied. The influence of the type of filler and the filler content on the crystallization behavior, the degradation properties, and on the tensile properties was investigated for sPP/CNF, sPP/CB, and sPP/MWNT composites.

### **6.1.1 Dispersion of the Fillers and Adhesion of the Polymer to the Filler**

Ultrasound can serve to separate particles that are agglomerated and held together by high attractive forces by the following mechanism. By oscillation of the sonicator tip, the solvent molecules are excited into vibration around their mean position. This causes pressure differences in the liquid, the pressure being high in places with many molecules and low in places with few molecules. If the pressure becomes too low, and the distance between molecules becomes large, the liquid is converted to gas in these places. The consequence is the formation of cavitation bubbles that collapse shortly afterwards. During this collapse, the local pressure becomes extremely high, allowing for the separation of particles in the surroundings of the bubbles<sup>[136]</sup>.

Preliminary experiments had shown that MWNTs were present in large agglomerates in the polymer matrix if they were used without any pre-treatment. For an improved dispersion of the MWNTs, they were sonicated in a toluene suspension in an ultrasonic bath for 30 minutes prior to the addition of MAO-solution. After a pre-reaction time of approximately 24 hours, metallocene 1 was added and this activated catalyst was then introduced into the reactor that was already filled with toluene saturated with propylene. This treatment improved the dispersion but was insufficient for the separation of the nanotube-bundles, as well. A microscopic photograph of the molten nanocomposite is shown in Fig. 10. Agglomerates with diameters of 0.05 mm and more are visible throughout the whole sample.

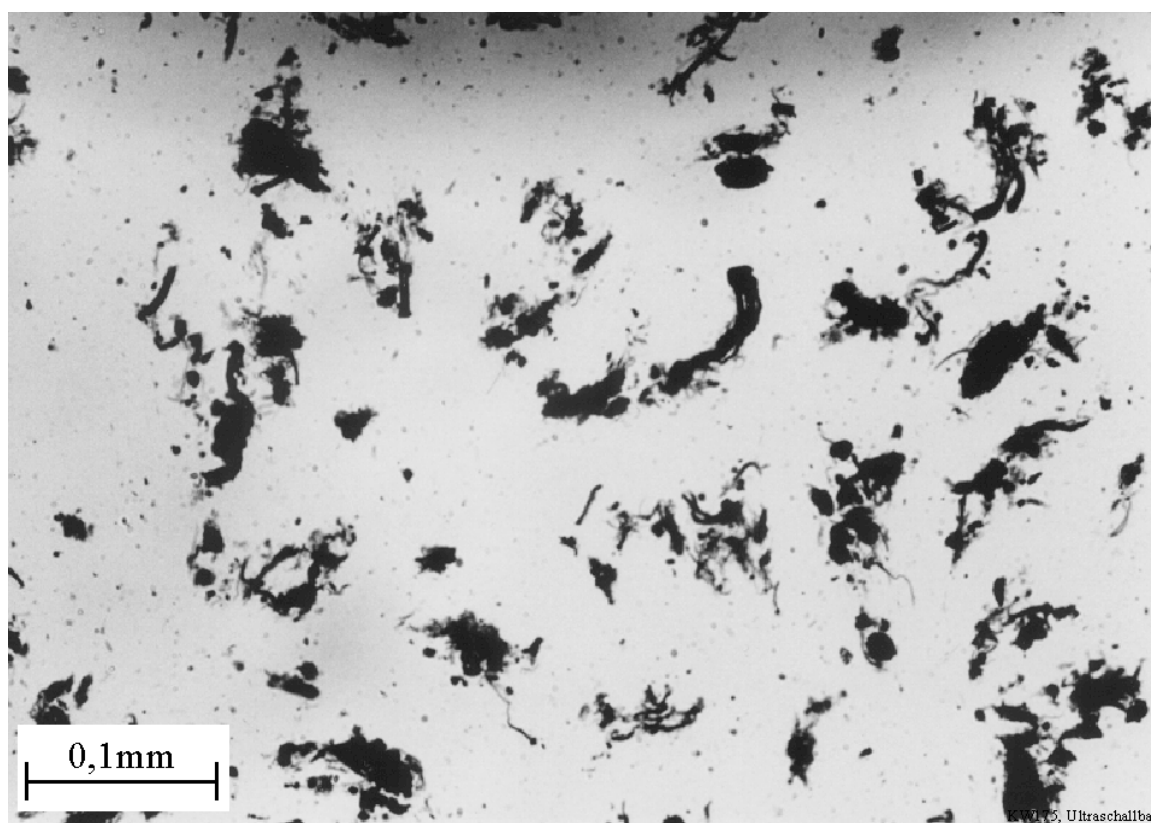


**Fig. 10: Microscopic Photograph of a sPP/MWNT-nanocomposite prepared after sonication of the nanotubes in an ultrasonic bath.**

For the above reasons, the subsequent dispersions of CNFs, CB and MWNTs in toluene were performed with a Sonopuls homogenizer HD 2200 equipped with a KE 76 sonotrode. The nanofillers were heated in vacuum and flushed with argon prior to the addition of toluene. The influence of the ultrasonic amplitude, which is a measure for the energy input, and the duration of the sonication on the dispersion of the respective nanofillers was investigated. The amplitude was varied from 10 to 50 % and the sonication time lay between 5 and 120 min. The degree of dispersion was determined by microscopy of the nanocomposites in the molten state. The quality of the filler wetting by the polymer matrix can be estimated from scanning electron microscopy (SEM) micrographs. A good wetting is an indication for a good adhesion.

### **6.1.2 Pre-Reaction of the Fillers with MAO**

Some polymerizations were performed without pre-reaction with MAO as described in detail in the experimental section. The fillers were introduced into the toluene-charged reactor immediately after sonication, and the polymerization was started by application of the metallocene after saturation with propylene was completed.

In case of the polymerizations with pre-reaction, the nanofiller suspension was stirred with MAO-solution for 24 hours after the ultrasonic treatment. The metallocene was then added to this suspension before introduction of the mixture into the toluene-charged reactor that had been saturated with propylene before.

Any hydroxyl or carboxyl groups present on the filler surface can react with added MAO to form a heterogeneous cocatalyst and, upon addition of the metallocene, a heterogeneous catalyst. This procedure is commonly used to attach MAO to silica surfaces<sup>[137]</sup>. Hydroxyl groups are also present on the surface of the purified carbon nanotubes, which were used in this study. This led to the conclusion that it should be possible to fix the cocatalyst on their surface by the above procedure (see Fig. 11).

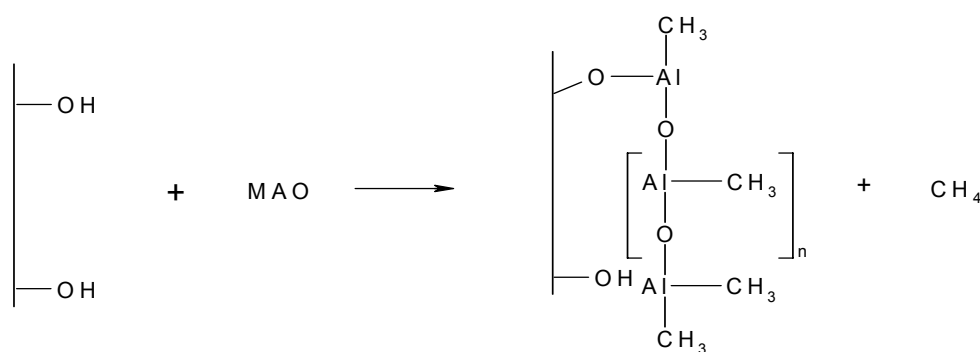


**Fig. 11: Reaction of MAO with hydroxyl groups on the surface of the filler.**

By reaction with the so formed cocatalyst, the metallocene could be indirectly heterogenized on the filler (Fig. 12), enabling it to polymerize propylene directly on the surface of the filler.

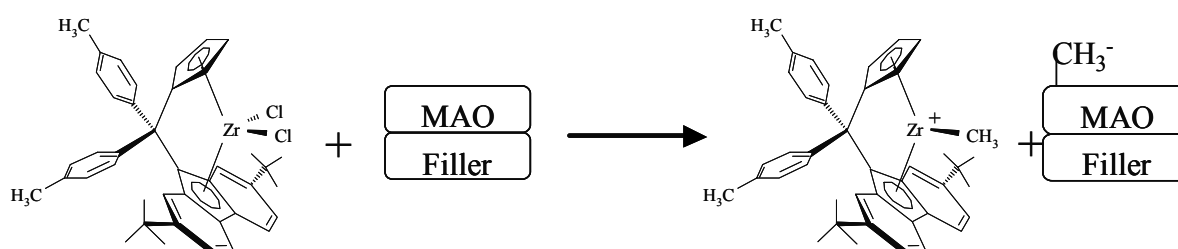


**Fig. 12: Indirect heterogenization of metallocene 1.**

### 6.1.3 Crystallization Behavior of the Nanocomposites

The crystallization behavior of polymers plays an important role during the processing of these materials. By reduction of the cooling time required for part solidification, cycle times can be shortened. This can be accomplished by the incorporation of nucleating agents into the neat polymer which speed up the crystallization. The crystallization kinetic influences the

morphology, which in turn affects the mechanical properties of a semi-crystalline polymer<sup>[86,91]</sup>. Important parameters for the characterization of the crystallization behavior are the crystallization temperature ( $T_c$ ), the melting temperature ( $T_m$ ), and the half-time of crystallization ( $t_{0.5}$ ). Additionally, the rate constant of crystallization ( $K$ ) and the Avrami exponent ( $n$ ) obtained from Avrami analysis of isothermal crystallization experiments are interesting parameters.

#### 6.1.3.1 Melting and Crystallization Temperature and Crystallinity

The values for the crystallization and melting temperatures were obtained from non-isothermal DSC measurements described in detail in the experimental section. The enthalpy of fusion of 100 % crystalline pure iPP is  $8.7 \pm 1.6$  kJ/mol<sup>[138]</sup>, corresponding to 207 J/g. Different values have been reported for the enthalpy of fusion of 100 % crystalline sPP. Wang et al. reported values of 6.9 kJ/mol and 8.7 kJ/mol (based on per propylene unit) which correspond to 164 J/g and 207 J/g, respectively<sup>[139]</sup>. As these values differ significantly, the reported crystallinities can only be taken as an estimate.

#### 6.1.3.2 Halftime of Crystallization

The half-time of crystallization is a measure for the crystallization speed and is defined as the time taken from the onset of the crystallization (point A in Fig. 13) until 50 % completion of the crystallization process. The total enthalpy of crystallization was obtained by integration of the area under the crystallization curve (from point A to C in Fig. 13). The time after which half the value of the total enthalpy of crystallization was reached was taken as crystallization half-time.

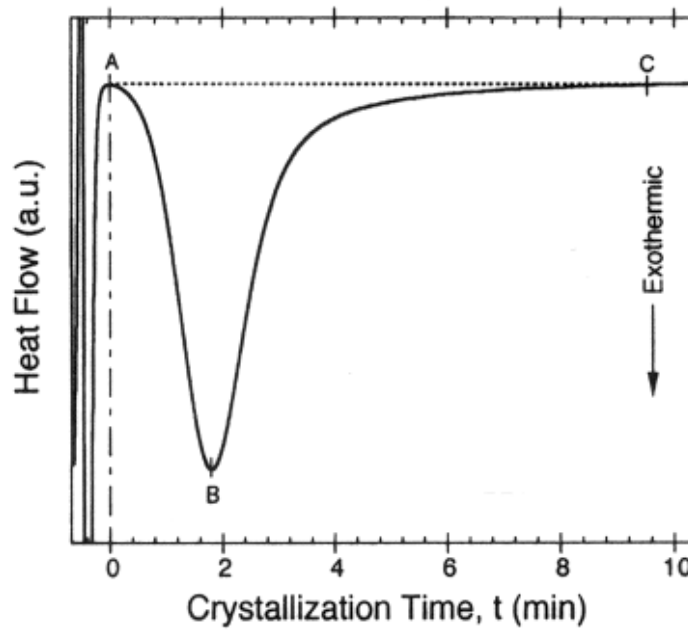


Fig. 13: Schematic representation of a DSC trace and baseline (dotted line) taken from reference [140].

### 6.1.3.3 Avrami Analysis

A kinetic theory of crystallization taking into account the dimension of the crystallite growth was derived by Avrami<sup>[141-144]</sup> (Eq. 1). The development of the crystalline fraction ( $X_c$ ) with the time is described with the Avrami crystallization constant ( $K$ ) and the Avrami exponent ( $n$ ) being suitable parameters. A larger value of  $K$  indicates a faster crystallization of the material. It should be noted, that the Avrami equation is, strictly speaking, only applicable for low crystallinities, that is, in the early stages of the crystallization.

$$1 - X_c = e^{-Kt^n}$$

**Eq. 1: Avrami equation with  $X_c$  crystalline volume fraction at time  $t$  and constant temperature,  $K$  and  $n$  Avrami parameters.**

This equation can also be written in the logarithmic form which is the basis for the Avrami plot.

$$\ln[-\ln(1 - X_c)] = \ln K + n \ln t$$

**Eq. 2: Double logarithmic form of the Avrami equation.**

The Avrami parameters ( $K$  and  $n$ ) can be obtained from a least squares fit of the experimental data to a double logarithmic plot of  $\ln[-\ln(1-X_c)]$  versus  $\ln(t)$  which is shown for an sPP/MWNT nanocomposite in Fig. 14. The Avrami exponent  $n$  is obtained as the slope of the



least-square fit, and the value for the Avrami crystallization rate constant is the antilogarithmic value of the y-intercept of the fit<sup>[140]</sup>. It is important to only use the parts of the plots where the experimental data shows a linear dependence of  $\ln[-\ln(1-X_c)]$  on  $\ln(t)$  because the theory is only applicable in this region. The use of data from the non-linear region can yield incorrect data.

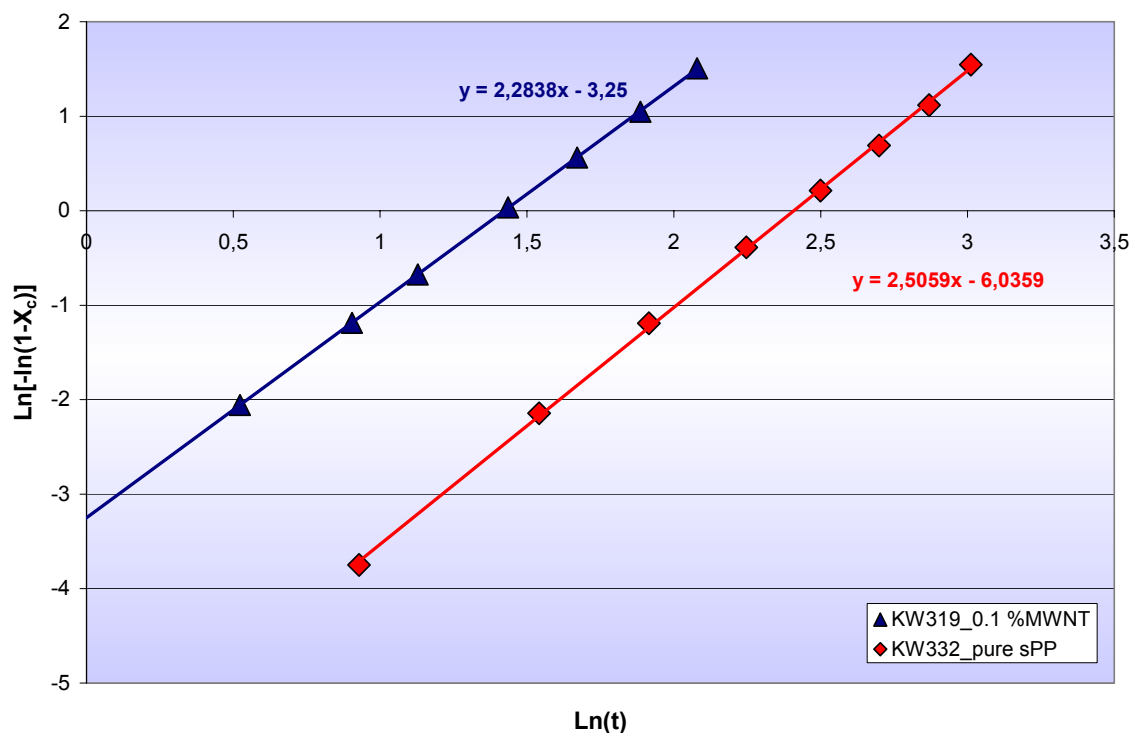


Fig. 14: Avrami plot for an exemplary sPP/MWNT nanocomposite containing 0.1 % carbon nanotubes.

The values for the Avrami exponent should be in the range of 1-4, and are an indication of the mechanism of nucleation and the geometry of the crystal growth (Tab. 1). According to the original theory, they should be integer, but when fitting experimental data, non-integer values are often obtained. This can be due to an inaccurate set of the onset of crystallization<sup>[86]</sup>.

Tab. 1: Significance of the Avrami exponent  $n$

$n$	nucleation and growth mechanism
$3 + 1 = 4$	Spherulitic growth + random nucleation
$3 + 0 = 3$	Spherulitic growth + instantaneous nucleation
$2 + 1 = 3$	Disc-like growth + random nucleation
$2 + 0 = 2$	Disc-like growth + instantaneous nucleation
$1 + 1 = 2$	Rod-like growth + random nucleation
$1 + 0 = 1$	Rod-like growth + instantaneous nucleation

For the application to values determined by DSC measurements, it is assumed that the differential area under the crystallization curve with time corresponds to the changes in crystallinity<sup>[140]</sup>.  $X_c$  is defined as the relative crystallinity at time  $t$ . Since it was assumed, that the crystallinity is linearly proportional to the enthalpy released during crystallization, the relative crystallinity at time  $t$  was taken as the ratio of the integral of the enthalpy at time  $t$  to the enthalpy over the whole crystallization time. It was assumed that crystallization was complete when the exothermic trace converged to the baseline (Point C in Fig. 13).

The crystallization kinetics of pure sPP samples were investigated by Supaphol et al<sup>[140]</sup>. When the isothermal crystallization temperature was raised from 60 °C to 95 °C the values of the Avrami exponent increased from 2.31 to 3.17 for sPP1 ( $M_w = 165,000$  g/mol,  $rrrr = 77\%$ ,  $M_w/M_n = 2.2$ ) and from 2.07 to 2.88 for sPP2 ( $M_w = 133,000$ ,  $rrrr = 74.6$  and  $M_w/M_n = 3.6$ ), which was attributed to a lower amount of athermal nuclei. The values for the rate constant  $K$  were found to increase with decreasing temperature and lay in the range of  $2.5 \cdot 10^{-4}$  to  $1.75 \cdot 10^{-1}$  and  $1.89 \cdot 10^{-4}$  to  $1.02 \text{ min}^{-n}$ .

#### 6.1.4 Thermal Stability of the Nanocomposites

Polyolefins are quite flammable<sup>[135]</sup> which is a reason for the frequent incorporation of flame retardants into this material to reduce the heat release during combustion. The thermal stability of the nanocomposites in this study was determined by thermogravimetric analysis (TGA). TGA provides information about the percental change of mass of a sample with respect to the temperature of the sample. Important parameters that can be gathered from TGA measurements are the extrapolated onset of degradation ( $T_{on}$ ) and the temperature of maximum weight loss rate (inflection point of the curve,  $T_{max}$ ) which are shown in Fig. 15. They were determined by evaluation of the data according to Marsh using Proteus software available for the TGA used in this study.

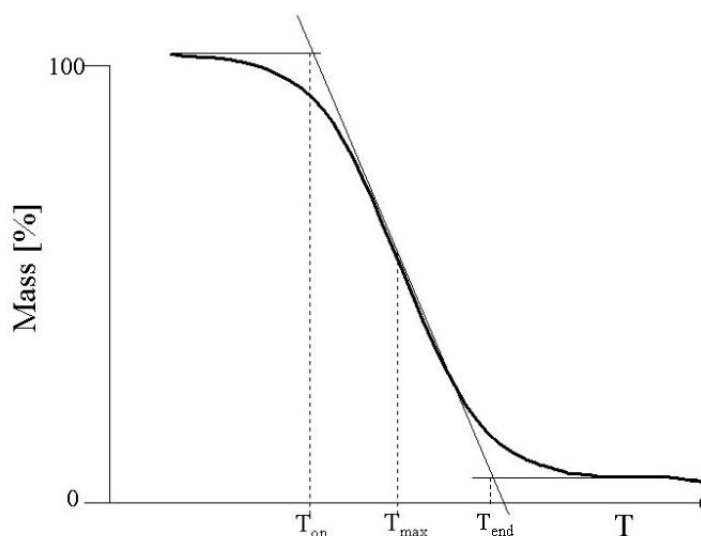


Fig. 15: Schematic representation of a TGA-curve with  $T_{on}$ ,  $T_{max}$ , and  $T_{end}$ .

### 6.1.5 Electrical Conductivity of the Nanocomposites

The electrical conductivity of polymers is important when the material is used in the packaging of electronic devices. It is desirable that the polymer be conductive to prevent it from taking up electrostatic charge, which might damage the content of the package. Most polymers are insulators, which makes the addition of conductive fillers necessary for this kind of application. Carbon black is often used for this task, but also carbon nanotubes and carbon nanofibers have been used because they require a lesser amount to be incorporated to achieve conductivity<sup>[55,92]</sup>. If carbon black is used, filler contents as high as 15 to 20 wt.-% can be necessary to ensure a sufficient conductivity. This, in turn, can lead to a deterioration of the mechanical properties<sup>[87]</sup>. Protection against electrostatic discharge can be accomplished by lowering the surface resistivity to values between  $10^5$  to  $10^{12}$   $\Omega$ /square, a low resistivity being more favorable.

The surface resistivity, which is the inverse of the conductivity, of the prepared sPP/CNF and sPP/MWNT nanocomposites was evaluated using two-point measurements. For these experiments, the films also used for the tensile tests were employed. A good contact between electrodes and polymer film was ensured by application of conductive colloidal graphite suspension as described in the experimental section. From these measurements, the resistivity ( $\rho$ ) was determined. A characteristic quantity that can be calculated from these measurements is the  $\log(\rho)$ , which can be plotted versus the weight-percentage of filler incorporated in the

nanocomposite. The percolation threshold is the filler content at which the  $\log(\rho)$  drops dramatically and the composite thus becomes conductive (see Fig. 16).

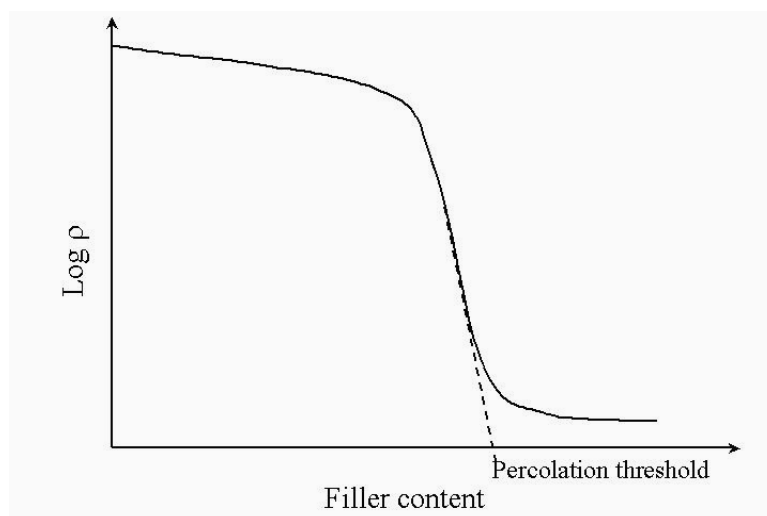


Fig. 16: Schematic representation of the dependence of the resistivity ( $\rho$ ) on the filler content.

### 6.1.6 Tensile Properties of the Nanocomposites

If fibers are incorporated into polymeric matrices, the main loads can be supported by the fibers instead of by the matrix. To realize this, a good bonding of the matrix to the fiber is important to prevent the latter from being pulled out upon application of strain. Fibers can then increase strength, stiffness, and toughness of the composite material<sup>[145]</sup>.

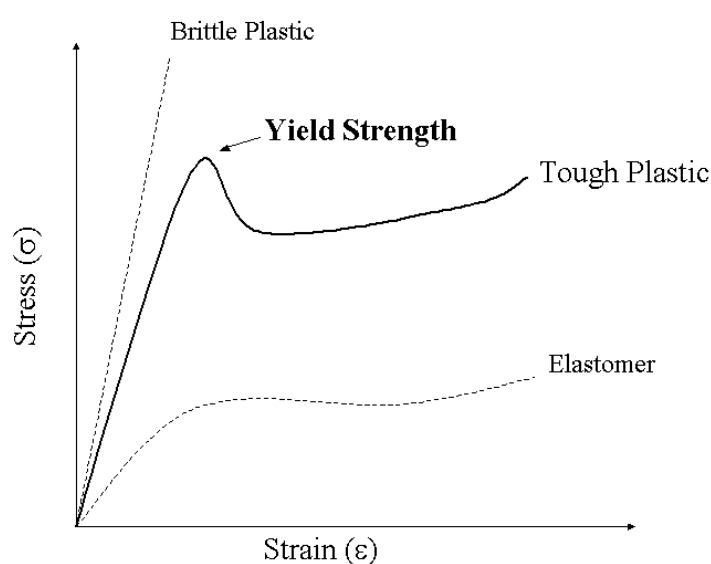


Fig. 17: Stress-strain behavior of different types of polymers.

The tensile tests were performed on test bars cut from films that had been obtained by hot-pressing of the nanocomposites. The elongation of the samples in dependence of the force

exerted was monitored. The strain ( $\epsilon$ ) and stress ( $\sigma$ ) for the samples were calculated by normalization of these values to the sample dimension. Typical stress-strain curves for different types of polymers are shown in Fig. 17<sup>[145]</sup>.

Brittle plastics show a linear dependence of the strain on the applied stress. Elastomers, which exhibit rubber elasticity, are characterized by a non-linear dependence of the strain on the stress. Tough plastics (for example polypropylene) initially show an almost linear increase of the strain when the stress applied is raised. At some point (yield strength) the plastic flow in these materials begins. The stress stays almost constant while elongation proceeds, the material showing clearly nonlinear viscoelastic properties in this region. This process is often accompanied by a necking of the sample. Before the rupture, a strain hardening occurs and the stress increases significantly with increasing strain.

The elongation at break, which is measured in percent, is the end-point of the stress-strain curve, signifying the rupture of the polymer sample. For tough plastics, it can be of the order of several hundred percent. The elastic modulus (Young's Modulus,  $E$ ) is given by the initial slope of the stress-strain curve, where deformation is reversible. The Young's modulus is a measure for the elasticity. A high Young's modulus is characteristic of a rather rigid material that shows little elongation when a force is applied. A softer material has a relatively low elastic modulus. It was determined with the help of the following equation (Eq. 3).

$$E = \frac{\sigma_{(0,25)} - \sigma_{(0,05)}}{\left(\frac{\epsilon_{(0,25)}}{100} - \frac{\epsilon_{(0,05)}}{100}\right)}$$

**Eq. 3: Determination of the elastic modulus ( $E$  = elastic modulus,  $\sigma(\epsilon)$  = stress at strain  $\epsilon$  [MPa],  $\epsilon$  = strain [%]).**

The yield strength (also yield strength) was taken as the maximum stress before necking occurred. This parameter is important for applications of polymers because the material must not be subjected to forces higher than the yield stress. Otherwise, an irreversible deformation takes place.

## 6.2 Polypropylene/Monospher Nanocomposites

Polymerizations of propylene in the presence of Monosphers were performed with [(p-MePh)<sub>2</sub>C(Cp)(2,7-bis-<sup>t</sup>BuFlu)]ZrCl<sub>2</sub>/MAO (**1** in scheme 1) in toluene slurry and in the gasphase and with *rac*-[Et-(IndH<sub>4</sub>)<sub>2</sub>]ZrCl<sub>2</sub> (**2** in scheme 1). The cocatalyst for these slurry polymerizations was prepared by impregnation of M250 with MAO. To be able to perform an indirect heterogenization of the metallocene, the cocatalyst was examined regarding the adhesion of MAO to M250. The storage stability of the resulting M250/MAO-cocatalyst was tested to render the preparation of a bigger amount of the cocatalyst possible. This was necessary to ensure a comparability of the experiments.

The effect of different amounts of MAO used for the impregnation of M250 was investigated in polymerizations with the catalyst M250/MAO/**1**. The most suitable M250/MAO/**1** species was chosen for propylene polymerizations under various conditions. In the following tests, the polymerization temperature, propylene concentration, and metallocene amount were varied to detect their influence on activity, polymer properties and envelopment of the silica spheres. Furthermore, gasphase polymerizations were carried out with the same catalyst system. The aim was to further improve the dispersion of the filler in the matrix polymer.

### 6.2.1 Adhesion and Stability

For the indirect heterogenization of the metallocene, it was necessary to ensure a good adhesion of the MAO to the M250. It was, therefore, tested by adding the metallocene to a suspension of M250/MAO in toluene and stirring the mixture for 10 minutes to form the active species. The dispersion was then filtrated to determine whether catalyst leaching had taken place and if active species were present in the filtrate. This was applied to the reactor containing triisobutylaluminium (TIBA) as scavenger and toluene saturated with propylene to start the polymerization. Neither propylene consumption, nor polymer formation was observed. This led to the conclusion, that the filtrate was obviously not active in propylene polymerization. In a next step, the solid residue of M250/MAO/**1** was suspended in toluene and applied to the reactor via a pressure lock. Propylene consumption and the formation of polypropylene was observable, proving that the solid residue acted as an active polymerization catalyst. Therefore, it was concluded that catalyst leaching was negligible for the subsequent polymerizations.

To determine whether MAO-impregnated M250 is suitable for storage, 2.55g M250 were impregnated with 11 ml of MAO-solution (corresponding to 420 mg MAO/g M250) as described in the experimental section. Directly after preparation, 2 weeks and 11 weeks after preparation, slurry polymerizations of propylene were carried out with this cocatalyst. They were performed in toluene at a propylene pressure of 2 bar (corresponding to 1.38 mol/l) at 30 °C. 2 mmol of TIBA were added as scavenger. The amount of M250/MAO was 0.55 g, and that of metallocene 1 was  $1.3 \cdot 10^{-6}$  mol. As can be seen from Tab. 2, the activity decreased only slightly even after a storage of 11 weeks. From a value of 3,700  $\text{kg}_{\text{Pol}}/(\text{mol}_{\text{Zr}} \cdot \text{h} \cdot \text{mol}_{\text{Mon}}/\text{l})$  it decreased to 89 % of the initial value after two weeks and to 81 % of the original activity after 11 weeks. Because of the relatively good stability, it was reasonable to prepare a larger amount of M250/MAO. Polymerizations under different polymerization conditions could consequently be carried out with the same cocatalyst to ensure their comparability.

**Tab. 2: Stability of supported MAO/M250 species.**

Weeks after Preparation	Activity [ $\text{kg}_{\text{Pol}}/(\text{mol}_{\text{Zr}} \cdot \text{h} \cdot \text{mol}_{\text{Mon}}/\text{l})$ ]	Filler Content <sup>a</sup> [%]
0	3,700	11
2	3,300	9
11	3,000	10

(Polymerization conditions: polymerization temperature (Tp) 30°C, polymerization time (tp) 30 min, propylene concentration (cp) 1.38 mol/l (2 bar), solvent 200 ml of toluene, amount of [(p-MePh)<sub>2</sub>C(Cp)(2,7-bis-tBuFlu)]ZrCl<sub>2</sub>  $1.3 \cdot 10^{-6}$  mol, amount of M250/MAO 0.55 g, amount of triisobutylaluminium (TIBA) 2 mmol, a: differences in filler content originate from different amounts of polymer formed)

## 6.2.2 Variation of MAO Amount

To find the minimum amount of MAO needed to activate the metallocene and in order to determine whether the applied amount of MAO had any influence on the envelopment of the silica spheres, different amounts of MAO were applied to the silica spheres for heterogenization. All other conditions (solvent volume, polymerization temperature, amount of M250/MAO, polymerization time, catalyst amount) were kept constant. Several polymerizations were performed with each batch of M250/MAO to determine the optimum amount of MAO for the impregnation. The results are shown in Fig. 18.

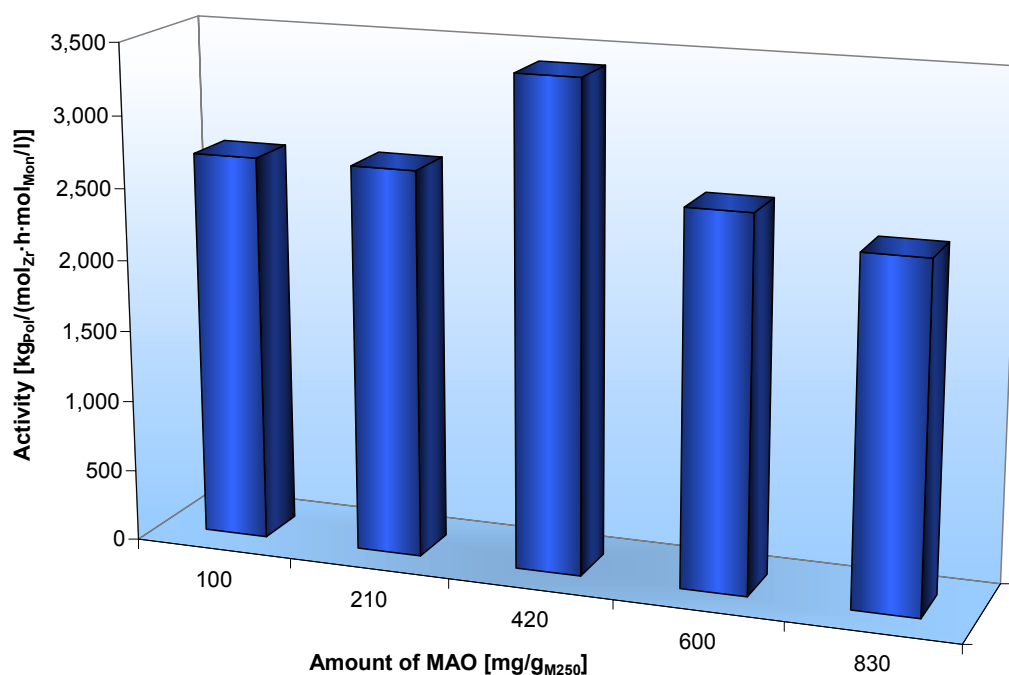


**Fig. 18:** Activity related to the amount of MAO applied to M250. (Polymerization conditions: polymerization temperature ( $T_p$ ) 30°C, polymerization time ( $t_p$ ) 30 min, propylene concentration ( $c_p$ ) 1.38 mol/l (2 bar), solvent 200 ml of toluene, amount of [(p-MePh)<sub>2</sub>C(Cp)(2,7-bis-tBuFlu)]ZrCl<sub>2</sub>  $1.3 \cdot 10^{-6}$  mol, amount of M250/MAO 0.55 g, amount of triisobutylaluminium (TIBA) 2 mmol)

The average activity of the M250/MAO/1 catalysts varied according to the amount of MAO applied for the preparation of the cocatalyst. In polymerizations with a cocatalyst containing 100 mg MAO/g M250 or 210 mg MAO/g M250, the activity was 2,700 kg<sub>Pol</sub>/(mol<sub>Zr</sub>·h·mol<sub>Mon</sub>/l). The maximum activity of 3,400 kg<sub>Pol</sub>/(mol<sub>Zr</sub>·h·mol<sub>Mon</sub>/l) was reached when a MAO amount of 420 mg/g M250 was used for the impregnation. For higher amounts of 600 and 830 mg MAO/g M250, the activity of the corresponding catalysts decreased to 2,600 and 2,400 kg<sub>Pol</sub>/(mol<sub>Zr</sub>·h·mol<sub>Mon</sub>/l), respectively. All detected melting temperatures lay in the region of 140 °C with no distinct trend visible regarding the applied amount of MAO. The same is true for the molar masses ranging from 500,000 to 600,000 g/mol.

The coverage of the silica spheres with polypropylene can be seen in Fig. 19 and Fig. 20. They show two examples of SEM micrographs for an amount of 100 mg MAO/g M250 and 420 mg/g M250, respectively. It is apparent, that in both cases most of the silica spheres were covered with polymer and only a few were not. There was no trend seen regarding the influence of the MAO-amount on the filler envelopment. This is also true for the other amounts of MAO that were investigated.



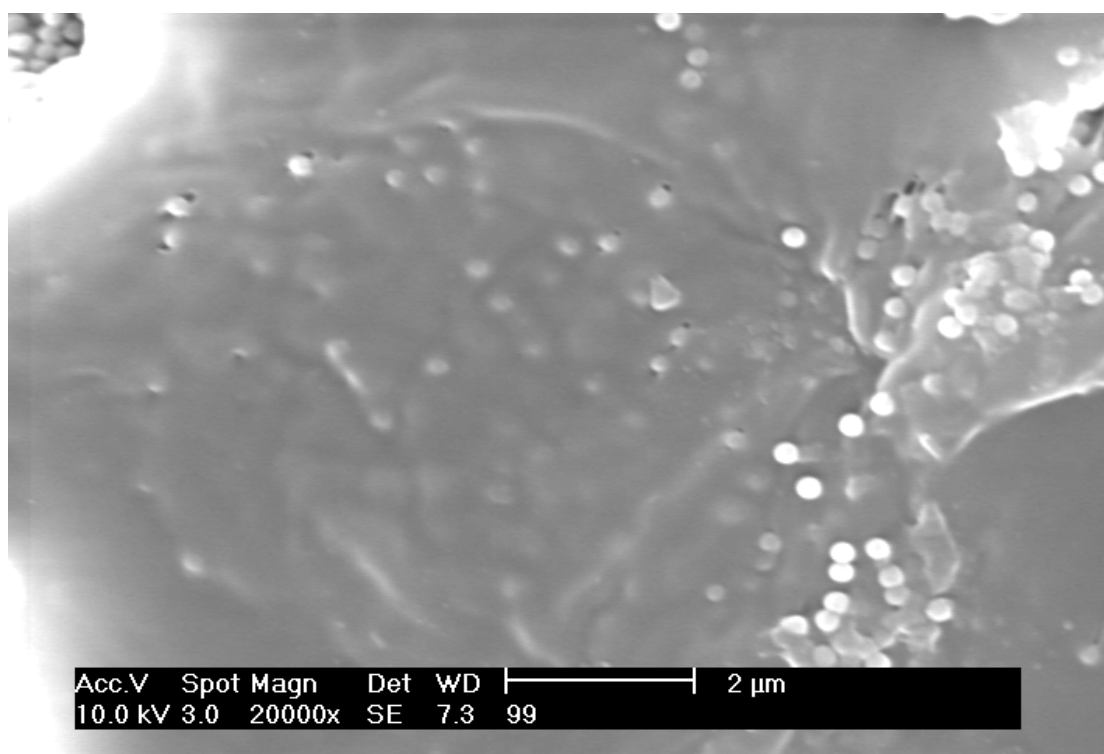


**Fig. 19:** SEM micrograph of M250-filled sPP synthesized with M250/MAO (100 mg MAO/g M250) as cocatalyst.

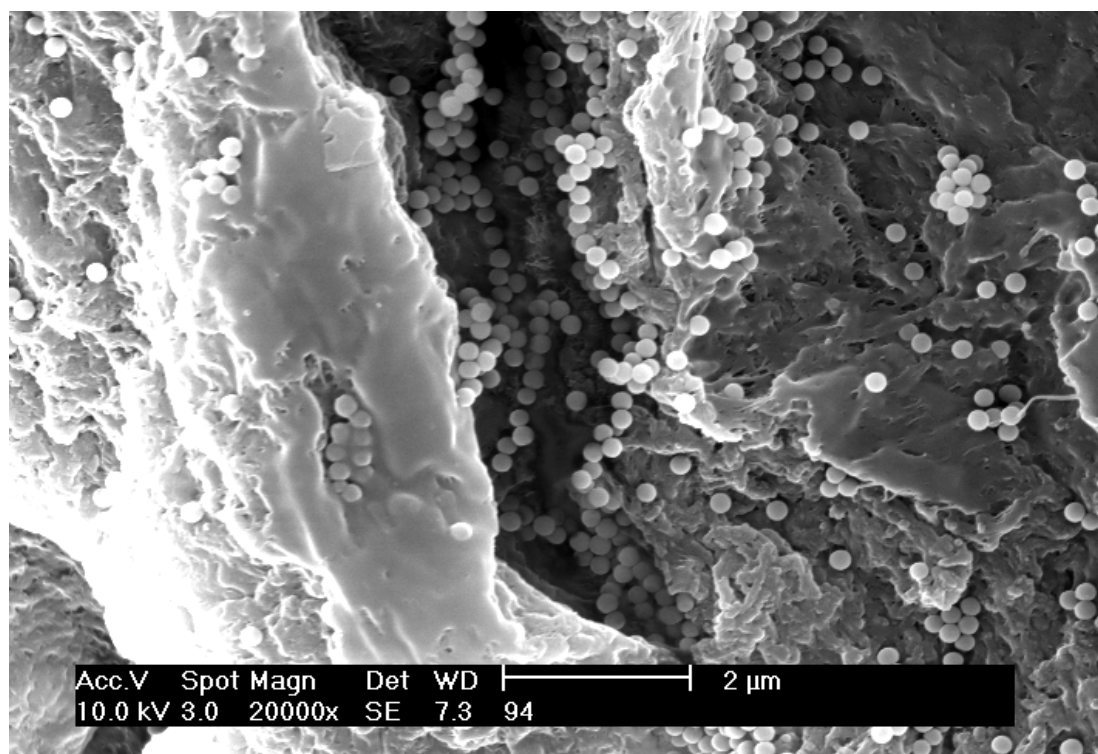


**Fig. 20:** SEM micrograph of M250-filled sPP synthesized with M250/MAO (420 mg MAO/g M250) as cocatalyst.

The monosphers impregnated with 420 mg MAO/g M250 showed the highest activity as cocatalyst in propylene polymerization. The melting temperatures lay in the region of 138 – 142 °C with a hardly perceptible tendency to rise with rising amount of MAO. The molecular

weight was found to generally lie between 500,000 and 600,000 g/mol, and the fraction of the rrrr pentad was around 91%, where detected.

The envelopment of the silica spheres with the matrix polymer and the polymer properties were obviously largely independent of the amount of MAO used for the preparation of the cocatalyst. It was, therefore, concluded that the cocatalyst providing the highest activity (420 mg MAO/g M250) should be used in all subsequent polymerizations.

### 6.2.3 Variation of Temperature, Propylene Concentration and Catalyst Amount

To reach the goal of a better dispersion and envelopment of the silica spheres with polypropylene, the influence of the polymerization conditions was investigated. To ensure comparability among the results, one batch of M250/MAO was synthesized as described above and used as cocatalyst for all subsequent slurry polymerizations. The first condition to be varied was the polymerization temperature. All polymerizations were carried out in 200 ml toluene mixed with 2 mmol of TIBA as scavenger. The amount of M250/MAO was kept constant at 0.55g, and the polymerization time lay between 30 and 180 minutes, depending on the temperature. The corresponding results for 0 °C, 30 °C and 60 °C are listed in Tab. 3.

**Tab. 3: Average activity and polymer properties in relation to polymerization temperature, propylene concentration and catalyst amount.**

Entry	Polymerization Temperature [°C]	Propylene Concentration [mol/l]	Catalyst Amount [mol]	Activity [kg <sub>Pol</sub> /(mol <sub>Zr</sub> ·h·mol <sub>Mon</sub> /l)]	Melting Point [°C]	Molecular Weight [g/mol]
1	0	1.4	$1.30 \cdot 10^{-6}$	600	149	790,000
2	30	0.6	$1.40 \cdot 10^{-6}$	1,800	137	370,000
3	30	1.4	$1.30 \cdot 10^{-6}$	2,300	141	560,000
4	30	1.4	$6.60 \cdot 10^{-7}$	2,300	139	n. d.
5	30	1.4	$3.20 \cdot 10^{-7}$	1,100	140	n. d.
6	30	3.5	$6.00 \cdot 10^{-7}$	2,500	142	640,000
7	60	1,4	$7,00 \cdot 10^{-7}$	3,000	121	220,000

(Polymerization conditions: polymerization time (tp) 30 – 180 min, solvent 200 ml of toluene, amount of M250/MAO 0.55 g, amount of triisobutylaluminium (TIBA) 2 mmol; n. d. = property was not detected)

As can be seen from entries 1, 3, and 7 (Tab. 3), a higher polymerization temperature expectedly induced a higher activity. This was also in accordance with the results from

solution-polymerizations<sup>[146]</sup>. The average activity of the polymerizations with M250/MAO/1 as cocatalyst was much lower than that of comparable homogeneous polymerizations with MAO/1. For 0 °C it was only 600 kg<sub>Pol</sub>/(mol<sub>Zr</sub>·h·mol<sub>Mon</sub>/l) with the heterogeneous system M250/MAO/1 as compared to 2,000 kg<sub>Pol</sub>/(mol<sub>Zr</sub>·h·mol<sub>Mon</sub>/l) for the homogeneous polymerization. At 30 °C it was 2,300 as compared to 5,200 kg<sub>Pol</sub>/(mol<sub>Zr</sub>·h·mol<sub>Mon</sub>/l) and at 60 °C it amounted to 2,400 as compared to 9,500 kg<sub>Pol</sub>/(mol<sub>Zr</sub>·h·mol<sub>Mon</sub>/l). As expected, the highest melting temperatures (see Tab. 3) of 149 °C were reached for polypropylenes synthesized at 0 °C, then decreased to 141 °C at 30 °C polymerization temperature and to 121 °C at a polymerization temperature of 60 °C, corresponding to a sinking syndiotacticity.

Interestingly, the SEM micrographs (Fig. 21, Fig. 22 and Fig. 23) clearly show a lack of influence of the polymerization temperature on the degree of coverage of the silica spheres. Some spheres are still not covered at all, while others are completely covered with polymer. The magnification is 20,000 times, 20,000 times and 50,000 times, and the filler content 35 %, 15 % and 9 %, respectively.

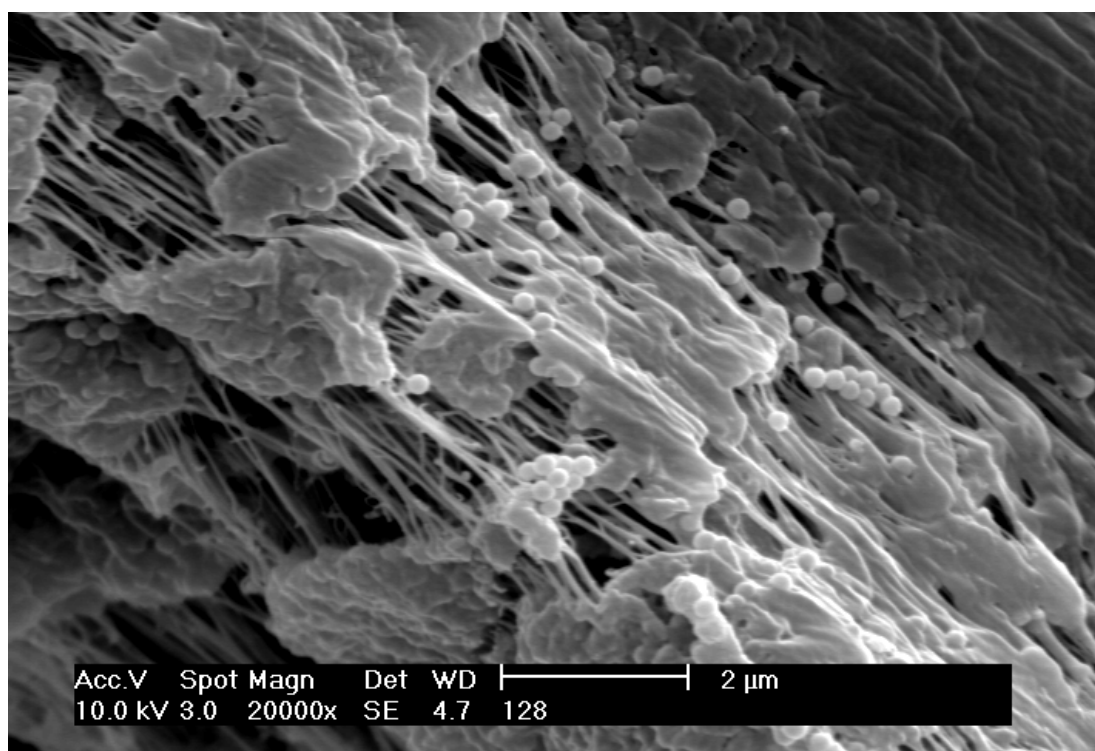


Fig. 21: SEM micrograph of M250-filled sPP synthesized at a polymerization temperature of 0°C.

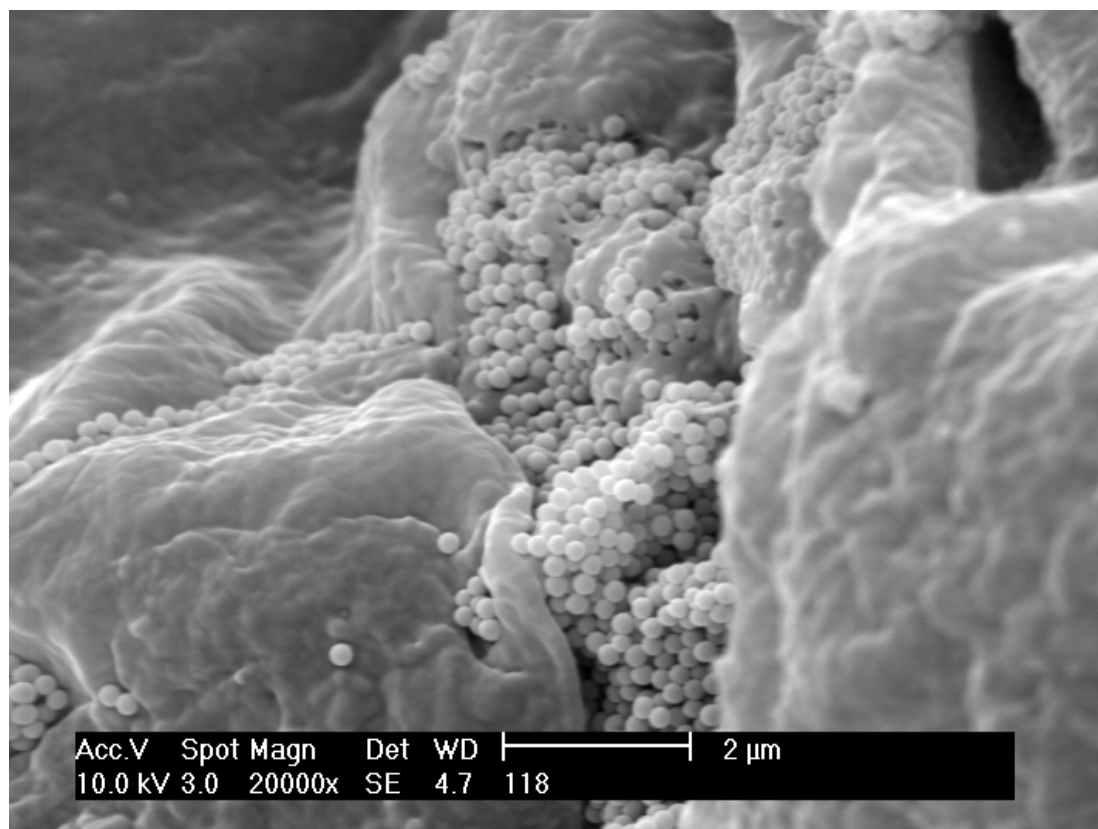


Fig. 22: SEM micrograph of M250-filled sPP synthesized at a polymerization temperature of 30°C.

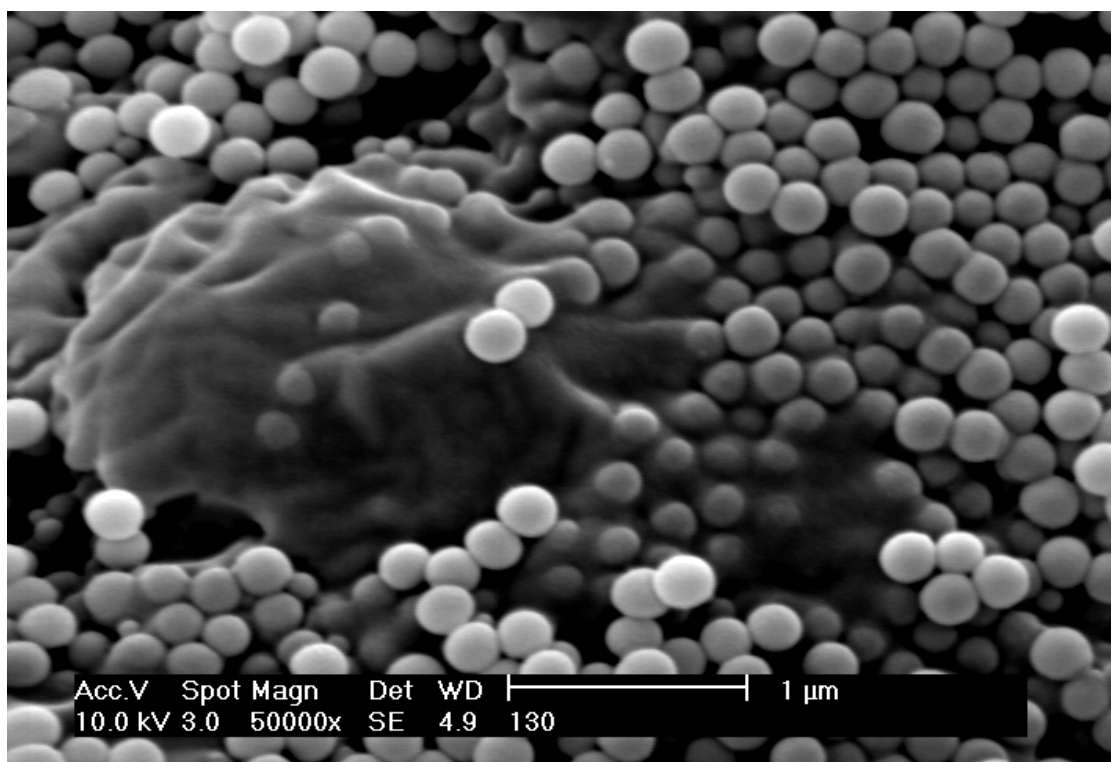


Fig. 23: SEM micrograph of M250-filled sPP synthesized at a polymerization temperature of 60°C.

The next parameter to be investigated was the concentration of propylene in the reaction mixture. It was varied in the range from 0.6 to 3.5 mol/l. According to Tab. 3 (entries 2,3,6), hardly any dependence of the activity, lying between 1,800  $\text{kg}_{\text{Pol}}/(\text{mol}_{\text{Zr}} \cdot \text{h} \cdot \text{mol}_{\text{Mon}}/\text{l})$  and 2,500  $\text{kg}_{\text{Pol}}/(\text{mol}_{\text{Zr}} \cdot \text{h} \cdot \text{mol}_{\text{Mon}}/\text{l})$ , on the concentration was found. Only at a propylene concentration as low as 0.6 mol/l, the average activity sank to 1,800  $\text{kg}_{\text{Pol}}/(\text{mol}_{\text{Zr}} \cdot \text{h} \cdot \text{mol}_{\text{Mon}}/\text{l})$ , and was, therefore, inferior to activities in polymerizations with a higher propylene concentration. Likewise, the melting point of approximately 137 °C lay about 4 °C below that of the polypropylene from the slurry polymerizations at 1.4 mol/l propylene at otherwise same conditions. For the highest propylene concentration of 3.5 mol/l, the melting temperature lies in the same range as for polymers produced at a concentration of 1.4 mol propylene per liter. The molecular weight was naturally influenced by the monomer concentration and increased from 370,000 to 640,000 g/mol for propylene concentrations of 0.6 to 3.5 mol/l, respectively.

The SEM micrographs for the polymerizations at a propylene concentration of 0.6 and 3.5 mol/l did not show any improvement in the degree of coverage of the silica microspheres as can be seen from Fig. 24 and Fig. 25. The filler content of the nanocomposite prepared at 0.6 mol/l propylene was approximately 25 % and 10 % for the one prepared at 3.5 mol/l.

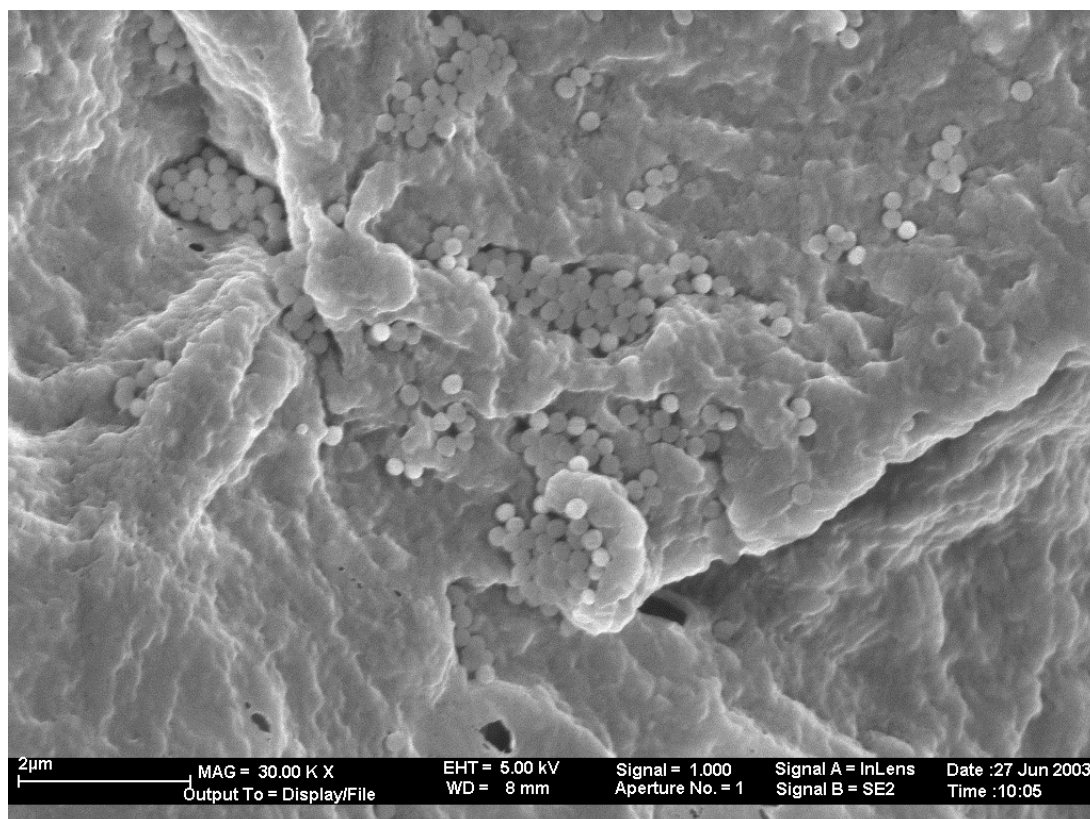
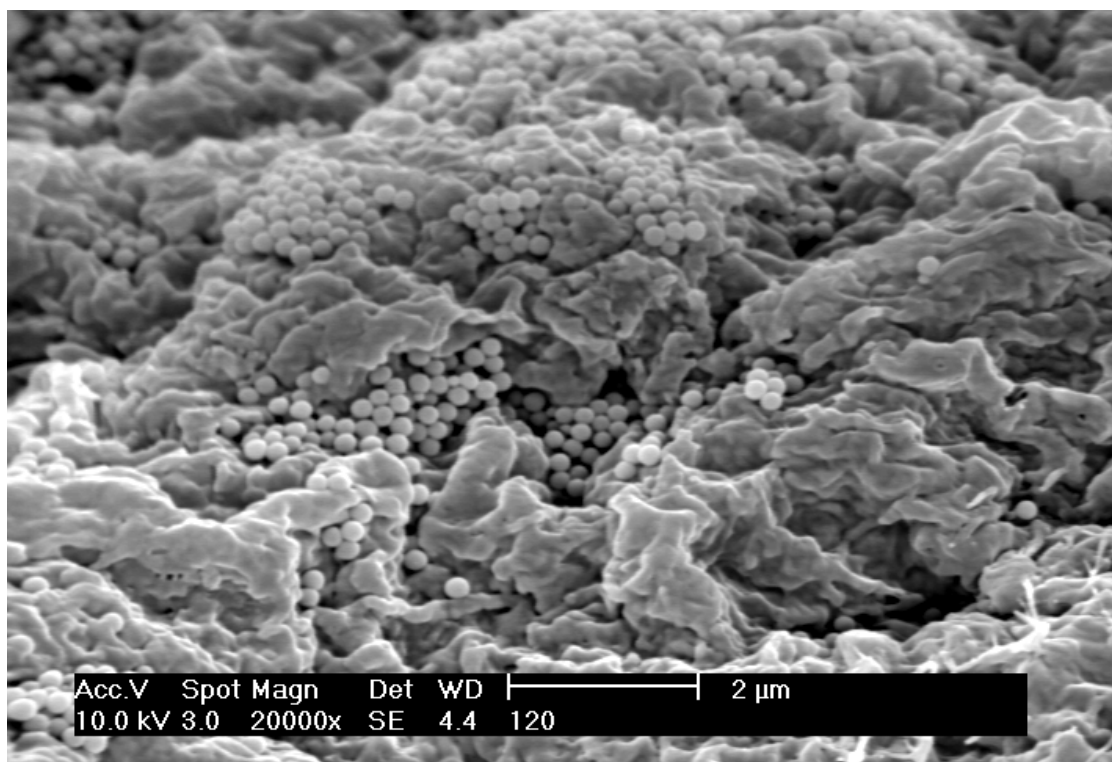


Fig. 24: SEM micrograph of M250-filled sPP synthesized at a propylene concentration of 0.6 mol/l .



**Fig. 25:** SEM micrograph of M250-filled PP synthesized at a propylene concentration of 3,5 mol/l .

It is obvious that the propylene concentration has only a minor effect on the activity, the melting point, and the coverage of M250, but a distinct effect on the molecular weight.

To determine whether the number of active centers on the monospher surface had any influence on their coverage with polypropylene during the subsequent polymerization, the metallocene amount applied to the M250/MAO was reduced to slow down polymer formation.

It is clearly seen from Tab. 3 (entries 3-5), that the activity remained approximately constant as long as the catalyst amount was reduced to not less than  $6.6 \cdot 10^{-7}$  mol. Upon a further reduction to  $3.2 \cdot 10^{-7}$  mol, the activity diminished to only 1,100  $\text{kg}_{\text{Pol}}/(\text{mol}_{\text{Zr}} \cdot \text{h} \cdot \text{mol}_{\text{Mon}}/\text{l})$ , as compared to 2,300  $\text{kg}_{\text{Pol}}/(\text{mol}_{\text{Zr}} \cdot \text{h} \cdot \text{mol}_{\text{Mon}}/\text{l})$  for the initially used fourfold amount of catalyst, even though the activity is normalized to the metallocene amount. The melting points were in the range from 139-141 °C for all investigated catalyst amounts. The envelopment of the silica spheres, however, could not be improved by this method as can be seen from Fig. 26 showing an sPP/M250 nanocomposite synthesized with a catalyst amount of only  $3.2 \cdot 10^{-7}$  mol. The filler content of this nanocomposite was 21 %.

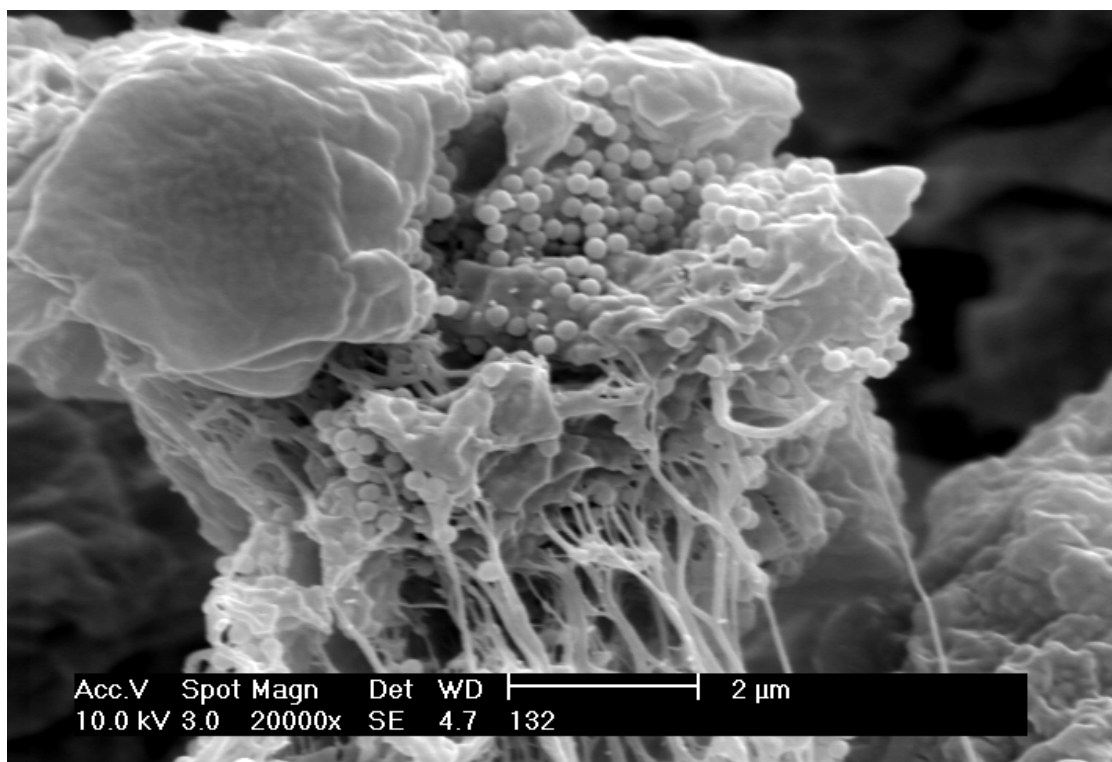


**Fig. 26:** SEM micrograph of M250-filled PP synthesized with a metallocene amount of  $3,2 \cdot 10^{-7}$  mol.

As discussed above, the variation of polymerization temperature, monomer concentration and metallocene amount did partly affect the polymer properties such as melting temperature and molecular weight and the polymerization activity; whereas, no distinct effect on the quality of the envelopment of the silica spheres was observed. It was concluded that a good dispersion of the M250 and adhesion of the polypropylene to the fillers could possibly be inhibited by interactions of the growing polymer chain with the solvent present during the polymerizations.

#### 6.2.4 Gasphase Polymerizations

To prevent interactions between the polymer chains and the solvent, and thus facilitate the envelopment of the silica-spheres, it was decided to perform the subsequent polymerizations of propylene in a stirred-bed gasphase reactor. The propylene concentration was set to 0.2 mol/l and the catalyst amount to  $7 \cdot 10^{-6}$  mol. The activity of  $300 \text{ kg}_{\text{Pol}}/(\text{mol}_{\text{Zr}} \cdot \text{h} \cdot \text{mol}_{\text{Mon}}/\text{l})$  that could be reached employing these polymerization conditions lies well below that for the slurry polymerization ( $2,300 \text{ kg}_{\text{Pol}}/(\text{mol}_{\text{Zr}} \cdot \text{h} \cdot \text{mol}_{\text{Mon}}/\text{l})$ ). In contrast, the melting point of  $141 \text{ }^\circ\text{C}$  lay in the same range as the melting point for slurry polymerizations with M250/MAO/1 at  $30 \text{ }^\circ\text{C}$  and 1.4 mol/ propylene. A filler content as high as 40 to 45 % could be realized in these gasphase polymerizations. More importantly, a good dispersion of M250 in the polymer matrix was achieved in the gasphase polymerization of propylene with M250/MAO/1. It is



evident from Fig. 27 and Fig. 28, that almost all nanospheres are well covered with polymer, and that the M250 are hardly aggregated. They are well dispersed throughout the whole matrix.

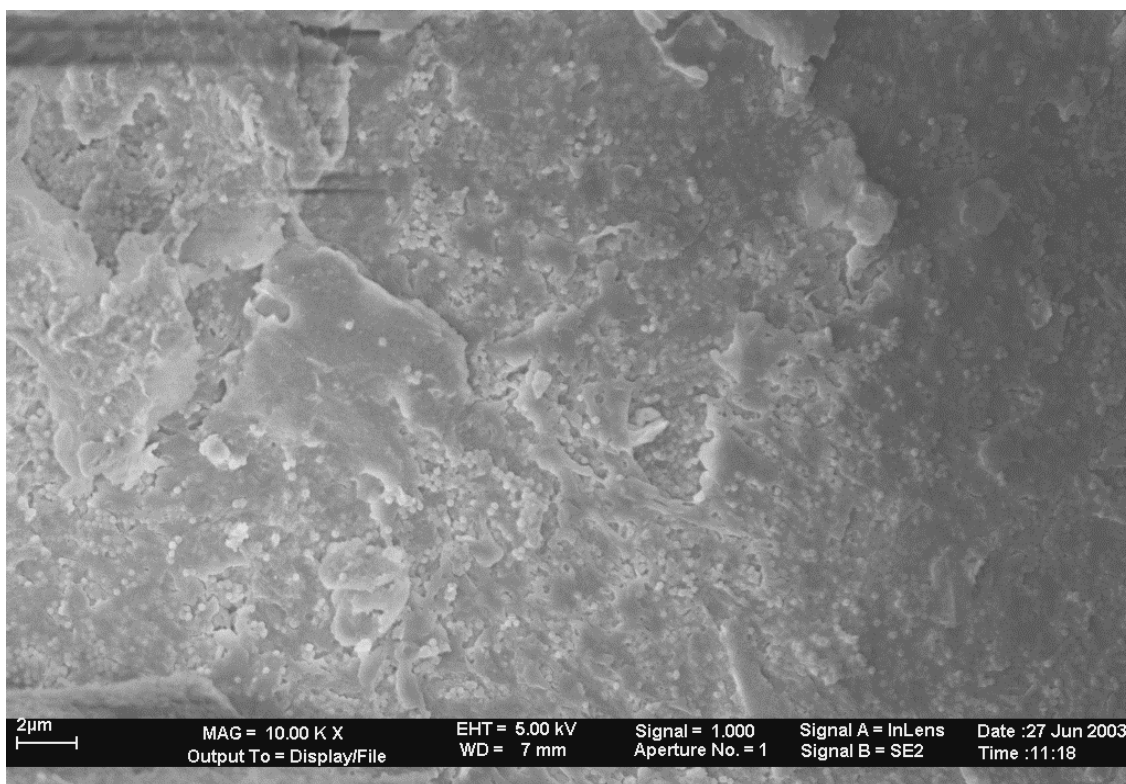


**Fig. 27:** SEM micrograph of M250-filled sPP synthesized in a gas phase polymerization.

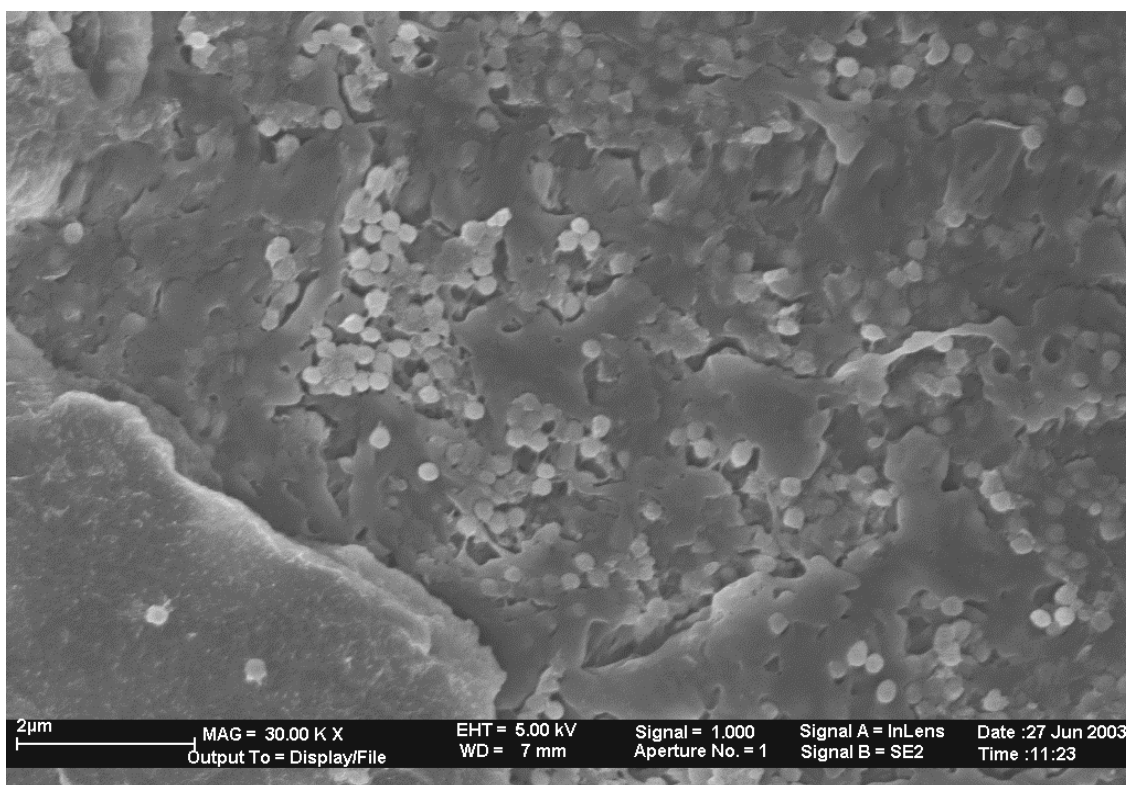


**Fig. 28:** SEM micrograph of M250-filled sPP synthesized in a gas phase polymerization.



The good results in the gasphase polymerization of propylene with M250/MAO/1 led to analogous polymerizations with *rac*-[Et-(IndH<sub>4</sub>)<sub>2</sub>]ZrCl<sub>2</sub>. The polymerization was carried out at 30 °C for 60 min with a metallocene amount of  $6.25 \cdot 10^{-6}$  mol. The propylene concentration remained the same (0.2 mol/l) and 0.55 g M250/MAO prepared as described above were used as cocatalyst.

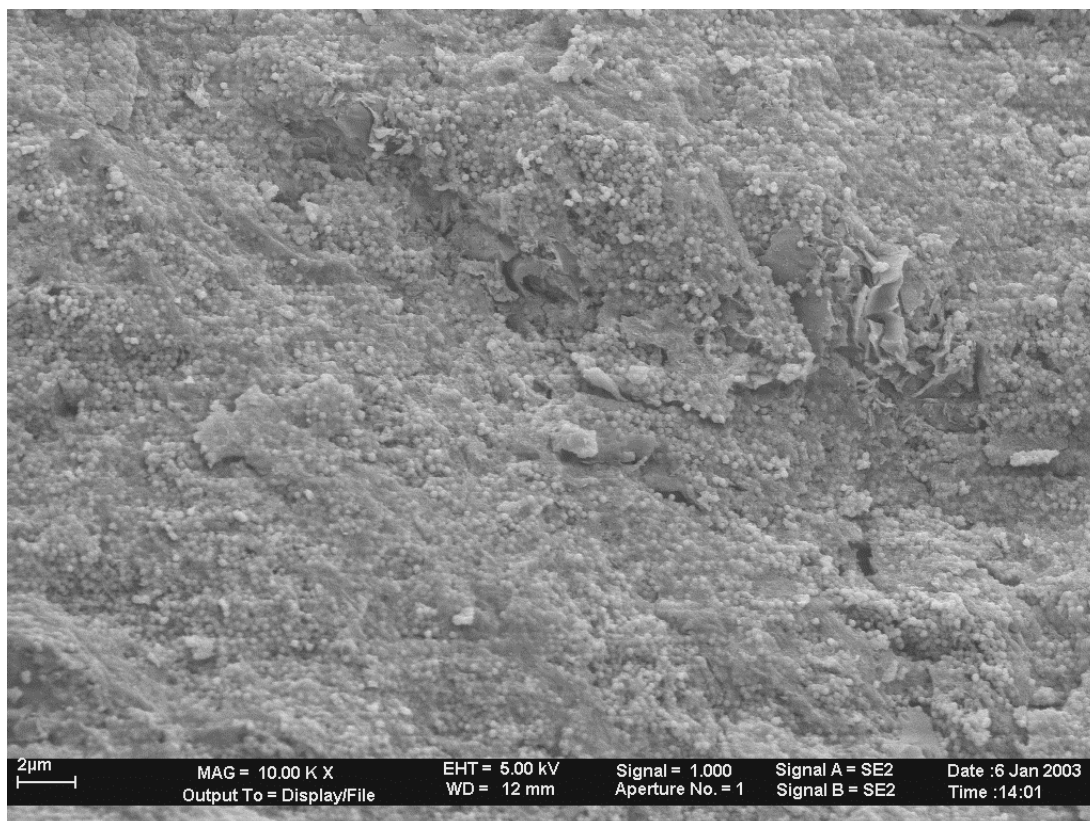


**Fig. 29: SEM micrograph of M250-filled iPP synthesized in a gas phase polymerization with *rac*-[Et-(IndH<sub>4</sub>)<sub>2</sub>]ZrCl<sub>2</sub>.**

With this system, an activity of  $400 \text{ kg}_{\text{Pol}}/(\text{mol}_{\text{Zr}} \cdot \text{h} \cdot \text{mol}_{\text{Mon}}/\text{l})$  and a maximum loading of 60 wt-% could be reached. The melting temperature of the isotactic polypropylene nanocomposite containing 50% monosphers was found to be 138 °C. Fig. 29 shows an electron micrograph (10,000-fold magnification) of this nanocomposite that was taken from a molten sample. The dispersion of the silica spheres in the isotactic polypropylene matrix is very even. Fig. 30 shows an electron micrograph (50,000-fold magnification) of the same composite without melting before the shot. A very good dispersion of the monosphers in the polymer matrix is obvious, as well as an even better coverage than in the case of the syndiotactic polypropylene/M250 nanocomposite produced with M250/MAO/1. The thickness of the polypropylene layer covering the monosphers can be approximated to lie between 30 and 100 nm.

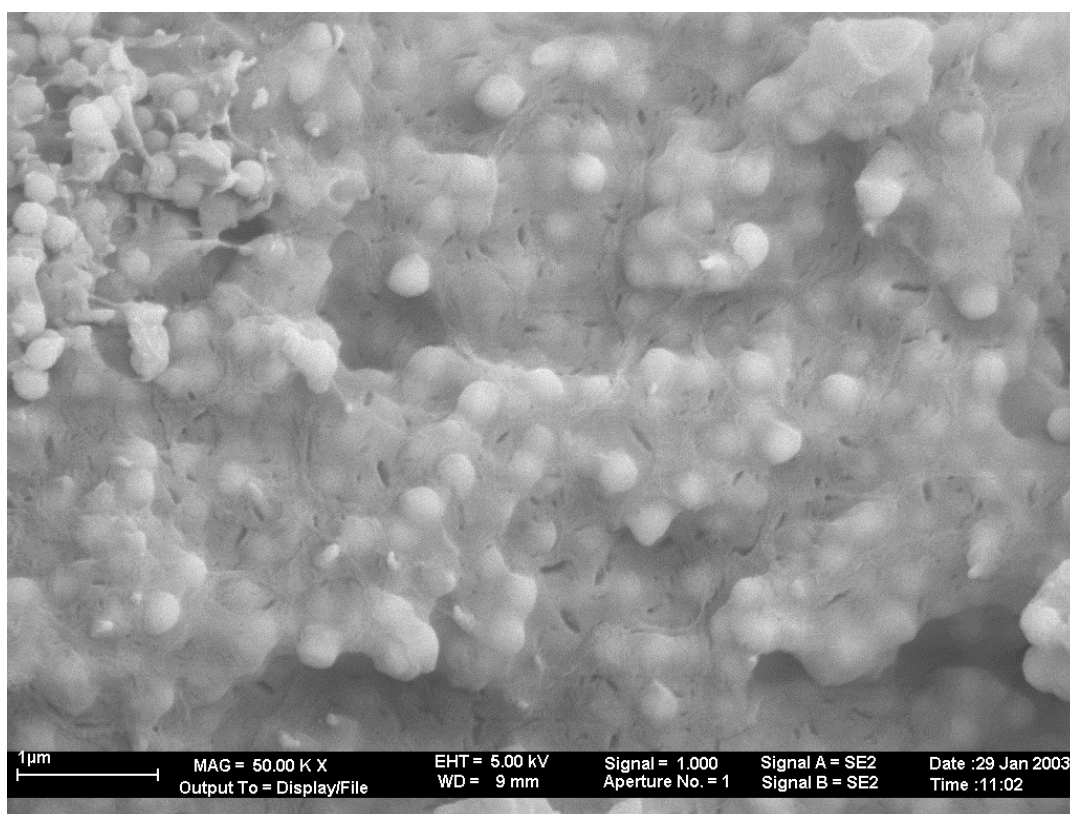


**Fig. 30:** SEM micrograph of M250-filled PP synthesized in a gas phase polymerization with *rac*-[Et-(IndH<sub>4</sub>)<sub>2</sub>]ZrCl<sub>2</sub>.

### 6.3 Polypropylene/Glass Fiber Nanocomposites

PP/GF composites have been prepared by *in situ* polymerization of propylene in the presence of pre-treated glass fibers before<sup>[83]</sup>. First, the GF were subjected to treatment with MAO that was followed by quenching with acidified ethanol and drying. 9-Decen-1-ol and MAO were added to these fibers, and then propylene was copolymerized with the alcohol on the fiber surface. Clusters and layers of PP on the surface were obtained, depending on the amount of alcohol used. The PP close to the GF could not be extracted with hot heptane, indicating a good interfacial adhesion.

In this work, a different approach was used. The cocatalyst for the performed slurry polymerizations was prepared by impregnation of glass fibers with MAO. Before the impregnation, some of the glass fibers were pretreated with sodium hydroxide as described in the experimental section to improve the adhesion of the polypropylene matrix to the glass fibers. These glass fibers were then used as cocatalysts for the subsequent slurry polymerizations of propylene with *rac*-[Et-(IndH<sub>4</sub>)<sub>2</sub>]ZrCl<sub>2</sub> (**2** in scheme 1).

When the polymerization was carried out with those glass fibers that had not been treated with KOH, the activity was about 600 kg<sub>Pol</sub>/(mol<sub>Zr</sub>·h·mol<sub>Mon</sub>/l) and the melting temperature was approximately 140 °C. As can be seen from Fig. 31, the resulting composite with a glass fiber content of around 20 weight-% was very heterogeneous, and hardly any glass fibers were covered by the polymer matrix.

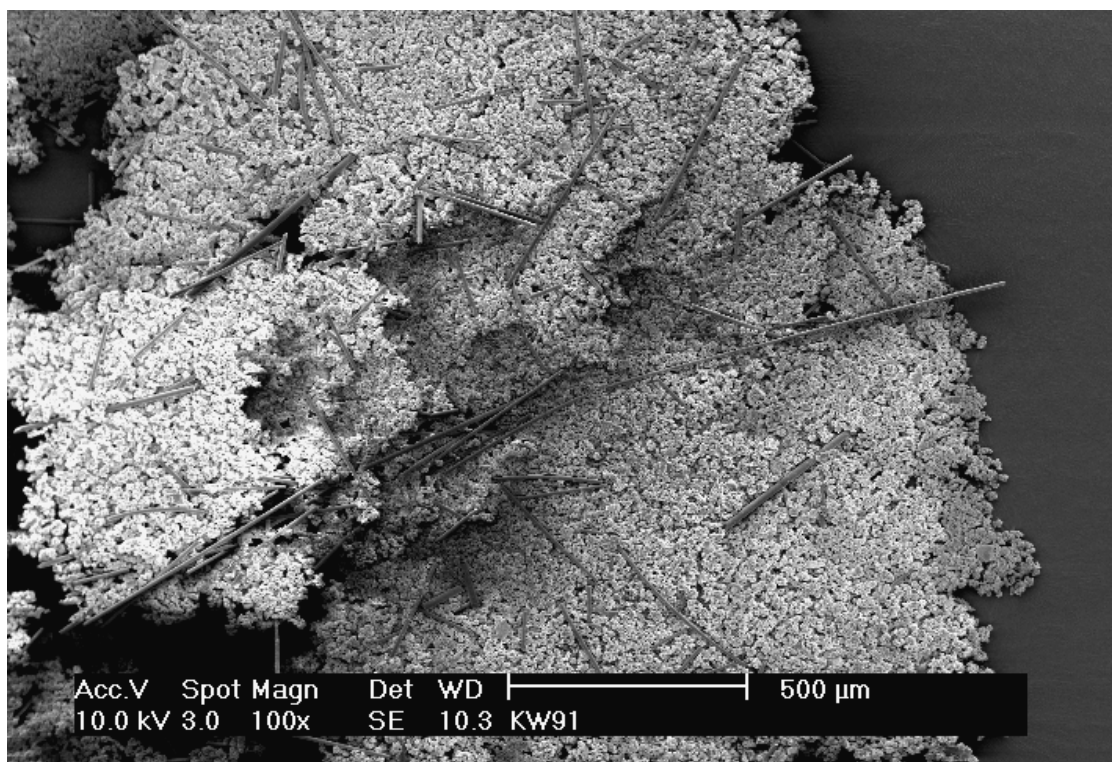


Fig. 31: SEM micrograph showing an iPP composite prepared from untreated glass fibers.

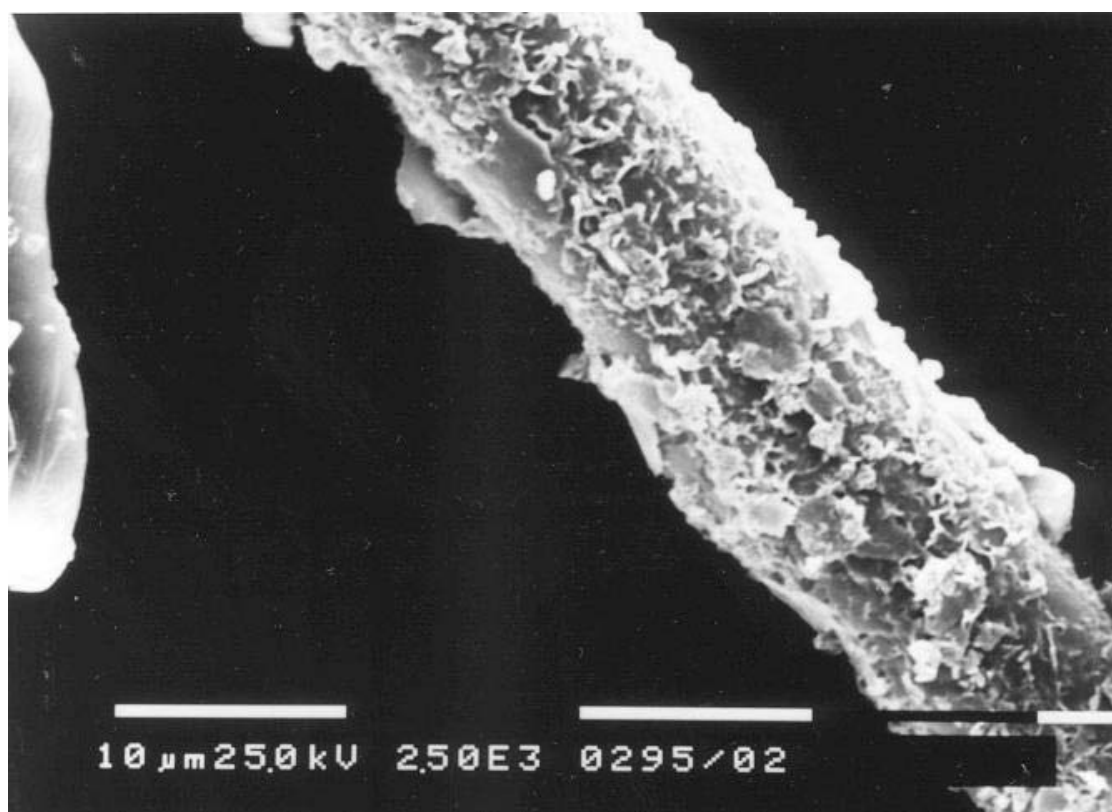
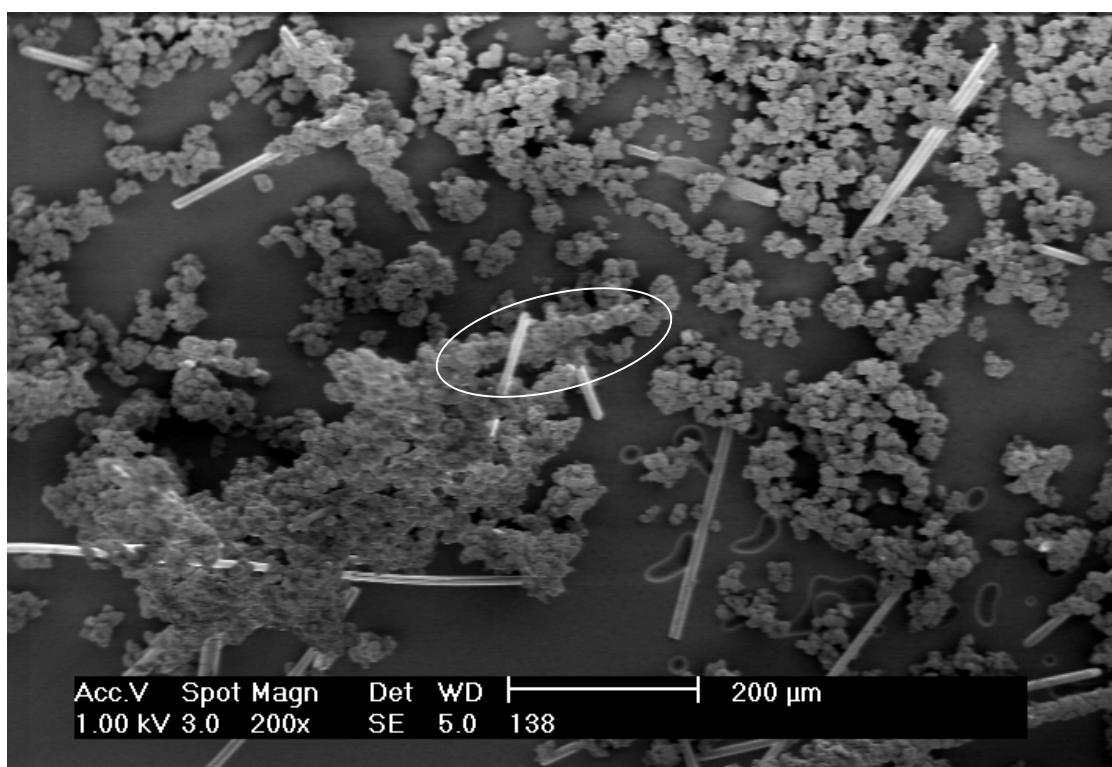


Fig. 32: Glass fiber after treatment with hot KOH solution (magnification 2500x, 1dash corresponds to 10μm).

To improve the interfacial adhesion, the glass fibers were pretreated with a KOH solution before reaction with the MAO. The aim was to roughen the surface of the glass fibers in order

to make it more accessible for the MAO and eventually for the polymer. Fig. 32 shows a glass fiber that has been treated with KOH. The rough surface is well visible. In contrast to that, the surface before the treatment with KOH was smooth.

Using a relatively low concentration of the potassium hydroxide solution, a cocatalyst (GF/MAO) was prepared showing approximately the same activity as the one that had been prepared without the KOH treatment. In a composite containing 10 wt-% GF, a lot of the polypropylene was still not attached to the glass fibers as Fig. 33 shows. Compared to the composite prepared with un-prereacted glass fibers, a definite improvement is visible. Indicated by the white ellipse is a fiber that is completely covered with polymer, for example. At a 5000-fold magnification (Fig. 34), the roughened surface of the glass fibers can be seen. The polymer is mostly attached to the surface of the filler in this case.



**Fig. 33: SEM micrograph showing an iPP composite prepared from glass fibers that had been treated with 1 molar KOH solution (magnification: 200x).**

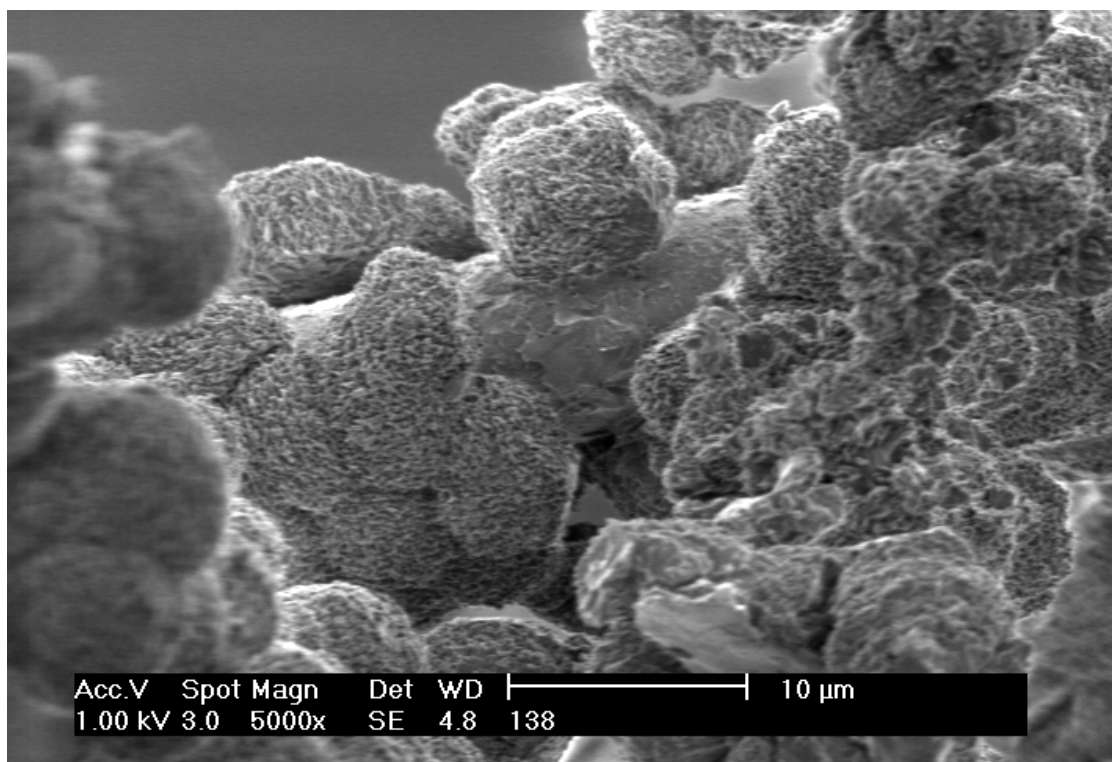


**Fig. 34:** SEM micrograph showing an iPP composite prepared from glass fibers that had been treated with 1 molar KOH solution (magnification: 5000x).

To further improve the interfacial properties of the composite, a higher concentration of 2.5 mol/l KOH was chosen for the treatment of the glass fibers prior to their impregnation with MAO. There was no effect on the activity, which remained unchanged around  $600 \text{ kg}_{\text{Pol}}/(\text{mol}_{\text{Zr}} \cdot \text{h} \cdot \text{mol}_{\text{Mon}}/\text{l})$ . However, the coverage of the glass fibers with the polymer was very much improved (Fig. 35 and Fig. 36). For a composite containing 20 wt-% GF, almost all fibers appear to be wrapped in polypropylene at a 150-fold magnification. Hardly any fiber surfaces without polymer are to be seen. The bigger magnification shows an example of the complete coverage of one of the fibers with polymer.

This supports the theory that the MAO reacts directly with the filler surface to form a heterogeneous cocatalyst for olefin polymerization. After addition of the metallocene, the active polymerization catalyst would thus be anchored to the filler surface and could start the polymerization of propylene directly from the surface of the glass fibers, leading to a good coverage of the filler with the iPP.

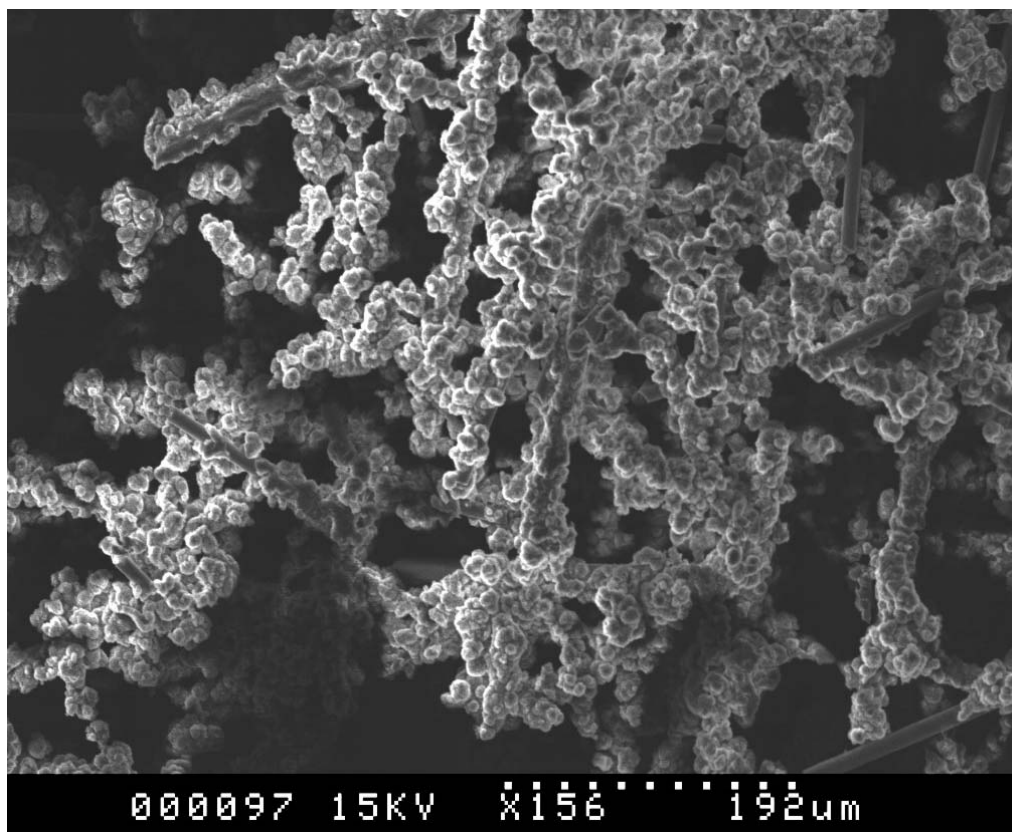


Fig. 35: SEM micrograph showing an iPP composite prepared from glass fibers that had been treated with 2.5 molar KOH solution (magnification: 150x).

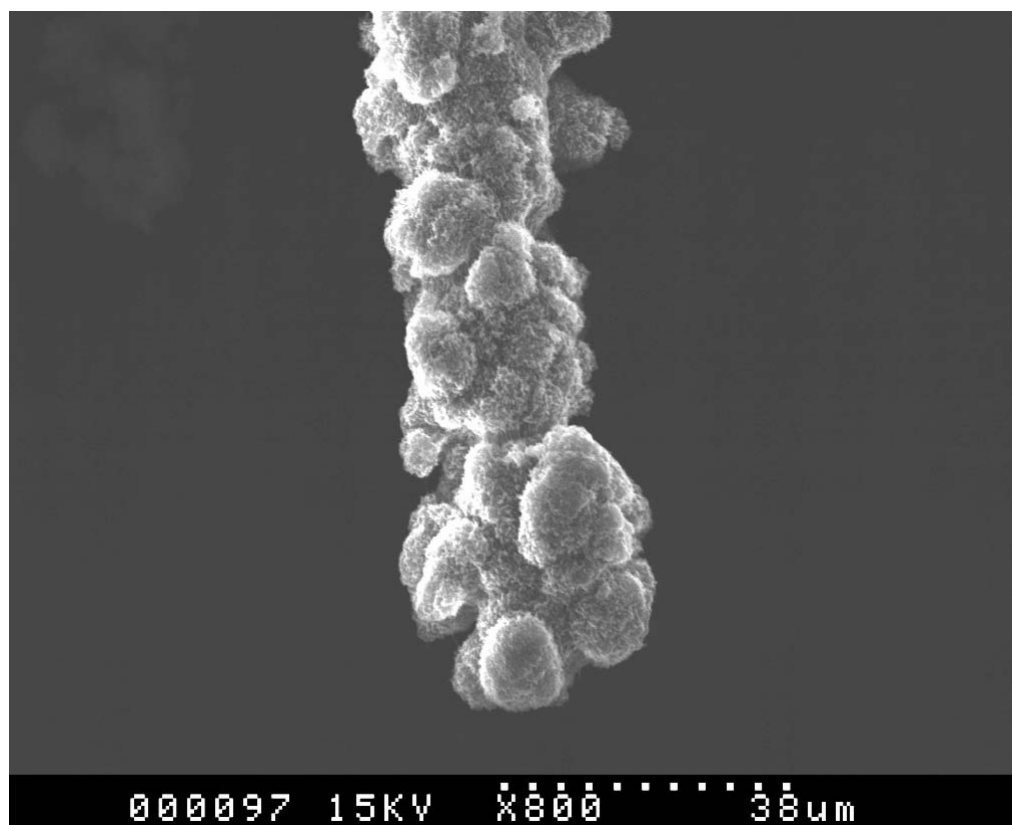


Fig. 36: SEM micrograph showing an iPP composite prepared from glass fibers that had been treated with 2.5 molar KOH solution (magnification: 800x).

The above pictures show that iPP/GF composites were successfully prepared by *in situ* polymerization of propylene with the metallocene *rac*-[Et-(IndH4)<sub>2</sub>]ZrCl<sub>2</sub> and a cocatalyst synthesized from glass fibers and MAO. The best results, that is, a uniform coverage of the fillers, were obtained when the glass fibers had been etched with KOH before the reaction with MAO. From the uniform distribution of polymer on the surface, it was concluded that large parts of the cocatalyst were indeed anchored on the surface of the fibers during the polymerization.



## 6.4 Isotactic Polypropylene/Carbon Nanofiber Nanocomposites

iPP/CNF nanocomposites were synthesized after sonication of the fillers with the sonopuls homogenizer based on the results from preliminary experiments by *in situ* polymerizations of propylene with metallocene **2**. The amplitude was varied from 10 to 50 % of the maximum amplitude to determine its influence on the dispersion of the CNFs and the polymer properties. These experiments were performed with and without pre-reaction. In addition to that, the sonication time was varied between 5 and 120 min. The results were then compared to determine the best reaction conditions for the preparation of nanocomposites with different filler contents.

The synthesized nanocomposites with different nanofiber loading were then examined with regard to their crystallization behavior. An investigation of the tensile properties was not performed because it was impossible to obtain films by hot-pressing of the nanocomposite material. Because of the low molecular weight in the range of 40,000 to 50,000 g/mol, the polymer melt had a very low viscosity. Moreover, the strain in the polymer films upon cooling became strong enough to break the films into pieces.

One film of an iPP/CNF nanocomposite containing 1 % carbon nanofibers could be obtained that was big enough to perform conductivity measurements, but no conductivity was observed for this filler content.

### 6.4.1 Dispersion of the Carbon Nanofibers

The influence of the ultrasonic amplitude and the sonication time on the dispersion of the carbon nanofibers was investigated. These experiments were performed with and without pre-reaction. The amplitude did not show an influence on the activity of the propylene polymerization, nor did the sonication time, but the pre-treatment of the filler did (see Fig. 37). In experiments without pre-reaction, the activity of between 5,000 and 7,000  $\text{kg}_{\text{Pol}}/(\text{mol}_{\text{Zr}} \cdot \text{h} \cdot \text{mol}_{\text{Mon}}/\text{l})$  lay in the range of that of the polymerizations without filler (average activity: 6,600  $\text{kg}_{\text{Pol}}/(\text{mol}_{\text{Zr}} \cdot \text{h} \cdot \text{mol}_{\text{Mon}}/\text{l})$ ). In contrast to that, the activity in polymerizations with pre-reaction lay much below that of propylene polymerizations without filler. It was only 1,000 to 2,000  $\text{kg}_{\text{Pol}}/(\text{mol}_{\text{Zr}} \cdot \text{h} \cdot \text{mol}_{\text{Mon}}/\text{l})$ .

This could be due to a partial destruction of the MAO during the pre-reaction with the CNFs. Any impurities present on the surface of the carbon nanofibers could react with the MAO, thereby reducing the amount of MAO present for the activation of the catalyst. Another possible reason is the more complex polymerization process that involves several steps in which the catalyst could come in contact with air. As only  $9 \cdot 10^{-7}$  mol catalyst were used for the polymerizations, already a small amount of oxygen or other impurities could have a great impact on the activity of the system.

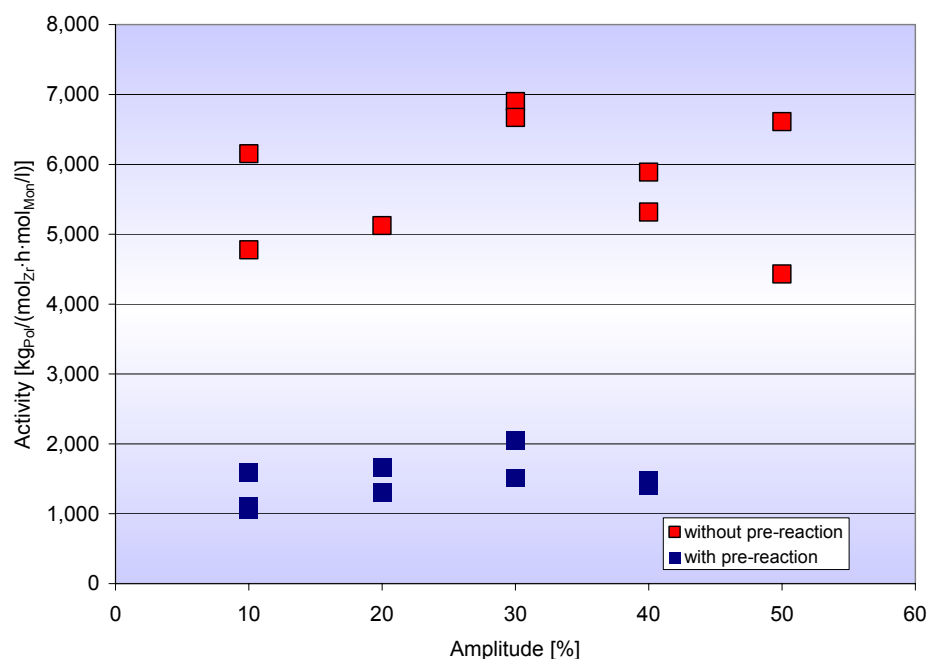
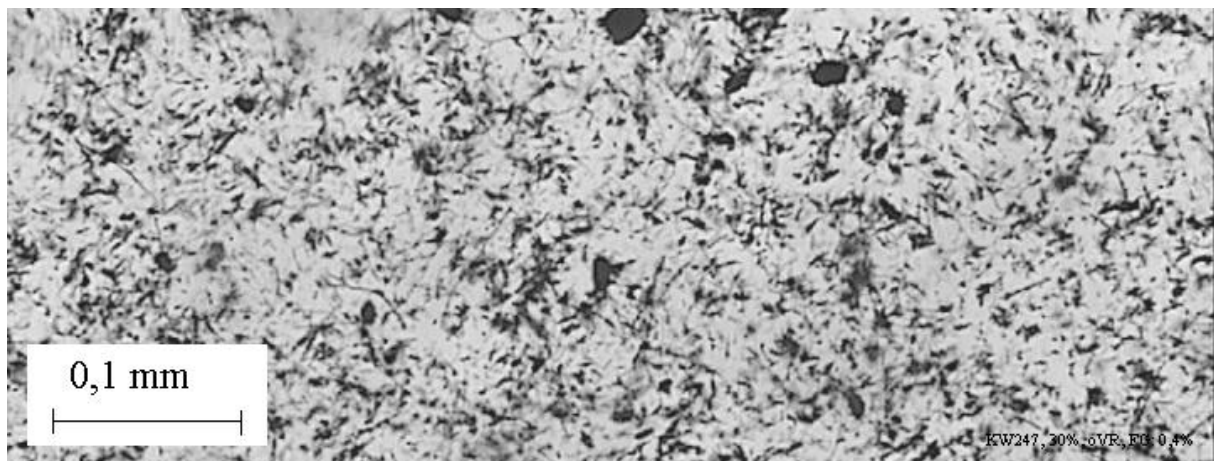
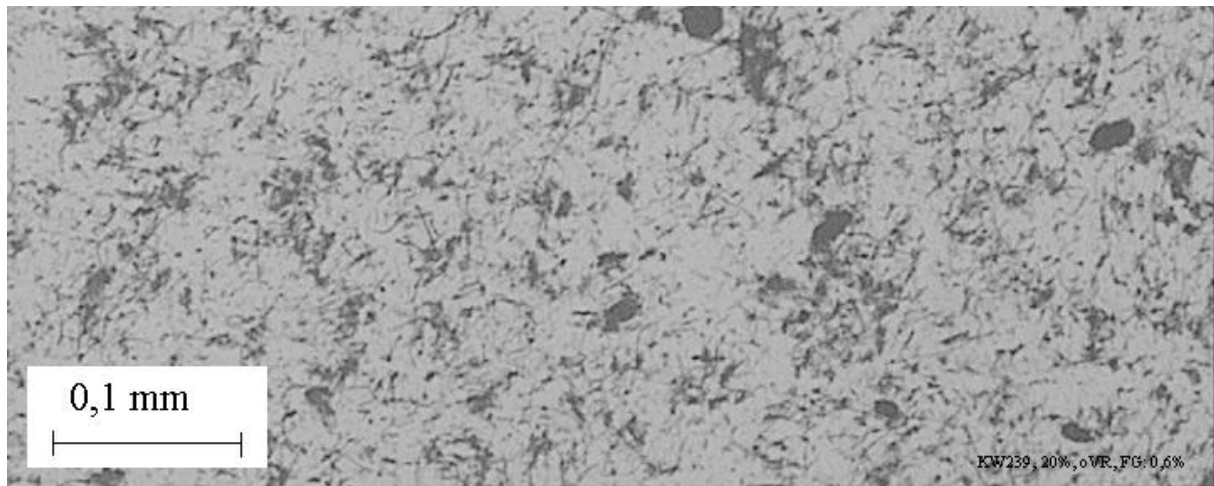
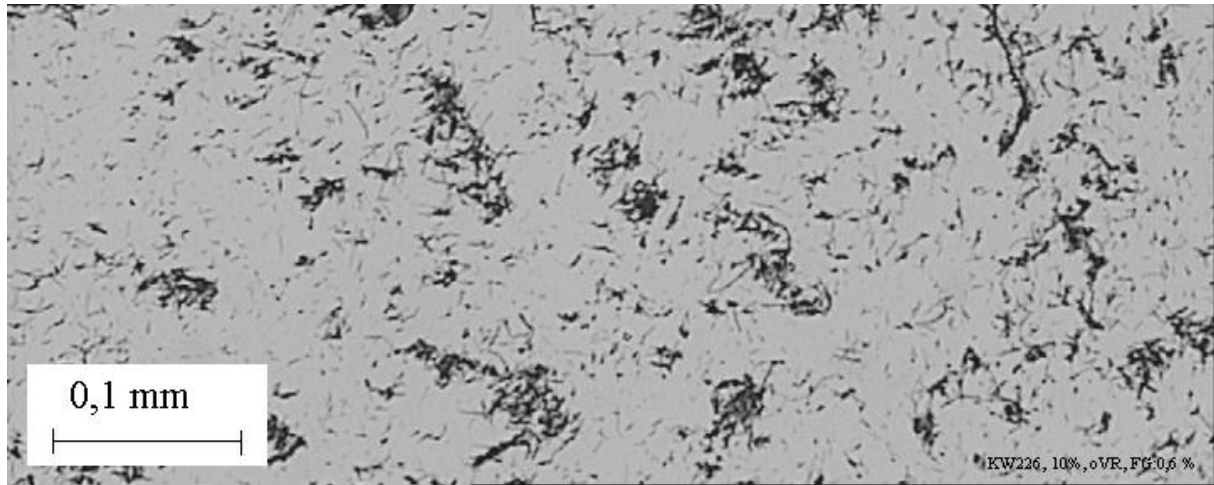


**Fig. 37: Influence of the ultrasonic amplitude and the pre-treatment on the activity of the propylene polymerization.**

The microstructures of some nanocomposites were investigated by NMR experiments to be sure that the isotacticity was close to that of the pure polymer. This was done to exclude differences in polymer microstructure as possible reason for differences in other polymer properties. The amount of mmmm-pentads lay between 87 and 89 % and therefore in the range of that of the neat polymer.

In polymerizations without pre-reaction, the ultrasonic amplitude was varied from 10 % to 50 % of the maximum amplitude. The resulting nanocomposites were examined with regard to the quality of distribution of the CNFs in the polymer matrix by microscopy of the nanocomposite melt. All filler contents lay between 0.4 and 0.6 %. It can be seen from Fig. 38 that the dispersion of the CNFs in the polymer matrix became slightly better when a higher

ultrasonic amplitude was used. An amplitude of 40 % proved to be sufficient to destroy bigger aggregates of carbon nanofibers.



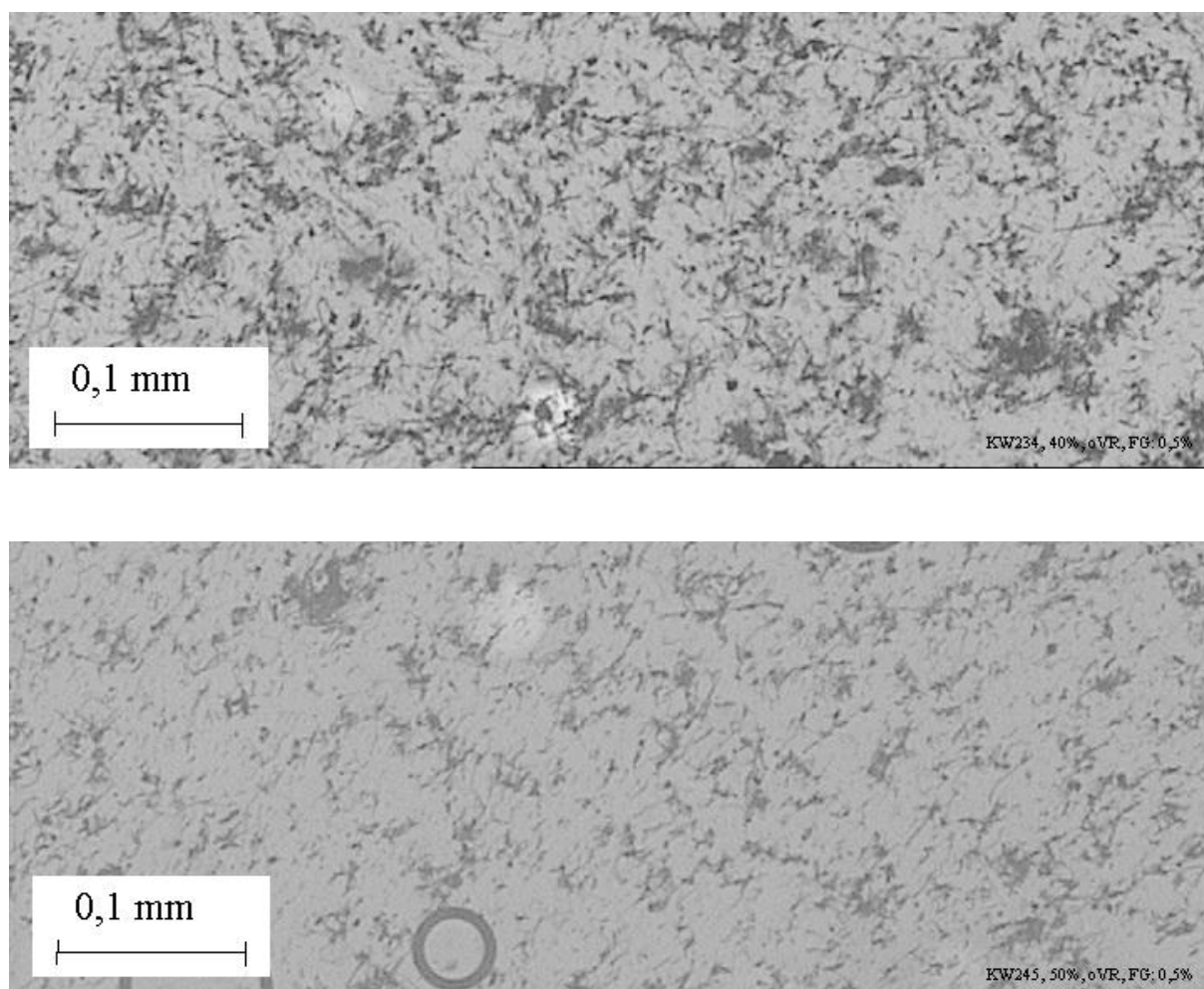


**Fig. 38: Microscopic photographs of iPP/CNF nanocomposites prepared without pre-reaction after ultrasonication with an amplitude of 10 %, 20 %, 30 %, 40 %, and 50 %, respectively.**

The following Fig. 39 shows the dispersion of carbon nanofibers in the polymer matrix of nanocomposites prepared with pre-reaction. Also in this case, a better dispersion was obtained when a higher ultrasonic amplitude was applied. The filler contents of the respective samples lay between 1 and 4 %. At amplitudes of 30 and 40 %, almost no agglomerates of CNFs were detected.

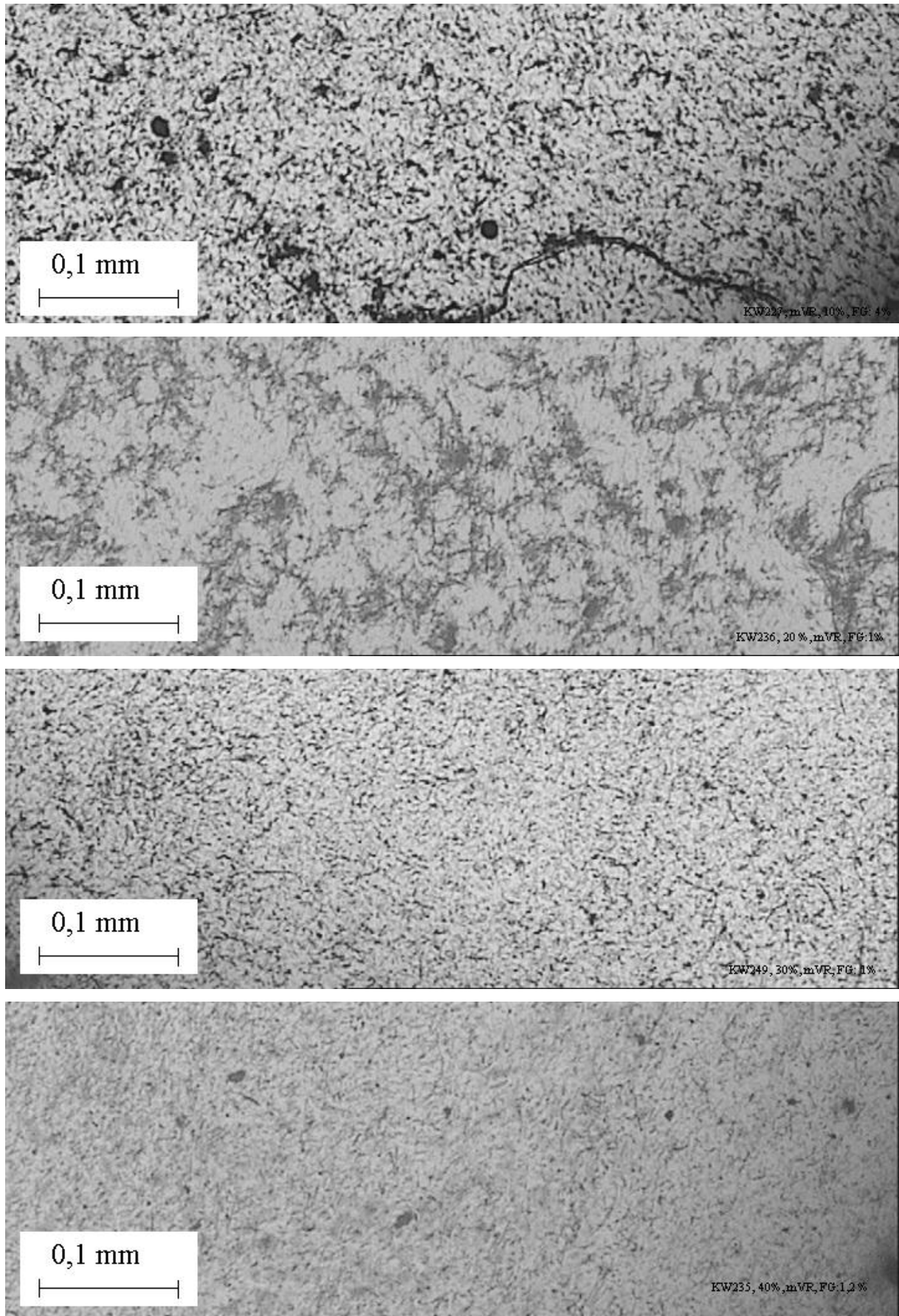


**Fig. 39: Microscopic photographs of iPP/CNF nanocomposites prepared with pre-reaction after ultrasonication with an amplitude of 10 %, 20 %, 30 %, and 40 %, respectively.**



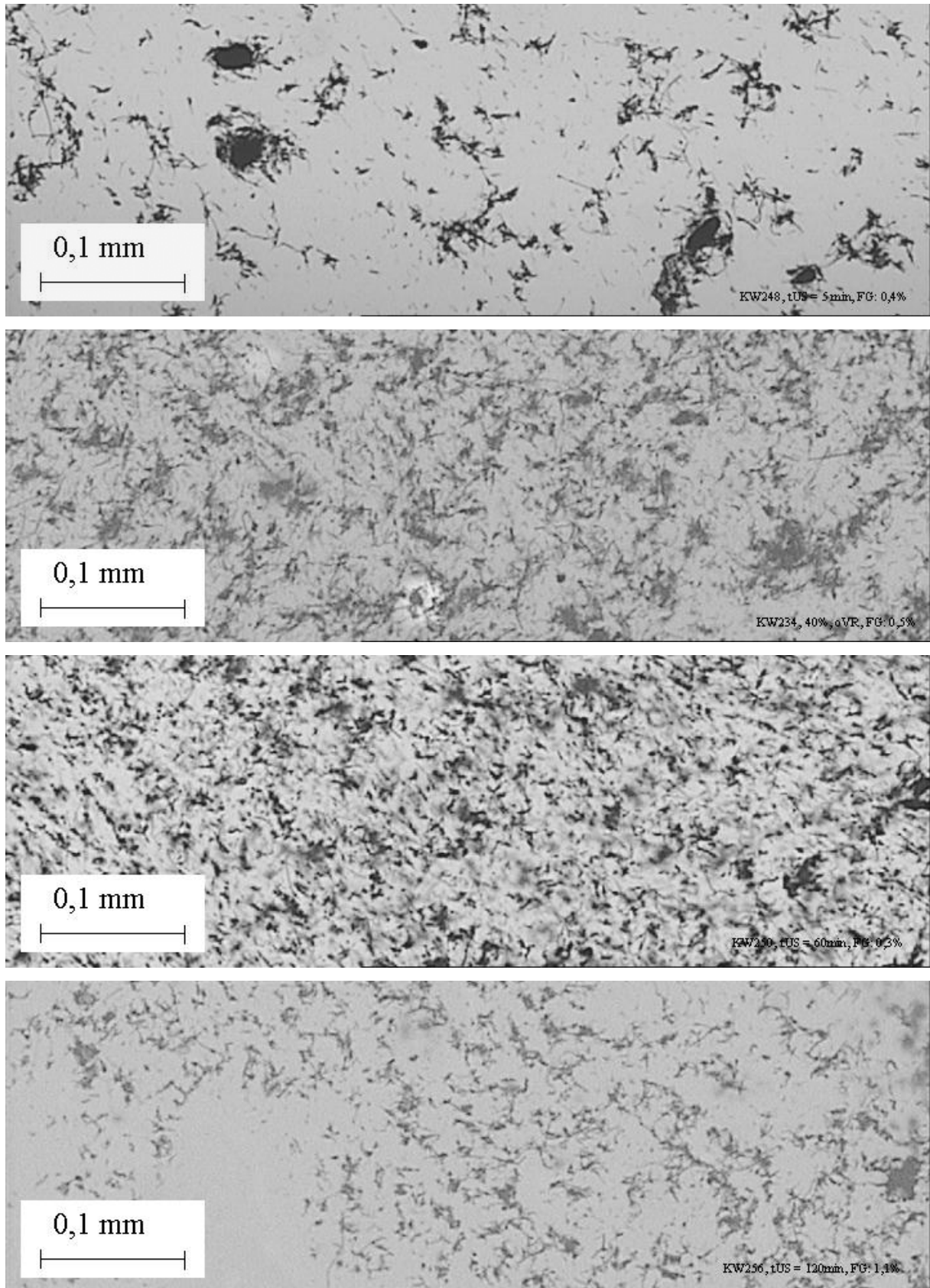


**Fig. 40:** Microscopic photographs of iPP/CNF nanocomposites prepared without pre-reaction after ultrasonication with an amplitude of 40 % for 5, 15, 60, and 120 min, respectively.

Fig. 40 shows microscopic photographs of iPP/CNF nanocomposites prepared without pre-reaction after different sonication times. The CNFs had been sonicated with an ultrasonic amplitude of 40 % for 5, 15, 60, and 120 minutes. It can be clearly seen that the dispersion of the nanotubes improved greatly with increasing sonication time.

From the above results, it was decided to perform the subsequent polymerizations without pre-reaction because the pre-reaction of the nanofibers with MAO did not lead to a significantly better dispersion of the CNFs. Additionally, the activity was much better with this method. The ultrasonic amplitude was set to 20 % and the sonication time to 15 minutes. It has been noted earlier that fillers with a high aspect ratio can be destroyed by the application of extreme forces. Consequently, it was decided to perform the following polymerizations after the pre-treatment described above. Under these conditions, the filler content was varied by incorporation of different amounts of CNFs.

#### **6.4.2 Adhesion of the Polypropylene Matrix to the Carbon Nanofibers**

The adhesion of the isotactic polypropylene to the carbon nanofibers was investigated by SEM of fracture surfaces. The results are shown in the following pictures. Fig. 41 shows a 10,000 times magnification of an iPP/CNF nanocomposite prepared with pre-reaction of the CNFs with MAO after sonication with an ultrasonic amplitude of 20 % for 15 minutes. The picture shows an aggregate of nanofibers. The individual fibers are separated by polymer which is more obvious from Fig. 42 showing a higher magnification (30,000 times) of the same nanocomposite. It can also be seen from this picture, that fiber pull-out has happened to a certain degree which is obvious from the holes in the polymer matrix.

Some of the nanofibers visible on the surface of the polymer are relatively short. This is probably due to damage by the sonication of the fibers before polymerization. Another possible reason is the presence of short fibers in the starting material. These would then show up more often on the surface of the polymer because they are easily pulled out of the PP when this is broken to obtain the surface observable by SEM.

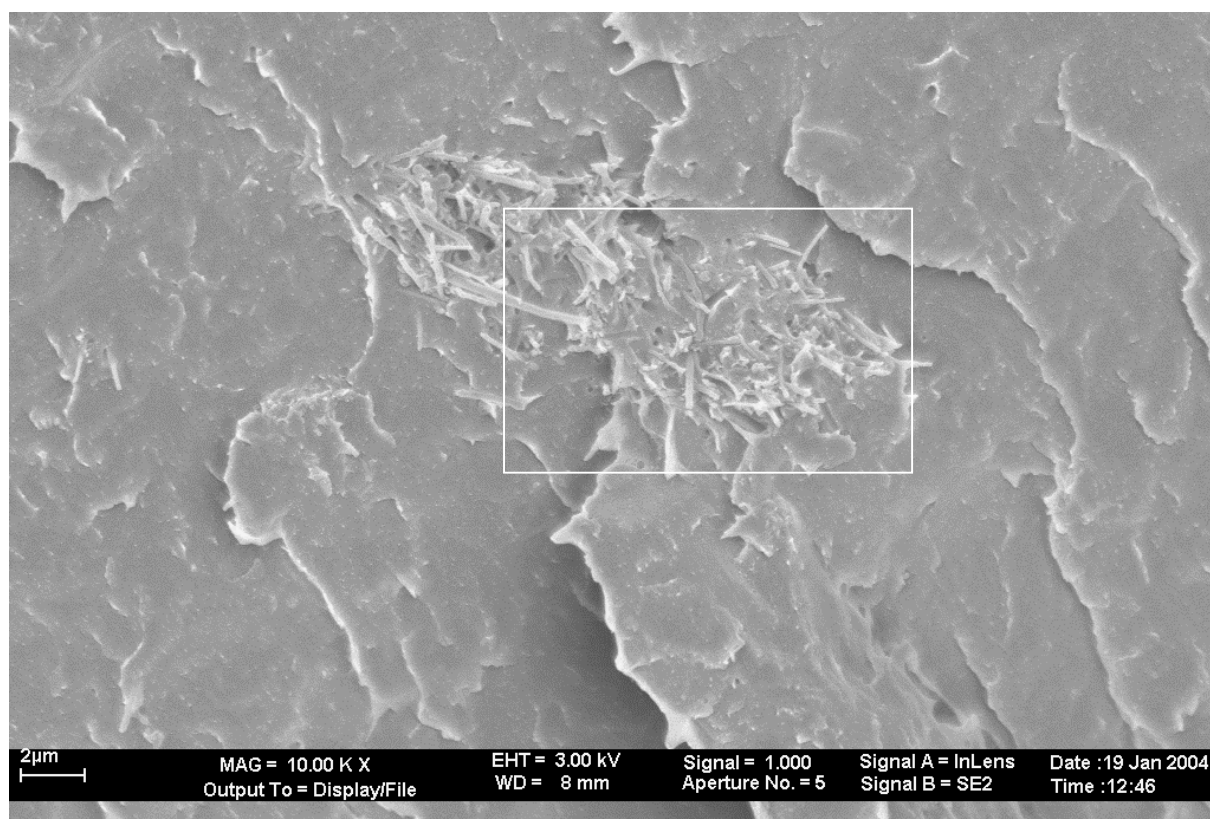


**Fig. 41:** SEM micrograph (magnification 10,000 times) of an iPP/CNF nanocomposite containing 1 % nanofibers prepared with pre-reaction (amplitude 20 %) (KW236).

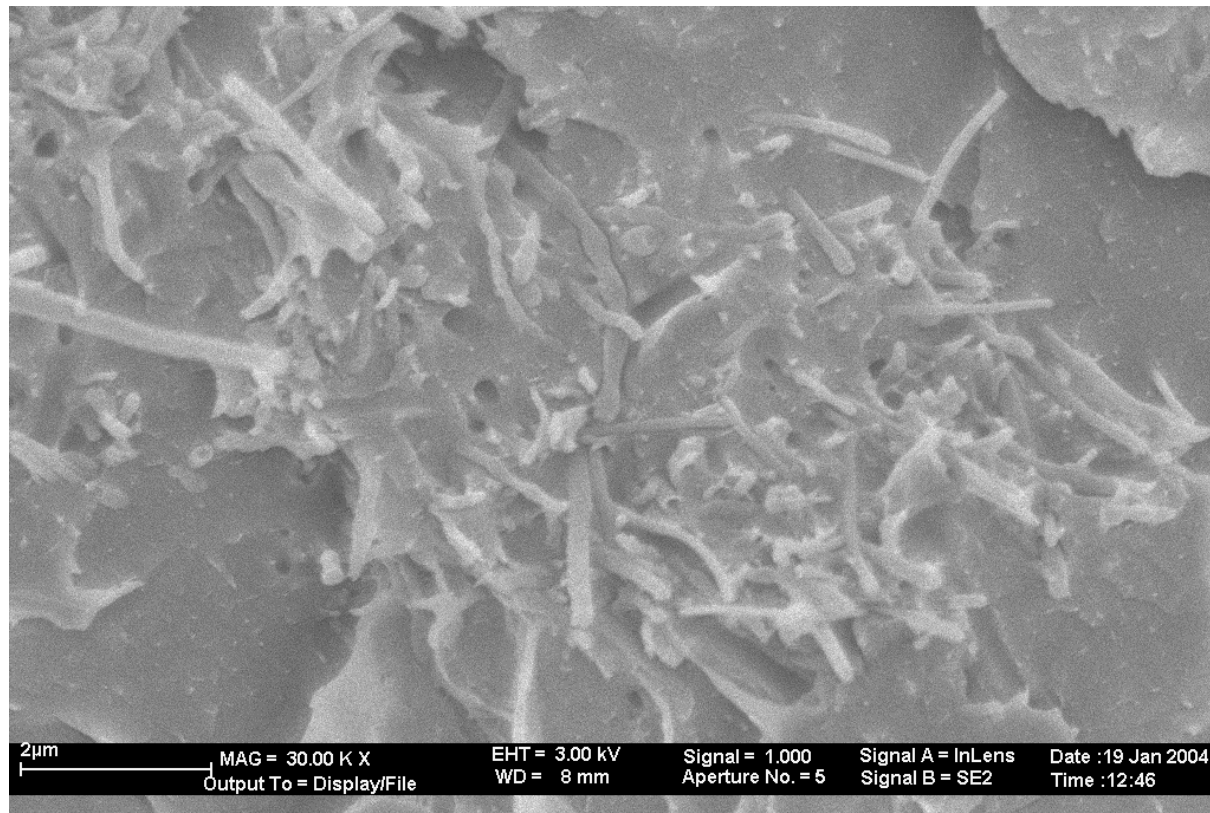


**Fig. 42:** SEM micrograph (magnification 30,000 times) of an iPP/CNF nanocomposite containing 1 % nanofibers prepared with pre-reaction (amplitude 20%) (KW236).



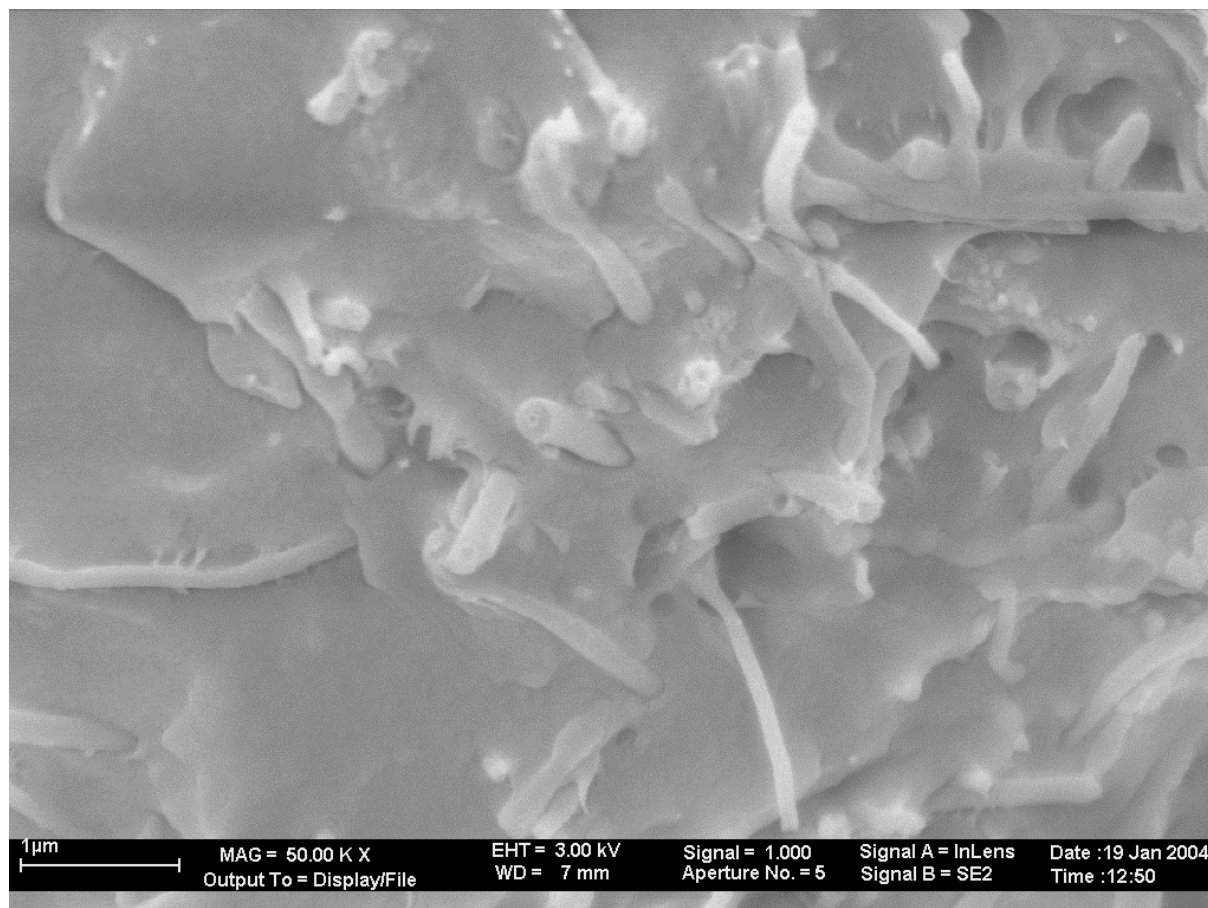


**Fig. 43: SEM micrograph (magnification 50,000 times) of an iPP/CNF nanocomposite containing 0.6 % nanofibers prepared without pre-reaction (amplitude 20 %) (KW239).**

Fig. 43 shows the 50,000 fold magnification of an iPP/CNF nanocomposite prepared without pre-reaction after sonication of the CNFs with an amplitude of 20 % for 15 minutes. Also in this case, fiber pull-out was observed to a certain extent. Some CNFs seem to be relatively short but most of them are still long. Wetting can be seen to some extent but in not very pronounced.

### **6.4.3 Crystallization and Melting Behavior of the iPP/CNF Nanocomposites**

#### **6.4.3.1 Melting Temperature and Crystallinity**

The melting temperatures were in the same range as for the pure iPP having a melting point of 136 °C. The presence of carbon nanofibers did not show any influence on the crystallinity which lay in the same range of that of comparable pure iPP (36 - 39 %).

#### **6.4.3.2 Crystallization Temperature**

In contrast to that, the crystallization temperature was influenced by the presence of the carbon nanofibers (see Fig. 44). The crystallization temperature of the pure isotactic

polypropylene was 104 °C, whereas, the crystallization temperature of the iPP/CNF nanocomposites ranged between 106 and 110 °C. A trend of rising crystallization temperature with rising filler loading was observed, the highest being 110 °C. This fact points to a nucleating effect of the carbon nanofibers.

The increase in crystallization temperature was higher than that found by Sandler et al. They found an 5 °C increase of the crystallization temperature upon addition of 7 % carbon nanofibers<sup>[86]</sup>. The same improvement could be achieved by the addition of only 1 % CNF in this work. This could be due to the different synthesis method used here, possibly leading to a more homogeneous distribution of the CNFs.

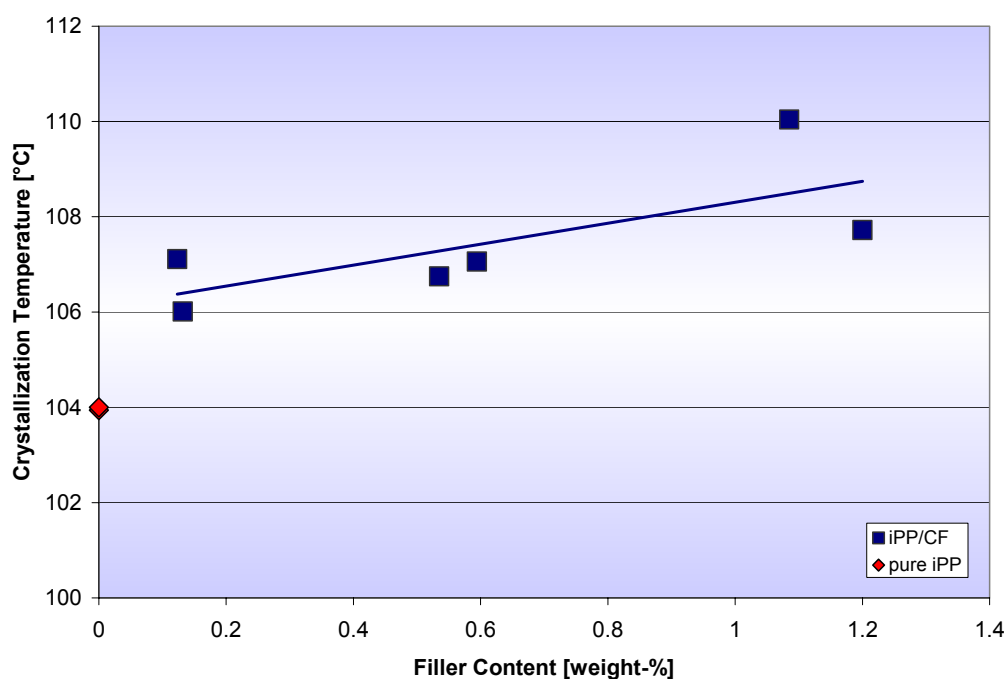


Fig. 44: Influence of the filler content on the crystallization temperature of the iPP/CNF nanocomposites.

#### 6.4.3.3 Half-time of Crystallization

For further proof of this hypothesis, the half-time of crystallization of several iPP/CNF nanocomposites with different filler contents was determined and compared to that of the pure iPP. The results are shown Fig. 45. The half-time of crystallization increased with increasing isothermal crystallization temperature as expected. It is obvious that the half-time of crystallization of the iPP/CNF nanocomposites was largely independent of the filler content of the composite. It was decreased to roughly one-third of the value for pure iPP in all cases.

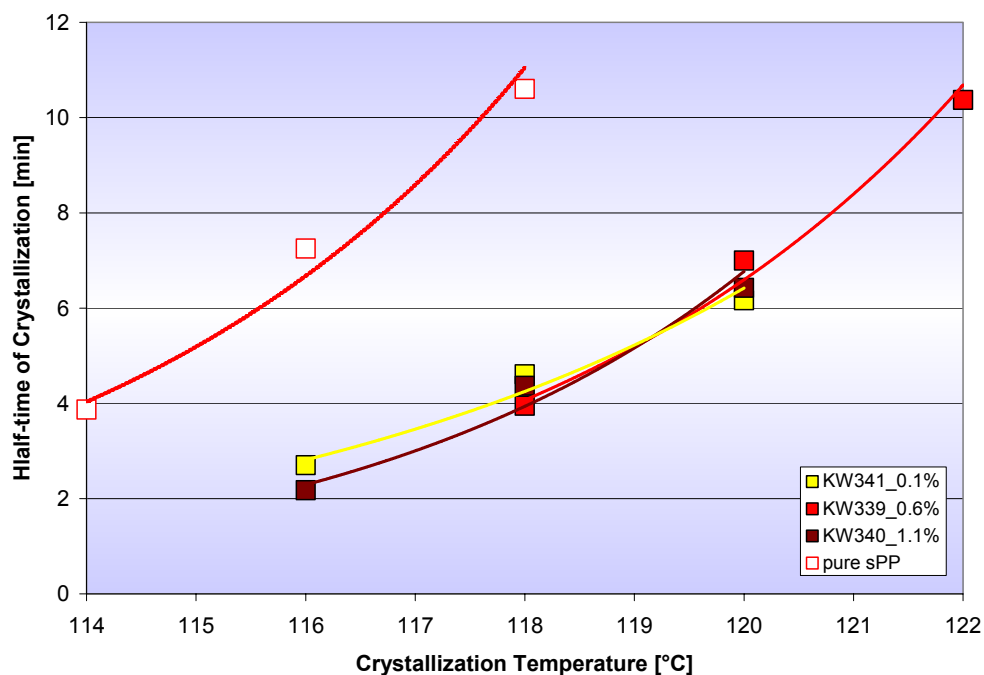


Fig. 45: Influence of the crystallization temperature and the filler content on the half-time of crystallization ( $t_{0.5}$ ) of iPP/CNF nanocomposites.

#### 6.4.3.4 Avrami Analysis

The rate constant of crystallization and the Avrami parameters were determined by Avrami analysis of the data obtained by isothermal crystallization measurements. The influence of the isothermal crystallization temperature and the filler content on the rate constant of crystallization is shown in Fig. 46. It can be clearly seen that the rate of crystallization slowed down with rising crystallization temperature. It is also obvious from the results obtained that the crystallization process was sped up drastically in the presence of higher filler loadings. Already at a filler content of 0.1 %, the rate constant of crystallization at 118 °C was 16 times that of pure iPP, rising to 45 times that value for the iPP/CNF nanocomposite containing 1.1 % carbon nanofibers.

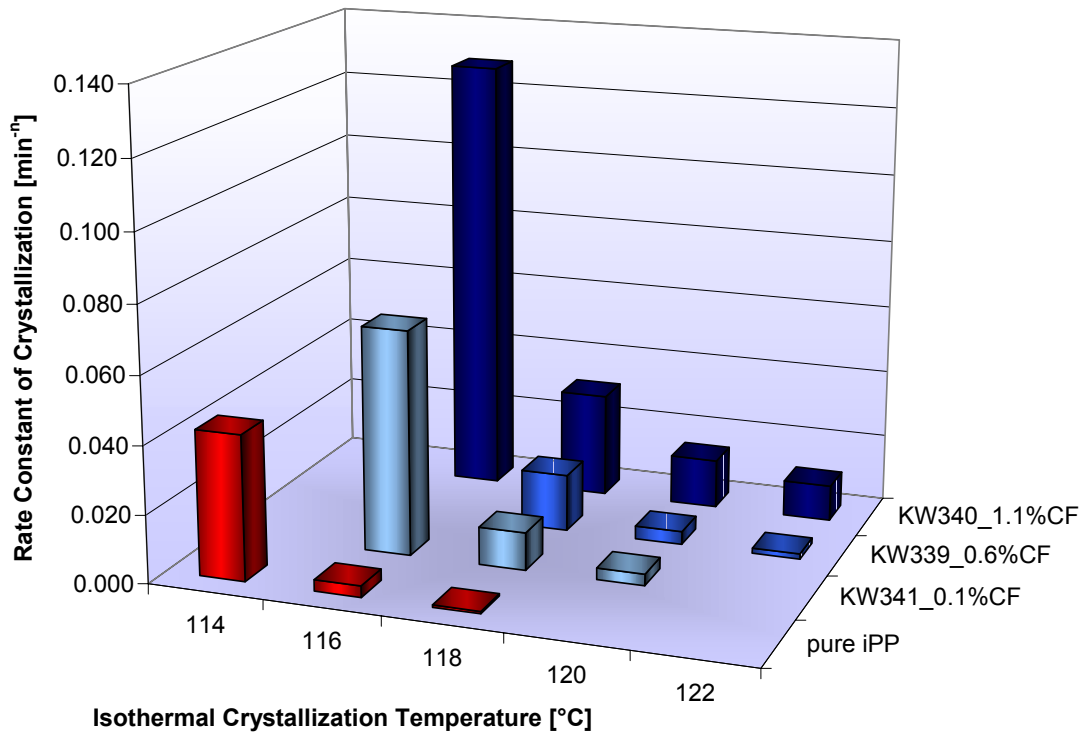


Fig. 46: Influence of the filler content and the isothermal crystallization temperature on the rate constant of crystallization (K) of the iPP/CNF nanocomposites.

## **6.5 Syndiotactic Polypropylene/Carbon Nanofiber Nanocomposites**

Based on the results from the preliminary experiments, sPP/CNF nanocomposites were synthesized by *in situ* polymerization of propylene with metallocene **1** after sonication of the fillers with the sonopuls homogenizer. To determine the influence of the ultrasonic amplitude and the pretreatment on the dispersion of the CNFs and the polymer properties, the former was varied from 10 to 50 % of the maximum amplitude. This set of experiments was performed with and without pre-reaction. The best reaction conditions for the preparation of nanocomposites with different filler contents were determined by comparison of the results. The sPP/CNF nanocomposites with different filler loadings were then examined with regard to their crystallization behavior, their thermal degradation properties, their electrical conductivity, and their tensile properties. In addition to this, the quality of the interfacial adhesion was estimated from SEM micrographs.

### **6.5.1 Dispersion of the Carbon Nanofibers**

Fig. 47 shows microscopic photographs of sPP/CNF nanocomposites. The fillers were sonicated for 15 minutes at an amplitude of 10, 20 or 40 % in a toluene suspension prior to the polymerization. No pre-reaction with MAO took place. The distribution of the CNF (Fig. 47) seemed to be a bit more homogeneous at higher amplitude, but the effect is not very pronounced. The filler content of all samples is approximately 0.5 weight-%. In all cases, agglomerates of CNFs were present. The biggest one can be seen in the nanocomposite prepared with CNFs sonicated at an amplitude of 10 %. It is about 0.04 mm in diameter. The size of the agglomerates became smaller when a higher amplitude was used.

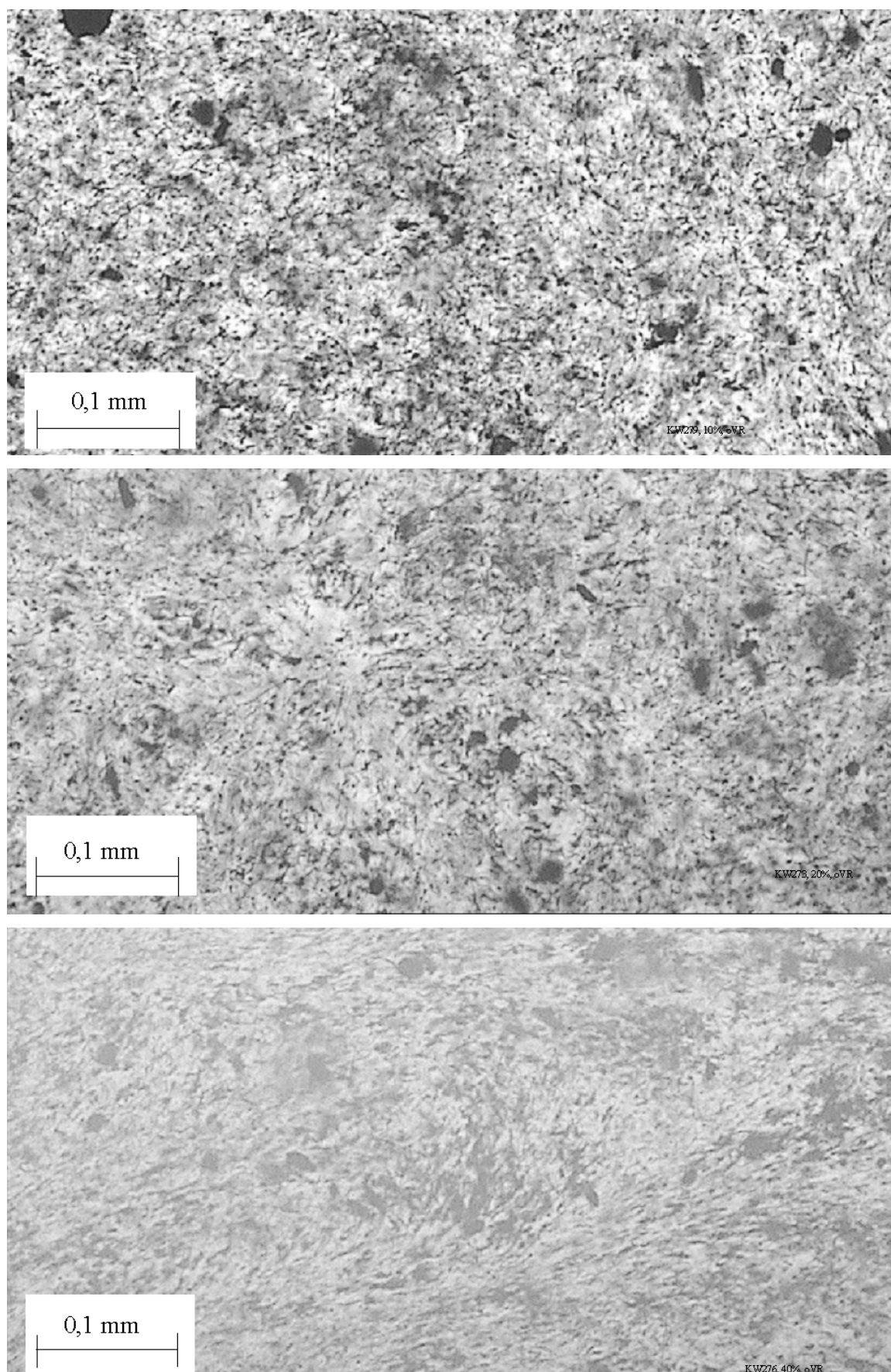


**Fig. 47: Microscopic photographs of sPP/CNF nanocomposites prepared without pre-reaction after sonication of the filler with an ultrasonic amplitude of 10 %, 20 %, and 40 %, respectively.**

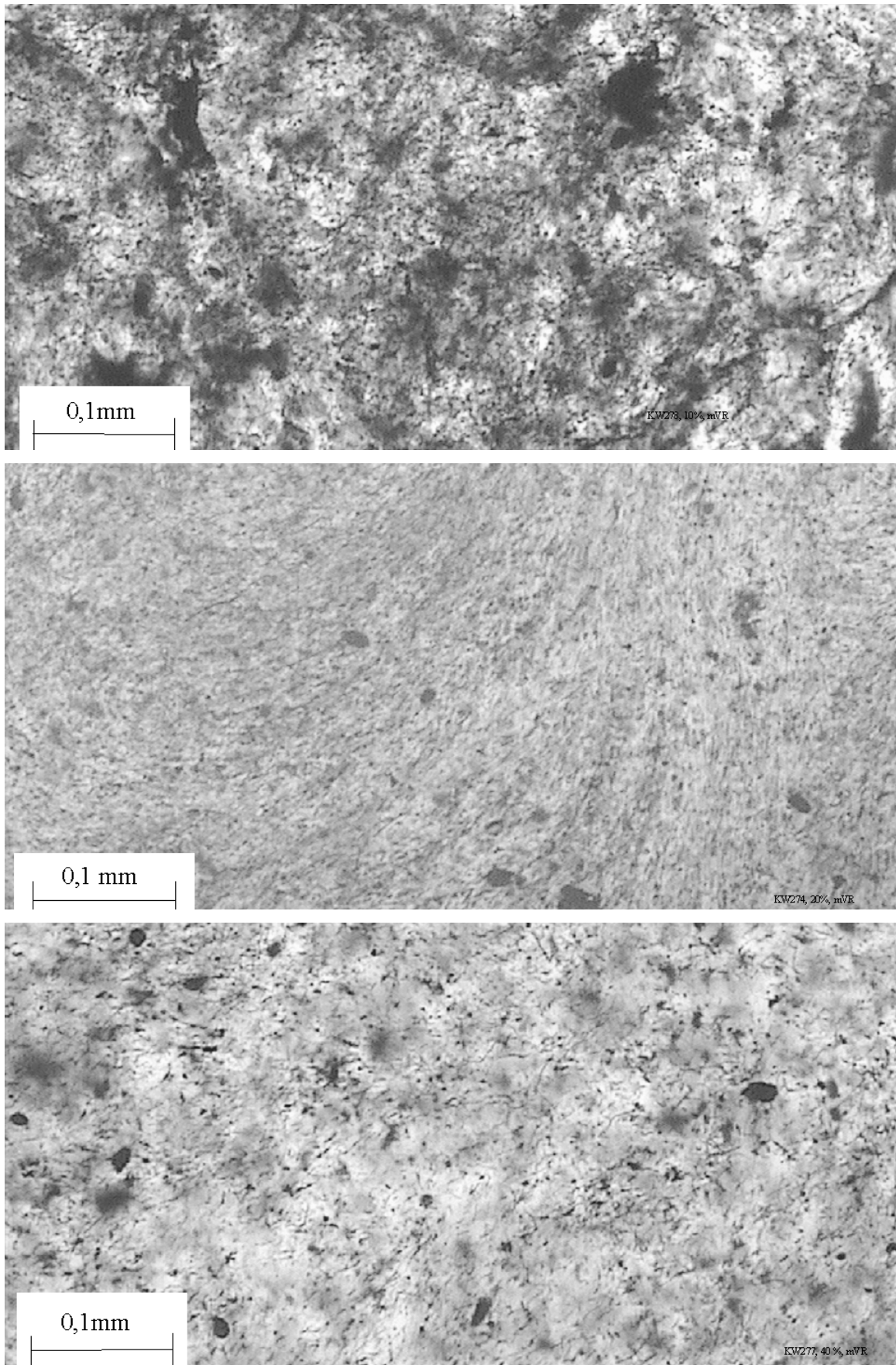


**Fig. 48:** Microscopic photographs of sPP/CNF nanocomposites prepared with pre-reaction after sonication of the filler with an ultrasonic amplitude of 10 %, 20 %, and 40 %, respectively.



A better dispersion of the fillers at higher amplitudes is also evident from Fig. 48, even though they show nanocomposites with different filler contents (0.8 weight-% in the sample prepared at 10 % amplitude, 0.6 weight-% in that prepared at 20 % and 0.4 weight-% in the one prepared at an amplitude of 40 %). These samples were prepared after pre-reaction of the sonicated fillers with MAO for 24 hours. It is evident from the above pictures that the pre-reaction does not influence the homogeneity of the CNF-dispersion in the matrix to a great extent.

**Tab. 4: Activities of propylene polymerizations after different pre-treatments of the CNFs.**

<b>Pre-reaction</b>	<b>Ultrasonic Amplitude [%]</b>	<b>Sonication Time [min]</b>	<b>Activity [kg<sub>Pol</sub>/(mol<sub>Zr</sub>·h·mol<sub>Mon</sub>/l)]</b>
<b>no</b>	10	15	3,500
<b>no</b>	20	15	4,000
<b>no</b>	40	15	4,800
<b>yes</b>	10	15	2,200
<b>yes</b>	20	15	2,400
<b>yes</b>	40	15	4,900

The activity of the catalyst (see Tab. 4) lay between 3,500 and 5,000 kg<sub>Pol</sub>/(mol<sub>Zr</sub>·h·mol<sub>Mon</sub>/l) and, therefore, in the same range as in homogeneous polymerizations with the same metallocene (4,300 kg<sub>Pol</sub>/(mol<sub>Zr</sub>·h·mol<sub>Mon</sub>/l)). It was somewhat lower in polymerizations after pre-reaction of the filler with MAO.

From the above results, it was concluded that the ultrasonic amplitude should be high enough to allow for a separation of the CNFs but not so high as to lead to an undesirable degradation of the fibers. As the pre-reaction with MAO had not improved the polymer properties or the dispersion of the filler in the matrix significantly, the following conditions were chosen for the subsequent polymerizations. The amplitude was set to 20 %, the sonication time to 15 minutes and the polymerizations were carried out without pre-reaction. Under these conditions, the filler content was varied by incorporation of different amounts of CNFs. The results are shown in Fig. 49.



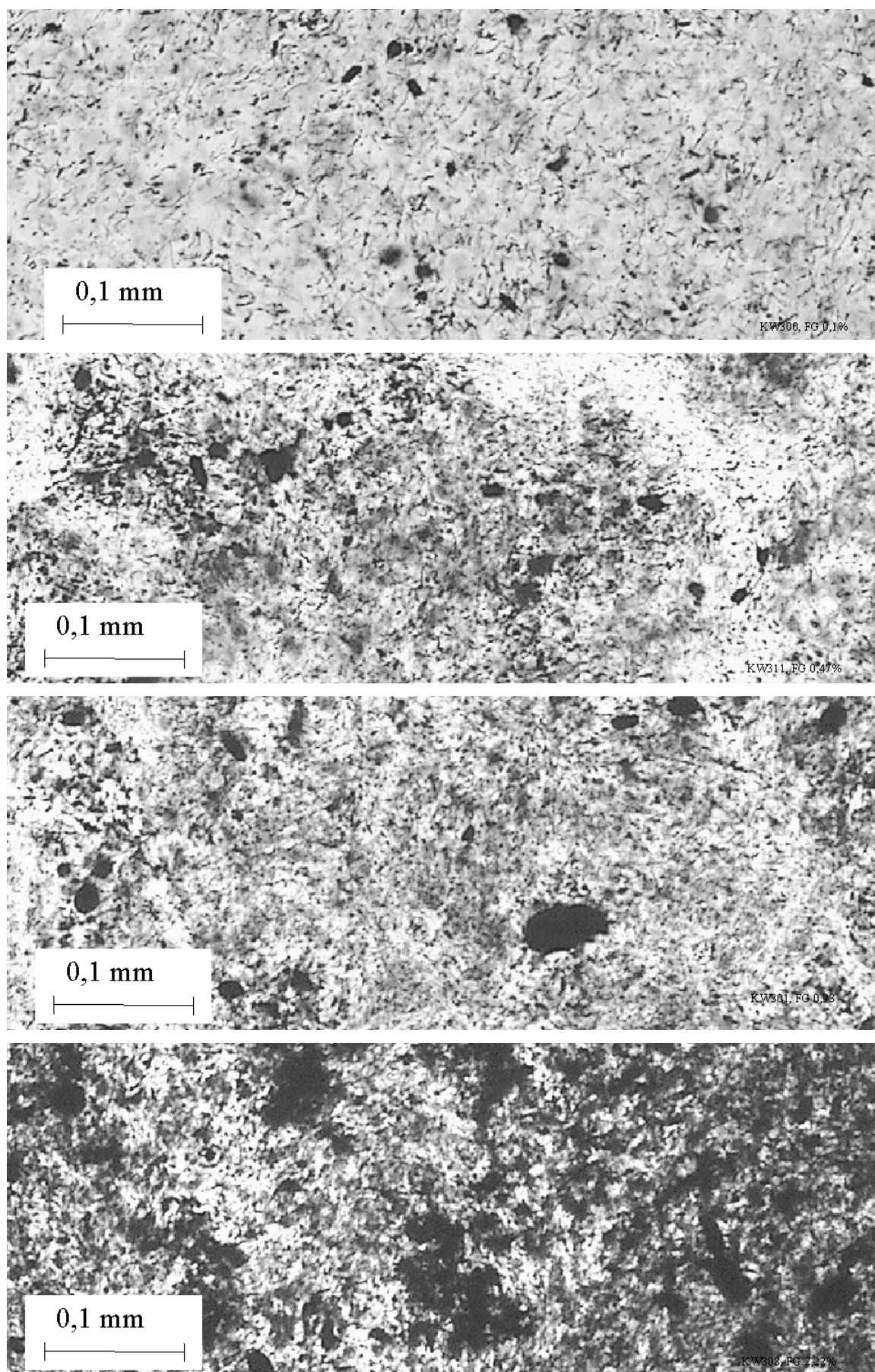


**Fig. 49: Microscopic photographs of sPP/CNF nanocomposites with filler contents of 0.1%; 0.5%; 0.9%; and 2.2%, respectively (amplitude 20 %, sonication time 15 min, without pre-reaction).**

It is observable in the above photographs, that the dispersion of the CNFs in the sPP matrix was not perfect. Some agglomerates were still present in the nanocomposite, but also regions with a very good distribution are visible. The dispersion at lower filler contents was naturally somewhat better, but also at a filler content as high as 2.2 %, the dispersion was still good. Going to higher filler contents, the distance between CNFs gets very small, and the microscopic photographs were almost totally black. The activities were found to range from 4,000 to 5,500  $\text{kg}_{\text{Pol}}/(\text{mol}_{\text{Zr}} \cdot \text{h} \cdot \text{mol}_{\text{Mon}}/\text{l})$ , which is in the same region as in the homogeneous polymerizations with the same metallocene. The polymer properties are summarized in Tab. 5 at the end of this chapter.

### **6.5.2 Adhesion of the Polypropylene Matrix to the Carbon Nanofibers**

The quality of the adhesion of the matrix sPP to the CNFs was estimated from SEM micrographs. It can be seen if the wetting of the fibers by the polymer is good or poor from these pictures. Fig. 50 shows a 100,000 fold magnification of an sPP/CNF nanocomposite containing 0.6 % nanofibers. It is evident that the wetting of the fibers by the polymer is quite good. Some parts of the fibers seem to be without polymer coverage, but other parts are well covered with polymer. In addition to that, a bundle of nanofibers with polymer in between the single fibers is visible. A good wetting can also be seen in Fig. 51, which shows an sPP/CNF nanocomposite with 0.6 % filler content at a magnification of 50,000 times. It is easily observed, that the polymer is attached to the fiber sticking out of the surface.

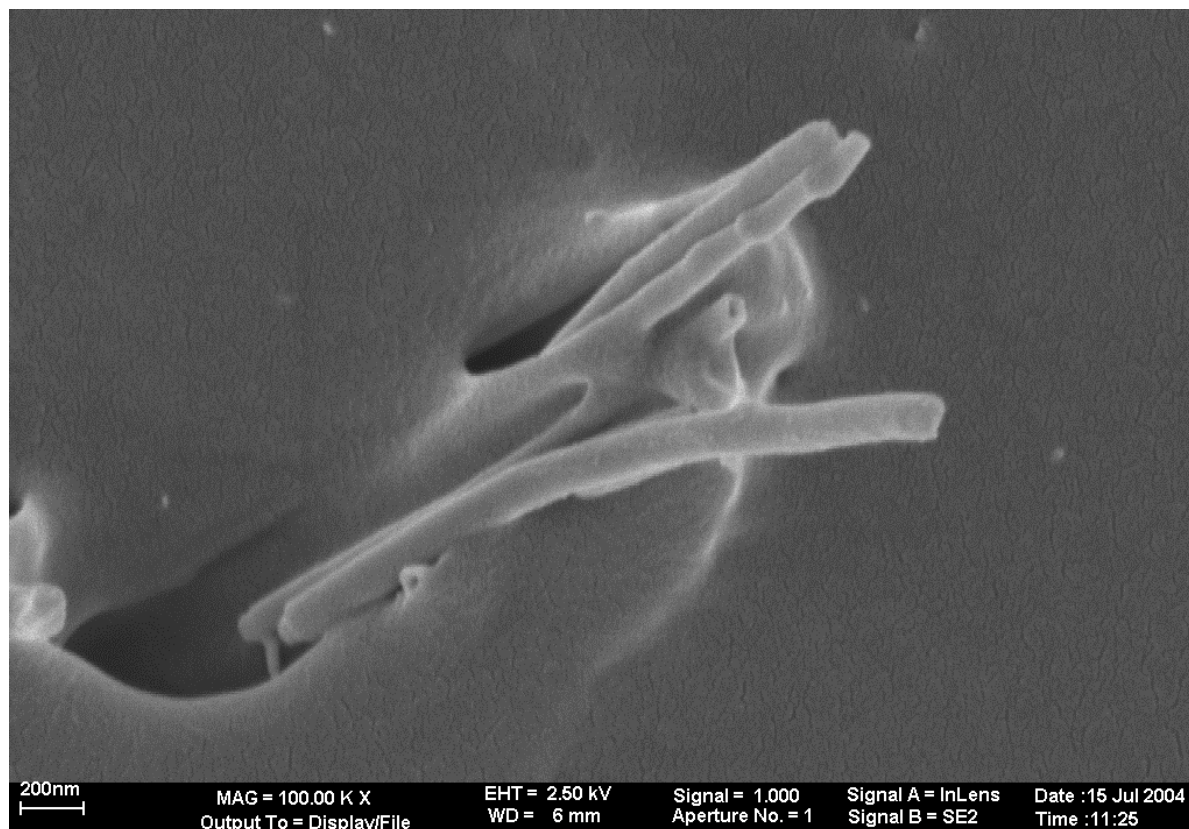


**Fig. 50:** SEM micrograph (magnification 100,000 times) of an sPP/CNF nanocomposite containing 0.9 % nanofibers (KW301).

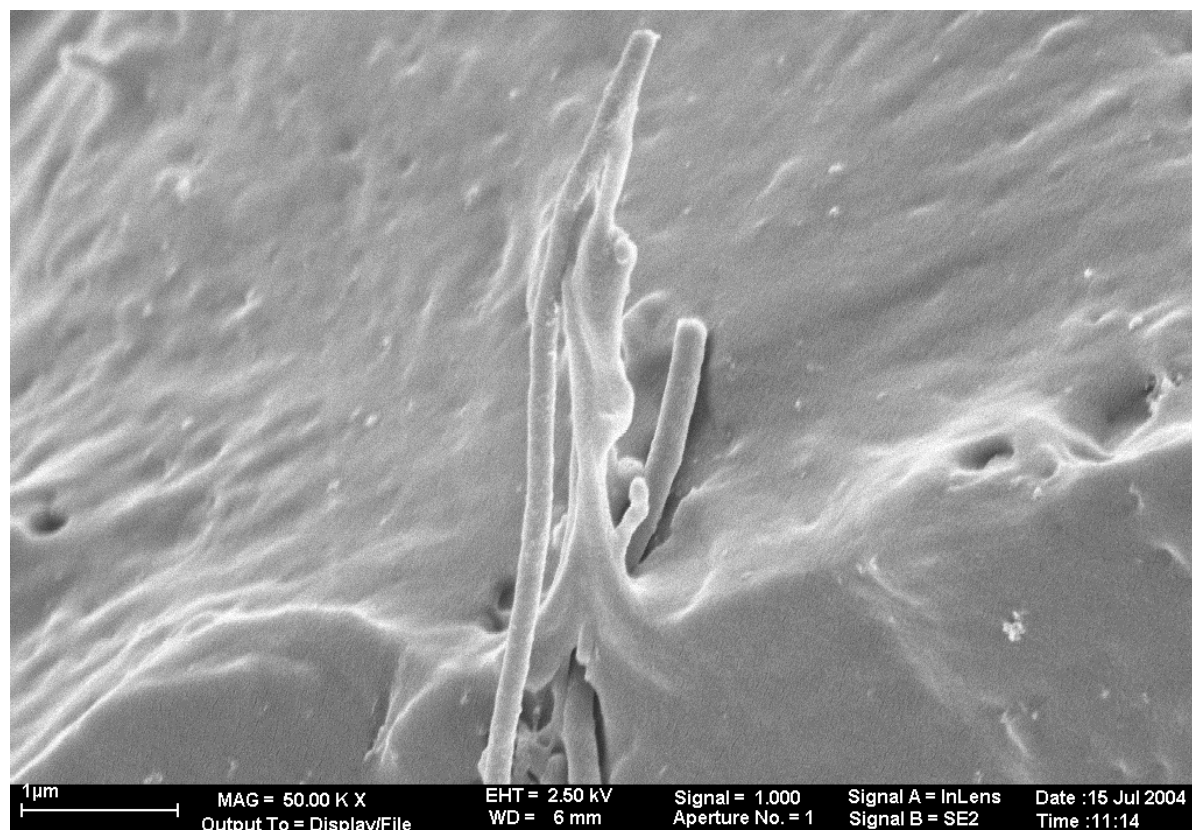


**Fig. 51:** SEM picture (magnification 50,000 times) of an sPP/CNF nanocomposite containing 0.6 % nanofibers (KW304).

An sPP/CNF nanocomposite with a higher filler loading (2.2 %) is shown in Fig. 52 and Fig. 53 at magnifications of 10,000 and 75,000, respectively.

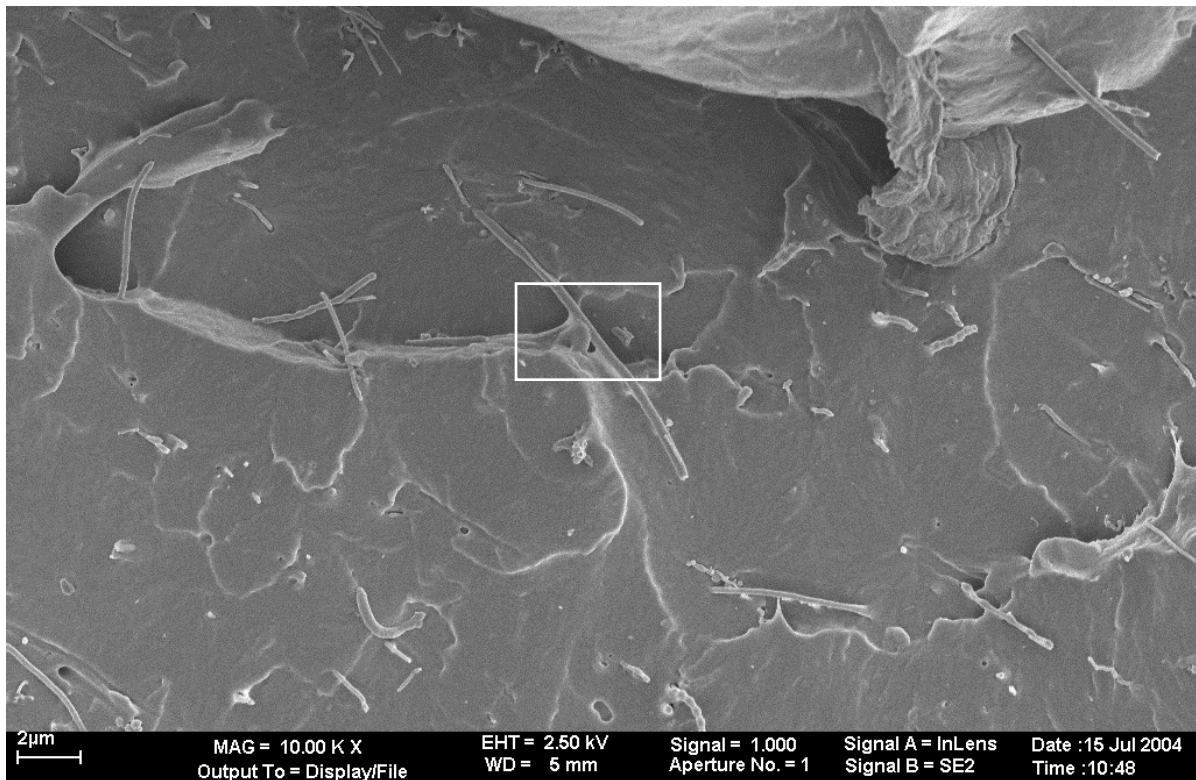


**Fig. 52:** SEM micrograph (magnification 10,000 times) of an sPP/CNF nanocomposite containing 2.2 % carbon nanofibers (KW308).

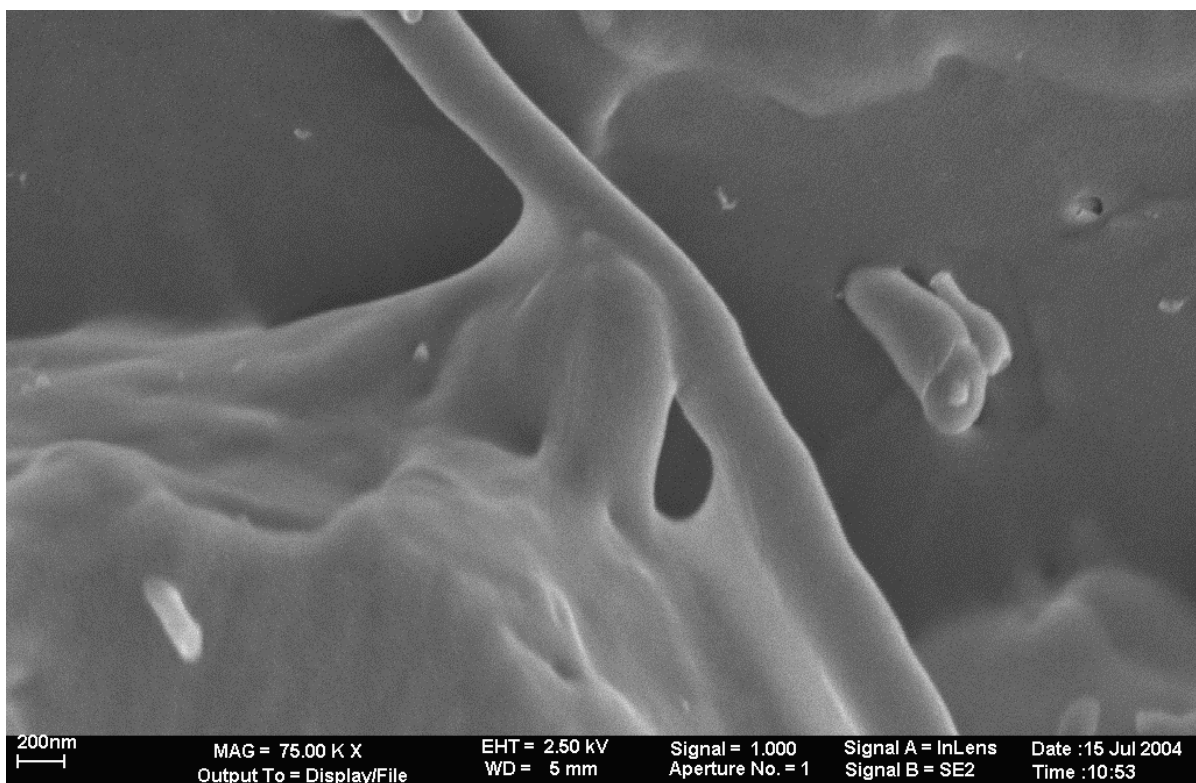


**Fig. 53:** SEM micrograph (magnification 75,000 times) of an sPP/CNF nanocomposite containing 2.2 % nanofibers (KW308).

The lower magnification shows an even distribution of the fibers without bundle-formation in the polymer matrix. Most of them are located partly in the polymer and are partly sticking out of the surface of the polymer. Hardly any of fiber pull-out is visible in this picture. A good wetting is seen in the higher magnification of the indicated area. The fiber even seems to form a bridge between two parts of the polymer in this picture.

### **6.5.3 Crystallization and Melting Behavior of the sPP/CNF nanocomposites**

#### **6.5.3.1 Melting Temperature and Crystallinity**

The melting temperature was characterized by one peak at 139 to 142 °C in most cases (see Tab. 5 at the end of this chapter). No influence of the filler on the molecular weight was found. It ranged between 360,000 and 400,000 g/mol for the sPP/CNF composites as compared to 400,000 g/mol for the neat sPP.

The crystallinity as determined by integration of the melting peak was independent of the filler content. If a value of 164 J/g for the 100 % crystalline sPP is taken as reference (see section 6.1), the crystallinity ranged between 27 and 29 %, being roughly the same as in the pure sPP samples. It was independent of the filler content of the nanocomposites. These results are in accordance with values obtained by Sandler et al, who found that incorporation of 7 % of Pyrograph III CNFs into isotactic PP by melt-compounding did not change the melting temperature, the peak shape or the over all crystallinity, but did increase the crystallization temperature by 5°C<sup>[86]</sup>.

#### **6.5.3.2 Crystallization Temperatures**

The effect on the crystallization temperature is somewhat more pronounced (Fig. 54). It rose from 96 °C for the neat sPP to 98 °C for the sPP/CNF composite with a filler content of 0.1 % reaching a plateau at 101 °C for filler contents of more than 1 %.

An increase in the crystallization temperature was also found by Lozano et al. When iPP was melt-compounded with CNFs, the steepest slope was found at incorporations of CNFs lower than 5 %. The crystallization temperature was 114 °C for pure PP and 128 °C for a 5 % CNF composite. The melting temperature was largely unaffected by the presence of the nanofibers<sup>[128]</sup>.

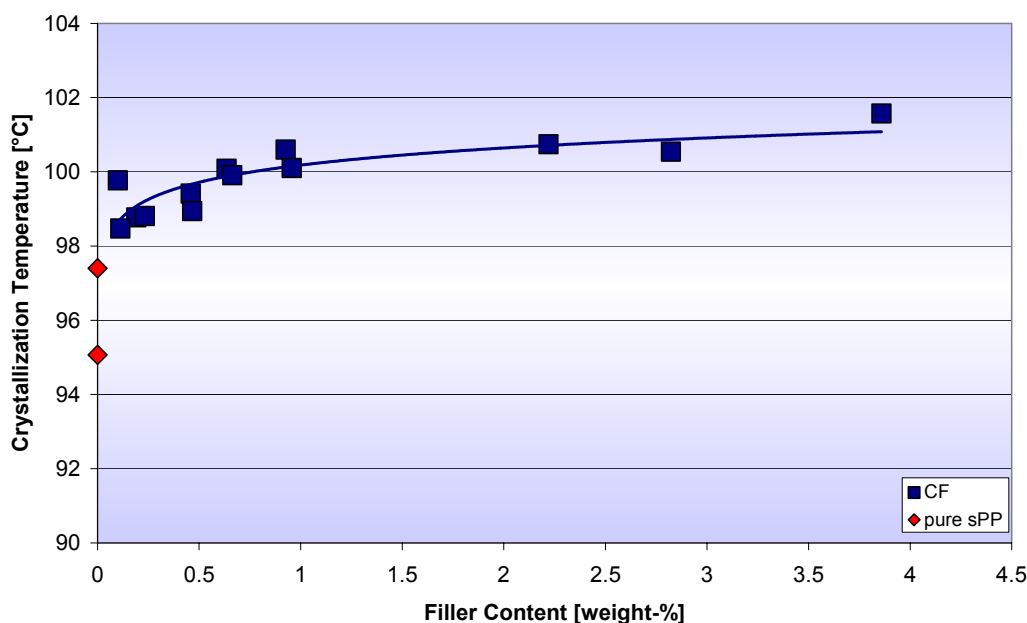


Fig. 54: Influence of the filler content on the crystallization temperature of the sPP/CNF nanocomposites.

### 6.5.3.3 Half-time of Crystallization

The half-time of crystallization provides information about the rate of crystallization. The data for the sPP/CNF nanocomposites with different filler contents and for the neat sPP is shown in Fig. 55 and Tab. 5.

With rising isothermal crystallization temperature, the  $t_{0.5}$  also increased for all samples tested as expected. The influence of the filler content was not very pronounced, though. One could expect that the half-time of crystallization should decrease with rising filler content because more fibers should provide for more nucleation sites. This is not in accordance with the experimental results, which is probably due to an inhomogeneous dispersion of the fillers in the polymer matrix. If the nanofibers are still partly agglomerated after the polymerization and an inhomogeneous nanocomposite is formed, the nucleation might not be induced by the individual fibers but by fiber bundles. This would lead to a reduced number of nucleation sites with regard to the filler content and in turn to a slower crystallization than might be expected for a perfectly homogeneous nanocomposite. This effect seems to be more pronounced for higher filler contents.



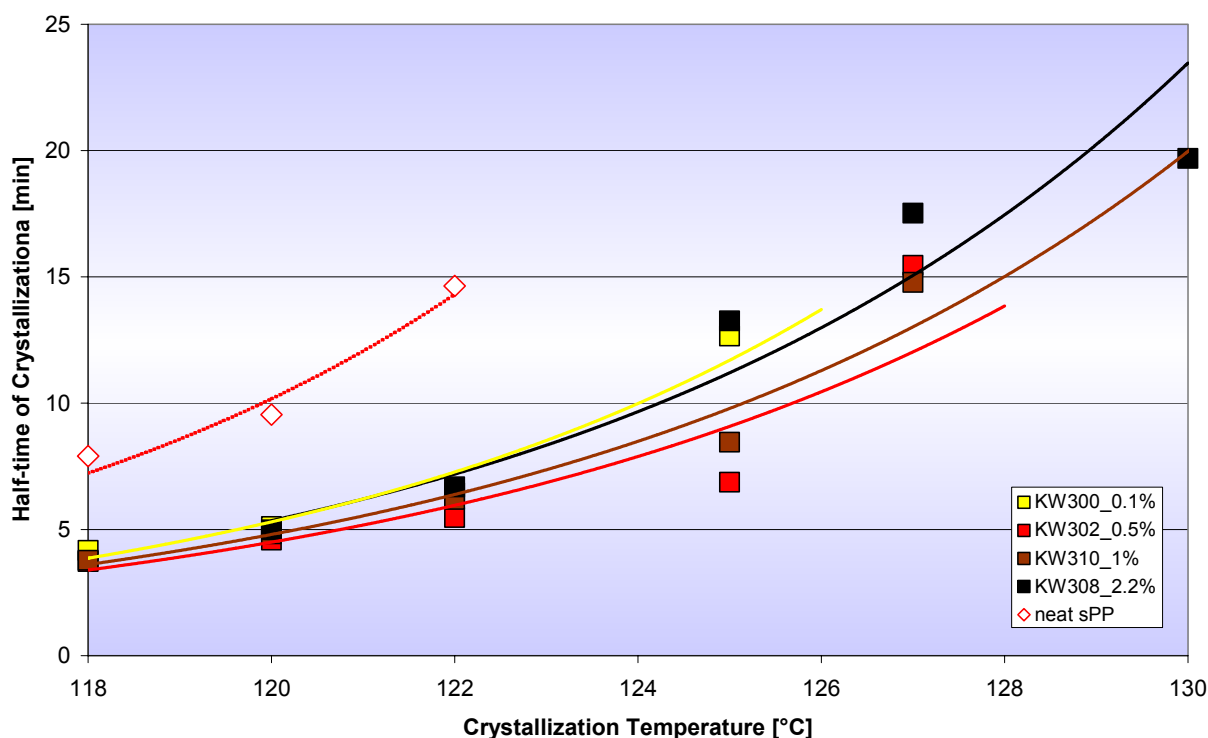


**Fig. 55: Influence of the crystallization temperature and the filler content on the half-time of crystallization ( $t_{0.5}$ ).**

One effect that can be clearly seen, though, is the tremendous reduction of the half-time of crystallization of the pure sPP upon addition of the carbon nanofibers. It was reduced to approximately one-half of the value for the pristine polymer at all temperatures investigated. This means that the crystallization of 50 % of the nanocomposite only took roughly half the time that is needed for the crystallization of 50 % of the neat polypropylene. It should be noted, that crystallization of the composite materials proceeded too fast at lower isothermal crystallization temperature to provide reliable results. At temperatures higher than those shown in the graph, the crystallization of the pure PP proceeded too slowly to be reliably detected by the DSC used. The reduction of the half-time of crystallization as described above can be taken as evidence for a nucleating effect of the carbon nanofibers in the sPP/CNF nanocomposites.

#### 6.5.3.4 Avrami Analysis

The analysis of the results obtained from DSC measurements according to the Avrami theory also shows that the carbon nanofibers acted as nucleating agents. The rate constant of crystallization ( $K$ ) obtained as antilogarithmic value of the y intercept of the least squares fitted line to the experimental data increased from  $1.7 \cdot 10^{-3} \text{ min}^{-n}$  for the pure sPP to  $9.4 \cdot 10^{-3} \text{ min}^{-n}$  for the composite containing 0.1 % CNF (see also Tab. 5). This can be explained

by the assumption that nucleation proceeds from the surface of the nanofibers when CNFs are present.

The influence of the filler content and the isothermal crystallization temperature on the rate constant of crystallization is shown in Fig. 56. It is noticeable that the rate of crystallization decreased with increasing isothermal crystallization temperature. The issue is not as clear with regard to the influence of the filler content. Up to a filler content of 0.5 %, the rate of crystallization increased for the respective crystallization temperatures. At higher filler loadings, the rate of crystallization decreased again but always stayed faster than in the pure polymer. This could be due to a hindered mobility of the polymer chains due to the presence of the high amounts of carbon nanofibers.

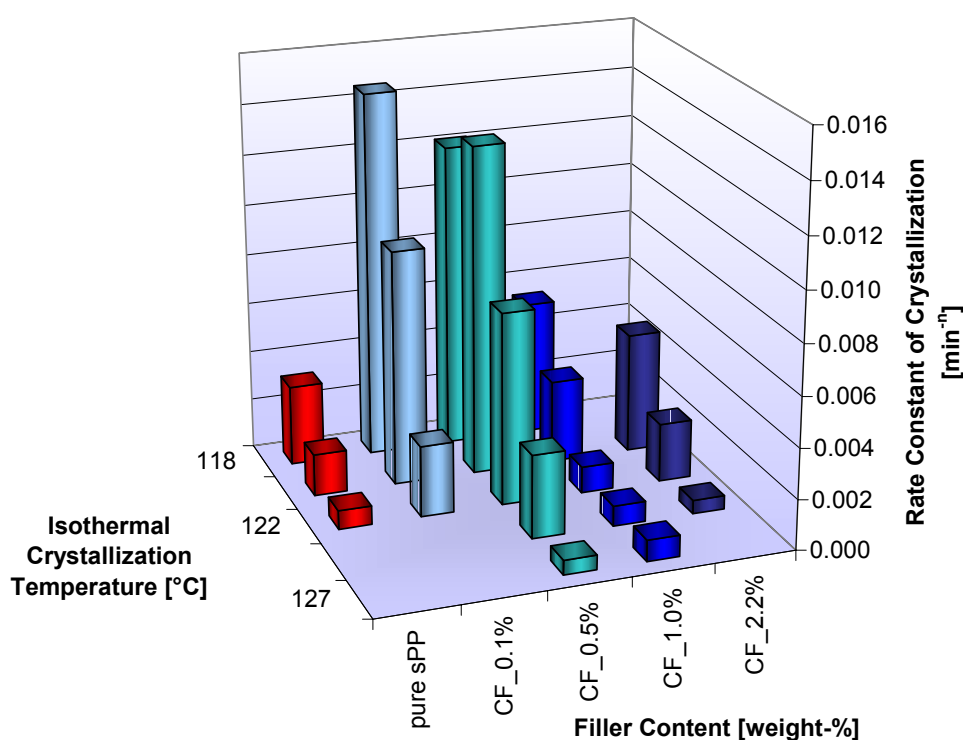


**Fig. 56:** Influence of the filler content and the isothermal crystallization temperature on the rate constant of crystallization (K) of the sPP/CNF nanocomposites.

The above findings are in accordance with results obtained by Sandler for melt-compounded iPP/CNF nanocomposites. They observed that the Avrami exponent dropped from 2.8 to 2.56 upon addition of the CNFs. This is consistent with a heterogeneous nucleation mechanism on the nanofiber surface<sup>[86]</sup>. Lozano et al found an increase in crystallization rate upon addition of CNF to a PP matrix. It increased from 0.0373 min<sup>-1</sup> for pure PP to 0.8664 min<sup>-1</sup> for a CNF/PP nanocomposite containing 60 % nanofibers<sup>[128]</sup>.



### 6.5.4 Thermal Stability of the sPP/CNF Nanocomposites

The degradation of the neat polymer and the nanocomposites was investigated using TGA at a heating rate of 5 °C/min. The results concerning the onset of degradation ( $T_{\text{on}}$ ), the temperature of maximum weight loss (inflection point,  $T_{\text{max}}$ ) and the end of degradation ( $T_{\text{end}}$ ) are shown in Fig. 57 and Tab. 5.

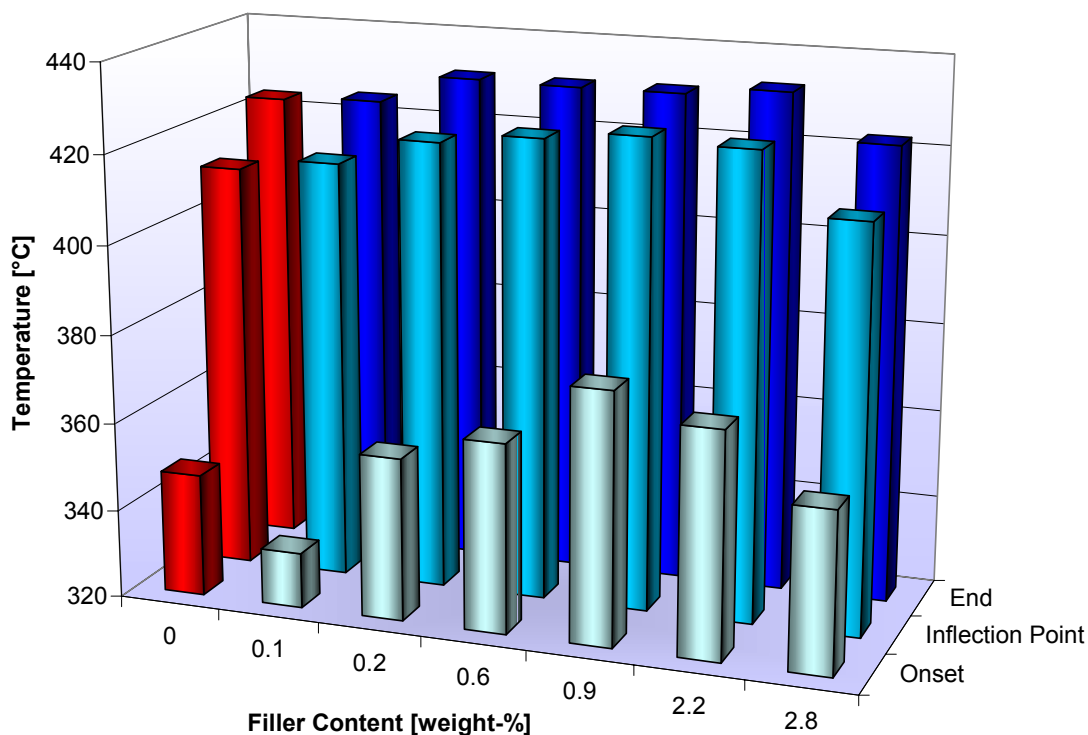


**Fig. 57: Influence of the filler content on the onset of degradation, the inflection point and the end of degradation of the pure sPP and the sPP/CNF nanocomposites as determined by TGA.**

The onset of degradation was generally at a higher temperature for the nanocomposites than for the pure polymer. The highest enhancement was found for the composite containing 0.9 % of carbon nanotubes, for which the onset of degradation was raised by approximately 30 °C as compared to the neat sPP. A general trend of rising onset of degradation with rising filler content was found up to a filler content of 0.9 %. After that, the onset of degradation appeared to sink again. With exception of the sample with 2.8 wt-% of CNFs, the  $T_{\text{max}}$  of the nanocomposites was also higher (by a maximum of 10 °C) than that of the neat polymer. Also in this case, a general increase in degradation temperature with increasing filler content followed by a decrease for filler contents higher than 0.9 % was observed. The same is true for the end of degradation temperature which was increased by a maximum of 10 °C. The increase in degradation temperature is a sign for an improved thermal stability of the composite as compared to the pure sPP.

Lozano et al. found an increase in the onset of degradation with increasing amount of CNFs incorporated into an iPP matrix by melt-mixing. The final degradation temperature was raised by 100 °C. This was attributed to a restricted mobility of the polymer chains caused by the CNFs [128].

### **6.5.5 Electrical Conductivity of the sPP/CNF Nanocomposites**

The conductivity of the samples with different filler contents was evaluated using two-point measurements. For these experiments, parts of the films also used for cutting the bones for the tensile tests were employed. A good contact between electrodes and polymer film was ensured by application of conductive colloidal graphite suspension as described in the experimental section. Most of the films investigated did not show any conductivity at all. Only the samples with filler contents as high as 2.8 % and 3.9 % exhibited a slight conductivity. The values for the resistivity ( $\rho$ ) were still quite high. They lay between  $10^8$  and  $10^9$  for the samples with 2.8 % and 3.9 %, respectively. Naturally, no trend was seen from these values, nor could a percolation threshold be determined. It is obvious, though, that this type of nanocomposite is generally conductive already at relatively low filler contents.

This is consistent with results obtained by Andrews<sup>[87]</sup> who could show that iPP/CNF nanocomposites show some conductivity. The surface resistivity was reduced to  $10^7$   $\Omega$ /square at a filler content of 5 vol.-% of CNFs. Lozano et al. found that the surface resistivity of iPP/CNF nanocomposites (purified) only dropped significantly when the filler amount exceeded 10 wt.-%. The volume resistivity dropped from  $10^{18}$  to approximately  $10^8$  at filler contents between 9 and 18 wt.-%<sup>[85]</sup>.

### **6.5.6 Tensile Properties of the sPP/CNF Nanocomposites**

The tensile properties of the sPP/CNF nanocomposites were obtained from the stress-strain curves of the materials. These were recorded for test bars that had been prepared from films obtained by hot-pressing of the nanocomposite powder. Exemplary stress-strain curves are shown in Fig. 58. It can be seen that the general shape of the curves is similar, and that the yield strength of the nanocomposites was higher for higher filler loadings. Coupled with this effect was an increase in brittleness of the nanocomposite with increasing filler content. This is obvious for the samples with filler contents of 2.2 and 2.8 %, respectively. The elongation at break which is characterized by the end of the respective curves was reduced considerably from more than 900 % to 350 %.

The elastic modulus that was calculated from the stress-strain curves showed a high degree of scattering. It was, therefore, impossible to detect a trend regarding the influence of the filler content on this parameter, and the results are not shown here.

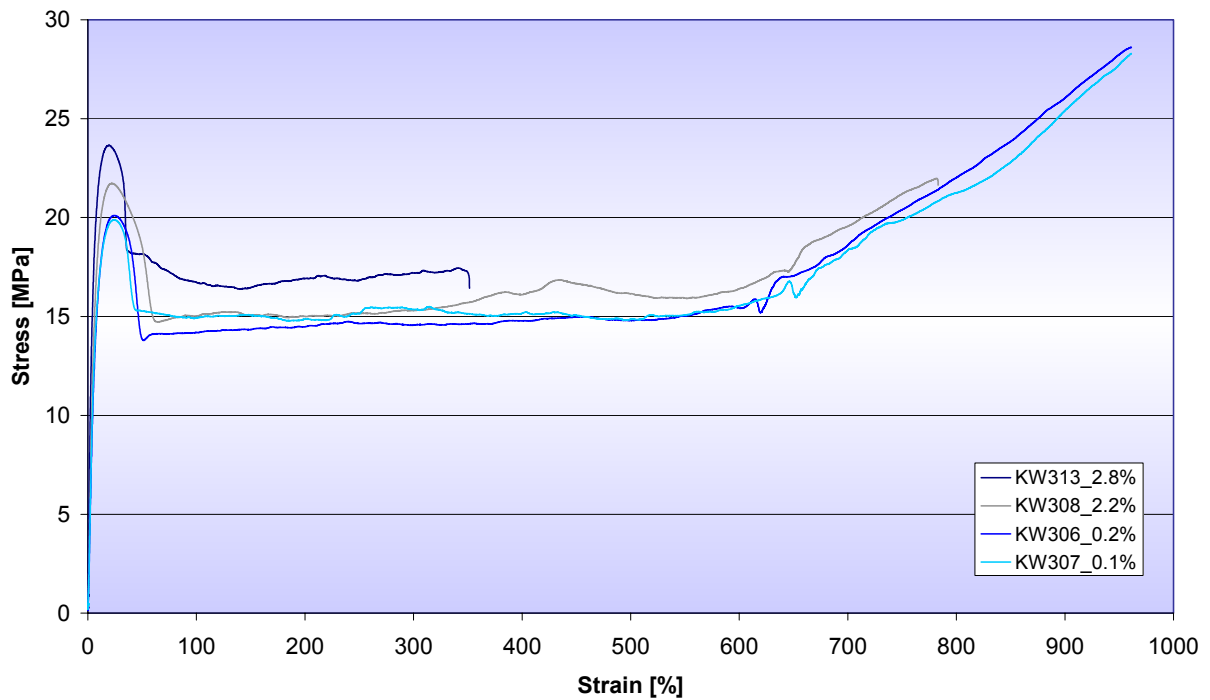


Fig. 58: Stress-strain behavior of exemplary sPP/CNF nanocomposites.

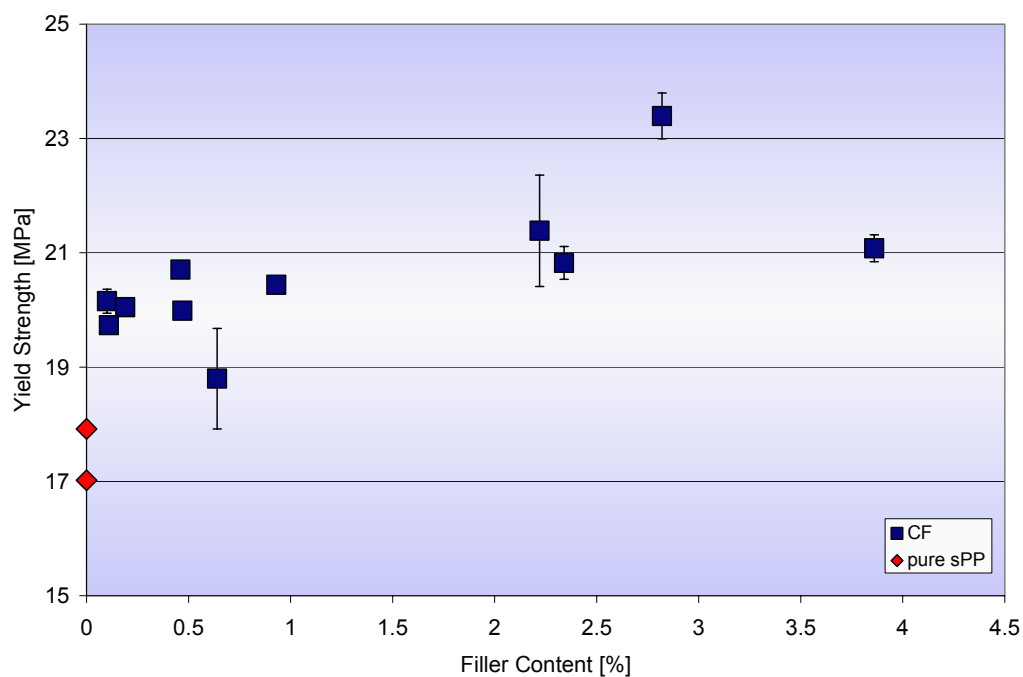
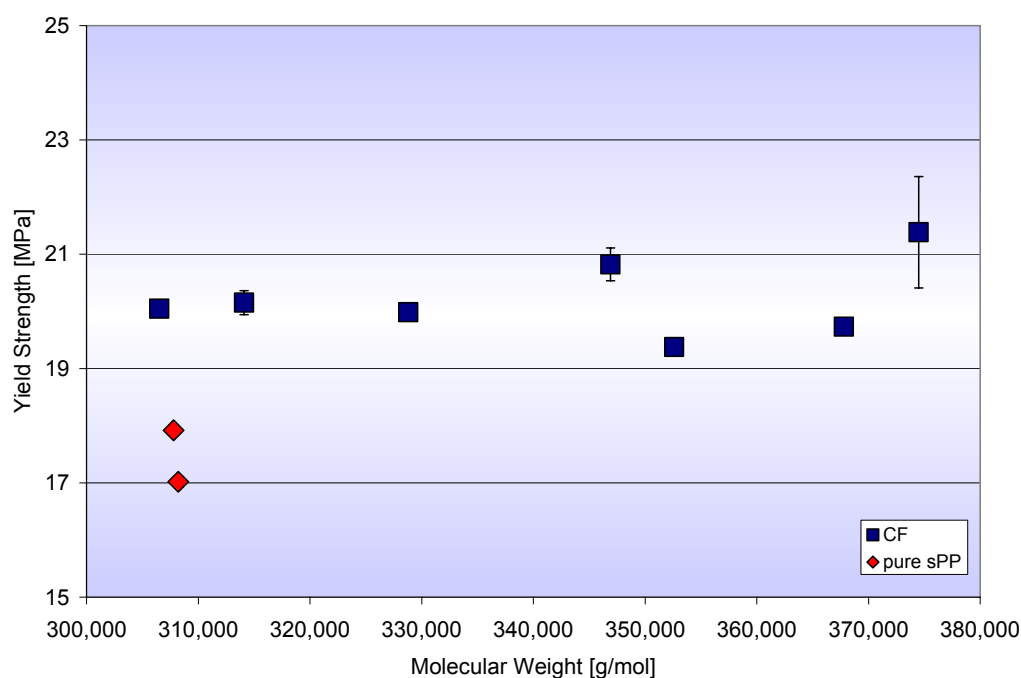


Fig. 59: Influence of the filler content on the yield strength of sPP/CNF nanocomposites.

The influence of the filler content on the yield strength of the sPP/CNF nanocomposites is shown in Fig. 59 and Tab. 5. It is apparent that the yield strength of the material could be improved by the addition of carbon nanofibers. This improvement was greater for higher filler loadings. At low CNF contents, the yield strength could be improved by 15 % as compared to the average yield strength of the pure polymer (17.5 MPa). When the filler content was raised to 1 % or more, an enhancement of the yield strength by 20 % could be accomplished.



**Fig. 60: Influence of the molecular weight on the yield strength of sPP/CNF nanocomposites.**

This enhancement of the yield strength was independent of the molecular weight of the nanocomposites. The influence of the mass-average of the molecular weight ( $M_w$ ) on the yield strength is shown in Fig. 60. Even though the molecular weight of the pure PP was at the low end of all materials investigated, no trend of higher yield strengths for materials with higher molecular weights was observed.

The results presented above are comparable to results from the literature to some extent. Tibbets et al prepared injection molded specimen of PP/CNF that showed a doubled yield strength with regard to the unfilled polymer and a quadrupled modulus. To achieve this, the fibers had to be ball-milled before the compounding to ensure a good dispersion in the polymer matrix<sup>[147]</sup>.

Lozano et al obtained iPP/CNF nanocomposites (5 % CNF) with a yield strength of 69 MPa which was 17 % higher than the value for the pure material. The yield strength decreased

under the value for raw PP at higher loadings. The elongation to break (167 %) was reduced considerably at 40 % CNF content (13 % elongation), meaning that the material had changed from ductile to brittle<sup>[128]</sup>.

An improvement of the yield strength could be accomplished by the preparation used in this study. It is probable that a higher degree of enhancement could be reached by an amelioration of the filler dispersion and a further enhancement of the interfacial adhesion.

**Tab. 5: Properties of some sPP/CNF nanocomposites.**

<b>Filler Content [wt.-%]</b>	<b>0</b>	<b>0.1</b>	<b>0.5</b>	<b>1</b>	<b>2.2</b>
<b>Activity [kg<sub>Pol</sub>/(mol<sub>Zr</sub>·h·mol<sub>Mon</sub>/l)]</b>	4,300	4,300	4,300	4,300	4,900
<b>Melting Temperature [°C]</b>	140	140	140	141	140
<b>Crystallization Temperature [°C]</b>	96	99	100	100	101
<b>Rate Constant of Crystallization [<math>\cdot 10^{-4} \text{ min}^{-n}</math>]</b>	7.5	28	77	10	23
<b>Half-time of Crystallization [min]</b>	14.6	6.4	5.5	6.2	6.7
<b>Degradation Temperature (T<sub>max</sub>) [°C]</b>	412	415	424	426	425
<b>Tensile Strength [MPa]</b>	17.5	19.9	19.8	20.4	21.1

<sup>a</sup>The rate constant of crystallization and the half-time of crystallization were determined from isothermal DSC measurements at 122 °C.

## **6.6 Syndiotactic Polypropylene/Carbon Nanotube Nanocomposites**

Based on the results from the preliminary experiments, sPP/MWNT nanocomposites were synthesized after sonication of the fillers with the sonopuls homogenizer by *in situ* polymerization of propylene with metallocene **1**. To determine the influence of the ultrasonic amplitude and the sonication time on the dispersion of the MWNTs and the polymer properties, it was varied from 10 to 40 % of the maximum amplitude, and the time was chosen between 15 and 120 minutes. The corresponding experiments were performed with and without pre-reaction and the results were compared to find out the best reaction conditions for the preparation of nanocomposites with different filler contents. These were then examined with regard to their crystallization behavior, their thermal degradation properties, their electrical conductivity, and their tensile properties. In addition to that, the adhesion of the matrix polymer to the MWNTs was investigated.

### **6.6.1 Dispersion of the Carbon Nanotubes**

For experiments without pre-reaction, the MWNTs were treated with ultrasound in a toluene suspension for 15 minutes prior to the polymerization. The amplitude was varied from 10 to 40 %, and no pre-reaction with MAO was carried out. As can be seen from Fig. 61, a higher ultrasonic amplitude led to a slightly better dispersion of the nanotubes. It was still not very good after treatment with an amplitude of 30%, though. The filler contents of the shown samples are 0.5 %, 0.7 %, and 0.6 % by weight for the amplitudes of 10%, 20 %, and 30 %, respectively. The activity (see Tab. 6) did not show any significant dependence on the amplitude used for the sonication of the fillers. It was 3,500 to 4,000  $\text{kg}_{\text{Pol}}/(\text{mol}_{\text{Zr}} \cdot \text{h} \cdot \text{mol}_{\text{Mon}}/\text{l})$  and, therefore, in the range of the activities for the polymerizations without MWNTs (4,300  $\text{kg}_{\text{Pol}}/(\text{mol}_{\text{Zr}} \cdot \text{h} \cdot \text{mol}_{\text{Mon}}/\text{l})$ ).

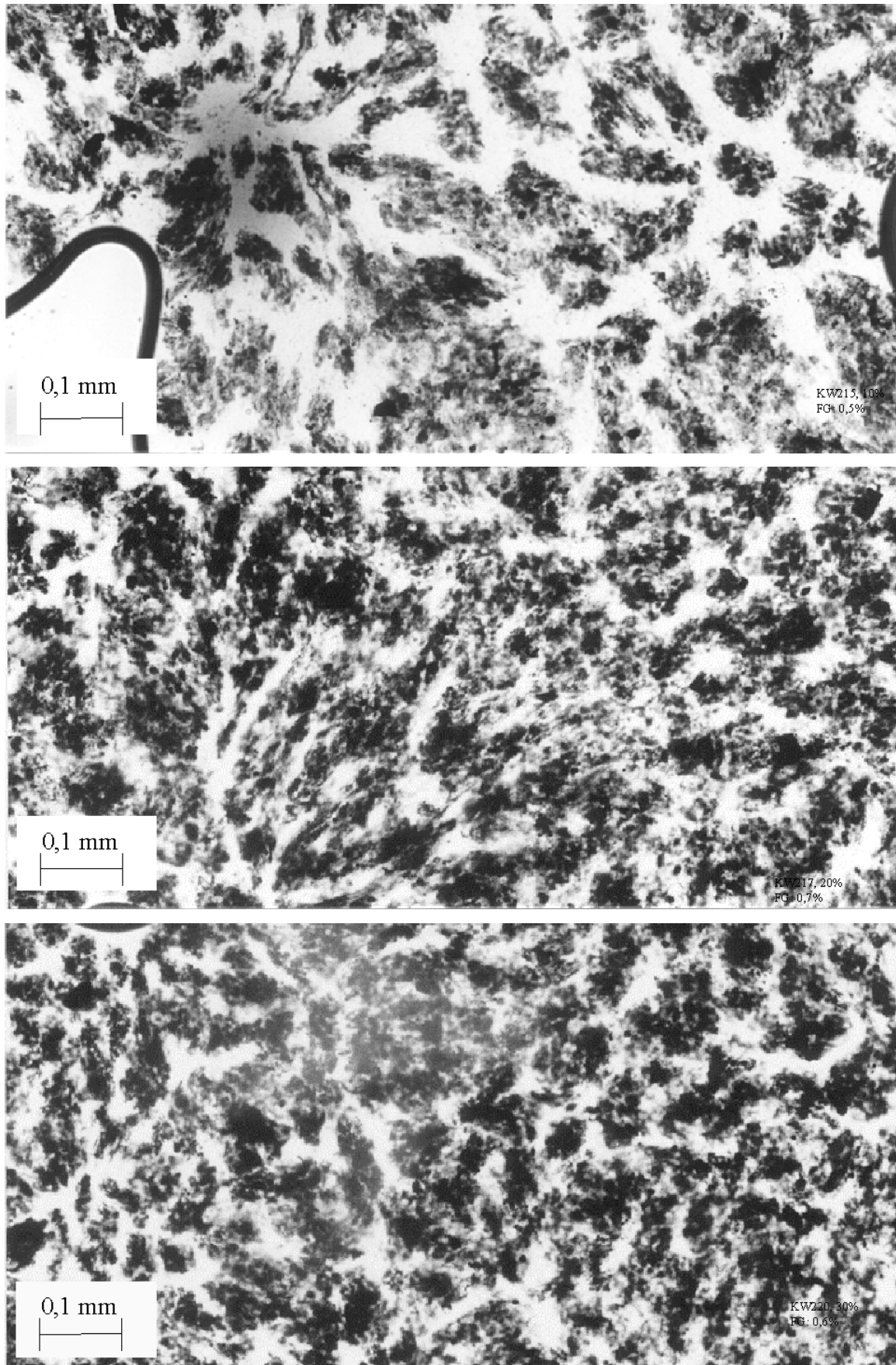


**Fig. 61:** Microscopic photographs of sPP/MWNT nanocomposites prepared without pre-reaction after sonication of the filler with an ultrasonic amplitude of 10 %, 20 %, and 30 %, respectively.

To improve the homogeneity of the dispersion, polymerizations were carried out after the same ultrasonic treatments, but this time a pre-reaction of the MWNTs with MAO for approximately 24 hours was performed. The results are shown in Fig. 62 .

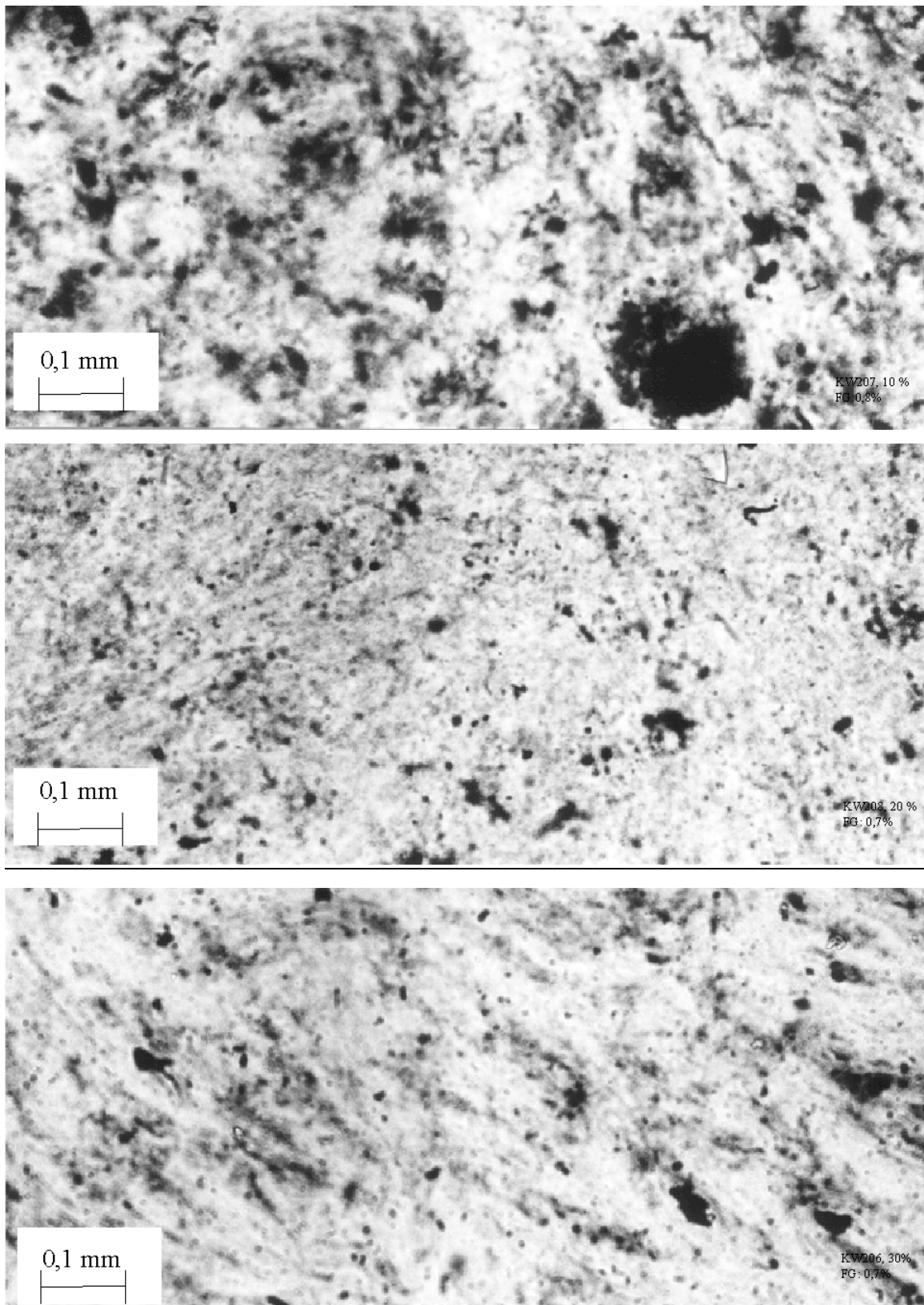


**Fig. 62:** Microscopic photographs of sPP/MWNT nanocomposites prepared with pre-reaction after sonication of the filler with an ultrasonic amplitude of 10 %, 20 %, and 30 %, respectively.



The improvement of the dispersion with rising ultrasonic amplitude was somewhat more pronounced when the sPP/MWNT nanocomposites were prepared with pre-reaction than when they were prepared without pre-reaction. In this case, the filler content of the samples pre-treated with an ultrasonic amplitude of 10 %, 20 %, and 30 % were 0.8 %, 0.7 %, and 0.7 %, respectively. The activity of 2,500 to 3,000  $\text{kg}_{\text{Pol}}/(\text{mol}_{\text{Zr}}\cdot\text{h}\cdot\text{mol}_{\text{Mon}}/\text{l})$  was below that for the polymerizations without nanotubes and for those in the presence of MWNTs but without pre-reaction.

**Tab. 6: Activities of propylene polymerizations after different pre-treatments of the MWNTs.**

Pre-reaction	Amplitude [%]	Sonication Time [min]	Activity [ $\text{kg}_{\text{Pol}}/(\text{mol}_{\text{Zr}}\cdot\text{h}\cdot\text{mol}_{\text{Mon}}/\text{l})$ ]
no	10	15	3,700
no	20	15	3,900
no	30	15	3,800
yes	10	15	2,600
yes	20	15	2,600
yes	30	15	2,600
yes	10	30	2,900
yes	10	60	2,600
yes	10	120	2,900

What is clearly more important than the effect of the amplitude is the effect of the pre-reaction with MAO on the dispersion. Obviously, the pre-reaction leads to a better distribution of the nanotubes in the sPP-matrix. This is in contrast to the results for the sPP/CNF composites, where the pre-treatment of the fillers had no influence on their degree of dispersion. This effect is probably due to the hydroxyl groups present on the surface of the MWNTs. As described in section 6.1.2, they could react with the MAO, thus anchoring the cocatalyst to the surface of the nanotubes. This would, on one hand, prevent the nanotubes from reagglomerating after the ultrasonic treatment because of repulsive forces between the MAO ions. On the other hand, it would lead to the polymer formation directly on the surface of the fillers. The growing polymer chains would then separate the MWNTs from each other during the polymerization.

In addition to the effect of the amplitude, the effect of the sonication time of the nanotubes on their distribution in the polymer matrix was investigated. The amplitude was set to 10 % and the sonication times were 15, 30, 60 and 120 minutes. The results are shown in Fig. 63 (note that the magnification in the first picture is smaller than in the rest).

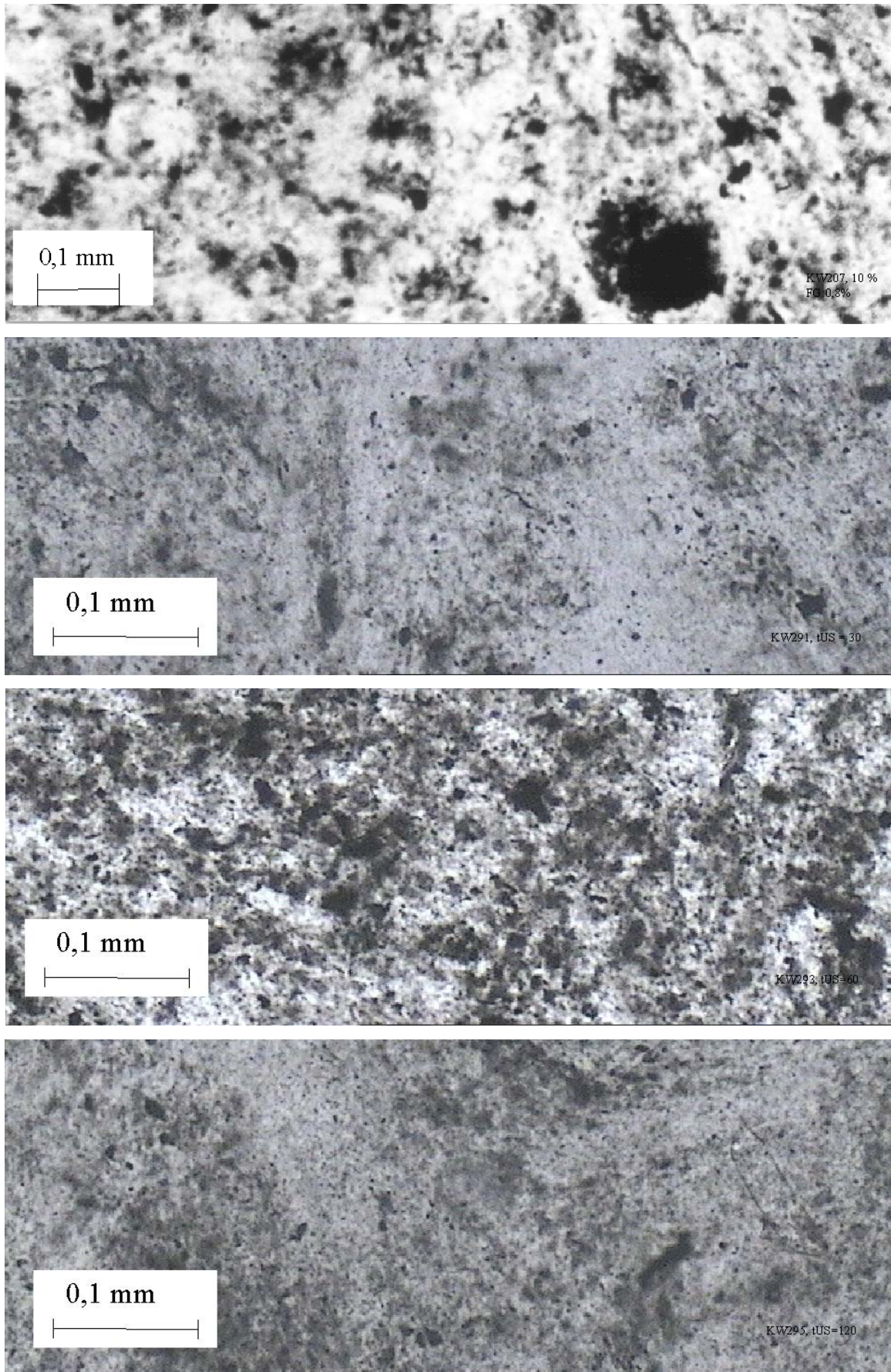


**Fig. 63:** Microscopic photographs of sPP/MWNT nanocomposites prepared with pre-reaction after sonication of the filler with an ultrasonic amplitude of 10 %, for 15, 30, 60 and 120 minutes, respectively.

It can be seen, that a longer sonication time generally improves the dispersion. The most homogeneous distribution is reached for the sPP/MWNT composite after sonication of the nanotubes for 120 minutes. This sPP/MWNT nanocomposite contains 0.5 % of nanotubes as compared to 0.8 %, 0.4 %, and 0.8 % for the samples that had been sonicated for 60, 30 and 15 minutes, respectively. The activities were still around  $2,500 \text{ kg}_{\text{Pol}}/(\text{mol}_{\text{Zr}} \cdot \text{h} \cdot \text{mol}_{\text{Mon}}/\text{l})$ .

For the subsequent polymerizations, an ultrasonic amplitude of 10 % and a sonication time of 60 minutes were chosen as a compromise between a dispersion as homogeneous as possible and the possible damage of the nanotubes due to high amplitudes or long sonication times<sup>[51]</sup>. A series of sPP/MWNT nanocomposites with filler contents between 0.1 and 0.9 weight-% was prepared and these materials were characterized with respect to their crystallization behavior, their thermal degradation, their electrical properties, and their tensile properties (The nanocomposite properties are summarized in Tab. 7 at the end of this chapter.). The adhesion of the matrix to the MWNTs was also investigated.

### **6.6.2 Adhesion of the Polypropylene to the Carbon Nanotubes**

The quality of the adhesion of the matrix sPP to the MWNTs was estimated by SEM. From these pictures, it can be seen if the wetting of the fibers by the polymer is good or poor. A good wetting, in turn, indicated a good adhesion. A 100,000-fold magnification of an sPP/MWNT nanocomposite containing 0.4 % carbon nanotubes is shown in Fig. 64. The arrow indicates a place where an individual tube can be seen above and below the polymer surface. This means that the tubes are actually wetted by the polymer. More nanotubes, which partly stick out of the polymer surface, can be seen in this picture, but no tube pull-out is visible.

The next picture (Fig. 65) shows a 10,000-fold magnification of an sPP/MWNT with 0.9 % of carbon nanotubes. On the left side of the picture, a large agglomerate of nanotubes is shown, which eventually is covered with polymer, as can be seen in the middle and on the right side of the picture. In larger magnifications, it can be seen that parts of the nanotubes in the bundle are covered with polymer to some extent.



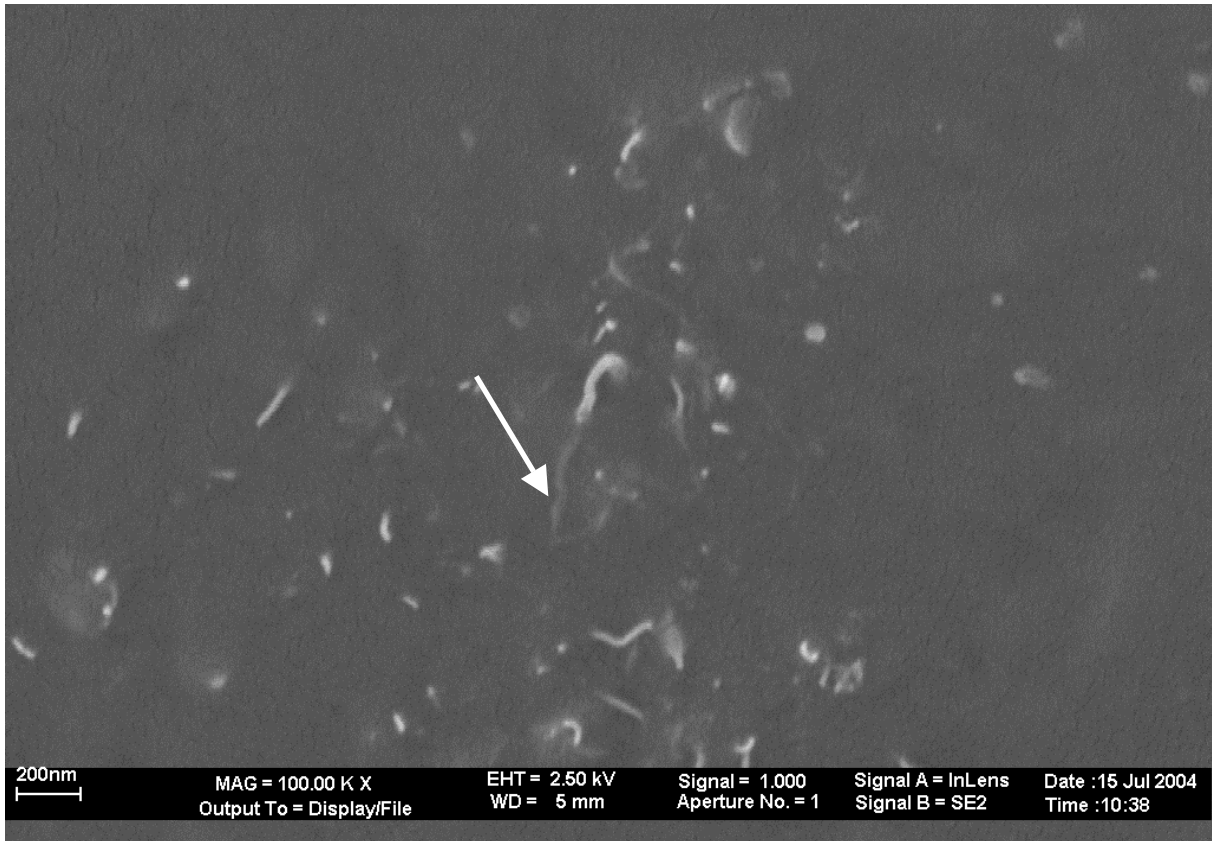


Fig. 64: SEM picture(magnification 100,000 times) of an sPP/MWNT nanocomposite containing 0.4 % nanotubes (KW318).

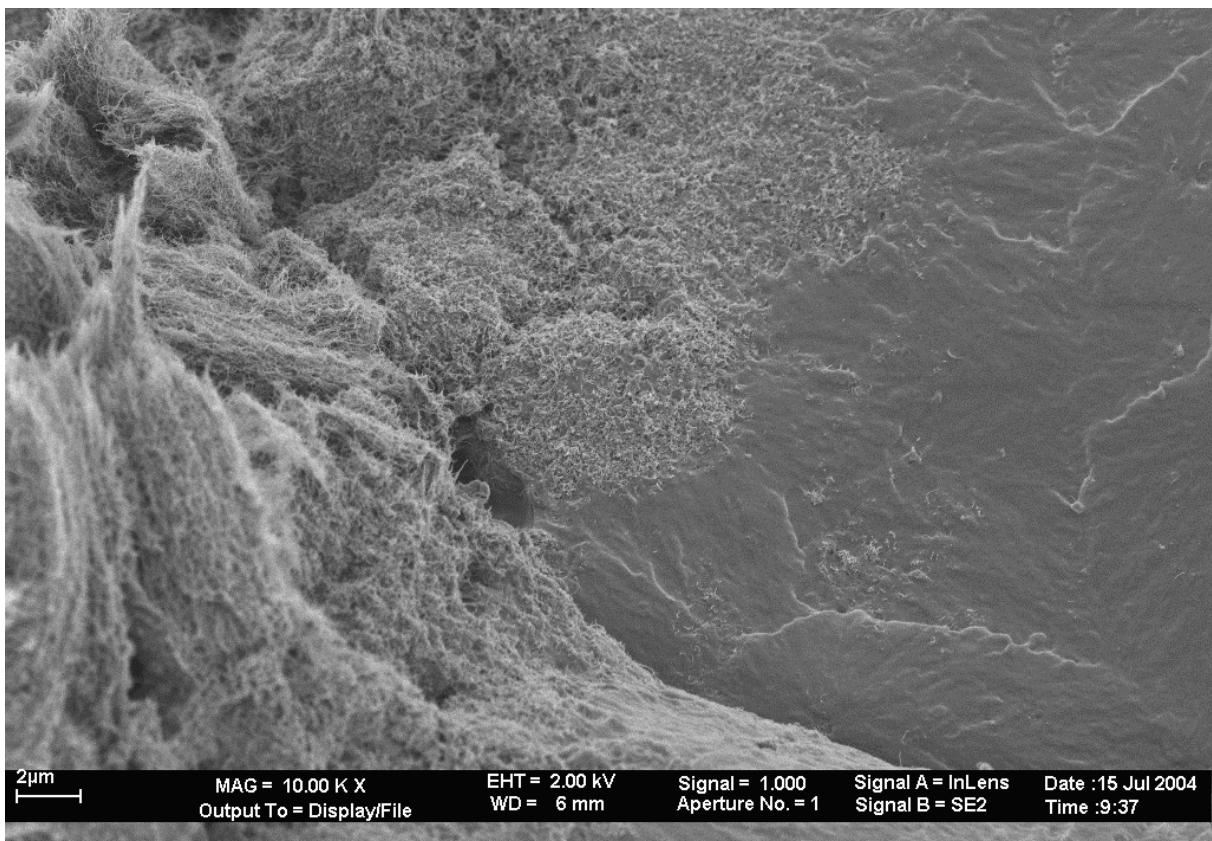


Fig. 65: SEM picture (magnification 10,000 times) of an sPP/MWNT nanocomposite containing 0.9 % nanotubes (KW323).

It is difficult to obtain sharp images at very high magnifications because the nanocomposite samples move in the electron beam. The following micrograph (Fig. 66) shows the highest magnification possible with the equipment at hand. It is a 120,000-fold magnification of the right part of Fig. 65 which is sufficiently large to make the observation of the single tubes possible. They are not present as bundles, but as individual tubes, which indicates a good dispersion in this region. Moreover, no pull-out of nanotubes out of the polymer matrix is observed. This is proof of a very good adhesion of the polymer matrix to the nanotube surface because otherwise MWNTs pointing straight out of the polymer surface and holes where they could have been pulled out of the polymer should have been observed. The inset in Fig. 66 indicates a well-wetted carbon nanotubes, which also is a sign of a good adhesion between the components of the nanocomposite. More individual nanotubes partly incorporated in the matrix and partly sticking out of it are visible throughout the image.



**Fig. 66:** SEM picture (magnification 120,000 times) of an sPP/MWNT nanocomposite containing 0.9 % of carbon nanotubes (KW323).

### 6.6.3 Crystallization and Melting Behavior of the sPP/MWNT Nanocomposites

#### 6.6.3.1 Melting Temperature and Crystallinity

The melting temperature of the sPP/MWNT nanocomposites was elevated slightly with regard to the pure sPP. The dependence on the filler content is shown in Fig. 67. A table of all polymer properties can be found at the end of this chapter (Tab. 3) All melting temperatures of the nanocomposites lay at least two to four degrees above those of the neat sPP, but showed hardly any dependence on the filler content. The enhancement of the melting temperature was only moderate but detected in all samples investigated.

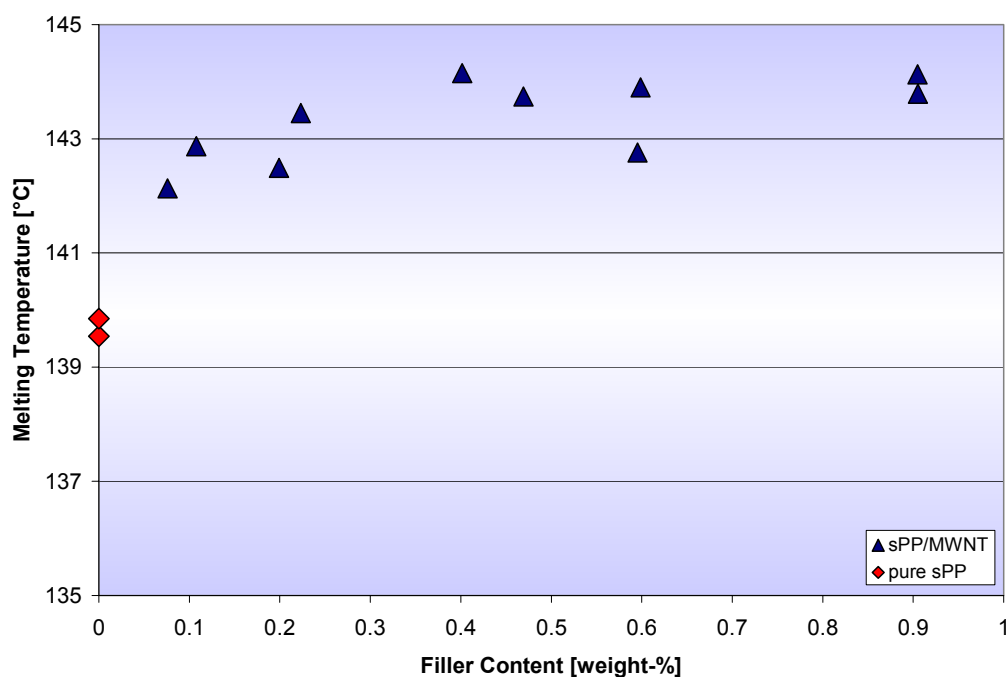


**Fig. 67: Influence of the filler content on the melting temperatures of the sPP/MWNT nanocomposites.**

The crystallinity as shown in Fig. 68 was also increased slightly with respect to the pure polymer as well. Also in this case, no trend regarding the dependence on the filler content is observed. All crystallinities were calculated from the melting peak of the second heat on the basis of a crystallization enthalpy of 164 J/g for the 100 % crystalline material<sup>[139]</sup>.

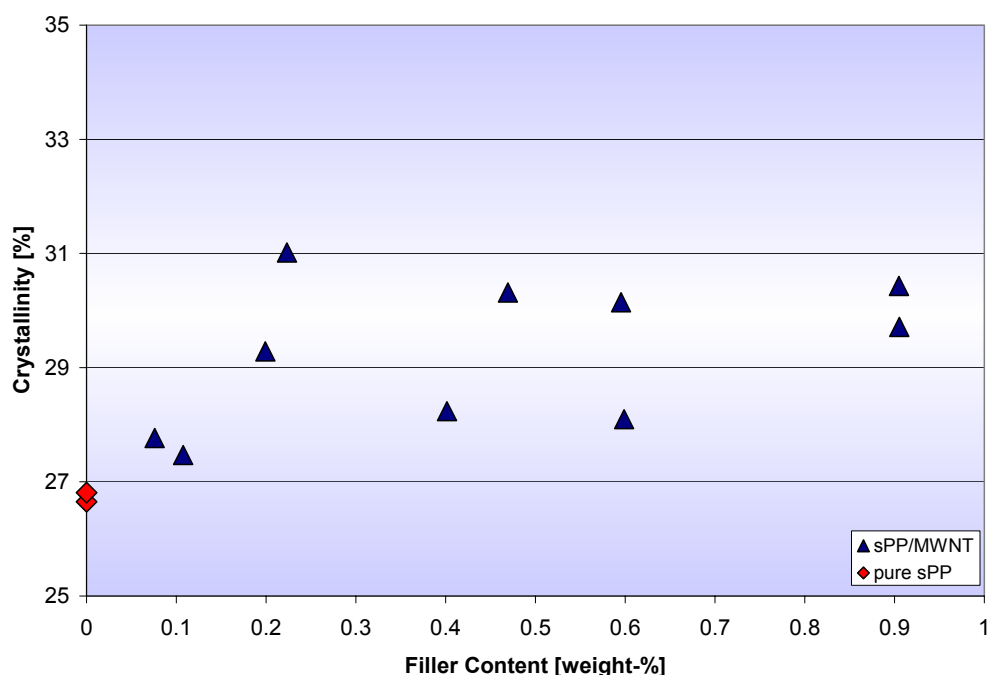


**Fig. 68: Influence of the filler content on the crystallinity of the sPP/MWNT nanocomposites.**

Some authors report that no changes in the melting peak shape or the melting temperature were found<sup>[86]</sup>, while others state that the melting as well as the crystallization peak were narrower in the nanocomposite than in the pure polymer<sup>[116]</sup>. The former investigated iPP/MWNT films obtained by solution casting, while the latter had prepared iPP/SWNT samples by a melt-compounding process. The differences in observation could thus be due to the different carbon nanotubes or the preparation process used.

With regard to the crystallinity, PP/SWNT nanocomposites that had been prepared by solution blending from PP and SWNT modified with octadecylamine have been examined. It seemed to remain approximately constant within experimental error, but the effect of the SWNTs on the crystallinity remained a bit obscure<sup>[131]</sup>.

In this work, a small enhancement of the melting temperature was found upon addition of 0.1 to 0.9 % of carbon nanotubes. At the same time, the melting temperature was independent of the filler content. The crystallinity with regard to the melting peak was very little enhanced for the nanocomposite in comparison to the pure sPP.

### 6.6.3.2 Crystallization Temperatures

A more pronounced effect of the filler content was observed for the crystallization temperatures (see Fig. 69 and Tab. 7). All crystallization temperatures of sPP/MWNT were



located above the crystallization temperature of pure sPP (96 °C). Already at a filler content as low as 0.1 weight-%, the crystallization temperature was raised by 5 °C in comparison to that of neat sPP. This effect was even more pronounced at higher filler contents. The nanocomposites containing 0.9 % MWNTs exhibited a crystallization temperature of 111 °C, which was 15 °C higher than that of pure sPP. A linear dependence of the crystallization temperature on the MWNT content was observed in the range of filler loadings investigated as is indicated by the straight line in Fig. 69.

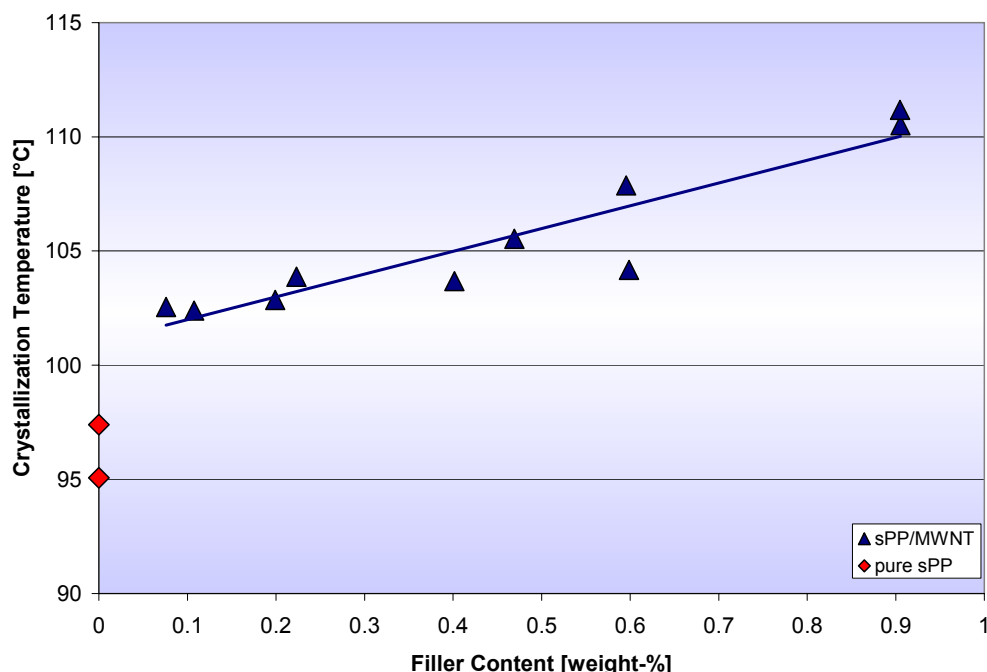


**Fig. 69: Influence of the filler content on the crystallization temperature of the sPP/MWNT nanocomposites.**

The rise in the crystallization temperature upon incorporation of carbon nanotubes is an indication of the nucleating ability of the MWNTs.

Agreement exists about the fact that the crystallization temperature of PP is raised by the addition of carbon nanotubes. The extent of the increase shows great differences, however.

The crystallization temperature of iPP/MWNT films obtained by solution casting was shifted to higher values by about 8 °C upon addition of 0.5 % of carbon nanotubes [86]. In contrast to that, the addition of 0.5 % SWNTs to PP/EPDM blends by melt-compounding led to a rise in crystallization temperature of 4 °C only. At higher filler loadings, even a lowering of the  $T_c$  was found<sup>[130]</sup>. In iPP/SWNT nanocomposites that had been prepared by solution blending of PP and SWNT modified with octadecylamine a filler content of 1.8 % SWNTs was necessary

to reach a 5 °C increase in crystallization temperature. The peak sharpened when SWNTs were present<sup>[131]</sup>.

A melt-compounded sample of PP/SWNT was subjected to isothermal and non-isothermal crystallization. The crystallization temperature of the composite containing 0.8 % SWNT was raised by 11 °C as compared to the neat polymer<sup>[116]</sup>. The differences in the effect of comparable amounts of carbon nanotubes are probably due to differences in the homogeneity of the dispersion in the polymer matrix and to the different types of nanotubes used.

In this work, an enhancement of the crystallization temperature of 5 to 15 °C of the sPP/MWNT nanocomposites in comparison to the pure polymer could be achieved. At a filler content of 0.5 weight-% of MWNTs, the crystallization temperature was raised by 10 °C which is a stronger increase more than in the publications cited above, even though the cooling rate was the same in all experiments. A possible reason is the different preparation method used in this work which could have led to a better dispersion of the nanotubes.

#### 6.6.3.3 Half-time of Crystallization

Generally, the half-times of crystallization increase with increasing temperatures, which could be confirmed for all materials investigated (Fig. 70 and Tab. 7). It was significantly lower for the sPP/MWNT nanocomposites than for the pristine polymer which is due to the nucleation of crystallite growth from the MWNT surface.

The comparison of the nanocomposites with different filler contents shows that the crystallization at a certain isothermal crystallization temperature proceeded faster when more MWNTs were incorporated in the polymer. If one takes a look at the half-time of crystallization at 122 °C, for example, it can easily be seen that it was significantly reduced when more carbon nanotubes were present. The half-time of crystallization at this temperature was 15 minutes for the pure polymer. When only 0.1 weight-% of carbon nanotubes were incorporated, it was lowered to one third of that value, accordingly, to only 5 minutes. When the percentage of MWNTs was raised to 0.2 % the half-time of crystallization is reduced by roughly one minute and at a filler content of 0.4 % by another 2 minutes to 2.3 minutes. The nanocomposite with a filler loading of 0.9 % crystallizes too fast to allow for the determination of the half-time of crystallization possible at this crystallization temperature.

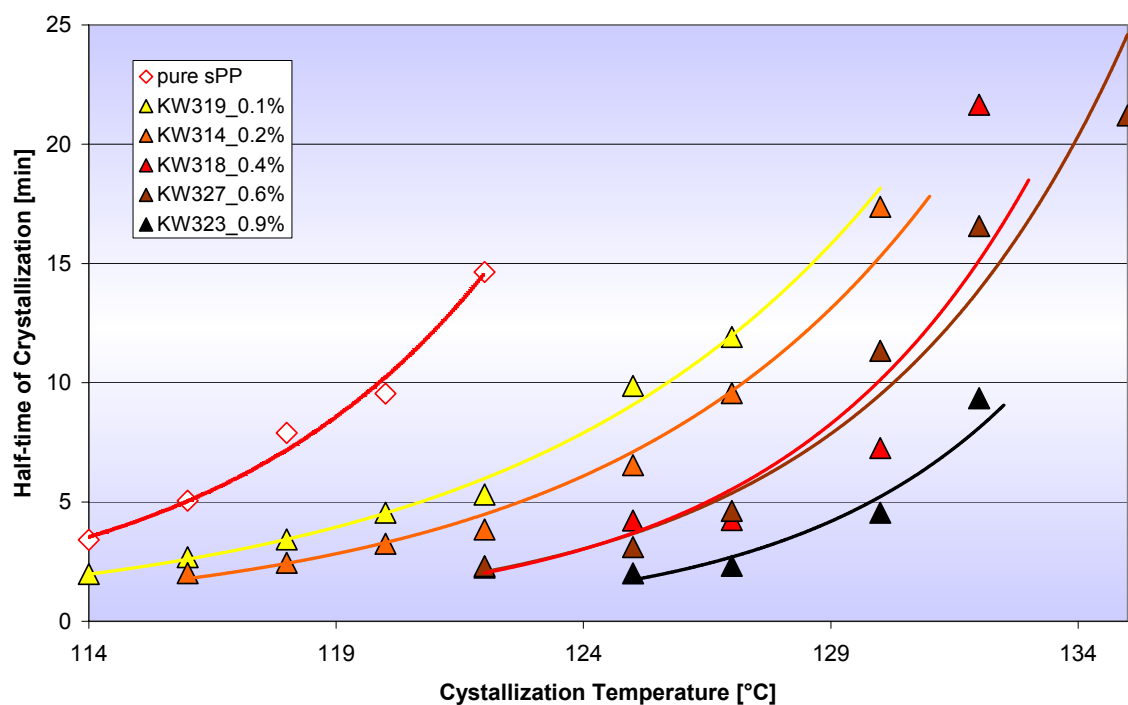


**Fig. 70: Half-time of crystallization of the sPP/MWNT nanocomposites at different isothermal crystallization temperatures.**

The same trends described in detail for the crystallization temperature of 122 °C can be seen for the other crystallization temperatures. It should be noted that the crystallization of the pure sPP and the nanocomposites with low filler loadings was too slow at higher isothermal crystallization temperatures to make a reliable determination with the DSC at hand possible.

The half-time of crystallization of CNT nanocomposites was found to decrease in all cited references with regard to the pure polymers. The half-time of crystallization of a PP nanocomposite containing 1 % of MWNTs prepared by solution mixing under sonication was, for instance, found to be reduced as compared to that of the neat PP<sup>[91]</sup>.

The crystallization half-time of PP/SWNT nanocomposites that had been prepared by solution blending from PP and SWNT modified with octadecylamine was also found to decrease by roughly a factor of two upon addition of SWNTs<sup>[131]</sup>. A reduction was also found for PP/EPDM/SWNT nanocomposites prepared by melt-compounding. In this case, the half-time of crystallization showed a minimum at 0.5 % SWNT (1/2 the time of that of the pure polymer). The authors attributed this to that fact that the SWNTs nucleate crystallite growth on one hand, but that they hinder the spherulite growth on the other hand<sup>[130]</sup>. An

inhomogeneous distribution of the carbon nanotubes at higher filler contents could also be the reason.

In accordance with the results presented above, the half-time of crystallization of the nanocomposites could also be reduced significantly for the samples prepared in this work. In contrast to other works<sup>[130,131]</sup>, a strong dependence of the half-time of crystallization on the filler content was found, indicating a faster crystallization for sPP/MWNT nanocomposites with higher filler loadings.

#### 6.6.3.4 Avrami Analysis

A closer look at the crystallization behavior of the nanocomposites confirms that the MWNTs acted as nucleating agents. The rate constant of crystallization ( $K$ ) and the Avrami parameter ( $n$ ) of the nanocomposites were determined from the respective Avrami plots as described in section 6.1.3.3. The rate constants of crystallization for the pure sPP and nanocomposites with different loadings of carbon nanotubes are shown in Fig. 71 (see also Tab. 7). The values that are not shown could not be determined with the DSC at hand either because crystallization proceeded too slowly or too fast at the respective temperatures for a reliable evaluation of the data.

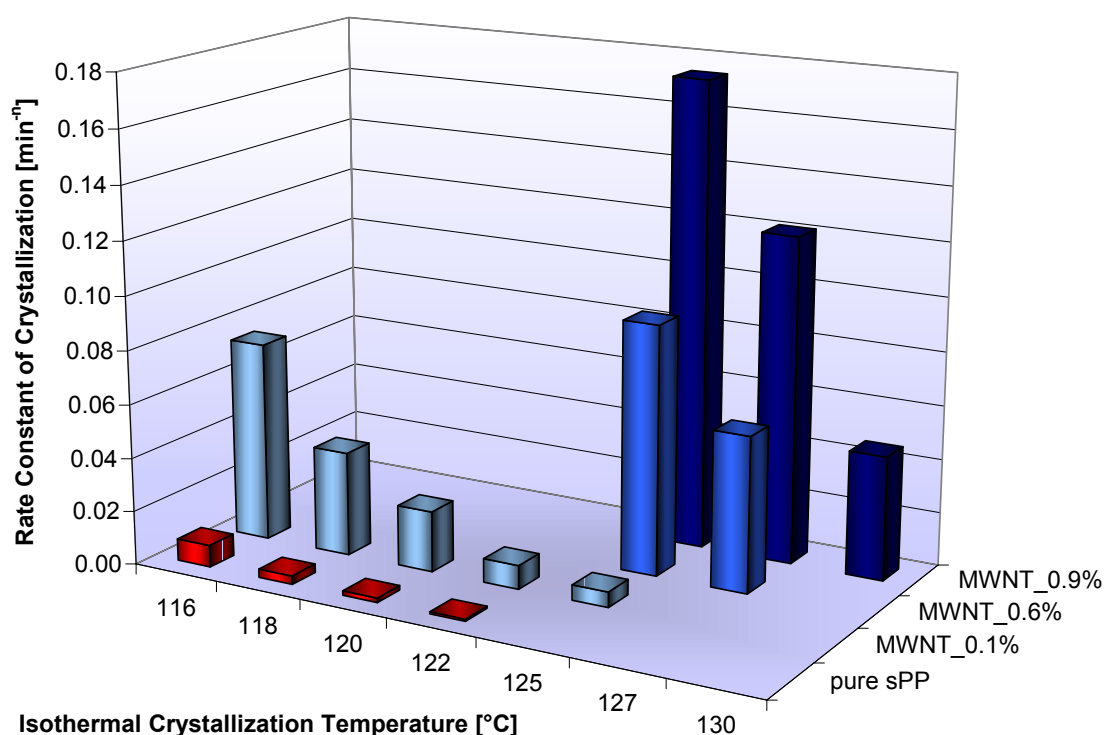


**Fig. 71: Influence of the filler content and the isothermal crystallization temperature on the rate constant of crystallization.**

From the values shown, it can be clearly seen that the pure sPP exhibited the lowest crystallization rate at all temperatures investigated. The crystallization also slowed down with increasing isothermal crystallization temperature as expected. When 0.1 weight-% of carbon nanotubes were incorporated into the polymer matrix, the crystallization rate constant at 118 °C was increased by 1100 % as compared to the pure PP.

A comparison of the crystallization behavior of the nanocomposites with different loadings at 125 °C shows that a larger percentage of filler in the polymer led to a faster crystallization of the material. The crystallization of the pure sPP could not be observed during the crystallization time of up to 1 hour, and also the crystallization of the nanocomposite containing 0.1 % MWNTs proceeded slowly with a rate constant of  $5.7 \cdot 10^{-3} \text{ min}^{-n}$ . In contrast to this, the nanocomposite containing 0.9 % carbon nanotubes crystallized with a rate constant of  $1.7 \cdot 10^{-1} \text{ min}^{-n}$ .

Analysis of the Avrami parameter (Fig. 72) shows a reduction in the dimensionality of the crystallite growth upon addition of carbon nanotubes to the PP matrix. This is evidenced by the reduction of the Avrami parameter from 2.5 for the neat polymer to values ranging from 2.3 to 1.6 depending on the amount of filler in the nanocomposite.

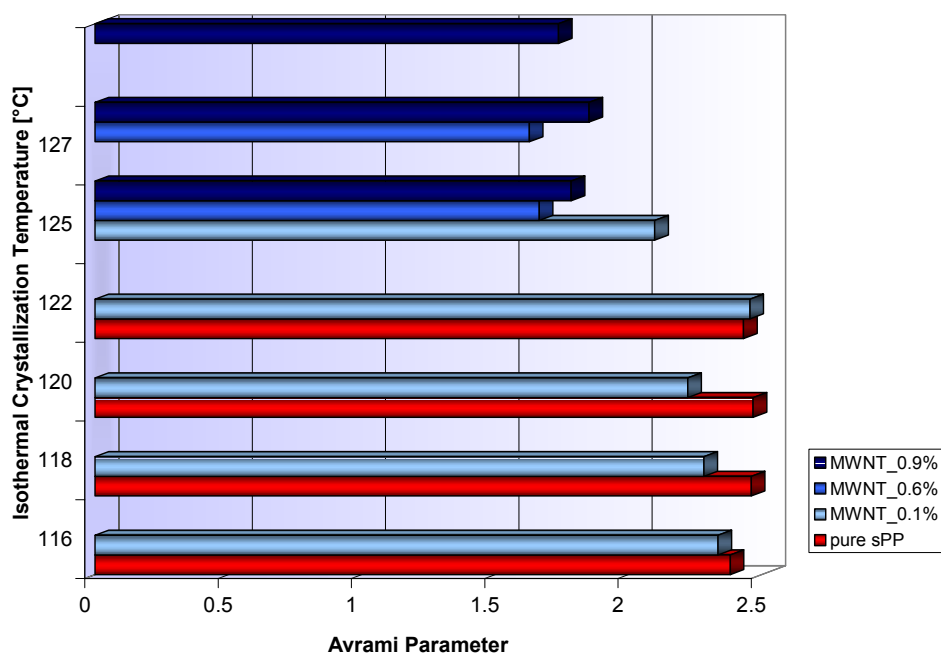


Fig. 72: Influence of the isothermal crystallization temperature and the filler content on the Avrami parameter (n).

Some of the results presented above are in accordance with publications regarding the effect of carbon nanotubes on the crystallization behavior of iPP. Controversial effects have been reported in different publications, which shall be discussed in comparison to results obtained in this work.

Agreement exists about the fact that the rate of crystallization is enhanced by the addition of carbon nanotubes to a polymer matrix. As discussed above, the reduction in half-time of crystallization has been taken as proof of this fact<sup>[91]</sup>. Additionally, some authors have performed Avrami analyses of their results to determine the rate constant of crystallization.

In several works, the rate of crystallization was found to be increased by addition of carbon nanotubes<sup>[86,116,130,131]</sup>. The influence of the filler content is discussed controversially, though. The rate of crystallization of PP in PP-EPDM blends with filler loadings of 0 to 1 % SWNTs prepared by melt-compounding was found to rise until a filler content of 0.5 % was reached. At higher filler loadings, the crystallization was slowed down again, still being faster than in the neat polymer, though<sup>[130]</sup>. The rate constant (K) of crystallization of PP/SWNT nanocomposites that had been prepared by solution blending from PP and SWNT modified with octadecylamine seemed to be unaffected by the amount of SWNT<sup>[131]</sup>.

In accordance with the above publications, a faster crystallization rate was also found in this work. Additionally, a strong dependence of the rate constant of crystallization on the filler content was observed. This effect was so strong that evaluation of the crystallization data for nanocomposites with a high filler content at low isothermal crystallization temperatures was impossible. The significant acceleration of the crystallization process observed is, therefore, dependant on the filler content. This is especially interesting because the slow crystallization rate of sPP has hindered its commercial application<sup>[6]</sup>.

The effect of the presence of carbon nanotubes on the Avrami parameter (n) has been discussed controversially. In iPP/MWNT films that had been prepared by solution casting, the Avrami exponent was found to drop from 3.1 for the pure polymer to 2.5 upon addition of 0.5 % of carbon nanotubes<sup>[86]</sup>. A reduction was also found for the Avrami exponent determined for PP/EPDM melt-blended with SWNTs. It decreased with increasing nanotube content from 2.46 to 2.00. The values were attributed to a heterogeneous nucleation followed by a diffusion controlled spherulitic crystalline growth<sup>[130]</sup>.

In contrast to this, the Avrami exponent ( $n$ ) for PP/SWNT nanocomposites that had been prepared by solution blending of PP and SWNT modified with octadecylamine was raised by the addition of 0.6 % carbon nanotubes. It had a value of approximately 2.8 as compared to values between 1.8 and 2.4 for the neat PP or the nanocomposite containing 1.8 % SWNTs<sup>[131]</sup>.

A higher Avrami exponent of the nanocomposite than in the pure polymer was also found in a melt-compounded sample of PP/SWNT. A value of 3.4 was observed for the nanocomposite as compared to 2.8 for the neat PP at an isothermal crystallization temperature of 130 °C. The value close to three implies a three-dimensional heterogeneous crystal growth<sup>[116]</sup>.

Here, a reduction of the Avrami parameter was observed upon addition of the MWNTs. The extent of the effect is not totally clear, though, because differences in isothermal crystallization temperatures also evoke differences in the Avrami parameter. As mentioned earlier, the nanocomposites with higher filler loadings could not be investigated at low  $T_{iso}$ , and the pure sPP crystallized too slowly at high  $T_{iso}$  to make a comparison of the data over wide ranges of isothermal crystallization temperatures possible. A reduction of the Avrami parameter would point to a reduction of the dimensionality of the crystallite growth by addition of carbon nanotubes. As the nucleation caused by the MWNTs can be considered spontaneous, a value of  $n$  lower than 2 implies a crystallite growth between disc-like and rod-like (see section 6.1.3.3).

#### **6.6.4 Thermal Stability of the sPP/MWNT Nanocomposites**

The degradation of the neat polymer and the nanocomposites containing MWNTs was investigated using TGA. Experiments were performed at a heating rate of 5 °C/min. The results are shown in Fig. 73 and Fig. 74 (see also Tab. 7). The mass loss of the nanocomposites with different filler loadings and the pure polymer are shown in dependence of the temperature. The general shape of the curves is similar, but some differences can be seen when an analysis of the data according to Marsh is performed. These results are represented in Fig. 74.

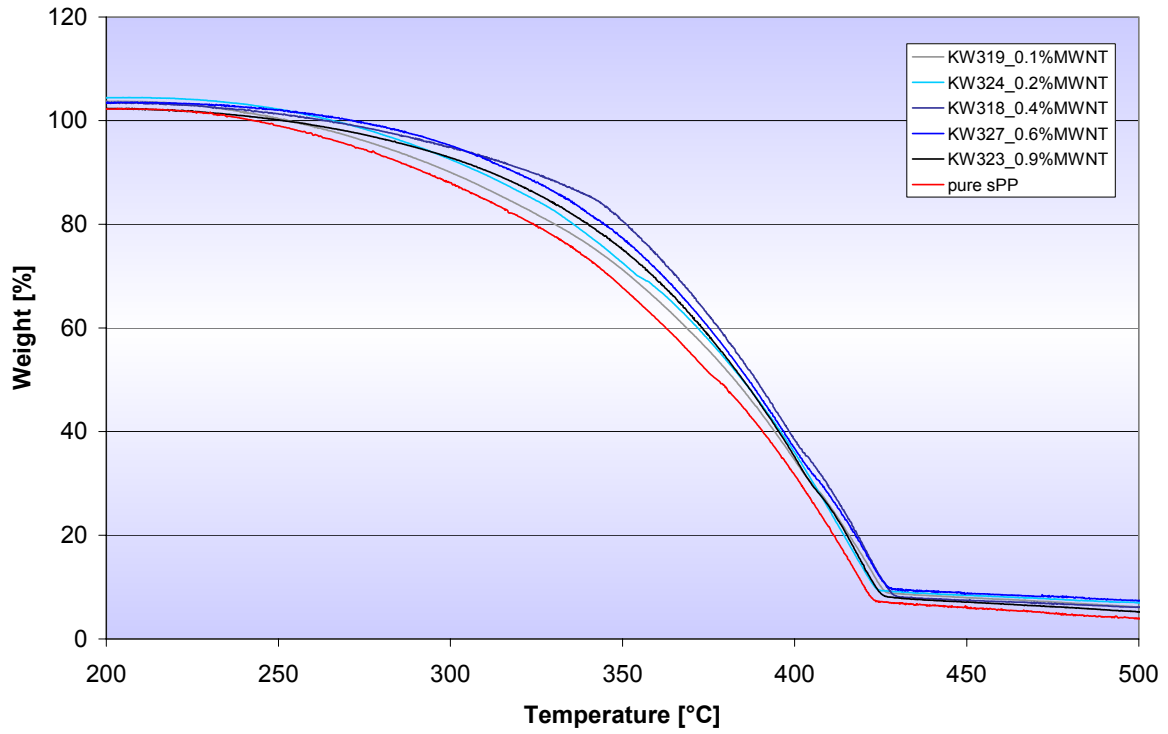


Fig. 73: Mass-loss of the sPP/MWNT nanocomposites in dependence on the temperature as determined by TGA.

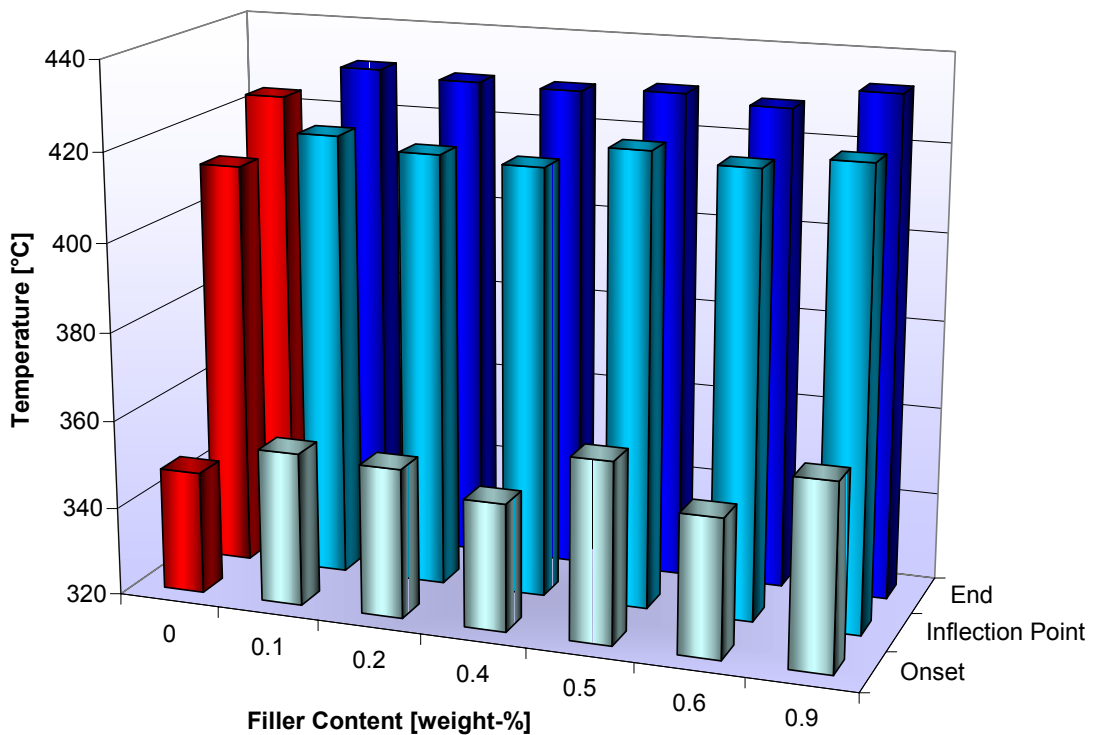


Fig. 74: Onset, inflection point and end of degradation of sPP/MWNT nanocomposites as determined by Marsh-analysis of the data obtained from TGA measurements.



It is obvious from this diagram that the onset of degradation, the inflection point ( $T_{\max}$ ), and the end of degradation were shifted to higher temperatures when carbon nanotubes were incorporated into the polymer. The three characteristic temperatures shown here have one thing in common: the enhancement was independent of the filler content in the range studied. A great difference in the extent of the improvement from one parameter to another was seen, though. The fact that no trend concerning the filler content was observable may be due to a high variance of the obtained data.

Some data is available in the literature concerning the degradation properties of iPP/MWNT nanocomposites. An enhancement of the degradation properties could be shown for nanocomposites containing 16 % MWNTs prepared by mixing of the components and subsequent hot pressing. These were subjected to TGA in air at a heating rate of 25 °C/min. The presence of the nanotubes raised the  $T_{\max}$  by 30 °C as compared to the neat PP, which was only a small further improvement compared to a filler content of 10 %[133].

Melt-compounded PP/MWNT nanocomposites were inspected with respect to their thermal degradation and flammability properties by TGA in nitrogen and in air at a heating rate of 10 °C/min. The composites showed a complex degradation behavior in air, showing multiple maxima in the weight loss rates. The authors attributed this to the presence of iron particles in the MWNTs. Furthermore, the results indicated that PP/MWNT nanocomposites burn much slower than the pure PP[135].

In another work, iPP/MWNT nanocomposites were prepared via melt-compounding and analyzed with respect to their degradation properties by TGA under nitrogen flow at a heating rate of 10 °C/min. At a content of 1 wt-% of MWNTs, the  $T_{\text{on}}$  was raised by 34 °C as compared to the pure PP and the  $T_{\max}$  was increased by only 7 °C. At a filler content of 5 % MWNTs, the  $T_{\text{on}}$  was increased by 74°C and the  $T_{\max}$  by 20 °C[132].

The relatively small effect of the MWNTs on the degradation behavior of the sPP in this work could, on one hand, be due to lower filler loadings than in most of the publications mentioned above. On the other hand, some authors have performed the measurements under nitrogen flow, whereas, the experiments in this work have been done in air. This should also influence the extent to which carbon nanotubes improve the stability of the nanocomposites. Detailed

analysis including nanocomposites with higher filler loadings would be necessary to further investigate the influence of the filler content on the degradation properties.

In addition to that, the heating rate plays an important role because the degradation of the polymeric material is shifted to higher temperatures at higher heating rates. In all cited publications, the heating rate was higher, generally leading to a higher degradation temperature.

### **6.6.5 Electrical Conductivity of the sPP/MWNT Nanocomposites**

The conductivity of the samples with different filler contents was evaluated using two-point measurements. None of the samples investigated showed any conductivity. This can be attributed to the fact that the filler content was very low. The highest amount of filler incorporated into the sPP matrix was 0.9 %. This was obviously not sufficient for the formation of a percolation network.

In contrast to this, iPP/MWNT nanocomposites prepared by melt-compounding have been shown to exhibit conductivity at filler incorporations as low as 0.05 vol.-%. The surface resistivity dropped to a value of  $10^5 \Omega/\text{square}$  at this filler content. A higher filler content was necessary when the nanotubes were aligned by fiber drawing of the nanocomposites<sup>[87]</sup>. The good conductivity is probably due to a more homogeneous dispersion than was accomplished in this work.

### **6.6.6 Tensile Properties of the sPP/MWNT Nanocomposites**

For the tensile test, films were prepared by hot-pressing of the nanocomposite powder. The stress-strain behavior was tested on test bars cut from these films. Some typical stress-strain curves are shown in Fig. 75. It can be seen that the general shape is similar for all sPP/MWNT nanocomposites tested. The high elongation at break (800 to 900 %) was reduced in some cases. This was probably caused by inhomogeneities of the films.

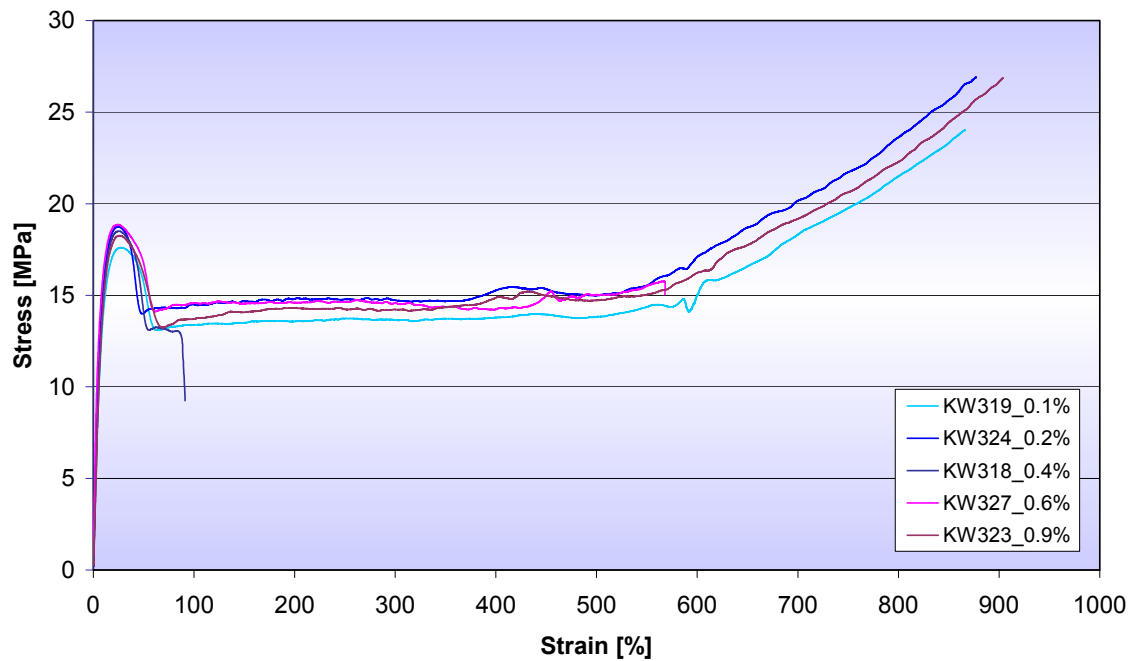


Fig. 75: Exemplary stress-strain curves of sPP/MWNT nanocomposites.

The influence of the filler content and the molecular weight on the yield strength of the nanocomposites is shown in Fig. 76 and Fig. 77, respectively (see also Tab. 7: Properties of some sPP/MWNT nanocomposites).

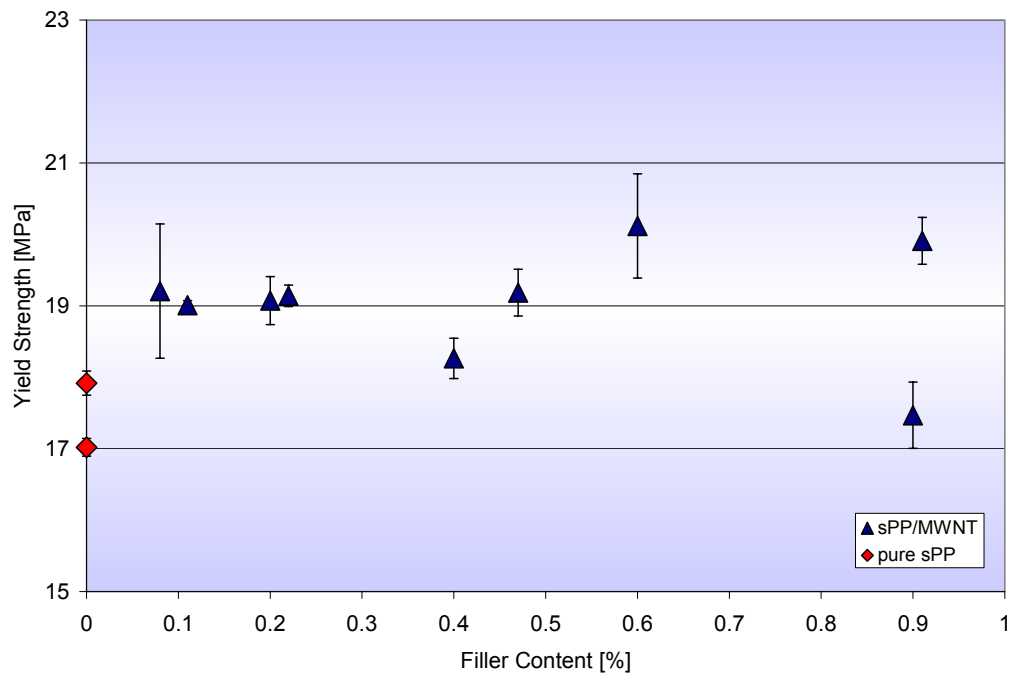
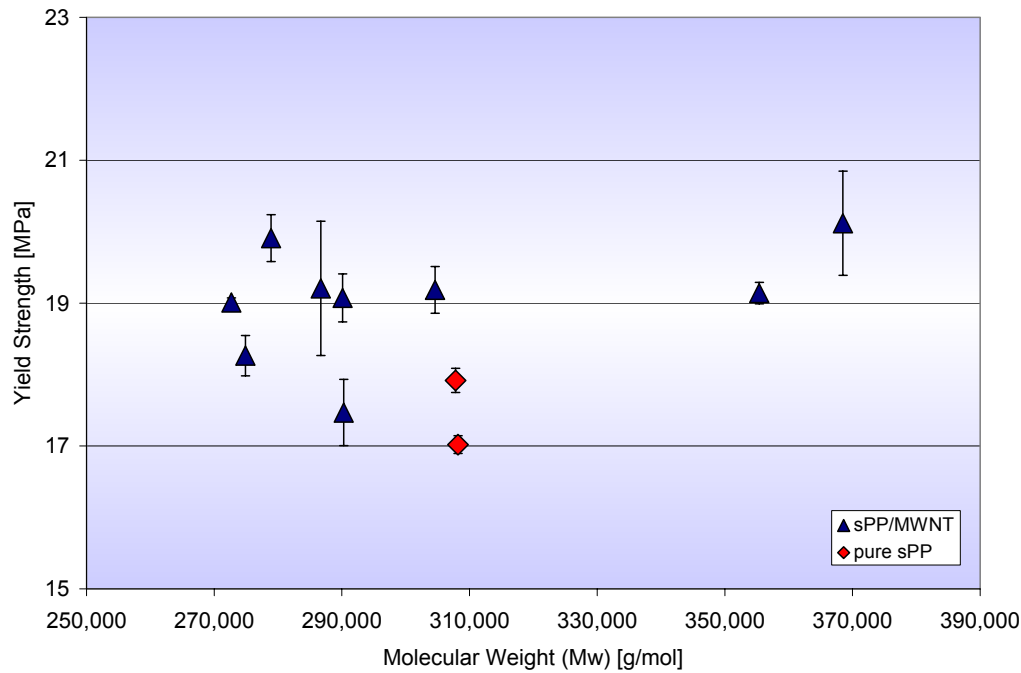


Fig. 76: Influence of the filler content on the yield strength of the sPP/MWNT nanocomposites.



**Fig. 77: Influence of the molecular weight on the yield strength of the sPP/MWNT nanocomposites.**

A slightly increased yield strength was found for the sPP/MWNT nanocomposites as compared to the neat polymer. The improvement lay between 10 and 15 %, and no clear trend regarding the filler content was detected in the range investigated. The yield strength was also independent of the mass average of the molecular weight. This means that improvements in the yield strength were not caused by a higher molecular weight of the nanocomposites.

The Young's moduli of the tested samples was calculated from the stress-strain curves. The values scattered very much, and, consequently, they are not reported here. No influence of the filler content on the modulus was detected.

Some publications are available dealing with the tensile properties of iPP/MWNT nanocomposites. The results are somewhat discordant. Andrews et al.<sup>[87]</sup> found that the elastic modulus of iPP/MWNT nanocomposites increased when the filler content increased from 0.05 to 12.5 vol.-%; whereas, the yield strength decreased for the same range of filler contents.

Fibers of PP/SWNT nanocomposites with a filler content of around 1 % prepared by melt-compounding and subsequent melt-spinning did not show any difference in yield strength compared to pure PP fibers. Also the modulus remained largely unchanged. This was probably due to a poor dispersion of the nanotubes<sup>[116]</sup>.

The relatively low degree of improvement of the composite properties as compared to the pure polymer achieved in this study could be attributed to a non-optimum distribution of the carbon nanotubes in the matrix. The SEM micrographs clearly show a good wetting of the nanotubes with the polymer in the regions with a homogeneous distribution. On the other hand, it could be seen from the microscopic and SEM images that regions of nanotube aggregates were still present in the polypropylene matrix. These could have led to premature failure of the material even though the MWNTs in some of these aggregates were wetted with polymer.

**Tab. 7: Properties of some sPP/MWNT nanocomposites.**

<b>Filler Content [wt.-%]</b>	<b>0</b>	<b>0.1</b>	<b>0.5</b>	<b>0.9</b>
<b>Activity</b> [kg <sub>Pol</sub> /(mol <sub>Zr</sub> ·h·mol <sub>Mon</sub> /l)]	4,300	3,000	3,500	4,100
<b>Melting Temperature [°C]</b>	140	142	144	144
<b>Crystallization Temperature [°C]</b>	96	103	105	111
<b>Rate Constant of Crystallization [<math>\cdot 10^{-4} \text{ min}^{-n}</math>]</b>	7.5	88	n.d.	n.d.
<b>Half-time of Crystallization [min]</b>	14.6	5.3	2.3	n.d.
<b>Degradation Temperature (T<sub>max</sub>) [°C]</b>	412	421	420	423
<b>Tensile Strength [MPa]</b>	17.5	19.1	19.2	18.7

<sup>a</sup>The rate constant of crystallization and the half-time of crystallization were determined from isothermal DSC measurements at 122 °C

## **6.7 Syndiotactic Polypropylene/Carbon Black Nanocomposites**

sPP/carbon black nanocomposites were synthesized for comparison with the nanocomposites containing fillers with high aspect ratios. The carbon black used was also nano sized with regard to its primary particles which had a diameter of 30 nm.

Based on the results from the preliminary experiments, sPP/CB nanocomposites were synthesized by *in situ* polymerization of propylene with metallocene **1** after sonication of the fillers with the sonopuls homogenizer. As the carbon black cannot aggregate in bundles due to its spherical shape, it was assumed that the ideal sonication conditions determined for the carbon nanofibers would also suffice for this type of filler. The CB was sonicated in toluene suspension at an ultrasonic amplitude of 20 % for 15 minutes. The polymerizations were carried out without pre-reaction as described in the experimental section.

A series of sPP/CB nanocomposites with filler contents between 0.1 and 1 weight-% was prepared, and these materials were characterized with respect to their crystallization behavior, their thermal degradation, their electrical properties, and their tensile properties (see also Tab. 8).

The average activity was between 4,000 and 5,000  $\text{kg}_{\text{Pol}}/(\text{mol}_{\text{Zr}} \cdot \text{h} \cdot \text{mol}_{\text{Mon}}/\text{l})$ , which is in the same range as the activity of 4,300  $\text{kg}_{\text{Pol}}/(\text{mol}_{\text{Zr}} \cdot \text{h} \cdot \text{mol}_{\text{Mon}}/\text{l})$  for the polymerizations without filler

### **6.7.1 Dispersion of the Carbon Black**

The dispersion of the carbon black was relatively good as can be seen from Fig. 78. Aggregates of carbon black are still visible, but at a magnification this low it can not be excluded that they were soaked with polymer. From the electron micrographs of sPP/CNF and sPP/CNT nanocomposites which showed wetting of the fillers even in the aggregates it is assumed that also the agglomerates in sPP/CB are partly penetrated by polymer.

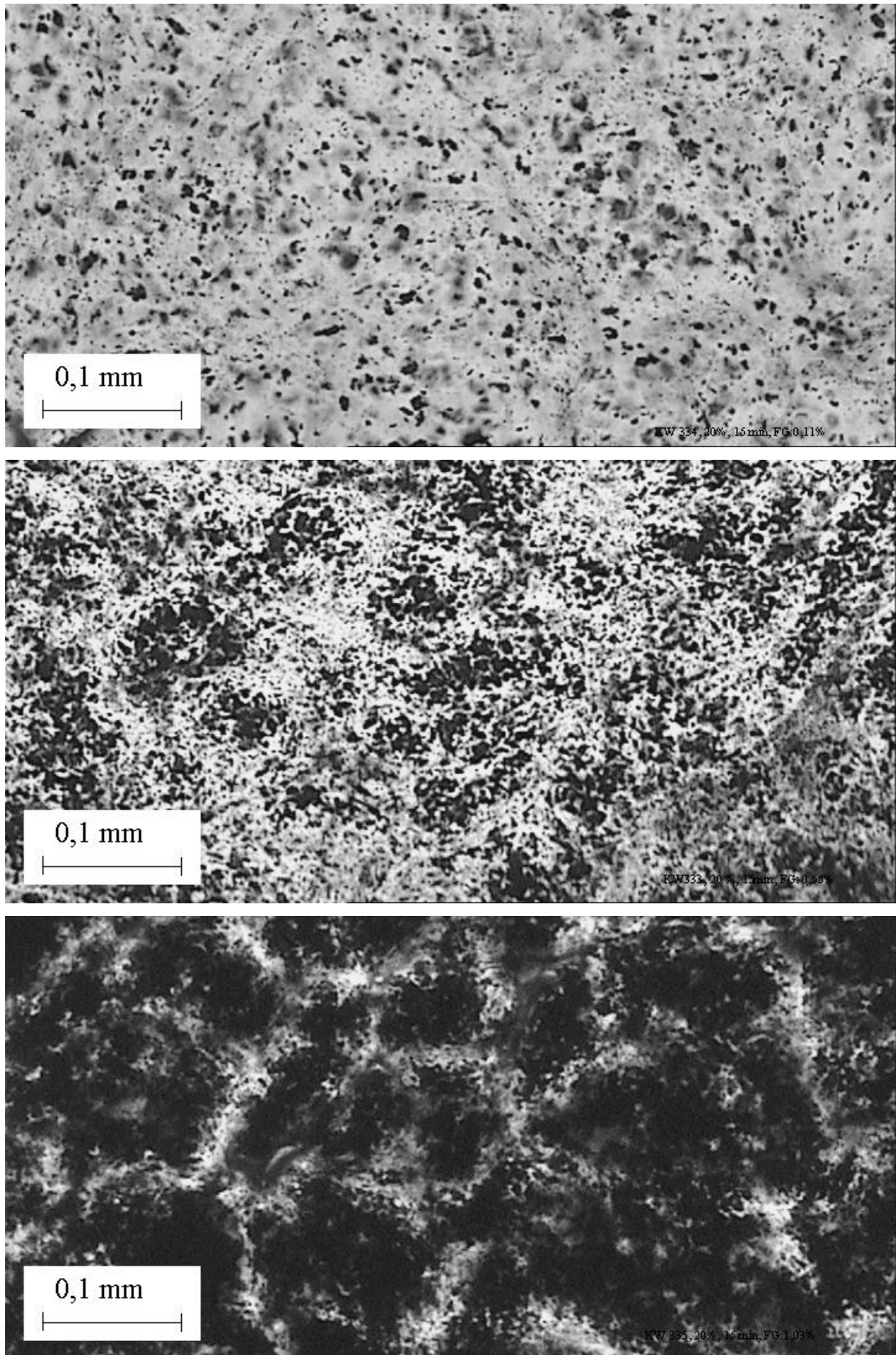


Fig. 78: Microscopic photographs of sPP/CB nanocomposites containing 0.1, 0.6 and 1% CB, respectively.

## 6.7.2 Crystallization and Melting Behavior of the sPP/CB Nanocomposites

### 6.7.2.1 Melting Temperature and Crystallinity

The melting temperatures of the sPP/CB nanocomposites were in the range of 139 to 141°C and, therefore, in the same region as for the neat polymer (see Tab. 8 at the end of this chapter). Also the crystallinity of 28 %, calculated with a value of 164 J/g (see section 6.1.3.1), was comparable to that of the pure polymer for all sPP/CB nanocomposites.

### 6.7.2.2 Crystallization Temperatures

The crystallization temperatures of the sPP/CB nanocomposites shown in Fig. 79 and Tab. 8 were elevated by 4 to 6 °C with respect to those of the pure polymer. A linear increase of the crystallization temperature with rising filler content was detected in the range of filler loadings studied.

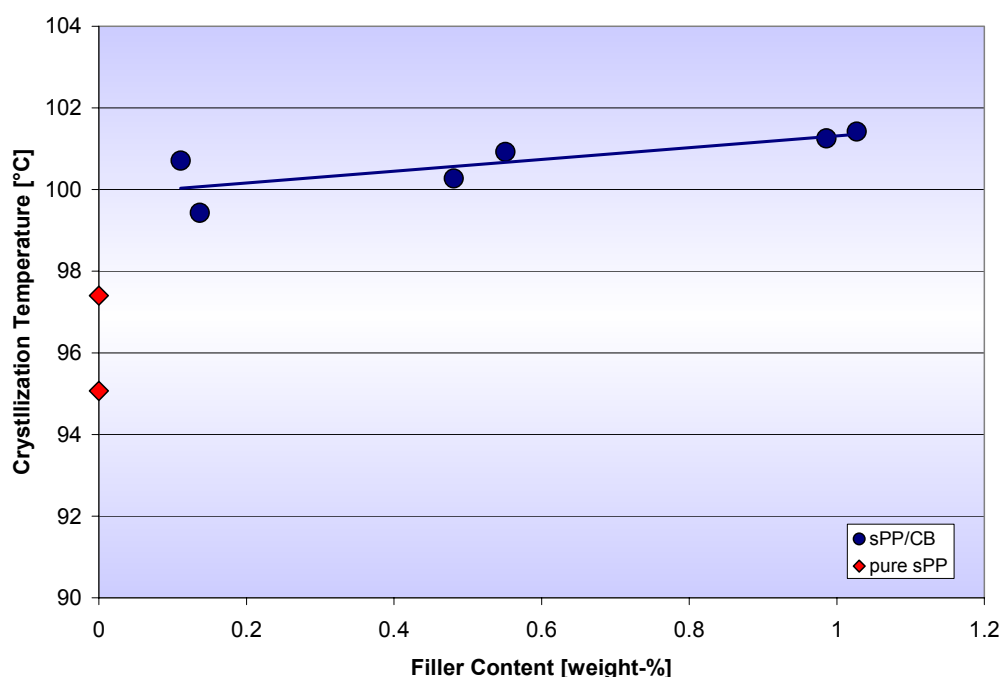


Fig. 79: Influence of the filler content on the crystallization temperature of the sPP/CB nanocomposites.

### 6.7.2.3 Half-time of Crystallization

The influence of the isothermal crystallization temperature and the filler content on the half-time of crystallization of the sPP/CB nanocomposites is shown in Fig. 80 and Tab. 8. Naturally, the crystallization half-time increased with increasing isothermal crystallization temperature because the crystallization proceeded more slowly. Although no significant differences in the half-time of crystallization were observed regarding the different filler



loadings, it should be noted that the crystallization proceeded faster in the presence of carbon black than in the pure polymer. The time that it took 50 % of the material to crystallize was reduced roughly by one-half upon addition of carbon black for all crystallization temperatures investigated.

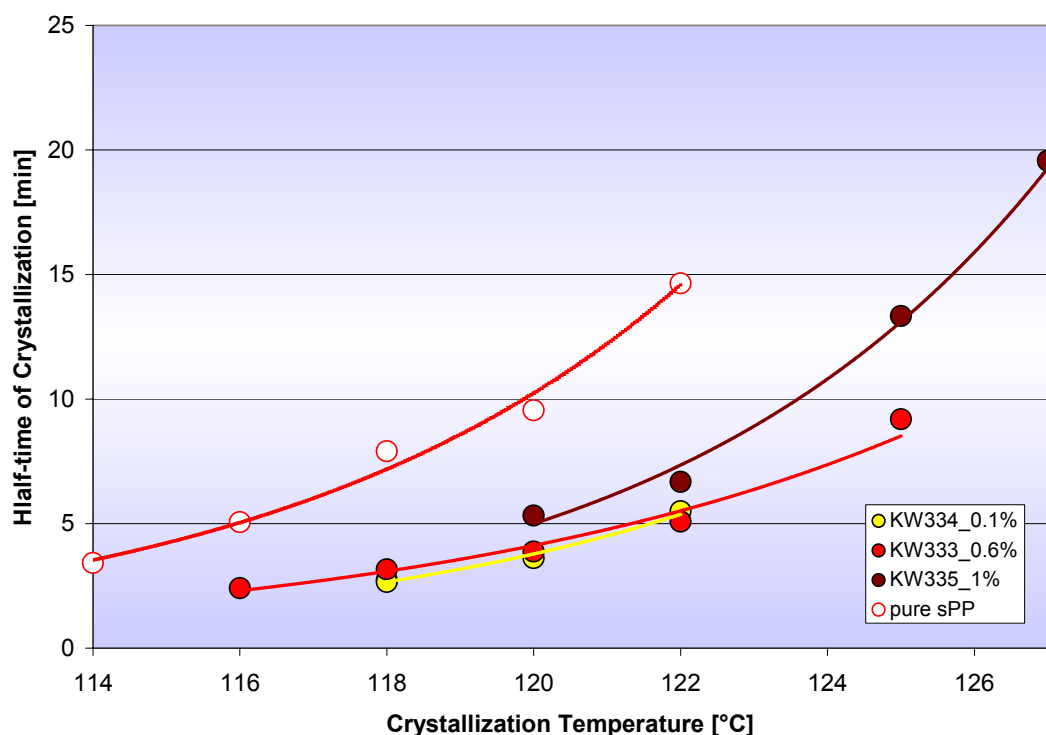


**Fig. 80:** Influence of the isothermal crystallization temperature on the half-time of crystallization of the sPP/CB nanocomposites.

#### 6.7.2.4 Avrami Analysis

An Avrami analysis of the data obtained from isothermal crystallization experiments was conducted also for the sPP/CB nanocomposites. The rate constant of crystallization of the sPP/CB nanocomposites is shown in Fig. 81 (see also Tab. 8). It is clearly seen that the rate of crystallization decreased with increasing isothermal crystallization temperature. This was expected and observed for all sPP/CB samples investigated. The incorporation of CB also increased the rate of crystallization for all samples tested. Up to a filler content of 0.6 %, the rate constant of crystallization increased with increasing content. The value was four times that of the pure polymer at an isothermal crystallization temperature of 120 °C for a filler loading of 0.6 %, for example. The rate of crystallization slowed down somewhat for higher loadings. This could be due to a hindered mobility of the polymer chains due to the presence of the fillers.

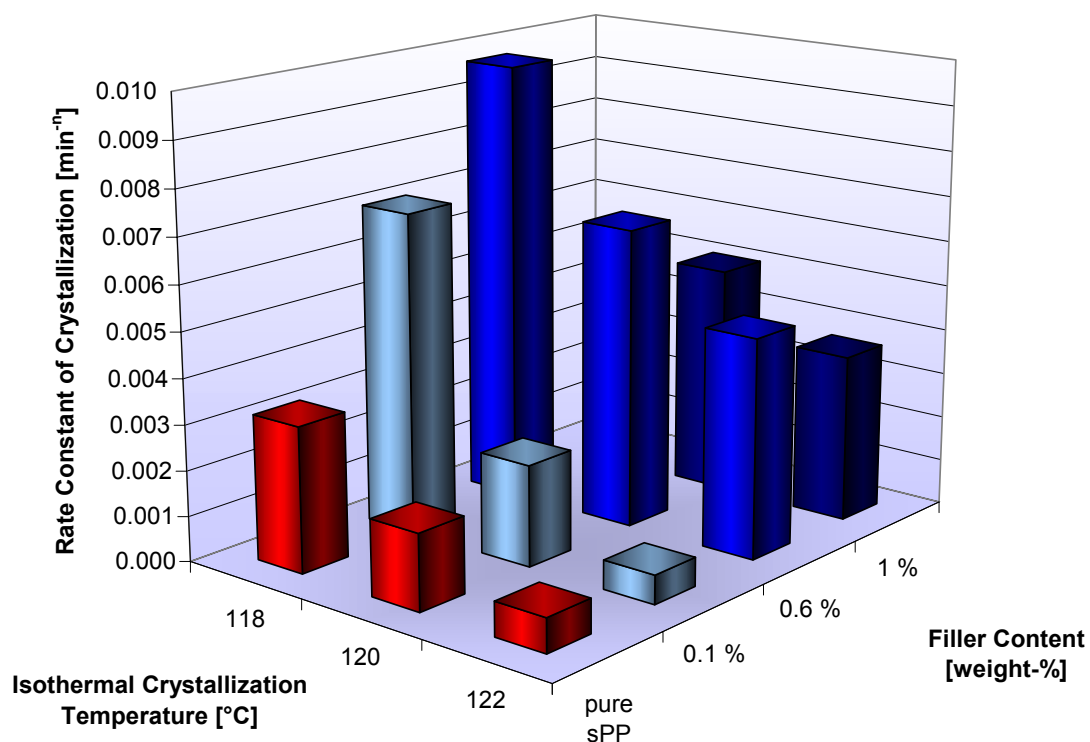


Fig. 81: Influence of the isothermal crystallization temperature and the filler content on the rate constant of crystallization of the sPP/CB nanocomposites.

### 6.7.3 Thermal Stability of the sPP/CB Nanocomposites

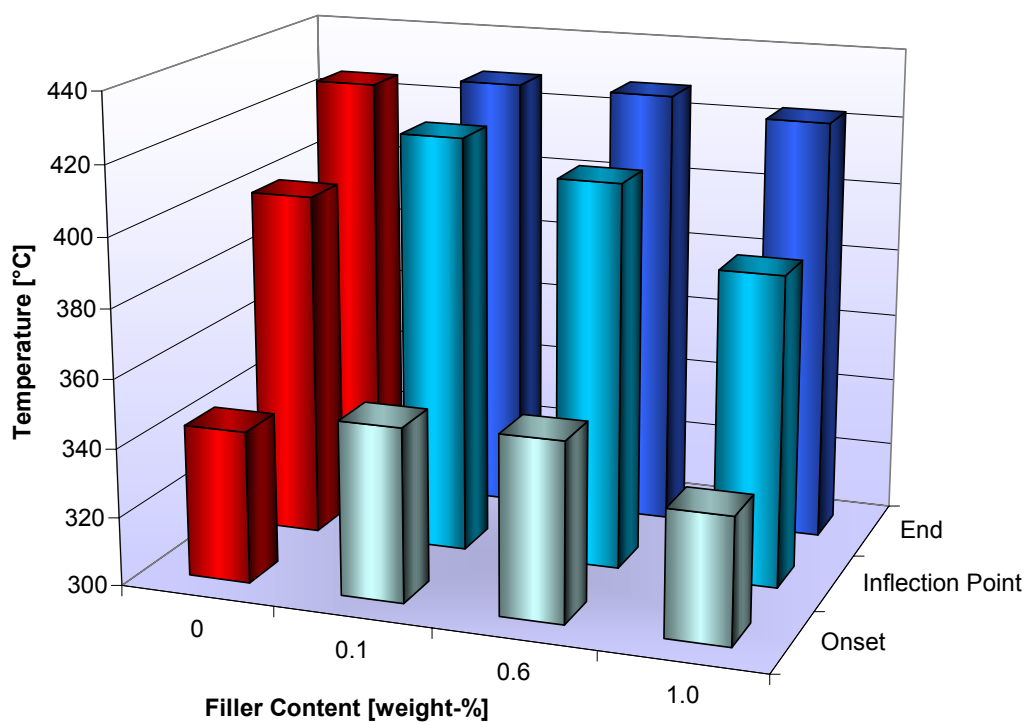


Fig. 82: Mass-loss of the sPP/CB nanocomposites in dependence of the temperature as determined by TGA.

The degradation behavior of the sPP/CB nanocomposites was investigated using TGA at a heating rate of 5 °C. The results for different filler loadings in comparison with the results for the pure sPP are shown in Fig. 73 and Tab. 8.

Low filler contents seemed to stabilize the polymeric matrix with regard to the degradation temperature. This was evident for the low filler content of only 0.1 % of carbon black. The onset of crystallization was raised by 6 °C and the inflection point by 20 °C as compared to the neat polymer, whereas, the end of degradation was reached at roughly the same temperature. Similar results were obtained for a filler content of 0.6 %. In contrast to this, the high filler content of 1 % led to lowered degradation temperatures. Not only onset but also inflection point and end of degradation took place at lower temperatures than in the pure polymer.

#### **6.7.4 Electrical Conductivity of the sPP/CB Nanocomposites**

The conductivity of the samples with different filler contents was evaluated using two-point measurements as described in the experimental section. None of the films investigated showed any conductivity.

#### **6.7.5 Tensile Properties of the sPP/CB Nanocomposites**

The tensile properties of the sPP/CB nanocomposites were determined in a similar manner as for the other nanocomposites. The influence of the filler content on the yield strength is depicted in Fig. 83 (see also Tab. 8). It shows that the presence of carbon black only has a minor impact on the yield strength of the polymer which was raised by 1.5 MPa on average upon addition of carbon black.

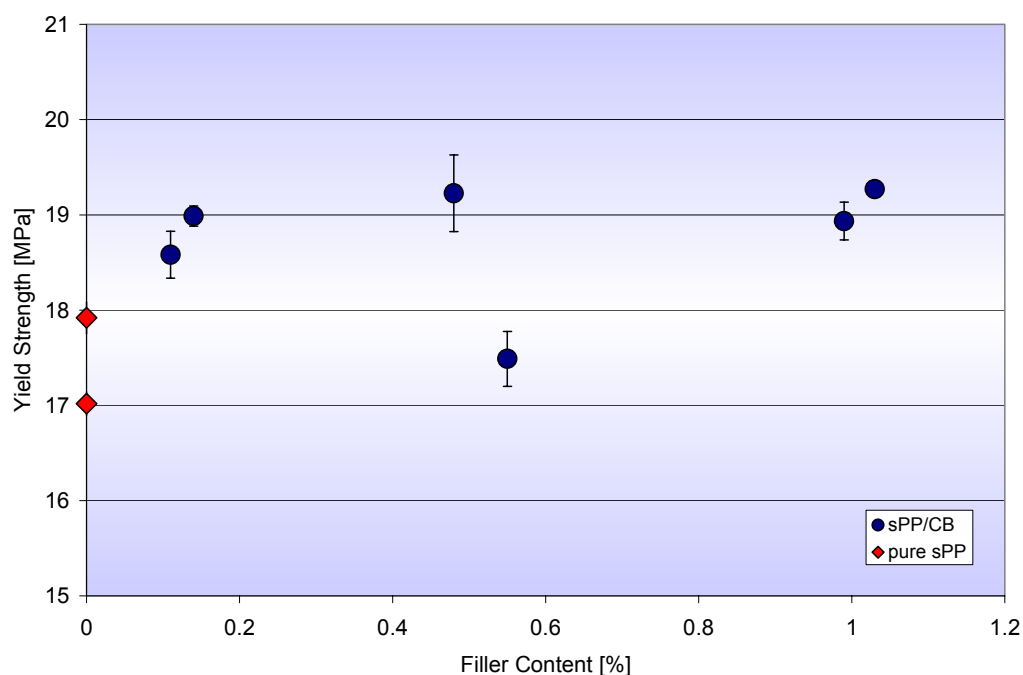


**Fig. 83:** Influence of the filler content on the yield strength of the sPP/CB nanocomposites.

The elastic modulus exhibited a high degree of scattering and is not shown here. In comparison to the neat polymer, the elongation at break remained approximately unchanged for the range of filler contents investigated.

**Tab. 8:** Properties of some sPP/CB nanocomposites.

Filler Content [wt.-%]	0	0.1	0.5	1
<b>Activity</b> [kg <sub>Pol</sub> /(mol <sub>Zr</sub> ·h·mol <sub>Mon</sub> /l)]	4,300	4,800	4,500	4,700
<b>Melting Temperature [°C]</b>	140	141	139	139
<b>Crystallization Temperature [°C]</b>	96	100	101	101
<b>Rate Constant of Crystallization [<math>\cdot 10^{-4} \text{ min}^{-1}</math>]</b>	7.5	6.4	48	37
<b>Half-time of Crystallization [min]</b>	14.6	7.6	5.1	6.7
<b>Degradation Temperature (T<sub>max</sub>) [°C]</b>	412	421	412	390
<b>Tensile Strength [MPa]</b>	17.5	18.8	18.4	19.1

<sup>a</sup>Rate constant of crystallization and half-time of crystallization were determined from isothermal DSC measurements at 122 °C.

## **6.8 COMPARISON OF sPP/CNF, sPP/MWNT AND sPP/CB NANOCOMPOSITES**

### **6.8.1 PP/GF and PP/M250 Nanocomposites**

PP/glass fiber and PP/monospher nanocomposites were successfully synthesized in this work. A homogeneous dispersion of the fillers in the matrix was achieved by different pre-treatments involving the heterogenization of the cocatalyst on the filler surface. Etched glass fibers could be well covered with polypropylene by *in situ* polymerization of propylene in toluene. The preparation of homogeneous PP/M250 nanocomposites required the gas-phase polymerization of propylene.

### **6.8.2 PP/CNF, PP/MWNT and PP/CB Nanocomposites**

#### **6.8.2.1 Dispersion of the Fillers in the Polymer Matrix**

Different pre-treatments before the polymerization were necessary to achieve a homogeneous distribution of the fillers used in this study. The carbon black, which has a low aspect ratio, and the carbon nanofibers could be separated quite well by sonication with ultrasound. They were then directly used in polymerizations of propylene without pre-reaction. This yielded nanocomposites with a satisfactory distribution of the nanofiller. The dispersion of the carbon nanotubes turned out to be more difficult. They were also sonicated with ultrasound but had to be subjected to a 24 hour pre-treatment with MAO to ensure a satisfactory distribution in the polymer matrix.

As was shown in the respective chapters, carbon nanofibers and carbon nanotubes were wetted well by the polypropylene. Nevertheless, aggregated nanofillers were still present in the composites. Some of these agglomerates were soaked with polymer, while the nonofillers remained un-wetted in others. This surely has an impact on other nanocomposite properties like the yield strength. Only in iPP/CNF samples some cases of fiber pull-out were detected. In general, SEM micrographs showed a good wetting of the fillers and no fiber or nanotube pull-out indicating a good interfacial adhesion.

#### **6.8.2.2 Crystallization and Melting Behavior**

The melting temperature and crystallinity of the sPP/CNF and the sPP/CB nanocomposites was largely unaffected by the presence of the fillers and their percentage (see Fig. 84). They

lay in the same region as the melting temperature of pure sPP. In contrast to this, the melting temperatures of sPP/MWNT nanocomposites were raised by 2 to 4 °C in comparison to those of the pure polypropylene. This can probably be attributed to a stabilization of the crystallites by the MWNTs.

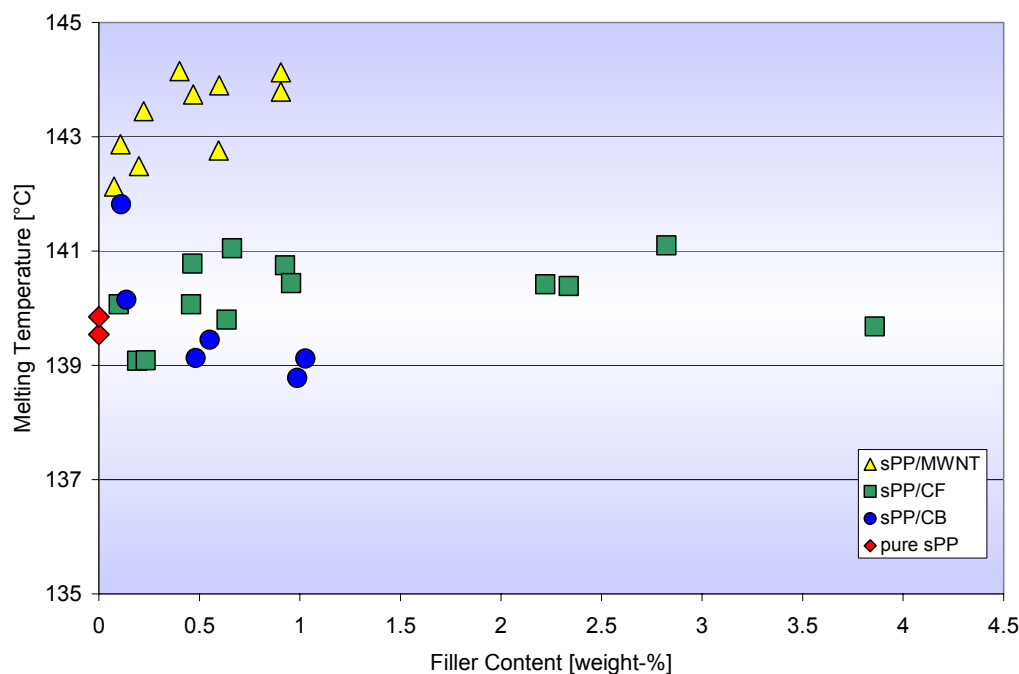


**Fig. 84: Influence of the filler and filler content on the melting temperature of the respective nanocomposites.**

The dependence of the crystallization temperature on the nature and the amount of the filler is shown in Fig. 85. It is obvious that the presence of all types of fillers led to an increase in the crystallization temperature of the respective nanocomposites in comparison to the pure polymer. This effect was much more pronounced for the sPP/MWNT nanocomposites than for the other two. In the case of CB or CNF as fillers, the crystallization temperature was raised by 4 to 6 °C depending on the filler loading. The enhancement (5 to 15 °C) of the crystallization temperature of sPP/MWNT nanocomposites was much more pronounced.

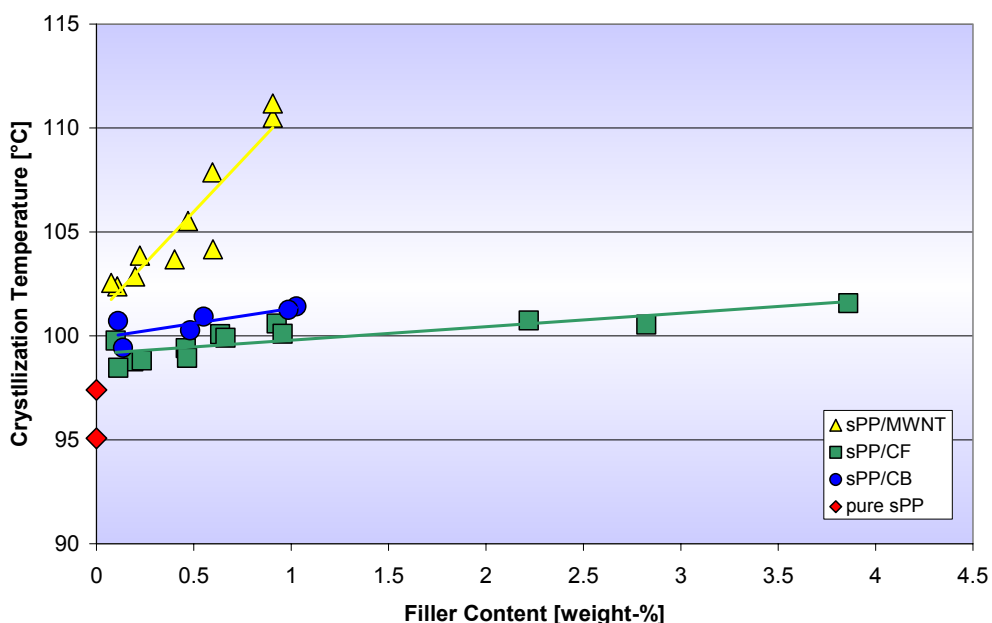


**Fig. 85: Influence of the filler and the filler content on the crystallization temperature of the respective nanocomposites.**

The above results are in accord with those obtained by Sandler et al who investigated the crystallization and melting behavior of iPP/MWNT and iPP/CNF nanocomposites prepared by melt-compounding. They found that incorporation of 7 % of Pyrograph III CNF or 0,5 % MWNT into isotactic PP did not change the melting temperature, the peak shape or the overall crystallinity. The crystallization temperature of the iPP/CNF nanocomposite increased by 5°C. It also increased for the iPP/MWNT nanocomposite, but the extent was not reported<sup>[86]</sup>.

For a further investigation of the crystallization behavior, the different nanocomposites were compared with respect to their isothermal crystallization behavior. Some exemplary DSC traces for isothermal crystallizations at 120 °C are shown in Fig. 86. The filler contents of all nanocomposites were close to 0.5 %. It can be clearly seen that the crystallization process took longest for the pure polypropylene. The green curve shows an sPP/CNF nanocomposite that crystallized faster than the neat polymer (red curve). The crystallization of the sPP/CB nanocomposite (blue trace) proceeded faster and that of the sPP/MWNT nanocomposite (yellow curve) was even faster. In fact, it was too fast at this temperature to supply reliable materials for Avrami analysis, which was performed to obtain the rate constant of crystallization  $k$  and the Avrami parameter  $n$ . Furthermore, the half-time of crystallization was determined.

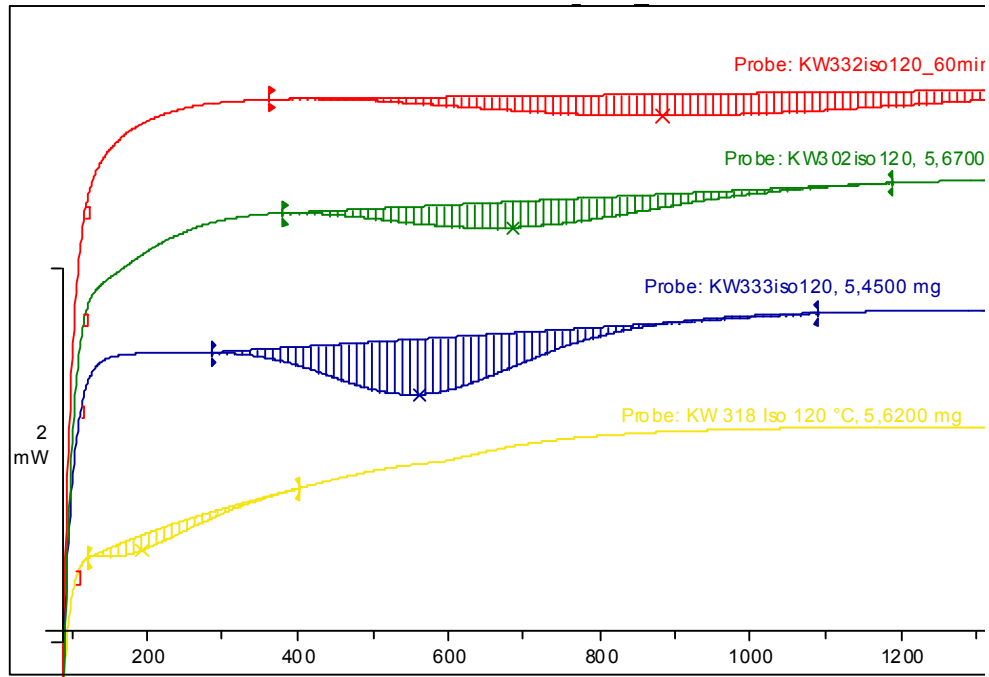


**Fig. 86:** Exemplary DSC traces of the different types of nanocomposites and the pure polypropylene (red: pure sPP, green: sPP/CNF, blue: sPP/CB, yellow: sPP/MWNT).

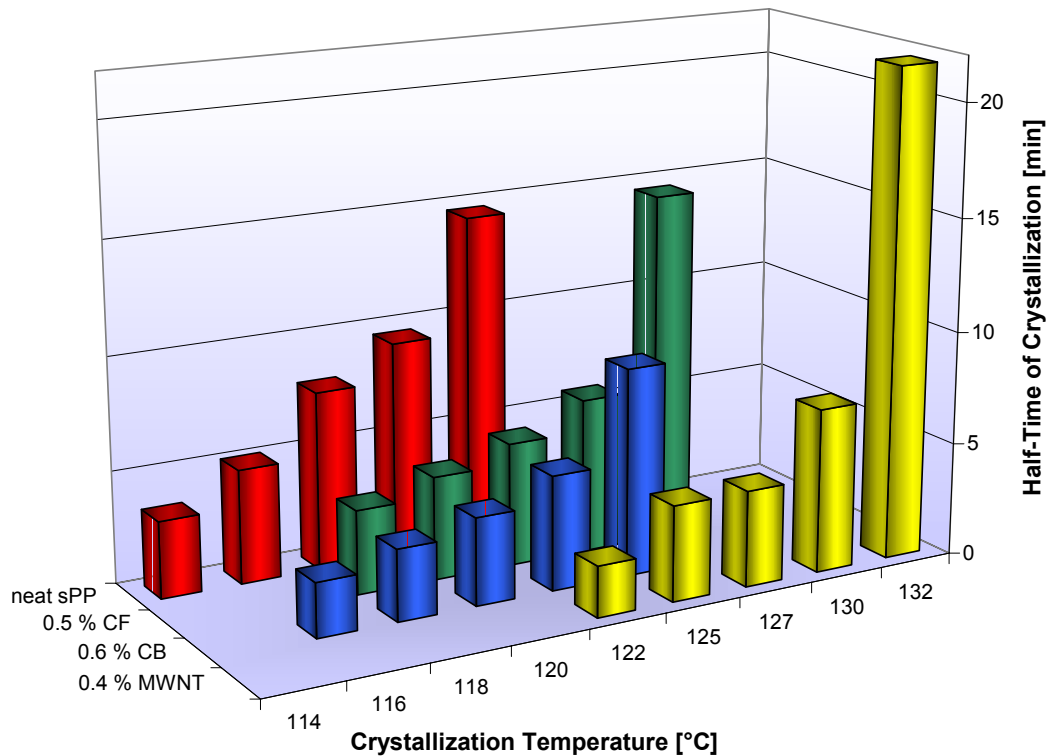


**Fig. 87:** Influence of the type of filler and the isothermal crystallization temperature on the half-time of crystallization of the respective nanocomposites.

Fig. 87 shows the half-times of crystallization of the different types of nanocomposites with a filler content close to 0.5% in dependence on the type of filler and the isothermal crystallization temperature.



crystallization temperature. It is obvious that the half-time of crystallization was shorter all types of composites than for the neat polymer at the same temperatures. Consequently, the crystallization of all nanocomposites proceeded faster than that of the pure PP. The half-time of crystallization of carbon nanofibers and carbon black were comparable. In contrast to that, the addition of carbon nanotubes to the polymer matrix led to a much stronger decrease of the crystallization half-time showing the superiority of MWNTs as nucleating agents.

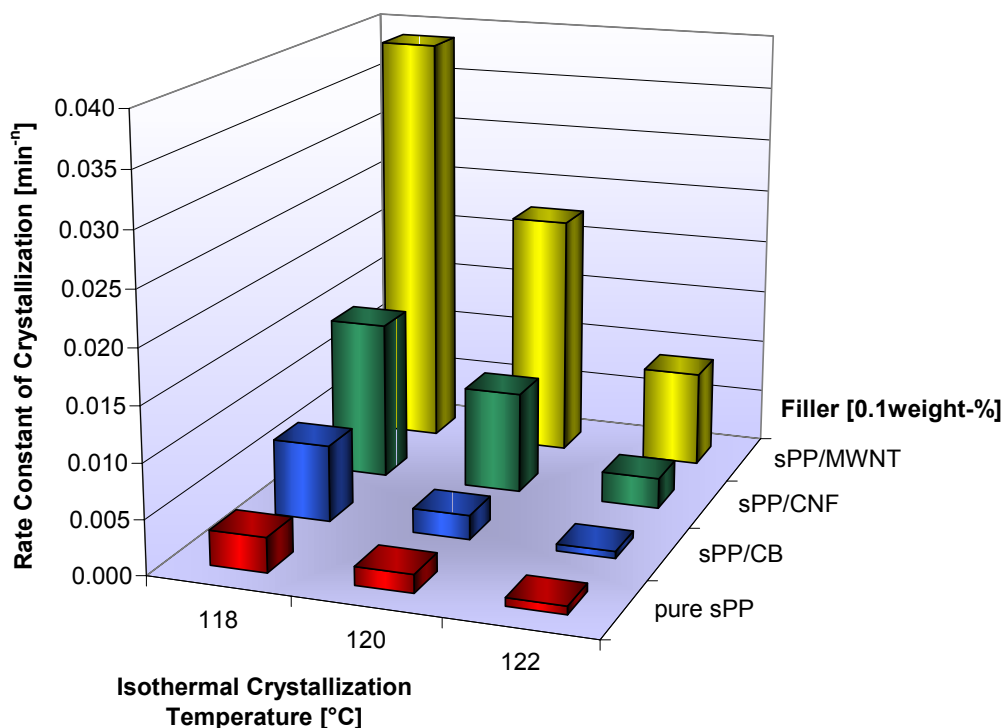


**Fig. 88: Influence of the type of filler and the isothermal crystallization temperature on the rate of crystallization.**

The effect of the nature of the filler and the isothermal crystallization temperature on the rate constant of crystallization is depicted in Fig. 88. It is apparent that the rate constant of crystallization decreased with increasing crystallization temperature. Additionally, it was smallest for the pure polymer meaning that the crystallization of this material proceeded with an inferior speed as compared to the filled polymers. The fillers with high aspect ratio (CNFs and MWNTs) showed a better nucleation ability than the spherical carbon black as can be seen by comparison of the respective rate constants of crystallization.

From the above findings, a distinct difference in the nucleating ability of the fillers can be deduced. This ability is, for example, important during the fabrication of injection molded parts because a faster crystallization enables the producer to reduce the cycle times. While the

nucleation ability of carbon black and carbon nanofibers is comparable in spite of their different geometry, carbon nanotubes act as much more efficient nucleating agents. This could be due to their smaller size compared to the CNFs. If well dispersed, the volume fraction occupied by MWNTs at the same filler loading (weight-%) would be higher and more nucleation sites would therefore be present. Another difference to be considered is the different surface of the nanotubes.

This behavior is in accordance with results obtained by Sandler et al. They found that carbon nanotubes were more effective nucleating agents than CNF in iPP nanocomposites that had been prepared by melt-compounding<sup>[86]</sup>. The authors attributed this to their smaller size.

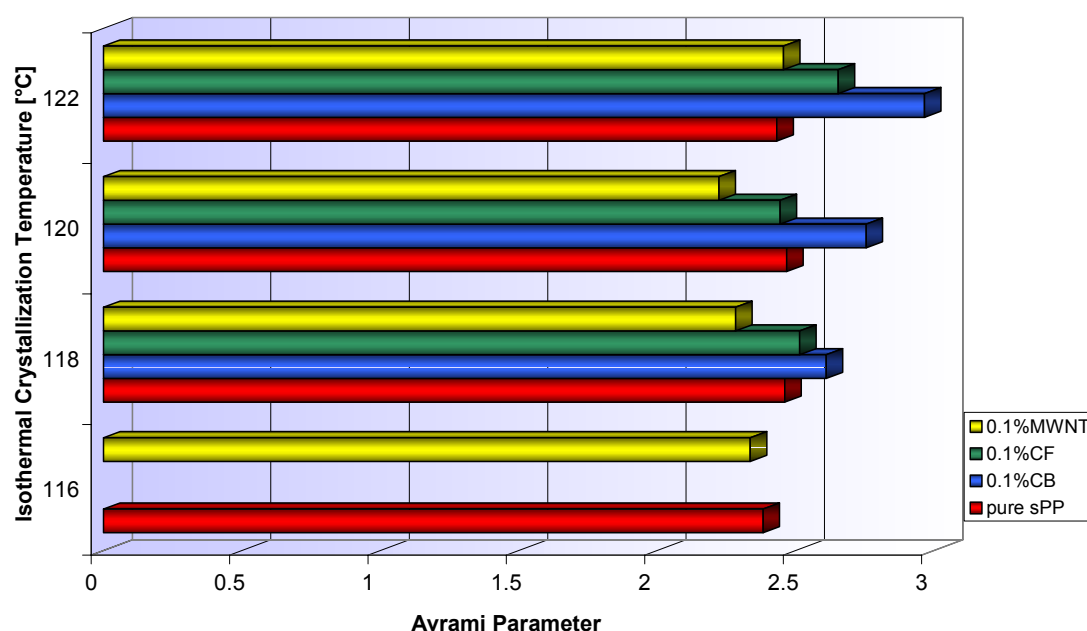


**Fig. 89:** Influence of the type of filler and the isothermal crystallization temperature on the Avrami parameter.

The influence of the type of filler and the isothermal crystallization temperature on the Avrami parameter is illustrated in Fig. 89. In case of carbon black as filler, the Avrami parameter increased. This is in contrast to the expectation that the Avrami parameter should be reduced by the presence of fillers because these fillers impede the crystallite growth. A possible reason is the difficult determination of the onset of crystallization in some cases. If the onset of crystallization is not determined correctly, this can have great influence on the Avrami plot and, therefore, on the calculation of the Avrami parameter. Another potential explanation is the spherical shape of the carbon black. If the crystallization started on the surface of these particles, the crystallite growth would proceed in three dimensions. In

conjunction with a spontaneous nucleation by the CB an Avrami parameter of 3 would be expected which is almost reached in some of the composites.

For carbon nanofibers, the Avrami parameter was mostly close to the value for the pure sPP. When nanotubes were used as fillers, the Avrami parameter was usually reduced with regard to the neat polymer indicating that MWNTs reduce the dimensionality of the crystallite growth. Nevertheless, the influence of the filler type on the Avrami parameter is not very clear. It is, as the rate constant of crystallization, very sensitive to differences in the onset of crystallization which was set manually.

### 6.8.2.3 Degradation Behavior

The degradation properties of the nanocomposites were investigated using thermo-gravimetric analysis. The results are shown in Fig. 90. It was observed that the presence of fillers usually led to a stabilization of the polymer against thermal degradation. This stabilization was intensified at higher filler loadings for sPP/CNF and sPP/MWNT nanocomposites. The inflection point of degradation lay up to more than 20 °C above that of the pure polymer. In the case of carbon black as filler a stabilization was seen at small contents. The degradation of the polymeric matrix proceeded faster than that of the pure polymer at a filler loading of 1 %.

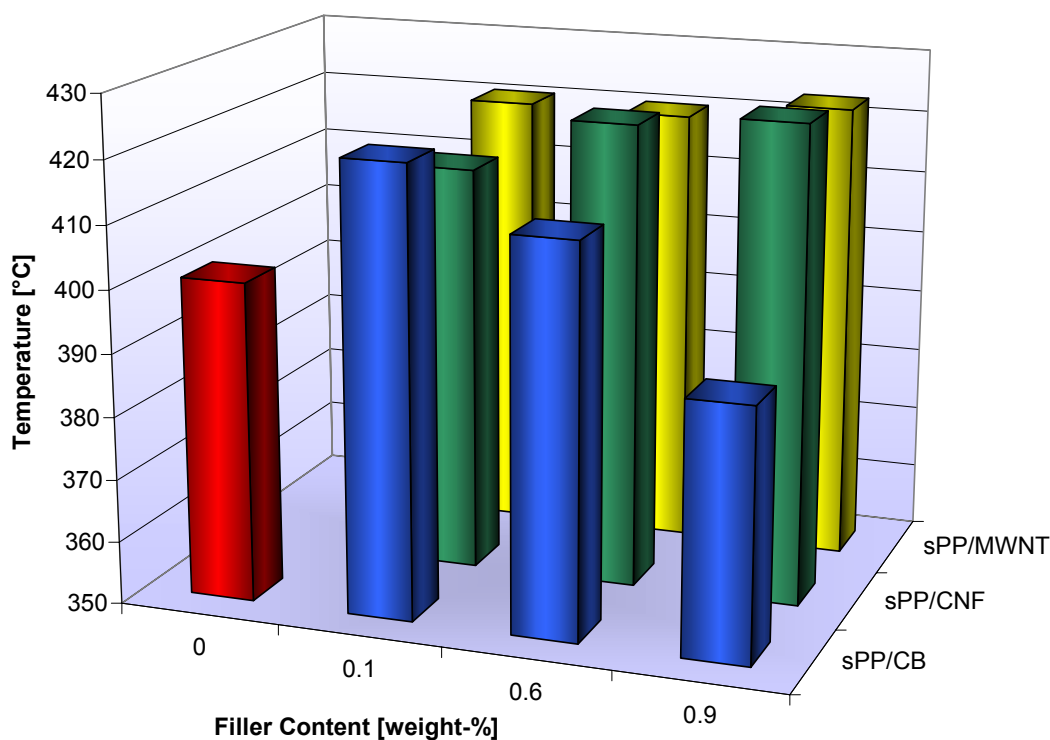


**Fig. 90:** Influence of the type of filler and the filler content on the degradation behavior of the respective nanocomposite (shown is the inflection point of the weight-loss curve).

The stabilization of the polymer matrix by CNFs and MWNTs can be attributed to the fact that the chain movement is restricted in the presence of the solid fillers. Further investigations with higher filler amounts could help to clarify the situation.

#### 6.8.2.4 Conductivity

With the exception of the sPP/CNF nanocomposites with filler loadings of 2.8 and 3.9 %, none of the prepared nanocomposites were conductive which was probably due to the lower filler contents. A beginning conductivity could be observed with the higher filler loadings only prepared with carbon nanofibers as fillers. This points to the conclusion that a conductivity of this type of nanocomposite is possible on principle, which has already been shown for iPP nanocomposites<sup>[55,85]</sup>. The filler loadings investigated in this work were obviously too low for the formation of conductive pathways, which are necessary for the nanocomposite to be conductive.

#### 6.8.2.5 Tensile Properties

The tensile properties were investigated by recording of the stress strain curves of the synthesized nanocomposites. The yield strength was calculated from the stress-strain behavior and is shown in Fig. 91.

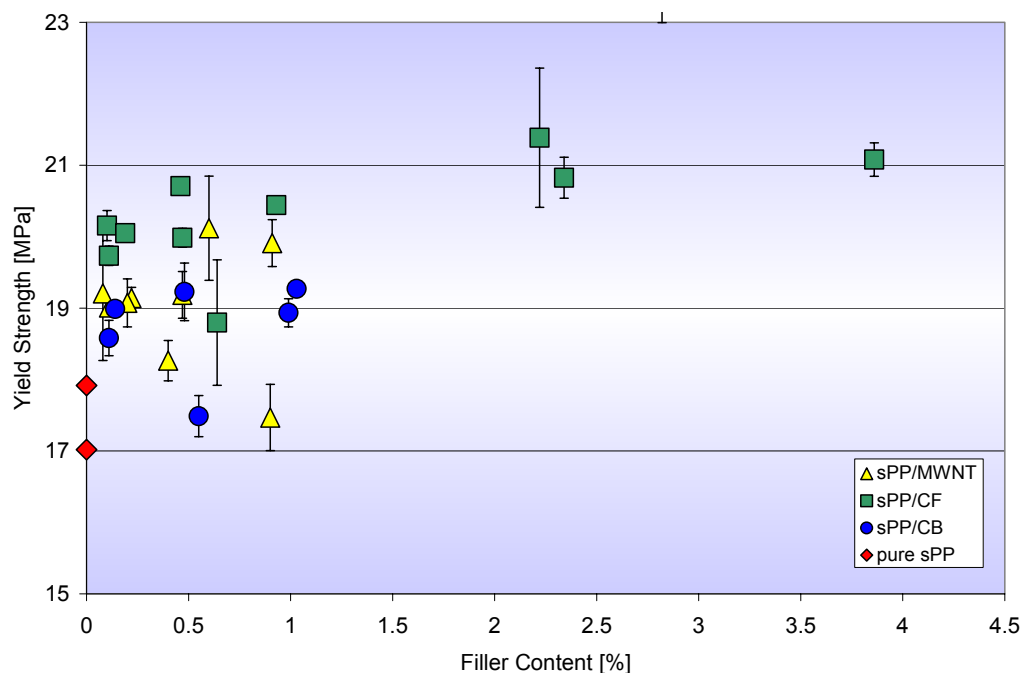


**Fig. 91: Influence of the type of filler and the filler content on the yield strength of the respective nanocomposites.**

The yield strength of almost all of the nanocomposites lay above that of the pure polymer. The highest improvement of the yield strength was found for carbon nanofibers as fillers, which enhanced the yield strength by up to 20 % as compared to the neat polymer. The improvement of 10 to 15 % that could be reached by the addition of carbon nanotubes or carbon black was smaller. This could have different reasons the first one being the very small filler contents investigated.

Furthermore, the carbon black is a more or less spherical filler meaning that the potential reinforcement achievable should be smaller than for the other fillers that have a high aspect ratio<sup>[39]</sup>. On the other hand, it should be relatively easy to disperse it well. As was shown in section 6.7.1, the dispersion was good but not perfect, which could also play a role in the strengthening of the material.

The MWNTs should theoretically provide for a better reinforcement than the CNFs because of their better mechanical strength, their smaller size, and their higher uniformity. Two effects, in addition to the low filler loadings, could have prevented a better reinforcement in this work. First, the dispersion of the carbon nanotubes has proven to be problematical. The choice of the sonication time and amplitude was made according to preliminary experiments with different times and amplitudes but also keeping in mind that a prolonged ultrasonic treatment can destroy the tubes which are then less useful in reinforcement because of a smaller aspect ratio and other possible defects. On the other hand, sonication at amplitudes too small or for a time period too short would not separate the bundles of MWNTs sufficiently. The presence of bundles effectively leads a reduction of the aspect ratio because the bundle diameter is naturally larger than that of a single tube. The pre-treatment of the carbon nanotubes with MAO has improved the dispersion greatly, but in SEM images few aggregates of MWNTs were still visible. These are likely to act as stress concentrators leading to a premature failure of the material.

Secondly, the interfacial adhesion of the matrix to the filler is crucial for the performance of the nanocomposite. Improvement is still possible but the SEM images all show a good wetting of the isolated nanotubes and no tube pull-out, which is an indication of an already very good adhesion of the matrix to the filler.

## 7 CONCLUSIONS AND PROSPECTS

Different PP nanocomposites were prepared in this study by *in situ* polymerization of propylene with metallocene/MAO catalysts in the presence of the respective fillers. By incorporation of the fillers, the thermal stability and the yield strength could be somewhat improved. Additionally, the fillers, especially the MWNTs, acted as nucleating agents, meaning that they significantly accelerated the crystallization process.

Extensive experiments were conducted to achieve a homogeneous dispersion of the carbon nanofibers and carbon nanotubes in the polymer. Further improvement is desirable to create materials with a truly homogeneous distribution and homogeneous properties throughout the whole material. This would be especially important regarding the tensile properties of the nanocomposites synthesized. Some inhomogeneities could explain the relatively high scattering of the values from different measurements of the yield strength.

The wetting of the CNFs by isotactic polypropylene was good, but fiber pull-out was visible to some extent. Wetting of the nanofillers by syndiotactic polypropylene was very good. This is an indication of a good adhesion of the matrix to the filler, which is important for an efficient load transfer. Nevertheless, the tensile properties improved only slightly upon addition of the nanofillers to the sPP. It would, therefore, be interesting not only to further improve the dispersion but also to stabilize the filler matrix interface. This could be accomplished by different methods. A modification of the carbon nanotube surface to create more hydroxyl or carboxyl groups by acid treatment would lead to more anchorage points for the MAO. The adhesion could be enhanced by an improved adsorption of the cocatalyst in this way. Moreover, the so obtained MWNT/MAO could be cleaned from unused MAO as was done for the preparation of PP/M250 nanocomposites to obtain a truly heterogeneous cocatalyst.

Most nanocomposites prepared in this work were synthesized with different filler contents to investigate the effect of the filler loadings on the properties of the materials. The range of filler contents was relatively small, though. With increasing filler content, the rate of crystallization increased. This effect was especially pronounced for carbon nanotubes which acted as excellent nucleating agents for sPP. No clear trend was observed regarding the effect

of the filler loading on the thermal stability. The investigation of nanocomposites with higher filler contents could clarify the influence of the filler loading on these properties.

Moreover, some sPP/CNF nanocomposites with relatively high filler content could be shown to be slightly conductive. Nanocomposites with higher filler contents would surely be more conductive, and also MWNT and CB nanocomposites should be conductive at sufficiently high loadings. Even contents of 5 % and more would still be much lower than the 20 to 30 % of conventional CB needed for this task.

## 8 Experimental Part

### 8.1 Materials

All manipulations of compounds were carried out by standard Schlenck, vacuum, and glove box techniques.

#### 8.1.1 Gases

Argon (purity  $\geq 99.996\%$ ) was purchased from Linde and was purified further by Oxisorb of Messer-Griesheim. Propylene was obtained from Gerling, Holz & Co. Handels GmbH, Germany (purity  $\geq 95\%$ ) and purified using 2 columns ( $V = 5 \cdot 200$  cm) filled with molecular sieve (4 Å) and BASF-Catalyst R3-11. Ethen was purchased from Linde and was purified as propylene.

#### 8.1.2 Solvents

Toluene used as solvent for polymerizations and for the metallocenes was purchased from various suppliers, dried over potassium hydroxide for several days, degassed, and purified by passing through columns similar to those used for the purification of propylene. It was stored in a gas-tight vessel under argon and was let directly into the reactor for polymerizations.

#### 8.1.3 Fillers

##### 8.1.3.1 Silica gel

Silica gel 60 (0.04 – 0.063 mm, BET-surface 480-540 m<sup>2</sup>/g) was purchased from Merck and dried for several days at 120 °C prior to use.

##### 8.1.3.2 Monospher 250

Monosphers 250 were supplied by Merck. Parts of them were dried at 150 °C in vacuum over night prior to use.

##### 8.1.3.3 Glassfibers

The glassfibers (FG 400/060) were kindly supplied by Schwarzwälder Textil-Werke Heinrich Kautzmann GmbH, Germany. Parts of them were directly impregnated with MAO, the rest was etched with a 1 molar or 2.5 molar KOH-solution during 2 h at 90 °C, filtered, washed until neutral, dried and then impregnated with MAO.



#### 8.1.3.4 Carbon nanofibers

Carbon nanofibers (CNF, pyrograph III) from Applied Science, Inc. were supplied by the research group of Prof. Schulte, Technical University Hamburg Harburg (TUHH). Their average diameter is 100 nm and their length lies in the mm-region. Before use, the CNF were heated in vacuum to remove adherent water.

#### 8.1.3.5 Multi-Walled Carbon nanotubes

Thin straight and coiled multi-walled carbon nanotubes (MWNT, as prepared or purified (>95 %)) were purchased from Nanocyl S. A., Belgium. Their diameter is approximately 15 – 25 nm and their length is up to 50  $\mu\text{m}$ . The MWNT were dried in vacuum prior to use.

#### 8.1.3.6 Carbon Black

Carbon Black was kindly supplied by the group of Prof. Schulte, TUHH. The average diameter of the primary particles was 30 nm. These were agglomerated into aggregates of 150 to 300 nm, which were again agglomerated.

### 8.1.4 **Metallocenes**

The metallocene [(p-MePh)<sub>2</sub>C(Cp)(2,7-bis-tBuFlu)]ZrCl<sub>2</sub> was synthesized in our workgroup<sup>[146]</sup>. The metallocene *rac*-[Et(IndH4)<sub>2</sub>]ZrCl<sub>2</sub> was purchased from Witco. They were used as  $2 \cdot 10^{-3}$  or  $1.25 \cdot 10^{-3}$  molar solutions in toluene which were stored in the freezer prior to use.

### 8.1.5 **Cocatalyst and Scavenger**

Methylaluminoxane (MAO) was purchased from Witco as a 10%-solution in toluene. It was filtered over a D4 fritted glass filter, and toluene and trimethylaluminum (TMA) were removed under vacuum. The MAO was then used as a 100 mg/ml solution in dry toluene.

For polymerizations in the gas-phase, a suspension of SiO<sub>2</sub>/MAO (purchased from Witco) in toluene with a concentration of 100 mg/ml and a total percentage of aluminum of 23 % was used. Triisobutylaluminium (TIBA) was purchased from Aldrich and used as a 1mmol/ml solution in toluene. TMA was used as an approximately 30%-solution.

### 8.1.6 **Quench-Solution**

The quench-solution was prepared from 200 ml hydrochloric acid (37 %), 425 ml ethanol and 1450 ml demineralized water.

## **8.2 Pretreatment of the Fillers**

### **8.2.1 Silica Gel**

The silica gel was heated in vacuum twice and purged with argon several times. The solid was dispersed in 20 ml of toluene before the appropriate amount of MAO-solution was added. After the reaction time of 0.5 to 1 h, the solid residue was filtered off, washed six times with 5 ml of toluene each and then dried at room temperature for two hours in vacuum.

### **8.2.2 Glass Fibers**

The glass fibers were heated in vacuum twice and purged with argon several times. The appropriate amount of MAO (ca. 4ml/g GF) was added and the reaction time was 24 h. After that time, the GF/MAO was filtered off and washed with toluene several times.

Some of the glass fibers were contacted with TMA (ca. 1ml/g) for 24 h before the reaction with MAO was carried out analogous to the description above.

### **8.2.3 Monosphers 250**

Prior to the impregnation with MAO, the dried Monosphers were dispersed in 20 ml of toluene and dispersion was improved by sonication in an ultrasonic bath for 15 minutes. The desired amount of MAO-solution was added and the mixture was stirred for 24 h at room temperature. It was then filtered using a D4 fritted glass filter and washed 10 times with 5 ml of toluene each. After drying for 4 h under vacuum at room temperature the resulting cocatalyst (M250/MAO) was stored in the glove box. Before polymerization, the following pre-activation was carried out: 0.55 g of M250/MAO were dispersed in 5 ml of toluene under stirring for 10 minutes. The metallocene was added and the dispersion was stirred for another 10 minutes to activate the catalyst. It was afterwards introduced into the reactor.

### **8.2.4 Carbon Nanotubes and Nanofibers**

The carbon nanofibers (5-250 mg) and nanotubes (5-50 mg) were sonicated in a toluene (12ml) suspension using a Sonopuls homogenizer HD 2200 equipped with a KE 76 sonotrode. The amplitude (10 – 50 %) and the sonication time (5 – 120 min) were varied to achieve an optimum separation and thus distribution of the fillers in the polymer. The sonicated fillers were then either introduced directly into the toluene-charged reactor (without pre-reaction) or stirred with MAO-solution (generally 2 ml) for 24 h (with pre-reaction) before introduction into the reactor.

### 8.3 Polymerizations

All polymerizations were carried out in a 1 l glass reactor (Büchi AG, Ulster, Switzerland, Fig. 92 and Fig. 93). It was heated to 90 °C in vacuum for 1h and then flushed with argon several times prior to use.

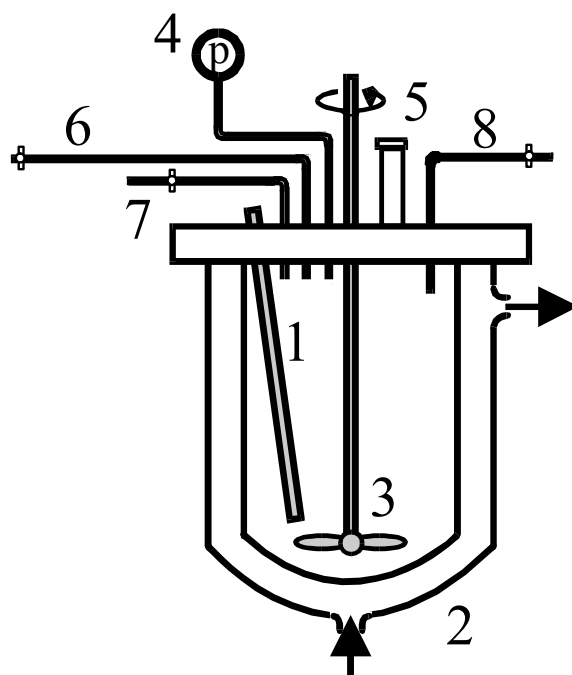


Fig. 92: Reactor used for solution- and slurry-polymerizations (1 thermometer, 2 thermostat, 3 stirrer, 4 manometer, 5 septum/pressure lock, 6 monomer (ethene or propylene)/pressure-release valve, 7 argon/vacuum, 8 toluene).

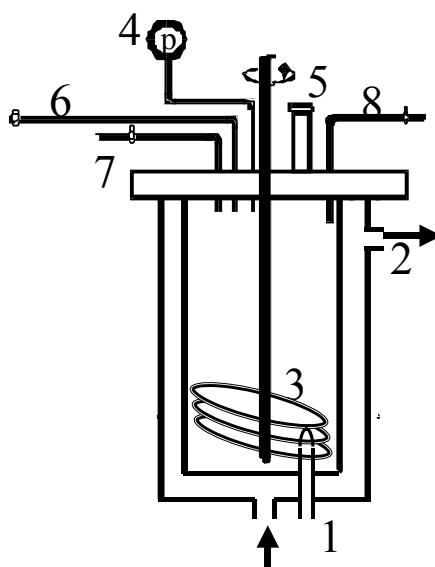


Fig. 93: Reactor used for polymerizations in the gas-phase (1 thermometer, 2 thermostat, 3 stirrer, 4 manometer, 5 septum/pressure lock, 6 propylene/pressure-release valve, 7 argon/vacuum, 8 toluene).

### 8.3.1 Polymerizations in the Presence of Monosphers

For slurry polymerizations, the reactor (Fig. 92) was charged with 200 ml of toluene, heated to the desired polymerization temperature and 2 ml of TIBA-solution were added. The solution was saturated with propylene at the desired pressure using a mass-flow controller (Brooks instruments, 5850 series). After the saturation was complete, the pre-activated catalyst (see section 8.2.3) was then introduced into the reactor using a pressure lock. Polymerizations were typically quenched after 0.5 – 2 h by addition of 5 ml of ethanol.

For gasphase polymerizations, a 1l glass reactor equipped with a helix-stirrer (Fig. 93) was charged with 200 ml of pre-dried sodium chloride before heating and purging with argon. After cool-down to the desired reaction temperature, 2 ml of TIBA-solution were added. The pre-activated catalyst (see section 8.2.3) and the stirred bed were dried under vacuum for 20 min after a reaction time of 10 minutes of the M250/MAO with the metallocene in toluene. Afterwards, the powder (M250/MAO/metallocene) was introduced into the reactor and the polymerization was started by applying a propylene pressure of 5 bar. After 1 h, the polymerization was stopped by degassing and evacuation. Polymers were stirred with 1.5 l of water over night, filtered and dried in vacuum at 60 °C. All polymerizations were carried out several times and differences in the activities lay under 20 % and differences of melting temperatures within the range of 2 °C.

### 8.3.2 Polymerizations in the Presence of Carbon Nanotubes and Carbon Nanofibers

In the case of the polymerizations without pre-reaction, the reactor (Fig. 92) was charged with 200 ml of toluene and heated to the desired polymerization temperature. MAO and the filler-suspension were introduced into the reactor and the dispersion was then saturated with propylene at the desired pressure using a mass-flow controller (Brooks instruments, 5850 series). The reaction was started by injection of the metallocene when saturation was completed.

In the case of the polymerizations with pre-reaction, the reactor was charged with 200 ml of toluene and heated to the desired polymerization temperature. 2 ml of TIBA solution (1mmol/ml toluene) were added to the toluene before saturation with propylene. The pre-activated catalyst-suspension (filler/MAO/metallocene) was introduced into the reactor when saturation was completed using a pressure lock. Polymerizations were typically quenched after 45 minutes by addition of 5 ml of ethanol. All polymers were stirred with a quench-

solution (see section 8.1.6) over night, filtered, washed and dried in vacuum at 60 °C over night.

## 8.4 Analytical Techniques

### 8.4.1 Filler Content

It was presumed that the whole amount of filler used for sonication was incorporated in the polymer. Consequently, the amount of filler in relation to the total polymer mass (weight-% ) was assumed to be the filler content.

### 8.4.2 <sup>13</sup>C-NMR-Spectroscopy

All <sup>13</sup>C-NMR-spectra were recorded <sup>1</sup>H-decoupled on a Bruker Ultrashield 400-Spectrometer at 100°C. The parameters of the measurements are listed in Tab. 9.

**Tab. 9: Parameters of NMR-measurements**

<b>Decoupling</b>	BB, Waltz 16 pulse program
<b>Frequency</b>	100.62 MHz
<b>Number of Scans</b>	1024
<b>Pulse Angle</b>	60°
<b>Relaxation Time</b>	5 s
<b>Sweep-Width:</b>	25126 Hz

Samples were prepared from approximately 200 mg polymer, 4 g trichlorobenzene and 0.5 g tetrachloroethane-d<sub>2</sub> (TCE-d<sub>2</sub>) in a 10 mm NMR-sample-tube. The chemical shift was measured relative to the TCE-d<sub>2</sub>-signal at 74.24 ppm, and spectra were evaluated using the program SpecView (ACD).

### 8.4.3 Differential-Scanning-Calorimetry (DSC)

Melting temperatures, T<sub>m</sub>, crystallization temperatures (T<sub>c</sub>) and glass-transition temperatures (T<sub>g</sub>) were determined by differential scanning microscopy (DSC) with a DSC 821e (Mettler-

Toledo) calibrated with indium ( $T_m = 156.6\text{ }^\circ\text{C}$ ), cyclopentane ( $T_m = -93.9\text{ }^\circ\text{C}$ ) and water ( $T_m = 0.0\text{ }^\circ\text{C}$ ). Generally, samples of 5-6 mg were used for DSC analysis. Data for the  $T_m$  was taken from the heating curve of the second heat at a heating rate of  $20\text{ }^\circ\text{C}/\text{min}$  in the range of  $-100$  to  $200\text{ }^\circ\text{C}$ . Crystallization temperatures,  $T_c$ , were determined by DSC from the cooling curve (cooling rate  $10\text{ }^\circ\text{C}/\text{min}$ ) after complete melting at  $200\text{ }^\circ\text{C}$  for 5 min. Isothermal crystallization was performed by quenching the sample to the desired temperature (cooling rate  $40\text{ }^\circ\text{C}/\text{min}$ ) after complete melting at  $200\text{ }^\circ\text{C}$  for 5 min.

#### 8.4.4 Electron Microscopy

Electron microscopy was performed on a Leo 1530 FE-REM at the Technical University Hamburg Harburg, on a Hitachi S-2500 in the research group of Prof. B. Albert at the Institute of Inorganic Chemistry, University of Hamburg, and on a FEG ESEM XL30 (Philips) at the University of Eindhoven. Some samples were sputtered with gold before the measurements.

#### 8.4.5 Microscopy

Microscopy was performed on an Olympus PH polarization microscope equipped with a Mettler heater and a Sony digital camera. The polymer was melted between glasses at  $200\text{ }^\circ\text{C}$  and pressed slightly before the photographs were taken.

#### 8.4.6 Viscosimetry

For some polymers, the viscosimetric molar weights were determined by viscosimetry at  $135\text{ }^\circ\text{C}$  using a Ubbelohde-Viscometer (capillary  $0a$ ,  $K = 0,005\text{ mm}^2/\text{s}^2$ ) and a Viskoboy 2.  $1\text{ mg}/\text{ml}$  solutions in  $50\text{ ml}$  decahydronaphthalin were used for the measurements that were carried out as described in [66].

#### 8.4.7 Gel-Permeation-Chromatography

Gel permeation chromatography was carried out with a Waters GPC 2000 Alliance system equipped with a refractive index detector, viscosimetric detector and a set of three columns, Styragel type. The particle size for each column was  $10\text{ }\mu\text{m}$ , and the pore sizes were  $10^3\text{ \AA}$  (HT3),  $10^4\text{ \AA}$  (HT4), and  $10^6\text{ \AA}$  (HT6). 1,2,4-Trichlorobenzene was used as solvent. The analyses were performed at  $140\text{ }^\circ\text{C}$  and  $1.0\text{ mL}/\text{min}$ . The columns were calibrated with narrow molar mass distribution polystyrene standards. The sample concentration was  $1\text{ mg}/\text{mL}$  and the injection volume  $215\text{ }\mu\text{L}$ . 2,6-Di-*tert*-butyl-4-methylphenol was used as thermostabilizer. The samples were filtered using a GPC vial equipped with a filter before the measurements to remove the filler. The Mark-Houwink constants were calculated automatically by the

Millenium software supplied by Waters from the values measured with the visco- and refractive index-detectors.

#### **8.4.8 Tensile Testing**

Polymer films were prepared by hot pressing at 200 °C. The samples for tensile testing were cut from these films. The testing was performed on a Zwick Z101 with distance encoder according to DIN EN ISO 527.2. The crosshead speed was 10 mm/min (1mm/min for measurement of the tensile modulus). The tensile modulus was calculated after normalization to the sample dimensions. The values for the yield strength were calculated from the measured data by normalization to the sample dimension. Several test bars were cut from each nanocomposite, and the yield strengths indicated are the average values obtained from the measurements conducted with these bars.

#### **8.4.9 Incineration**

M250 contents were determined by treatment of the M250-containing polymers by a bunsen burner and subsequent heating to 800 °C for 2 h. The resulting inorganic residue was weighed. Differences in filler contents of the synthesized polymers result from differences in activities because the same amount of cocatalyst (M250/MAO, 0.55g) was used in all polymerizations.

#### **8.4.10 Thermo-Gravimetric Analysis**

Thermo-Gravimetric Analysis (TGA) was carried out on a Netzsch STA 409C/CD in the research group of Prof. B. Albert, Institute of Inorganic Chemistry, University of Hamburg. Generally, samples of 25 mg were heated from 20 °C to 900 °C at a rate of 5 °C/min in air. The weight loss with rising temperature was monitored. The obtained curves of weight vs. temperature were evaluated according to Marsh with the Netzsch Proteus evaluation software. The extrapolated onset of degradation and the temperature corresponding to the highest mass-loss rate were thus accessible.

#### **8.4.11 Conductivity Measurements**

The conductivity measurements were carried out in the research group of Prof. Koning at the Technical University of Eindhoven, The Netherlands. The test were performed with the films that had been obtained by hot pressing (see section 8.4.8). To provide for a good contact of the electrodes with the nanocomposites, 4 parallel lines of 1 cm length with a distance of 1 cm from each other were drawn on the films with colloidal graphite in isopropanolic suspension.

The thickness ( $h$ ) of the films was measured with a Mitotoyo thickness meter three times. The resistance ( $R$ ) of the films was measured with the help of two-point measurements with a Keithley 220 Programmable Electrometer as the current source and a Keithley 6512 Programmable Electrometer as measuring device for the resistivity. The resistivity in  $\Omega\text{cm}$  was calculated according to (Eq. 4).

$$\rho \equiv \frac{Rwh}{l}$$

(Eq. 4)

The resistivity  $\rho$  can be obtained from the measured resistance  $R$  in  $\Omega$ , and dimensions  $w$ ,  $h$ , and  $l$  of the sample. As the lines drawn on the films were chosen to be 1 cm long and separated by 1 cm,  $w$  and  $l$  correspond to 1, and (Eq. 4) can be simplified to (Eq. 5).

$$\rho = Rh$$

(Eq. 5)

The values indicated are an average of two measurements.

## 8.5 Safety

The chemicals used in this work were disposed of in accordance with the Chemikaliengesetz and the Gefahrstoffverordnung<sup>[148]</sup>.

After separation into halogen-containing solvents, halogen-free solvents and aqueous solutions, the chemicals were disposed of in the appropriate containers.

MAO and its solutions were hydrolyzed carefully with 2-propanol, ethanol and water. After acidification with hydrochloric acid, the solutions were separated and disposed of as described above.

Solids and contaminated papers and filters were put into the appropriate containers.



The security data for the chemicals used in this work is listed in Tab. 10.

**Tab. 10: Security data concerning the chemicals used in this work.**

<b>Chemical Substance</b>	<b>Classification</b>	<b>Risk Phrases</b>	<b>Safety Phrases</b>
<b>MWNT</b>	T	48/23-38-36	22-29-36/37/39
<b>Ethanol</b>	F	11	(2)-7-16
<b>Ethylene</b>	F <sup>+</sup>	12	(2)-9-16-33
<b>Potassium Hydroxide</b>	C	35	2-26-37/39-45
<b>Methylaluminoxane</b>	F, C, Xn	14/15-17-35	16-23-30-36-43
<b>1-Propylene</b>	F	13	9-16-33
<b>Hydrochloric Acid, &gt;25 %</b>	C	34-37	2-26
<b>Toluene</b>	F, Xn	11-20	16-25-29-33
<b>1,2,4-Trichlorbenzene</b>	Xn, N	22-36/37/38-51/53	26-61
<b>Triisobutylaluminum</b>	F, C	11-14-17-34-48/20	16-26-36/37/39-43-45
<b>Trimethylaluminum</b>	F <sup>+</sup> , C	14-17-34	16-43a-45

## 9 LITERATURE

- (1) Galli, P.; Vecellio, G. *J. Polym. Sci. A* **2004**, *42*, 396-415.
- (2) Ko, H. Macro 2004, Paris, **2004**.
- (3) Del Duca, D.; Moore, E. P. In *Polypropylene Handbook*; Moore, E. P., Ed.; Hanser: München, **1996**.
- (4) Auriemma, F.; De Rosa, C. *J. Am. Chem. Soc.* **2003**, *125*, 13134-13147.
- (5) Moore, E. P. J. In *Polypropylene Handbook*; Moore, E. P. J., Ed.; Carl Hanser Verlag: Munich, Vienna, New York, **1996**.
- (6) Dotson, D. L. ; Milliken & Company: WO03/087175 A1, **2003**
- (7) Wolfsberger, A.; Gahleitner, M.; Wachholder, M. *Kunststoffe* **2002**, *92*, 44-51.
- (8) Oertel, C. G. In *Polypropylene Handbook*; Moore, E. P., Ed.; Hanser: München, **1996**.
- (9) Ullmann In *Ullmann's Encyclopedia of Industrial Chemistry*; Elvers, B., Hawkins, S., Schulz, G., Eds.; VCH: Weinheim, **1992**; Vol. A21.
- (10) Kashiwa, N. Macro 2004, Paris, **2004**.
- (11) Sherman, L. M. *Plasticstechnology* **2002**.
- (12) Bonte, Y.; Schweda, R. *Kunststoffe* **2001**, *91*, 262-266.
- (13) Atofina ; Atofina.; **2004**; Vol. 2004
- (14) Sinclair, K. B. *Macromol. Symp.* **2001**, *173*, 237-261.
- (15) Ziegler, K.; Holzkamp, E.; Breil, H.; Matin, H. *Angew. Chem.* **1955**, *67*, 541.
- (16) Wilke, G. *Angew. Chem.* **2003**, *115*, 5150-5159.
- (17) Natta, G.; Pino, P.; Corradini, P.; Danusso, F.; Mantika, E.; Mazzanto, G.; Moraglio, G. *J. Am. Chem. Soc.* **1955**, *77*, 541.
- (18) Corradini, P. *J. Polym. Sci. A* **2004**, *42*, 391-395.
- (19) Albizzati, E.; Giannini, U.; Collina, G.; Noristi, L.; Resconi, L. In *Polypropylene Handbook*; Moore, E. J., Ed.; Carl Hanser Verlag: Munich, Vienna, New York., **1996**.
- (20) Andresen, A.; Cordes, H.-G.; Herwig, J.; Kaminsky, W.; Merck, A.; Mottweiler, R.; Pein, J.; Sinn, H.-J.; Vollmer, H. *Angew. Chem.* **1976**, *88*, 689.
- (21) Kaminsky, W. *J. Polym. Sci. A* **2004**, *42*, 3911-3921.
- (22) Brintzinger, H. H.; Huttner, G.; Wild, R. R. W. P.; Zsolnai, L. *J. Organomet. Chem.* **1982**, *232*, 233.
- (23) Brintzinger, H. H.; Kaminsky, W.; Külper, K.; Wild, F. R. W. P. *Angew. Chem.* **1985**, *97*, 507.

- (24) Spaleck, W.; Antberg, M.; Dolle, V.; Klein, R.; Rohrmann, J.; Winter, A. *New J. Chem.* **1990**, *14*, 499.
- (25) Spaleck, W.; al, e. *Organometallics* **1994**, *13*, 954.
- (26) Ewen, J. A.; Jones, R. L.; Razavi, A. *J. Am. Chem. Soc.* **1988**, *110*, 6255-6256.
- (27) Aulbach, M.; Küber, F. *Ch. i. u.Z.* **1994**, *28*, 197.
- (28) Brintzinger, H.-H.; Fischer, D.; Mülhaupt, R.; Rieger, B.; Waymouth, R. *Angew. Chem.* **1995**, *107*, 1255-1283.
- (29) Beginn, U.; Keul, H.; Klee, D.; Möller, M.; Mourran, A.; Peter, K.; Weichold, O. *Nachrichten a. d. Chemie* **2004**, *52*, 324-331.
- (30) Bochmann, M. *Nachr. Chem. Techn. Lab.* **1993**, *41*, 1220.
- (31) Resconi, L.; Cavallo, L.; Fait, A.; Piemontesi, F. *Chem. Rev.* **2000**, *100*, 1253-1345.
- (32) Kaminsky, W.; Kuelper, K.; Brintzinger, H.-H.; Wild, F. R. *Angew. Chem. Int. E. Engl.* **1985**, *24*, 507.
- (33) Kawamura-Kuribayashi, H.; Koga, N.; Morokuma, K. *J. Am. Chem. Soc.* **1992**, *114*, 8687-8694.
- (34) Cavallo, L.; Guerra, G.; Vacatello, M.; Corradini, P. *Macromol.* **1991**, *24*, 1784-1790.
- (35) Miller, S. A.; Bercaw, J. E. *Organometallics* **2002**, *21*, 934-945.
- (36) Busico, V.; Cipullo, R. *Progr. Polym. Sci.* **2001**, *26*, 443-533.
- (37) Gomez, F. J.; Waymouth, R. M. *Macromol.* **2002**, *35*, 3358-3368.
- (38) Leino, R.; Gómez, F. J.; Cole, A. P.; Waymouth, R. M. *Macromolecules* **2001**, *34*, 2072-2082.
- (39) Mülhaupt, R.; Engelhardt, T.; Schall, N. *Kunststoffe* **2001**, *91*, 178-190.
- (40) Hohenberger, W. *Kunststoffe* **2002**, *92*, 86-91.
- (41) Mülhaupt, R.; Stricker, F. *Kunststoffe* **1997**, *87*, 482.
- (42) Zielonka Dissertation, University of Hamburg, **1991**.
- (43) Kaminsky, W.; Zielonka, H. *Polym. Adv. Technol.* **1993**, *4*, 415-422.
- (44) Zielonka, H. diploma thesis, University of Hamburg, **1988**.
- (45) Premalal, H. G. B.; Ismail, H.; Baharin, A. *Polymer Testing* **2002**, *21*, 833-839.
- (46) Siriwardena, S.; Ismail, H.; Ishiaku, U. S. *Polymer International* **2001**, *50*, 707-713.
- (47) Weigel, P.; Ganster, J.; Fink, H.-P.; Gassan, J.; Uihlein, K. *Kunststoffe* **2002**, *92*, 95-97.
- (48) Murr, L. E.; Soto, K. F. *J. Mat. Sci.* **2004**, *39*, 4941-4947.
- (49) Gusev, A. A. *Macromolecules* **2001**, *34*, 3081-3093.
- (50) Vacatello, M. *Macromolecules* **2001**, *34*, 1946-1952.

- (51) Lu, K. L.; Lago, R. M.; Chen, Y. K.; Green, M. L. H.; Harris, P. J. F.; Tsang, S. C. *Carbon* **1996**, *34*, 814-816.
- (52) Bergman, J. S.; Coates, G. W.; Chen, H.; Giannelis, E. P.; Thomas, M. G. *Chem. Commun.* **1999**, *21*, 2179-2180.
- (53) Morgan, A. B.; Gilman, J. W.; Jackson, C. L. *Macromolecules* **2001**, *34*, 2735-2738.
- (54) Wei, L.; Tang, T.; Huang, B. *J. Polym. Sci. A* **2004**, *42*, 941-949.
- (55) Andrews, R.; Jaques, D.; Qian, D.; Rantell, T. *Accounts of Chemical Research* **2002**, *35*, 1998-1017.
- (56) Alexandre, M.; Pluta, M.; Dubois, P.; Jérôme, R. *Macromol. Chem. Phys.* **2001**, *202*, 2239-2246.
- (57) Kawasumi, M.; Hasegawa, N.; Kato, M.; Usuki, A.; Okada, A. *Macromolecules* **1997**, *30*, 6333-6338.
- (58) Tjong, S. C.; Meng, Y. Z.; Hay, A. S. *Chem. Mater.* **2002**, *14*, 44-51.
- (59) Maiti, P.; Nam, P. H.; Okamoto, M.; Hasegawa, N.; Usuki, A. *Macromol.* **2002**, *35*, 2042-2049.
- (60) Reichert, P.; Nitz, H.; Klinke, S.; Brandsch, R.; Thomann, R.; Mülhaupt, R. *Macromol. Mater. Eng.* **2000**, *275*, 8.
- (61) Manias, E.; Touny, A.; Wu, L.; Strawhecker, K.; Lu, B.; Chung, T. C. *Chem. Mater.* **2001**, *13*, 3516-3523.
- (62) Dubois, P.; Alexandre, M.; Jérôme, R. *Macromol. Sym.* **2003**, *194*, 13-26.
- (63) Heinemann, J.; Reichert, P.; Thomann, R.; Mülhaupt, R. *Macromol. Rapid Commun.* **1999**, *20*, 423.
- (64) Ma, J.; Qi, Z.; Hu, Y. *J. Appl. Polym. Sci.* **2001**, *82*, 3611-3617.
- (65) Kaminsky, W.; Wiemann, K. *Expected Materials for the Future* **2003**, *3*, 6-12.
- (66) Wiemann, K. diploma thesis, University of Hamburg, **2001**.
- (67) Pluta, M.; Alexandre, M.; Blacher, S.; Dubois, P.; Jerome, R. *Polymer* **2001**, *42*, 9293-9300.
- (68) Schumann, H.; Widmaier, R.; Lnage, K. C. H.; Wassermann, B. C. *submitted* .
- (69) Alexandre, M.; Dubois, P. G.; Jerome, R. J. E. G.; Garcia-Marti, M.; Sun, T.; Garces, J. M.; Millar, D. M.; Kuperman, A. USA, WO 9947598, **1999**;WO 9947598.
- (70) Mülhaupt, R.; Heinemann, J.; Reichert, P.; Geprägs, M.; Queisser, J. In *Deutsches Patent- und Markenamt Deutschland*, **2000**
- (71) Tang, T.; Wei, L.; Huang, B. USA, US 2003055148, **2003**;US 2003055148.
- (72) Sun, T.; Garcés, M. *Adv. Mater.* **2002**, *14*, 128-130.

- (73) Rong, J.; Jing, Z.; Li, H.; Sheng, M. *Macromol. Rapid Commun.* **2001**, *22*, 329-334.
- (74) Du, Z.; Rong, J.; Zhang, W.; Jing, Z.; Li, H. *J. Mat. Sci.* **2003**, *38*, 4863-4868.
- (75) García, M.; van Zyl, W. E.; ten Cate, M. G. J.; Stouwdam, J. W.; Verweij, H.; Pimplapure, M. S.; Weickert, G. *Ind. Eng. Chem. Res.* **2003**, *42*, 3750-3757.
- (76) Zhang, W.; Yang, W. J. *J. Mat. Sci. Lett.* **2004**, *39*, 4921-4922.
- (77) Yao, Z.; Braidy, N.; Botton, G. A.; Adronov, A. *J. Am. Chem. Soc.* **2003**, *125*, 16015-16024.
- (78) Baskaran, D.; Mays, J. W.; Bratcher, M. S. *Angew. Chem.* **2004**, *116*, 2190-2194.
- (79) Xia, H.; Wang, Q.; Qiu, G. *Chem. Mat.* **2003**, *15*, 3879-3886.
- (80) Cochet, M.; Maser, W. K.; Benito, A. M.; Callejas, M. A.; Martinez, M. T.; Benoit, J.-M.; Schreiber, J.; Chauvet, O. *Chem. Commun.* **2001**, 1450-1451.
- (81) Park, C.; Ounaies, Z.; Watson, K. A.; Crooks, R. E.; J., S. J.; Lowther, S. E.; Connell, J. W.; Siochi, E. J.; Harrison, J. S.; St. Clair, T. L. *Chem. Phys. Lett.* **2002**, *364*, 303-308.
- (82) Tong, X.; Liu, C.; Dheng, H.-M.; Zhao, H.; Yang, F.; Zhang, X. *J. Appl. Polym. Sci.* **2004**, *92*, 3697-3700.
- (83) Barbosa, S. E.; Ferreira, M. L.; Damiani, D. E.; Capiati, N. J. *J. Appl. Polym. Sci.* **2001**, *81*, 1266-1276.
- (84) Ran, S.; Burger, C.; Sics, I.; Yoon, K.; Fang, D.; Kim, K.; Avila-Orta, C.; Keum, J.; Chu, B.; Hsiao, B. S.; Cokson, D.; Shultz, D.; Lee, M.; Viccaro, J.; Ohta, Y. *Colloid Polym. Sci.* **2004**, *282*, 802-809.
- (85) Lozano, K.; Bonilla-Rios, J.; Barrera, E. V. *J. Appl. Polym. Sci.* **2001**, *80*, 1162-1172.
- (86) Sandler, J.; Broza, k. G.; Nolte, M.; Schulte, K.; Lam, Y.-M.; Shaffer, M. S. P. *J. Macromol. Sci. B* **2003**, *42*, 479-488.
- (87) Andrews, R.; Jaques, D.; Minot, M.; Rantell, T. *Macromol. Mat. Eng.* **2002**, *287*, 395-403.
- (88) Thostenson, E. T.; Ren, Z.; Chou, T.-W. *Composites Sci. Technol.* **2001**, *61*, 1899-1912.
- (89) Kang, Z.; Wang, W.; Gao, L.; Lian, S.; Jiang, M.; Hu, C.; Xu, L. *J. Am. Chem. Soc.* **2003**, *125*, 13652-13653.
- (90) Ajayan, P. M. *Chem. Rev.* **1999**, *99*, 1787-1799.
- (91) Assouline, E. L., A.; Barber, A. H.; Cooper, C. A.; Klein, E.; Wachtel, E.; Wagner, H. D. *J. Polym. Sci. B* **2003**, *41*, 520-527.
- (92) Kim, I. *www.cepmagazine.org* **2001**.

- (93) Hyperion-catalysis ; [www.hyperion-catalysis.com](http://www.hyperion-catalysis.com)., **2004**
- (94) Beyer, G. *GAK* **2001**, *54*, 321-325.
- (95) Bharadwaj, R. K. *Macromol.* **2001**, *34*, 9189-9192.
- (96) Zilg, C.; Reichert, P.; Dietsche, F.; Engelhardt, T.; Mülhaupt, R. *Kunststoffe* **1998**, *88*, 1812.
- (97) Gorrasi, G.; Tortora, M.; Vittoria, V.; Kaempfer, D.; Mülhaupt, R. *Polymer* **2003**, *44*, 3679-3685.
- (98) Van Damme, H.; Burr, H. *Macromol. Sym.* **2003**, *194*, 1-12.
- (99) Zhang, W. D.; Shen, L.; Phang, I. Y.; Liu, T. *Macromol.* **2004**, *37*, 256-259.
- (100) Thostenson, E. T.; Chou, T.-W. *J. Phys. D: Appl. Phys.* **2003**, *36*, 573-582.
- (101) Kurauchi, T.; Okada, A.; Nomura, T.; Nishio, T.; Saegusa, S.; Deguchi, R. *SAE Technical Paper Series* **1991**, *910584*.
- (102) Okada, A.; Kawasumi, M.; Kurauchi, T.; Kamigaito, O. *Polym. Prep.* **1987**, *28*, 447.
- (103) Kojima, Y.; Usuki, A.; Kawasumi, M.; Okada, A.; Fukushima, Y.; Kurauchi, T.; Kamigaito, O. *J. Mater. Res.* **1993**, *8*, 1185.
- (104) Tudor, J.; O'Hare, D. *Chem. Commun.* **1997**, 603-604.
- (105) Kaempfer, D.; Thomann, R.; Mülhaupt, R. *Polymer* **2002**, *43*, 2909-2916.
- (106) Zanetti, M.; Camino, G.; Reichert, P.; Mülhaupt, R. *Macromol. Rapid Commun.* **2001**, *22*, 176-180.
- (107) Boucard, S.; Duchet, J.; Gérard, J. F.; Prele, P.; Gonzalez, S. *Macromol. Symp.* **2003**, *194*, 241-246.
- (108) Lehmann, B.; Friedrich, K.; Wu, C. L.; Zhang, M. Q.; Rong, M. Z. *J. Mat. Sci. Lett.* **2003**, *22*, 1027-1030.
- (109) Ruan, W. H.; Zhang, M. Q.; Z., T. M.; Friedrich, K. *J. Mat. Sci.* **2004**, *39*, 3475-3478.
- (110) Chan, C.-M.; Wu, J.; Li, J.-X.; Cheung, Y.-K. *Polymer* **2002**, *43*, 2981-2992.
- (111) Thio, Y. S.; Argon, A. S.; Cohen, R. E.; Weinberg, M. *Polymer* **2002**, *43*, 3661-3674.
- (112) Kumar, S.; Doshi, H.; Srinivasarao, M.; Park, J. O.; Schiraldi, D. A. *Polymer* **2002**, *43*, 1701-1703.
- (113) Finegan, I. C.; Tibbetts, G. g.; Glasgow, D. G.; Ting, J.-M.; Lake, M. L. *J. Mat. Sci.* **2003**, *38*, 3485-3490.
- (114) Hill, D. E.; Lin, Y.; Rao, A. M.; Allard, L. F.; Sun, Y.-P. *Macromol.* **2002**, *35*, 9466-9471.
- (115) Qian, D.; Dickey, E. C.; Andrews, R.; Rantell, T. *Appl. Phys. Lett.* **2000**, *76*, 2868-2870.

- (116) Bhattacharyya, A. R.; Sreekumar, T. V.; Liu, T.; Kumar, S.; Ericson, L. M.; hauge, R. H.; Smalley, R. E. *Polymer* **2003**, *44*, 2373-2377.
- (117) Ruan, S. L.; Gao, P.; Yang, X. G.; Yu, T. X. *Polymer* **2003**, *44*, 5643-5654.
- (118) Xia, H.; Wang, Q.; Li, K.; Hu, G.-H. *J. Appl. Polym. Sci.* **2004**, *93*, 378-386.
- (119) Blake, R.; Gun'ko, Y. K.; Coleman, J.; Cadek, M.; Fonseca, A.; Nagy, J. B.; Blau, W. *J. J. Am. Chem. Soc.* **2004**, *126*, 10226-10227.
- (120) Kearns, J. C.; Shambaugh, R. L. *J. Appl. Polym. Sci.* **2002**, *86*, 2079-2084.
- (121) Dupire, M.; Jacques, M. ; Fina Research S. A.: EP1054036, **2000**
- (122) Mylvaganam, K.; Zhang, L. C. *J. Phys. Chem. B* **2004**.
- (123) Wei, C. S., D.; Cho, K. *Nano Letters* **2002**.
- (124) Kharchenko, S. B.; Douglas, J. F.; Obrzut, J.; Grulke, E. A.; Migler, K. B. *Nature Mat.* **2004**, *3*, 564-568.
- (125) Bin, Y.; Kitanaka, M.; Zhu, D.; Matsuo, M. *Macromol.* **2003**, *36*, 6213-6219.
- (126) Calvert, P. *Nature* **1999**, *399*, 210-211.
- (127) Qian, J.; He, P. *J. Mat. Sci.* **2003**, *38*, 2299-2304.
- (128) Lozano, K.; Barrera, E. V. *J. Appl. Polym. Sci.* **2001**, *79*, 125-133.
- (129) Xie, X. L.; Aloys, K.; Zhou, X. P.; Zeng, F. D. *J. Therm. Anal. Cal.* **2003**, *74*, 317-323.
- (130) Valentini, L.; Biagiotti, J.; Kenny, J. M.; López Manchado, M. A. *J. Appl. Polym. Sci.* **2003**, *89*, 2657-2663.
- (131) Grady, B. P.; Pompeo, F.; Shambaugh, R. L.; Resansco, D. E. *J. Phys. Chem. B* **2002**, *106*, 5852-5858.
- (132) Seo, M.-K.; Park, S.-J. *Macromol. Mater. Eng.* **2004**, *289*, 368-374.
- (133) Watts, P. C. P.; Fearon, P. K.; Hsu, W. K.; Billingham, N. C.; Kroto, H. W.; Walton, D. R. M. *J. Mat. Chem.* **2003**, *13*, 491-495.
- (134) Kashiwagi, T.; Grulke, E.; Hilding, J.; Groth, K.; Harris, R.; Butler, K.; Shields, J.; Kharchenko, S.; Douglas, J. *Polymer* **2004**, *45*, 4227-4239.
- (135) Kashiwagi, T.; Grulke, E.; Hilding, J.; Harris, R.; Awad, W.; Douglas, J. *Macromol. Rapid Commun.* **2002**, *23*, 761-765.
- (136) Mason, T. J.; Lorimer, J. P. *Sonochemistry: Theory, Applications and Uses of Ultrasound in Chemistry*; Ellis Horwood: Chichester, **1988**.
- (137) Hlatky, G. G. *Chem. Rev.* **2000**, *100*, 1347-1376.
- (138) Brandrup, J.; Immergut, E. H. *Polymer Handbook*; 4 th ed.; Wiley: New York, **1998**.

- 
- (139) Wang, Z. G.; Wang, X.-H.; Hsiao, B. S.; Philips, R. A.; Medellin-Rodriguez, F. J.; Srinivas, S.; Wang, H.; Han, C. C. *J. Polym. Sci. B* **2001**, *39*, 2982-2995.
- (140) Supaphol, P.; Spruiell, J. E. *J. Macromol. Sci. B* **2000**, *B39*, 257-277.
- (141) Sperling, L. H. In *Introduction to Physical Polymer Science*; 2nd ed.; Sperling, L. H., Ed.; John Wiley & Sons: New York, Chichester, Brisbane, Toronto, Singapore, **1992**.
- (142) Avrami, M. *J. Chem. Phys.* **1939**, *7*, 1103-1112.
- (143) Avrami, M. *J. Chem. Phys.* **1940**, *8*, 212-224.
- (144) Wegner, G. *Polymere Werkstoffe - Chemie und Physik*; Georg Thieme Verlag: Stuttgart, New York, **1985**.
- (145) Sperling, L. H. In *Introduction to Physical Polymer Science*; Sperling, L. H., Ed.; John Wiley & Sons Inc.: New York, Chichester, Brisbane, Toronto, Singapore, **1992**.
- (146) Hopf, A. PhD thesis, Universität Hamburg, **2002**.
- (147) Tibbets, G. G.; Mc Hugh, J. J. *J. Mat. Res.* **1999**, *14*, 2871-2880.
- (148) *Gefahrstoffverordnung und Chemikaliengesetz, Anhang I-IV, MAK-Werte Liste etc., Technische Regeln für Gefahrstoffe*; Verlagsges. Weinheim, mbH, **1991**.



## **Declaration**

I declare to have developed the results presented in this thesis myself, and with the help of no other than the cited references and resources.

This work has not been presented to any inspecting authority in the same or a similar form before.

## **Erklärung**

Hiermit erkläre ich an Eides Statt, dass ich die vorliegende Arbeit selbständig erarbeitet und keine anderen als die angegebenen Quellen und Hilfsmittel zum Verfassen genutzt habe.

Die Arbeit ist zuvor in gleicher oder ähnlicher Form keiner Prüfungsbehörde vorgelegt worden.

Hamburg, November 2004



## Posters

A. Hopf, W. Kaminsky, F. Müller, K. Wiemann

„Hochsyndiotaktisches Polypropen durch neue Metallocen/MAO Katalysatoren“, Makromolekulares Kolloquium, Freiburg, Germany, February 20 – 22, 2002.

K. Wiemann, W. Kaminsky

„Nanocomposites durch in-situ Polymerisation von Propen mit Metallocen/MAO-Katalysatoren“, Informationskurs für Doktoranden, Bayer AG, Leverkusen, Germany, August 31 – September 5, 2003.

T. Seraidaris, K. Wiemann, W. Kaminsky

„Syndiotaktisches PP: Einfluss des Cokatalysators & Nanocomposites durch in-situ Polymerisation“, Hamburger Makromolekulares Symposium, Hamburg, Germany, September 8 – 9, 2003.

K. Wiemann, W. Kaminsky, F. Gojny, K. Schulte

„Nanocomposites of polypropylene and carbon nanofibers or carbon nanotubes formed by in-situ polymerization“, World Polymer Congress MACRO 2004, 40<sup>th</sup> IUPAC International Symposium on Macromolecules, Paris, France, July 4 – 9, 2004.

## Publications

W. Kaminsky, K. Wiemann, “Polypropene/silica nanocomposites synthesized by in-situ polymerization” *Expected Materials for the Future*, **2003**, 3, 6-12.

K. Wiemann, W. Kaminsky, F. Gojny, K. Schulte

„Nanocomposites of polypropylene and carbon nanofibers or carbon nanotubes formed by in-situ polymerization“, proceedings of World Polymer Congress MACRO 2004, 40<sup>th</sup> IUPAC International Symposium on Macromolecules, Paris, France, July 4 – 9, 2004.

W. Kaminsky, C. Piel, K. Wiemann

„Recent developments in metallocene catalysis“, Dechema Monographien, Wiley VCH, Vol 128, Polymer Reaction Engineering (H.-U. Moritz, K.-H. Reichert, eds.) Frankfurt, 2004, 131-140.

K. Wiemann, W. Kaminsky, F. Gojny, K. Schulte

Synthesis and properties of polypropylene/carbon nanofiber and polypropylene/carbon nanotube nanocomposites prepared by in-situ polymerization with metallocene/MAO catalysts, in preparation.



